

NOVEMBER 2023

AJNR

VOLUME 44 • PP 1241-1355

# AJNR

## AMERICAN JOURNAL OF NEURORADIOLOGY

Official Journal ASNR • ASFNR • ASHNR • ASPNR • ASSR  
NOVEMBER 2023 | VOLUME 44 | NUMBER 11 | WWW.AJNR.ORG

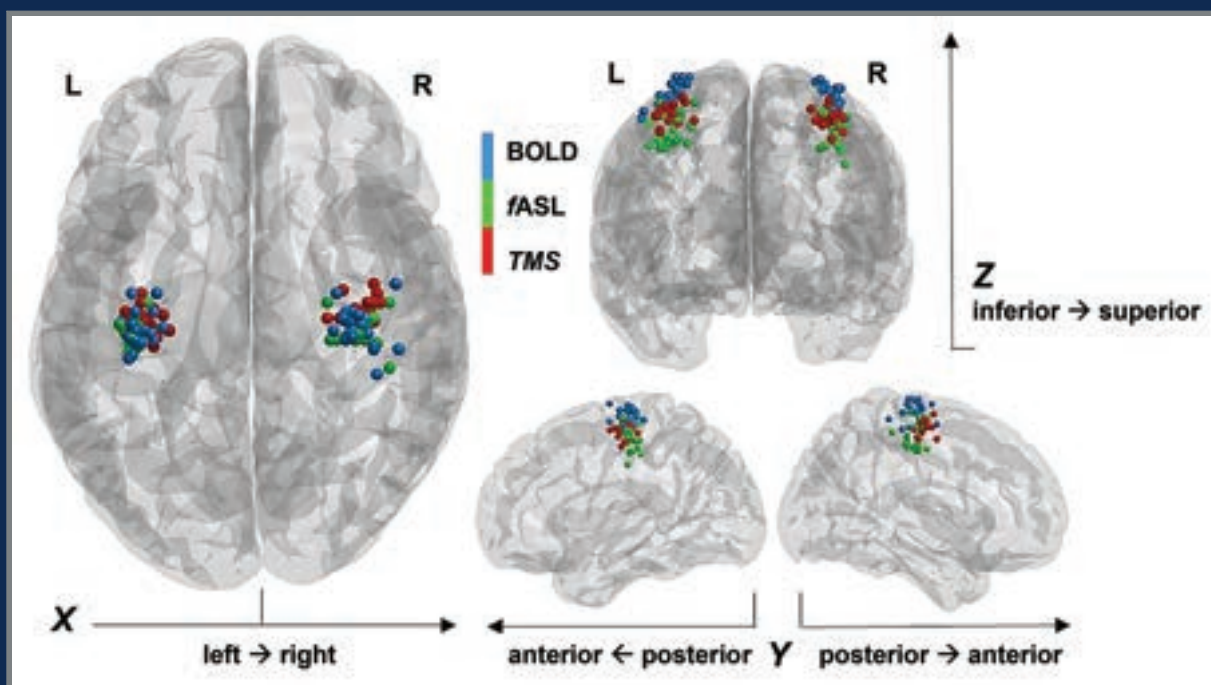
THE JOURNAL OF DIAGNOSTIC AND INTERVENTIONAL NEURORADIOLOGY

Screening blunt vascular injury in low-mechanism trauma

Specificity of functional arterial spin-labeling for preoperative assessment

Bone marrow enhancement associated with ruptured Rathke cleft cyst

Probabilistic scoring system of intracranial MRI findings for likelihood of discovering CSF leak



# FRED™ X™

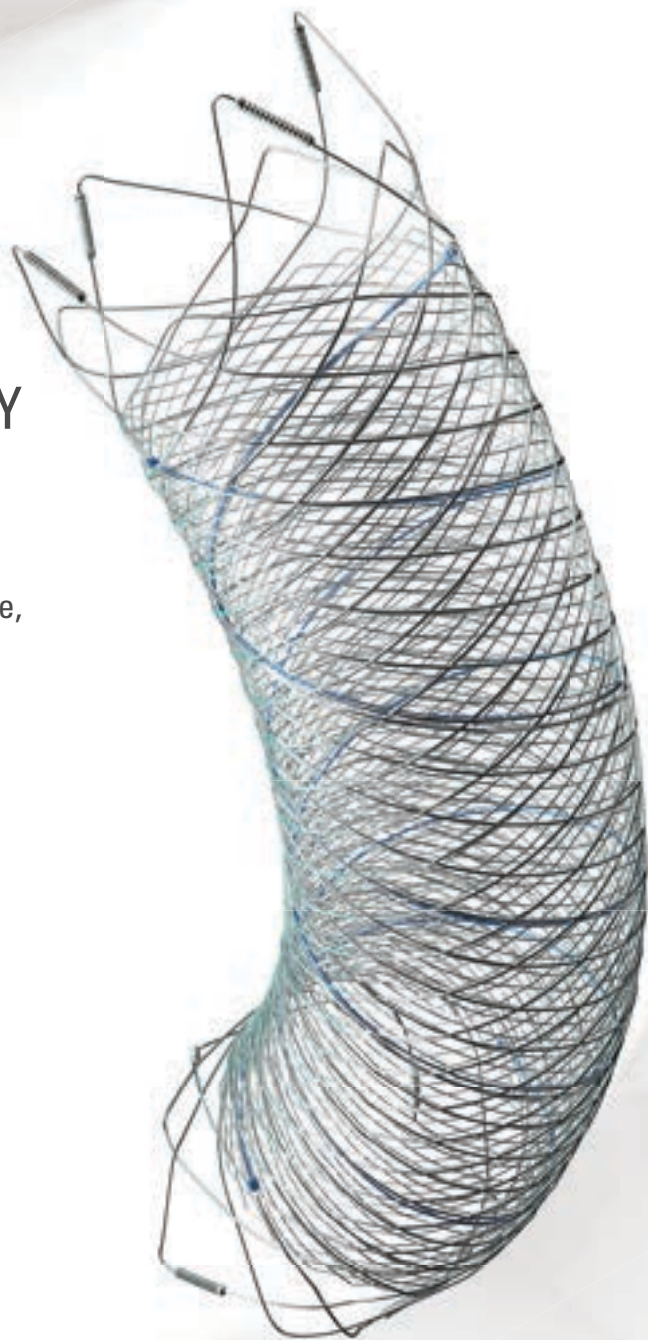
## Flow Diverter Stent

### THE NEXT ADVANCEMENT IN FLOW DIVERSION TECHNOLOGY

The FRED™ X Flow Diverter features the same precise placement and immediate opening of the FRED™ Device, now with X Technology. X Technology is a covalently bonded, nanoscale surface treatment, designed to:

- **REDUCE MATERIAL THROMBOGENICITY<sup>1</sup>**
- **MAINTAIN NATURAL VESSEL HEALING RESPONSE<sup>2,3,4</sup>**
- **IMPROVE DEVICE DELIVERABILITY AND RESHEATHING<sup>1</sup>**

The only FDA PMA approved portfolio with a 0.021" delivery system for smaller device sizes, and no distal lead wire.



For more information, contact your local MicroVention sales representative or visit our website. [www.microvention.com](http://www.microvention.com)



<sup>\*</sup> Data is derived from in vivo and ex vitro testing and may not be representative of clinical performance.

<sup>1</sup> Data on file

<sup>2</sup> Tanaka M et al. Design of biocompatible and biodegradable polymers based on intermediate water concept. Polymer Journal. 2015;47:114-121.

<sup>3</sup> Tanaka M et al. Blood compatible aspects of poly(2-methoxyethylacrylate) (PMEA) – relationship between protein adsorption and platelet adhesion on PMEA surface. Biomaterials. 2000;21:1471-1481.

<sup>4</sup> Schiel L et al. X Coating™: A new biopassive polymer coating. Canadian Perfusion Canadienne. June 2001;11(2):9.

**Indications for Use:** The FRED X System is indicated for use in the internal carotid artery from the petrous segment to the terminus for the endovascular treatment of adult patients (22 years of age or older) with wide-necked (neck width 4 mm or dome-to-neck ratio < 2) saccular or fusiform intracranial aneurysms arising from a parent vessel with a diameter 2.0 mm and 5.0 mm.

**Rx Only:** Federal (United States) law restricts this device to sale by or on the order of a physician. For Healthcare professionals intended use only.

MICROVENTION, FRED and HEADWAY are registered trademarks of MicroVention, Inc. in the United States and other jurisdictions. Stylized X is a trademark of MicroVention, Inc. © 2022 MicroVention, Inc. MM1222 US 03/22

# WEB™ 17

Aneurysm Embolization System

# LOWER PROFILE



## NEW SIZES



## MORE ACCESS OPTIONS



#### INDICATIONS FOR USE:

The WEB Aneurysm Embolization System is intended for the endovascular embolization of ruptured and unruptured intracranial aneurysms and other neurovascular abnormalities such as arteriovenous fistulae (AVF). The WEB Aneurysm Embolization System is also intended for vascular occlusion of blood vessels within the neurovascular system to permanently obstruct blood flow to an aneurysm or other vascular malformation.

#### POTENTIAL COMPLICATIONS:

Potential complications include but are not limited to the following: hematoma at the site of entry, aneurysm rupture, emboli, vessel perforation, parent artery occlusion, hemorrhage, ischemia, vasospasm, clot formation, device migration or misplacement, premature or difficult device detachment, non-detachment, incomplete aneurysm filling, revascularization, post-embolization syndrome, and neurological deficits including stroke and death. For complete indications, potential complications, warnings, precautions, and instructions, see instructions for use (IFU provided with the device).

VIA 21, 27, 33 - The VIA Microcatheter is intended for the introduction of interventional devices (such as the WEB device/stents/flow diverters) and infusion of diagnostic agents (such as contrast media) into the neuro, peripheral, and coronary vasculature.

VIA 17, 17 Preshaped - The VIA Microcatheter is intended for the introduction of interventional devices (such as the WEB device/stents/flow diverters) and infusion of diagnostic agents (such as contrast media) into the neuro, peripheral, and coronary vasculature.

The VIA Microcatheter is contraindicated for use with liquid embolic materials, such as n-butyl 2-cyanoacrylate or ethylene vinyl alcohol & DMSO (dimethyl sulfoxide).

The device should only be used by physicians who have undergone training in all aspects of the WEB Aneurysm Embolization System procedure as prescribed by the manufacturer.

RX Only: Federal law restricts this device to sale by or on the order of a physician.

For healthcare professional intended use only.



MicroVention Worldwide  
Innovator Center

PH +1.714.247.8000

35 Enterprise  
Aliso Viejo, CA 92656 USA  
MicroVention UK Limited  
MicroVention Europe, S.A.R.L.  
MicroVention Deutschland GmbH  
Website

PH +44 (0) 191 258 6777  
PH +33 (1) 39 21 77 46  
PH +49 211 210 798-0  
microvention.com



WEB™ and VIA™ are registered trademarks  
of Sequent Medical, Inc. in the United States.

©2021 MicroVention, Inc. MM1184 WW 11/2021

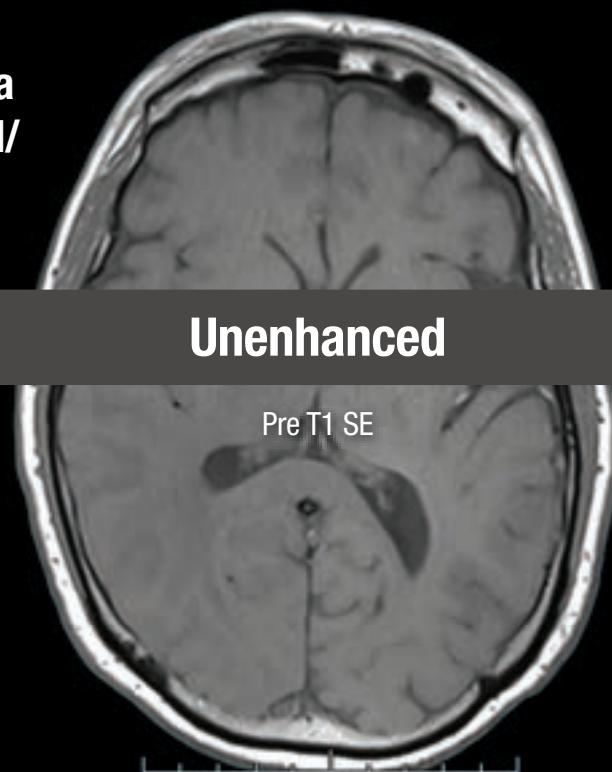


# THIS IS HALF Gd\*

**\*Effective contrast enhancement at half the gadolinium dose (0.05 mmol/kg) vs a macrocyclic GBCA at a dose of 0.1 mmol/kg in approved indications in the U.S.<sup>1-6†</sup>**

  
**Vueway®**  
(gadopiclenol) injection  
485.1 mg/mL

**NO COMPROMISE IN MRI FROM BRACCO,  
YOUR TRUSTED PARTNER**



<sup>†</sup>Phase III CNS Study Design (Study GDX-44-010): Intra-individual, crossover comparison of 0.05 mmol/kg VUEWAY (gadopiclenol) injection vs. 0.1 mmol/kg Gadavist® in MRI of the CNS. Patients with known or suspected CNS lesions. Three primary visualization endpoints (lesion border delineation, lesion internal morphology, degree of contrast enhancement). The CNS study included 256 patients with known or highly suspected CNS lesion(s) with a mean age of 57 years (range: 18-84 years), and 53% female patients.

Please see Brief Summary of Prescribing Information including Boxed Warning on adjacent page.

#### **VUEWAY® (gadopiclenol) solution for injection**

##### **Indications**

VUEWAY injection is indicated in adults and children aged 2 years and older for use with magnetic resonance imaging (MRI) to detect and visualize lesions with abnormal vascularity in:

- the central nervous system (brain, spine and surrounding tissues),
- the body (head and neck, thorax, abdomen, pelvis, and musculoskeletal system).

#### **IMPORTANT SAFETY INFORMATION**

##### **WARNING: NEPHROGENIC SYSTEMIC FIBROSIS (NSF)**

**Gadolinium-based contrast agents (GBCAs) increase the risk for NSF among patients with impaired elimination of the drugs. Avoid use of GBCAs in these patients unless the diagnostic information is essential and not available with non-contrasted MRI or other modalities. NSF may result in fatal or debilitating fibrosis affecting the skin, muscle and internal organs.**

- **The risk for NSF appears highest among patients with:**
  - Chronic, severe kidney disease (GFR < 30 mL/min/1.73 m<sup>2</sup>), or
  - Acute kidney injury.

- **Screen patients for acute kidney injury and other conditions that may reduce renal function. For patients at risk for chronically reduced renal function (e.g. age > 60 years, hypertension, diabetes), estimate the glomerular filtration rate (GFR) through laboratory testing.**
- **For patients at highest risk for NSF, do not exceed the recommended VUEWAY dose and allow a sufficient period of time for elimination of the drug from the body prior to any re-administration.**

##### **Contraindications**

VUEWAY injection is contraindicated in patients with history of hypersensitivity reactions to VUEWAY.

##### **Warnings**

Risk of **nephrogenic systemic fibrosis** is increased in patients using GBCA agents that have impaired elimination of the drugs, with the highest risk in patients with chronic, severe kidney disease as well as patients with acute kidney injury. Avoid use of GBCAs among these patients unless the diagnostic information is essential and not available with non-contrast MRI or other modalities.

**Hypersensitivity reactions**, including serious hypersensitivity reactions, could occur during use or shortly following VUEWAY administration. Assess all patients for any history of a reaction to contrast media, bronchial asthma and/or allergic disorders, administer VUEWAY only in



LIFE FROM INSIDE

65-year-old man – 3.0 T Siemens  
Brain metastasis from lung adenocarcinoma<sup>7</sup>

SE = Spin Echo. These are representative images from reference studies; individual results may vary.

**Gadopichlenol** 0.05 mmol/kg

Post T1 SE

**Gadobutrol** 0.1 mmol/kg

Post T1 SE

situations where trained personnel and therapies are promptly available for the treatment of hypersensitivity reactions, and observe patients for signs and symptoms of hypersensitivity reactions after administration.

**Gadolinium retention** can be for months or years in several organs after administration. The highest concentrations (nanomoles per gram of tissue) have been identified in the bone, followed by other organs (brain, skin, kidney, liver and spleen). Minimize repetitive GBCA imaging studies, particularly closely spaced studies, when possible.

**Acute kidney injury** requiring dialysis has occurred with the use of GBCAs in patients with chronically reduced renal function. The risk of acute kidney injury may increase with increasing dose of the contrast agent.

Ensure catheter and venous patency before injecting as **extravasation** may occur, and cause tissue irritation.

VUEWAY may **impair the visualization of lesions** seen on non-contrast MRI. Therefore, caution should be exercised when VUEWAY MRI scans are interpreted without a companion non-contrast MRI scan.

The most common adverse reactions (incidence  $\geq 0.5\%$ ) are injection site pain (0.7%), and headache (0.7%).

**You are encouraged to report negative side effects of prescription drugs to the FDA. Visit [www.fda.gov/medwatch](http://www.fda.gov/medwatch) or call 1-800-FDA-1088.**

**Please see BRIEF SUMMARY of Prescribing Information for VUEWAY, including BOXED WARNING on Nephrogenic Systemic Fibrosis.**

Manufactured for Bracco Diagnostics Inc. by Liebel-Flarsheim Company LLC - Raleigh, NC, USA 27616.

VUEWAY is a trademark of Bracco Imaging S.p.A.

All other trademarks and registered trademarks are the property of their respective owners.

**References:** 1. VUEWAY® (gadopichlenol) solution for injection, 485.1 mg/mL Full Prescribing Information and Patient Medication Guide. Monroe Twp., NJ: Bracco Diagnostics Inc.; September 2022. 2. Robic C, Port M, Rousseaux O, et al. Physicochemical and pharmacokinetic profiles of gadopichlenol: a new macrocyclic gadolinium chelate with high T1 relaxivity. *Invest Radiol.* 2019 Aug;54:475-484. 3. GADAVIST® (gadobutrol) Injection. Full Prescribing Information. Bayer HealthCare Pharmaceuticals Inc. Whippany, NJ; April 2022. 4. DOTAREM® (gadoterate meglumine) Injection. Full Prescribing Information. Guerbet LLC. Princeton, NJ; April 2022. 5. CLARISCAN™ (gadoterate meglumine) injection for intravenous use. Full Prescribing Information. GE Healthcare. Chicago, IL; February 2020. 6. ProHance® (Gadoteridol) Injection, 279.3 mg/mL Full Prescribing Information and Patient Medication Guide. Monroe Twp., NJ: Bracco Diagnostics Inc.; June 2022. 7. Loevner LA, Kolumban B, Hutóczki G, et al. Efficacy and safety of gadopichlenol for contrast-enhanced MRI of the central nervous system: the PICTURE randomized clinical trial. *Invest Radiol.* 2023 May;58(5):307-313.

Bracco Diagnostics Inc.  
259 Prospect Plains Road, Building H  
Monroe Township, NJ 08831 USA  
Phone: 609-514-2200  
Toll-Free: 1-877-272-2269 (U.S. only)  
Fax: 609-514-2446

© 2023 Bracco Diagnostics Inc.  
All Rights Reserved. US-VW-2300022 08/23



VISIT  
[VUEWAY.COM](http://VUEWAY.COM)  
FOR MORE  
INFORMATION

# Vueway™ (gadopiclenol) injection, for intravenous use

**BRIEF SUMMARY:** Please see package insert of full prescribing information.

## WARNING: NEPHROGENIC SYSTEMIC FIBROSIS (NSF)

Gadolinium-based contrast agents (GBCAs) increase the risk for NSF among patients with impaired elimination of the drugs. Avoid use of GBCAs in these patients unless the diagnostic information is essential and not available with non-contrast MRI or other modalities. NSF may result in fatal or debilitating fibrosis affecting the skin, muscle and internal organs.

- The risk for NSF appears highest among patients with:
  - Chronic, severe kidney disease (GFR < 30 mL/min/1.73 m<sup>2</sup>), or
  - Acute kidney injury.
- Screen patients for acute kidney injury and other conditions that may reduce renal function. For patients at risk for chronically reduced renal function (e.g. age > 60 years, hypertension, diabetes), estimate the glomerular filtration rate (GFR) through laboratory testing.
- For patients at highest risk for NSF, do not exceed the recommended Vueway dose and allow a sufficient period of time for elimination of the drug from the body prior to any re-administration [see Warnings and Precautions (5.1) in the full Prescribing Information].

## INDICATIONS AND USAGE

Vueway™ (gadopiclenol) is a gadolinium-based contrast agent indicated in adult and pediatric patients aged 2 years and older for use with magnetic resonance imaging (MRI) to detect and visualize lesions with abnormal vascularity in:

- the central nervous system (brain, spine, and associated tissues),
- the body (head and neck, thorax, abdomen, pelvis, and musculoskeletal system).

## CONTRAINDICATIONS

Vueway is contraindicated in patients with history of hypersensitivity reactions to gadopicholol.

## WARNINGS AND PRECAUTIONS

**Nephrogenic Systemic Fibrosis** Gadolinium-based contrast agents (GBCAs) increase the risk for nephrogenic systemic fibrosis (NSF) among patients with impaired elimination of the drugs. Avoid use of GBCAs among these patients unless the diagnostic information is essential and not available with non-contrast MRI or other modalities. The GBCA-associated NSF risk appears highest for patients with chronic, severe kidney disease (GFR < 30 mL/min/1.73 m<sup>2</sup>) as well as patients with acute kidney injury. The risk appears lower for patients with chronic, moderate kidney disease (GFR 30-59 mL/min/1.73 m<sup>2</sup>) and little, if any, for patients with chronic, mild kidney disease (GFR 60-89 mL/min/1.73 m<sup>2</sup>). NSF may result in fatal or debilitating fibrosis affecting the skin, muscle, and internal organs. Report any diagnosis of NSF following Vueway administration to Bracco Diagnostics Inc. (1-800-257-5181) or FDA (1-800-FDA-1088 or [www.fda.gov/medwatch](http://www.fda.gov/medwatch)).

Screen patients for acute kidney injury and other conditions that may reduce renal function. Features of acute kidney injury consist of rapid (over hours to days) and usually reversible decrease in kidney function, commonly in the setting of surgery, severe infection, injury or drug-induced kidney toxicity. Serum creatinine levels and estimated GFR may not reliably assess renal function in the setting of acute kidney injury. For patients at risk for chronically reduced renal function (e.g., age > 60 years, diabetes mellitus or chronic hypertension), estimate the GFR through laboratory testing.

Among the factors that may increase the risk for NSF are repeated or higher than recommended doses of a GBCA and the degree of renal impairment at the time of exposure. Record the specific GBCA and the dose administered to a patient. For patients at highest risk for NSF, do not exceed the recommended Vueway dose and allow a sufficient period of time for elimination of the drug prior to re-administration. For patients receiving hemodialysis, physicians may consider the prompt initiation of hemodialysis following the administration of a GBCA in order to enhance the contrast agent's elimination [see Use in Specific Populations (8.6) and Clinical Pharmacology (12.3) in the full Prescribing Information]. The usefulness of hemodialysis in the prevention of NSF is unknown.

**Hypersensitivity Reactions** With GBCAs, serious hypersensitivity reactions have occurred. In most cases, initial symptoms occurred within minutes of GBCA administration and resolved with prompt emergency treatment.

- Before Vueway administration, assess all patients for any history of a reaction to contrast media, bronchial asthma and/or allergic disorders. These patients may have an increased risk for a hypersensitivity reaction to Vueway.
- Vueway is contraindicated in patients with history of hypersensitivity reactions to Vueway [see Contraindications (4) in the full Prescribing Information].
- Administer Vueway only in situations where trained personnel and therapies are promptly available for the treatment of hypersensitivity reactions, including personnel trained in resuscitation.
- During and following Vueway administration, observe patients for signs and symptoms of hypersensitivity reactions.

**Gadolinium Retention** Gadolinium is retained for months or years in several organs. The highest concentrations (nanomoles per gram of tissue) have been identified in the bone, followed by other organs (e.g. brain, skin, kidney, liver, and spleen). The duration of retention also varies by tissue and is longest in bone. Linear GBCAs cause more retention than macrocyclic GBCAs. At equivalent doses, gadolinium retention varies among the linear agents with gadodiamide causing greater retention than other linear agents such as gadoxetate disodium, and gadobenate dimeglumine. Retention is lowest and similar

among the macrocyclic GBCAs such as gadoterate meglumine, gadobutrol, gadoteridol, and gadopicholol.

Consequences of gadolinium retention in the brain have not been established. Pathologic and clinical consequences of GBCA administration and retention in skin and other organs have been established in patients with impaired renal function [see Warnings and Precautions (5.1) in the full Prescribing Information]. There are rare reports of pathologic skin changes in patients with normal renal function. Adverse events involving multiple organ systems have been reported in patients with normal renal function without an established causal link to gadolinium.

While clinical consequences of gadolinium retention have not been established in patients with normal renal function, certain patients might be at higher risk. These include patients requiring multiple lifetime doses, pregnant and pediatric patients, and patients with inflammatory conditions. Consider the retention characteristics of the agent when choosing a GBCA for these patients. Minimize repetitive GBCA imaging studies, particularly closely spaced studies, when possible.

**Acute Kidney Injury** In patients with chronically reduced renal function, acute kidney injury requiring dialysis has occurred with the use of GBCAs. The risk of acute kidney injury may increase with increasing dose of the contrast agent. Do not exceed the recommended dose.

**Extravasation and Injection Site Reactions** Injection site reactions such as injection site pain have been reported in the clinical studies with Vueway [see Adverse Reactions (6.1) in the full Prescribing Information]. Extravasation during Vueway administration may result in tissue irritation [see Nonclinical Toxicology (13.2) in the full Prescribing Information]. Ensure catheter and venous patency before the injection of Vueway.

**Interference with Visualization of Lesions Visible with Non-Contrast MRI** As with any GBCA, Vueway may impair the visualization of lesions seen on non-contrast MRI. Therefore, caution should be exercised when Vueway MRI scans are interpreted without a companion non-contrast MRI scan.

## ADVERSE REACTIONS

The following serious adverse reactions are discussed elsewhere in labeling:

- Nephrogenic Systemic Fibrosis [see Warnings and Precautions (5.1) in the full Prescribing Information]
- Hypersensitivity Reactions [see Contraindications (4) and Warnings and Precautions (5.2) in the full Prescribing Information]

**Clinical Trials Experience** Because clinical trials are conducted under widely varying conditions, adverse reaction rates observed in the clinical trials of a drug cannot be directly compared to rates in the clinical trials of another drug and may not reflect the rates observed in clinical practice.

The safety of Vueway was evaluated in 1,047 patients who received Vueway at doses ranging from 0.025 mmol/kg (one half the recommended dose) to 0.3 mmol/kg (six times the recommended dose). A total of 708 patients received the recommended dose of 0.05 mmol/kg. Among patients who received the recommended dose, the average age was 51 years (range 2 years to 88 years) and 56% were female. The ethnic distribution was 79% White, 10% Asian, 7% American Indian or Alaska native, 2% Black, and 2% patients of other or unspecified ethnic groups.

Overall, approximately 4.7% of subjects receiving the labeled dose reported one or more adverse reactions.

Table 1 lists adverse reactions that occurred in > 0.2% of patients who received 0.05 mmol/kg Vueway.

TABLE 1. ADVERSE REACTIONS REPORTED IN > 0.2% OF PATIENTS RECEIVING VUEWAY IN CLINICAL TRIALS	
Adverse Reaction	Vueway 0.05 mmol/kg (n=708) (%)
Injection site pain	0.7
Headache	0.7
Nausea	0.4
Injection site warmth	0.4
Injection site coldness	0.3
Dizziness	0.3
Local swelling	0.3

Adverse reactions that occurred with a frequency < 0.2% in patients who received 0.05 mmol/kg Vueway included: maculopapular rash, vomiting, worsened renal impairment, feeling hot, pyrexia, oral paresthesia, dysgeusia, diarrhea, pruritus, allergic dermatitis, erythema, injection site paresthesia, Cystatin C increase, and blood creatinine increase.

## Adverse Reactions in Pediatric Patients

One study with a single dose of Vueway (0.05 mmol/kg) was conducted in 80 pediatric patients aged 2 years to 17 years, including 60 patients who underwent a central nervous system (CNS) MRI and 20 patients who underwent a body MRI. One adverse reaction (maculopapular rash of moderate severity) in one patient (1.3%) was reported in the CNS cohort.

## USE IN SPECIFIC POPULATIONS

**Pregnancy Risk Summary** There are no available data on Vueway use in pregnant women to evaluate for a drug-associated risk of major birth defects, miscarriage or other adverse maternal or fetal outcomes. GBCAs cross the human placenta and result in fetal exposure and gadolinium retention. The available human data on GBCA exposure during pregnancy and adverse fetal outcomes are limited and inconclusive (see Data). In animal reproduction studies, there were no adverse developmental effects observed in rats or rabbits with intravenous administration of Vueway during organogenesis (see Data). Because of the potential risks of gadolinium to the fetus, use Vueway only if imaging is essential during pregnancy and cannot be delayed. The estimated background risk of major birth defects and miscarriage for the indicated population(s) are unknown. All pregnancies have a background risk of birth defect, loss, or other adverse outcomes. In the U.S. general population, the estimated background risk of major birth defects and miscarriage in clinically recognized pregnancies is 2% to 4% and 15% to 20% respectively. Data Human Data Contrast enhancement is visualized in the placenta and fetal tissues after maternal GBCA administration. Cohort studies and case reports on exposure to GBCAs during pregnancy have not reported a clear association between GBCAs and adverse effects in the exposed neonates. However, a retrospective cohort study comparing pregnant women who had a GBCA MRI to pregnant women who did not have an MRI reported a higher occurrence of stillbirths and neonatal deaths in the group receiving GBCA MRI. Limitations of this study include a lack of comparison with non-contrast MRI and lack of information about the maternal indication for MRI. Overall, these data preclude

a reliable evaluation of the potential risk of adverse fetal outcomes with the use of GBCAs in pregnancy.

**Animal Data Gadolinium Retention:** GBCAs administered to pregnant non-human primates (0.1 mmol/kg on gestational days 85 and 135) result in measurable gadolinium concentration in the offspring in bone, brain, skin, liver, kidney, and spleen for at least 7 months. GBCAs administered to pregnant mice (2 mmol/kg daily on gestational days 16 through 19) result in measurable gadolinium concentrations in the pups in bone, brain, kidney, liver, blood, muscle, and spleen at one-month postnatal age.

**Reproductive Toxicology:** Animal reproduction studies conducted with gadopicholol showed some signs of maternal toxicity in rats at 10 mmol/kg and rabbits at 5 mmol/kg (corresponding to 52 times and 57 times the recommended human dose, respectively). This maternal toxicity was characterized in both species by swelling, decreased activity, and lower gestation weight gain and food consumption.

No effect on embryo-fetal development was observed in rats at 10 mmol/kg (corresponding to 52 times the recommended human dose). In rabbits, a lower mean fetal body weight was observed at 5 mmol/kg (corresponding to 57 times the recommended human dose) and this was attributed as a consequence of the lower gestation weight gain.

**Lactation Risk Summary** There are no data on the presence of gadopicholol in human milk, the effects on the breastfed infant, or the effects on milk production. However, published lactation data on other GBCAs indicate that 0.01% to 0.04% of the maternal gadolinium dose is excreted in breast milk. Additionally, there is limited GBCA gastrointestinal absorption in the breast-fed infant. Gadopicholol is present in rat milk. When a drug is present in animal milk, it is likely that the drug will be present in human milk (see Data). The developmental and health benefits of breastfeeding should be considered along with the mother's clinical need for Vueway and any potential adverse effects on the breastfed infant from Vueway or from the underlying maternal condition. Data In lactating rats receiving single intravenous injection of [<sup>147</sup>Gd]-gadopiclenol, 0.3% and 0.2% of the total administered radioactivity was transferred to the pups via maternal milk at 6 hours and 24 hours after administration, respectively. Furthermore, in nursing rat pups, oral absorption of gadopicholol was 3.6%.

**Pediatric Use** The safety and effectiveness of Vueway for use with MRI to detect and visualize lesions with abnormal vascularity in the CNS (brain, spine, and associated tissues), and the body (head and neck, thorax, abdomen, pelvis, and musculoskeletal system) have been established in pediatric patients aged 2 years and older.

Use of Vueway in this age group is supported by evidence from adequate and well-controlled studies in adults with additional pharmacokinetic and safety data from an open-label, uncontrolled, multicenter, single dose study of Vueway (0.05 mmol/kg) in 80 pediatric patients aged 2 to 17 years. The 80 patients consisted of 60 patients who underwent a CNS MRI and 20 patients who underwent a body MRI [see Adverse Reactions (6.1) and Clinical Pharmacology (12.3) in the full Prescribing Information].

The safety and effectiveness of Vueway have not been established in pediatric patients younger than 2 years of age.

**Geriatric Use** Of the total number of Vueway-treated patients in clinical studies, 270 (26%) patients were 65 years of age and over, while 62 (6%) patients were 75 years of age and over. No overall differences in safety or efficacy were observed between these subjects and younger subjects.

This drug is known to be substantially excreted by the kidney, and the risk of adverse reactions to this drug may be greater in patients with impaired renal function. Because elderly patients are more likely to have decreased renal function, it may be useful to monitor renal function.

**Renal Impairment** In patients with renal impairment, the exposure of gadopicholol is increased compared to patients with normal renal function. This may increase the risk of adverse reactions such as nephrogenic systemic fibrosis (NSF). Avoid use of GBCAs among these patients unless the diagnostic information is essential and not available with non-contrast MRI or other modalities. No dose adjustment of Vueway is recommended for patients with renal impairment. Vueway can be removed from the body by hemodialysis [see Warnings and Precautions (5.1, 5.3, 5.4) and Clinical Pharmacology (12.3) in the full Prescribing Information].

## OVERDOSAGE

Among subjects who received a single 0.3 mmol/kg intravenous dose of gadopicholol (6 times the recommended dose of Vueway), headache and nausea were the most frequently reported adverse reactions. Gadopicholol can be removed from the body by hemodialysis [see Clinical Pharmacology (12.3) in the full Prescribing Information].

**PATIENT COUNSELING INFORMATION** Advise the patient to read the FDA-approved patient labeling (Medication Guide).

**Nephrogenic Systemic Fibrosis** Inform the patient that Vueway may increase the risk for NSF among patients with impaired elimination of the drugs and that NSF may result in fatal or debilitating fibrosis affecting the skin, muscle and internal organs.

Instruct the patients to contact their physician if they develop signs or symptoms of NSF following Vueway administration, such as burning, itching, swelling, scaling, hardening and tightening of the skin; red or dark patches on the skin; stiffness in joints with trouble moving, bending or straightening the arms, hands, legs or feet; pain in the hip bones or ribs; or muscle weakness [see Warnings and Precautions (5.1) in the full Prescribing Information].

**Gadolinium Retention** Advise patients that gadolinium is retained for months or years in brain, bone, skin, and other organs following Vueway administration even in patients with normal renal function. The clinical consequences of retention are unknown. Retention depends on multiple factors and is greater following administration of linear GBCAs than following administration of macrocyclic GBCAs [see Warnings and Precautions (5.3) in the full Prescribing Information].

**Injection Site Reactions** Inform the patient that Vueway may cause reactions along the venous injection site, such as mild and transient burning or pain or feeling of warmth or coldness at the injection site [see Warnings and Precautions (5.5) in the full Prescribing Information].

**Pregnancy** Advise pregnant women of the potential risk of fetal exposure to Vueway [see Use in Specific Populations (8.1) in the full Prescribing Information].

## Rx only

US Patent No. 10,973,934  
Manufactured for Bracco Diagnostics Inc. by Liebel-Flarsheim Company LLC - Raleigh, NC, USA 27616.  
Toll Free: 1-877-272-2269 (U.S. only)  
Revised November 2022

# JOIN US! COMPREHENSIVE NEURORADIOLOGY COURSE

**February 1-3, 2024 • Cancun, Mexico / On-Demand**

ASNR's Comprehensive Neuroradiology Course offers you three days of image-rich neuroradiology review focused on:

**Adult Brain Imaging | Head and Neck Imaging | Spine Imaging  
Pediatric Neuroradiology | Advanced Imaging Techniques**

Join our award-winning faculty and engage in our interactive classroom environment, as well as during planned social and evening activities. Take advantage of a discounted, all-inclusive rate at the host hotel: the Hyatt Ziva Cancun!

*Can't attend in person? An on-demand option is also available!*

**Get all of the details and register now at  
[www.asnr.org/cnc24](http://www.asnr.org/cnc24).**

## Meet the Faculty

### **Joshua Nickerson, MD, FACR**

Professor, Division Chief of Neuroradiology, Oregon Health & Science University

### **Tabassum Kennedy, MD**

Professor, Division Chief of Neuroradiology, University of Wisconsin, Madison

### **Judith Gadde, DO, MBA**

Associate Professor, Northwestern University Feinberg School of Medicine;  
Pediatric Radiology Rotation Site Director, Lurie Children's Hospital of Chicago

### **Mahmud Mossa-Basha, MD**

Professor of Radiology, Vice Chair of Clinical Research and Clinical Transformation,  
University of Washington School of Medicine

### **Wende Gibbs, MD, MA**

Associate Professor, Director of Spine Imaging and Intervention, Barrow  
Neurological Institute

### **Ashley Aiken, MD,**

Professor of Radiology and Imaging Sciences, Vice Chair of Faculty Advancement,  
Emory University



# AJNR *go green*

***AJNR* urges American Society of Neuroradiology members to reduce their environmental footprint by voluntarily suspending their print subscription.**

The savings in paper, printing, transportation, and postage directly fund new electronic enhancements and expanded content.

The digital edition of *AJNR* presents the print version in its entirety, along with extra features including:

- Publication Preview
- Case Collection
- Podcasts
- The *AJNR* News Digest
- The *AJNR* Blog

It also reaches subscribers much faster than print. An electronic table of contents will be sent directly to your mailbox to notify you as soon as it publishes.

Readers can search, reference, and bookmark current and archived content 24 hours a day on [www.ajnr.org](http://www.ajnr.org).

ASNR members who wish to opt out of print can do so by using the *AJNR* Go Green link on the *AJNR* Website (<http://www.ajnr.org/content/subscriber-help-and-services>). Just type your name in the email form to stop print and spare our ecosystem.



# The ASNR Career Center

**The Go-To Job Site for Neuroradiology Employers and Job Seekers**

***For Job Seekers***

- Access to an expanded network of jobs via the National Healthcare Career Network
- Confidential resume posting
- Professional online profile

***For Employers***

- Employer resources to help you recruit top talent
- Multiple pricing options, including free Fellowship listings
- Resume search

**Start here: [careers.asnr.org](https://careers.asnr.org)**

UNITED STATES POSTAL SERVICE<sup>®</sup>

Home

PS Form 3526 Statement of Ownership, Management, and Circulation (All Periodicals Publications Except Requester Publications)

U.S. POSTAL SERVICE PERIODICALS  
STATEMENT OF OWNERSHIP - FORM 3526

Statement of Ownership Letters

You may type your entries into the online form 3526 below or upload the form file template to auto-populate the form.

Click here to download this form file template

☐ Upload Statement of Ownership Form File

\*Please review the entries on this page and click Continue to review the next page before submitting.

1. Company Name/Publication Title  
AMERICAN SOCIETY OF NEURORADIOLOGY/AINR

2. Publication Number  
532630

3. Filing Date (mm/dd/yyyy)  
09/20/2023

4. Issue Frequency  
MONTHLY

5. No. Issues Published Annually (required)  
12

6. Annual Subscription Price  
\$75.00

7. Complete Mailing Address of Known Office of Publication (not printer)  
Address Line 1 820 JORIE BLVD STE 300  
Address Line 2  
City OAK BROOK County DU PAGE State IL ZIP+4 60053-2281  
Country (630) 574-1487

8. Complete Mailing Address of Headquarters or General Business Office of Publisher  
Address Line 1 820 JORIE BLVD STE 300  
Address Line 2  
City OAK BROOK State IL ZIP+4 60053-2251  
Country

9. Full Names and Complete Mailing Addresses of Publisher, Editor, and Managing Editor (Do not leave blank)

Full Name AMERICAN SOCIETY OF NEURORADIOLOGY  
Address Line 1 820 JORIE BLVD STE 300  
Address Line 2  
City OAK BROOK State IL ZIP+4 60053-2251  
Country

Full Name KAREN HALM  
Address Line 1 820 JORIE BLVD STE 300  
Address Line 2  
City OAK BROOK State IL ZIP+4 60053-2251  
Country

10. Owner (Do not leave blank. If the publication is owned by a corporation, give the name and address of the corporation immediately followed by the names and addresses of all stockholders owning or holding 1 percent of the total amount of stock. If not owned by a corporation, give the names and addresses of the individual owners. If owned by a partnership or other unincorporated firm, give its name and address as well as those of each owner. If the publication is published by a government organization, give its name and address.)

Full Name Complete Mailing Address  
AMERICAN SOCIETY OF NEURORADIOLOGY 820 JORIE BLVD STE 300, OAK BROOK, IL 60053-2281

☐ Upload Owner Address File

☐ List of owners is in the publication file at the original entry office.

11. Known Bondholders, Mortgagees, and Other Security Holders Owning or Holding 1 Percent or More of Total Amount of Bonds, Mortgages, or Other Securities. If none, check box:

Full Name Complete Mailing Address

Statement of Ownership Form 3526 Page 1 Next Step: Address Verification

[Feedback](#) [Logout](#)  
Copyright © 1999-2023 USPS. All Rights Reserved.

U.S. POSTAL SERVICE PERIODICALS  
STATEMENT OF OWNERSHIP - FORM 3526

Home

PS Form 3526 Statement of Ownership, Management, and Circulation (All Periodicals Publications Except Requester Publications)

Statement of Ownership Letters

13. Company Name/Publication Title  
AMERICAN SOCIETY OF NEURORADIOLOGY/AINR

14. Issue Date for Circulation Data Below (mm/dd/yyyy)  
09/11/2023

15. Extent and Nature of Circulation

15. Extent and Nature of Circulation		14. Issue Date for Circulation Data Below (mm/dd/yyyy)	
		Average No. Copies Each Issue During Preceding 12 Months	No. Copies of Single Issue Published Nearest to Filing Date
a. Total Number of Copies (net press run)		0	0
b. Paid Circulation (By Mail and Outside the Mail)		1240	1231
c. Total Paid Distribution (Sum of 15b (1), (2), (3), and (4))		0	0
d. Free or Nominal Rate Outside County Copies Included on PS Form 3541		129	128
e. Free or Nominal Rate In-County Copies Included on PS Form 3541		77	73
f. Total Free or Nominal Rate Distribution (Sum of 15d (1), (2), (3), and (4))		1446	1432
g. Copies not Distributed		31	28
h. Total (Sum of 15f and 15g)		1477	1460
i. Percent Paid (15c divided by 15f times 100)		139	135
j. If total circulation includes electronic copies, report that circulation on lines below		1616	1595
a. Paid Electronic Copies		97.90 %	98.08 %
b. Total Paid Print Copies (Line 15c) + Paid Electronic Copies		0.00 %	0.00 %
c. Total Print Distribution (Line 15f) + Paid Electronic Copies			
d. Percent Paid (Both Print & Electronic Copies)			

☐ I certify that 90% of all my distributed copies (Electronic & Print) are paid above a nominal price.

17. Publication of Statement of Ownership  
☒ If the publication is a general publication, publication of this statement is required. Will be printed in the 11/08/2023 issue of this publication. ☐ Publication not required.

18. Signature and Title of Editor, Publisher, Business Manager, or Owner  
Signature Karen Halm Title Managing Editor Date 09/20/2023

Reason for Amendment

☒ I certify that all information furnished on this form is true and complete. I understand that anyone who furnishes false or misleading information on this form or who omits material or information requested on the form may be subject to criminal sanctions (including fines and imprisonment) and/or civil sanctions (including civil penalties).

Previous Step: Page 1 Page 2 Next Step: Save Document

[Feedback](#) [Logout](#)  
Copyright © 1999-2023 USPS. All Rights Reserved.



## Simplify the MOC Process



## Manage your CME Credits Online

Available to Members of Participating Societies

American Board of Radiology (ABR)  
American College of Radiology (ACR)  
American Roentgen Ray Society (ARRS)  
American Society of Neuroradiology (ASNR)  
Commission on Accreditation of Medical Physics Educational Programs, Inc. (CAMPEP)

Radiological Society of North America (RSNA)  
Society of Interventional Radiology (SIR)  
SNM  
The Society for Pediatric Radiology (SPR)

## CMEgateway.org

### It's Easy and Free!

Log on to CME Gateway to:

- View or print reports of your CME credits from multiple societies from a single access point.
- Print an aggregated report or certificate from each participating organization.
- Link to SAMs and other tools to help with maintenance of certification.

### American Board of Radiology (ABR) participation!

By activating ABR in your organizational profile, your MOC-fulfilling CME and SAM credits can be transferred to your own personalized database on the ABR Web site.

### Sign Up Today!

go to CMEgateway.org

# THE FOUNDATION OF THE ASNR



## **Apply Now!** Foundation of the ASNR Grants 2024 Cycle Is Now Open

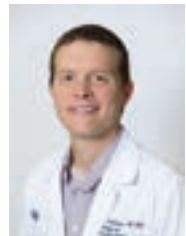
The Foundation of the ASNR's Grant Program is presented annually to support members of the ASNR who demonstrate great promise for future contributions to the field of neuroradiology.

*Visit [foundation.asnr.org](https://foundation.asnr.org) for all of the details and deadlines.*

## Research projects will now be funded at \$120,000 each!

### Foundation of the ASNR Grant Program 2022 Recipients Are Making an Impact

The primary goal of our study is to develop and evaluate a state-of-the-art automated pre- and postoperative glioblastoma volumetric segmentation algorithm at a high-volume brain tumor center. The significance of this study is that it will provide a new tool for automated, objective assessment of progression and/or treatment response in patients with glioblastoma. This grant has been instrumental in jumpstarting my research career as a junior academic neuroradiology faculty member. With this award I have been able to secure essential dedicated research time and personnel support to help achieve my early career research goals. All FASNRR donors should know that these awards make a difference and help build successful radiology research careers.



**Evan Calabrese,  
MD, PhD**  
*Duke University*

---

Paramagnetic rim lesions (PRLs) may serve as an imaging marker for the work up of multiple sclerosis (MS) progression and treatment. With the help of the ASNR foundation grant, we are working to establish a radiologic-histological correlation for PRLs. The study of PRLs and this research could clinically impact MS diagnosis and monitoring, may better determine the efficacy of existing therapeutic agents or stimulate development of new therapeutics, and overall may help reduce disability associated with disease progression. This work would not have been possible without the generous support of the Foundation.



**Emmanuel Obusez,  
MD**  
*Cleveland Clinic*





# The next generation GBCA from Guerbet is here

---



To learn more,  
scan QR code or visit  
[www.guerbet-us.com](http://www.guerbet-us.com)

# AJNR

## AMERICAN JOURNAL OF NEURORADIOLOGY

NOVEMBER 2023  
VOLUME 44  
NUMBER 11  
WWW.AJNR.ORG

Publication Preview at [www.ajnr.org](http://www.ajnr.org) features articles released in advance of print.  
Visit [www.ajnrblog.org](http://www.ajnrblog.org) to comment on AJNR content and chat with colleagues.

### EDITORIAL














- 1241 **A New Era Dawns at AJNR: Revamping the Editorial Board and Streamlining the Review Process** *Max Wintermark, MD*

### REVIEW ARTICLE

-  1242 **Ethical Considerations and Fairness in the Use of Artificial Intelligence for Neuroradiology** *C.G. Filippi, et al.*

ARTIFICIAL  
INTELLIGENCE

### GENERAL CONTENTS

-  1249 **Perfusion Collateral Index versus Hypoperfusion Intensity Ratio in Assessment of Collaterals in Patients with Acute Ischemic Stroke** *Brian Tsui, et al.*
-   1256 **DWI-Detected Ischemic Lesions after Endovascular Treatment for Cerebral Aneurysms: An Updated Systematic Review and Meta-analysis** *Abiel Berhe Habtezghi, et al.*
-  1262 **Mesoscopic Assessment of Microstructure in Glioblastomas and Metastases by Merging Advanced Diffusion Imaging with Immunohistopathology** *Urs Würtemberger, et al.*
-  1270 **Radiogenomics Provides Insights into Gliomas Demonstrating Single-Arm 1p or 19q Deletion** *Arian Lasocki, et al.*
-  1275 **Impact of Balloon Guide Catheters in Elderly Patients Treated with Mechanical Thrombectomy: Insights from the ROSSETTI Registry** *Mikel Terceño, et al.*
-   1282 **Considering Psychological and Cognitive Factors in Interventional Neuroradiology: A Systematic Literature Review** *Chiara Riccietti, et al.*
-   1291 **4D-DSA for Assessment of the Angioarchitecture and Grading of Cranial Dural AVF** *P.F. Samp, et al.*
-  1296 **Blunt Cerebrovascular Injury: Are We Overscreening Low-Mechanism Trauma?** *Kevin D. Hiatt, et al.*
-   1302 **Specificity of Quantitative Functional Brain Mapping with Arterial Spin-Labeling for Preoperative Assessment** *Giannina R. Iannotti, et al.*

NEUROVASCULAR/  
STROKE IMAGING

NEUROVASCULAR/  
STROKE IMAGING

BRAIN TUMOR  
IMAGING

BRAIN TUMOR  
IMAGING

NEUROINTERVENTION

NEUROINTERVENTION

NEUROINTERVENTION

EMERGENCY  
NEURORADIOLOGY

NEUROIMAGING  
PHYSICS/FUNCTIONAL  
NEUROIMAGING/  
CT AND MRI  
TECHNOLOGY

AJNR (Am J Neuroradiol ISSN 0195–6108) is a journal published monthly, owned and published by the American Society of Neuroradiology (ASNR), 820 Jorie Boulevard, Oak Brook, IL 60523. Annual dues for the ASNR include approximately 19% for a journal subscription. The journal is printed by Intellicor Communications, 330 Eden Road, Lancaster, PA 17601; Periodicals postage paid at Oak Brook, IL and additional mailing offices. Printed in the U.S.A. POSTMASTER: Please send address changes to American Journal of Neuroradiology, P.O. Box 3000, Denville, NJ 07834, U.S.A. Subscription rates: nonmember \$452 (\$530 foreign) print and online, \$320 online only; institutions \$520 (\$594 foreign) print and basic online, \$1029 (\$1103 foreign) print and extended online, \$380 online only (basic), \$825 online only (extended); single copies are \$35 each (\$40 foreign). Indexed by PubMed/MEDLINE, BIOSIS Previews, Current Contents (Clinical Medicine and Life Sciences), EMBASE, Google Scholar, HighWire Press, Q-Sensei, RefSeek, Science Citation Index, SCI Expanded, ReadCube, and Semantic Scholar. Copyright © American Society of Neuroradiology.



-  **1309** Prevalence of Cochlear-Facial and Other Non-Superior Semicircular Canal Third Window Dehiscence on High-Resolution Temporal Bone CT *Vladislav Razskazovskiy, et al.* **HEAD AND NECK IMAGING**
-  **1314** MR Imaging Appearance of Ruptured Rathke Cleft Cyst and Associated Bone Marrow Enhancement *Ian T. Mark, et al.* **HEAD AND NECK IMAGING**
-  **1318** The Influence of Non-aerated Paranasal Sinuses on DTI Parameters of the Brain in 6- to 9-Year-Old Children *Marjolein H.G. Dremmen, et al.* **PEDIATRIC NEUROIMAGING**
- 1325** Fetal MR Imaging Anatomy of the Transverse Temporal Gyrus (Heschl Gyrus) *Eleonora Piccirilli, et al.* **PEDIATRIC NEUROIMAGING**
-  **1332** Factors Predictive of Treatment Success in CT-Guided Fibrin Occlusion of CSF-Venous Fistulas: A Multicenter Retrospective Cross-Sectional Study *Andrew L. Callen, et al.* **SPINE IMAGING AND SPINE IMAGE-GUIDED INTERVENTIONS**
- 1339** Likelihood of Discovering a CSF Leak Based on Intracranial MRI Findings in Patients without a Spinal Longitudinal Extradural Collection: A New Probabilistic Scoring System *John C. Benson, et al.* **SPINE IMAGING AND SPINE IMAGE-GUIDED INTERVENTIONS**
-  **1345** Clinical Outcomes and Safety Comparison of Vertebroplasty, Balloon Kyphoplasty, and Vertebral Implant for Treatment of Vertebral Compression Fractures *Taibo Li, et al.* **SPINE IMAGING AND SPINE IMAGE-GUIDED INTERVENTIONS**
-  **1352** A Novel Patient-Positioning Device for Dynamic CT Myelography *Andrew L. Callen, et al.* **SPINE IMAGING AND SPINE IMAGE-GUIDED INTERVENTIONS**

### ONLINE FEATURES MEMORIAL

- E42** Professor Antonios (Anton) Valavanis, MD *Thierry A.G.M. Huisman, et al.*

### LETTER

- E45** Medicare Coverage of Amyloid PET: Implications for Clinical Practice *J. Ivanidze, et al.*

### BOOK REVIEWS *R.M. Quencer, Section Editor*

Please visit [www.ajnrblog.org](http://www.ajnrblog.org) to read and comment on Book Reviews.



Giannina, et al, performed dual-echo pseudocontinuous ASL and BOLD imaging to assess the performance of functional ASL for the delineation of the functional cortex during motor and somatosensory tasks in a cohort of healthy subjects.



Indicates Editor's Choices selection



Indicates Fellows' Journal Club selection



Indicates open access to non-subscribers at [www.ajnr.org](http://www.ajnr.org)



Indicates article with supplemental online data



Indicates article with supplemental online video



Evidence-Based Medicine Level 1



Evidence-Based Medicine Level 2

### EDITOR-IN-CHIEF

#### Max Wintermark, MD, MAS, FASFN, FICIS

*Frank T. McGraw Memorial Chair in the Study of Cancer  
Professor and Chair of Neuroradiology  
The University of Texas MD Anderson Center*

### DEPUTY EDITOR

#### Lubdha M. Shah, MD, MS

Professor of Radiology and Director of Spine Imaging  
Department of Radiology and Imaging Sciences  
University of Utah

### SPECIAL ADVISORS TO THE EDITOR-IN-CHIEF

#### Mauricio Castillo, MD, FACR

MA Mauro Distinguished Professor of Radiology  
University of North Carolina-Chapel Hill

#### Robert Quencer, MD

Professor Emeritus  
Department of Radiology  
University of Miami

### ARTIFICIAL INTELLIGENCE

#### Senior Editor

#### Reza Forghani, MD, PhD

Professor of Radiology & Artificial Intelligence  
Vice Chair of AI  
Director, Radiomics & Augmented Intelligence Laboratory (RAIL)  
Department of Radiology  
University of Florida College of Medicine

### Associate Editors

#### Andreas Rauschecker, MD, PhD

Assistant Professor-in-Residence  
Co-Executive Director and Clinical Director,  
Center for Intelligent Imaging (ci<sup>2</sup>)  
Department of Radiology & Biomedical Imaging  
University of California, San Francisco

#### Sam (Seyedmehdi) Payabvash, MD

Assistant Professor of Radiology  
Yale School of Medicine  
Connecticut

### BRAIN TUMOR IMAGING

#### Senior Editor

#### Ben Ellingson, MD

Professor and Director of MRI Research  
Director, UCLA Brain Tumor Imaging Laboratory  
Department of Radiological Sciences  
David Geffen School of Medicine  
University of California, Los Angeles

### Associate Editors

#### Ali Nabavizadeh, MD

Assistant Professor of Radiology  
Division of Neuroradiology  
University of Pennsylvania

#### Mark S. Shiroishi, MD, MS, FASFN

Assistant Professor, Division of Neuroradiology,  
Department of Radiology  
Director of Neuro-Oncology Imaging - USC Brain Tumor Center  
Chief of Pediatric Neuroradiology - Los Angeles General Medical Center  
Affiliated Faculty - USC Imaging Genetics Center  
Mark and Mary Stevens Neuroimaging and Informatics Institute  
Keck School of Medicine of USC  
University of Southern California

### EMERGENCY NEURORADIOLOGY

#### Senior Editor

#### Karen Buch, MD

Assistant Professor of Radiology  
Massachusetts General Hospital

### Associate Editors

#### Melissa A. Davis, MD, MBA

Vice Chair of Medical Informatics  
Associate Professor  
Department of Radiology and Biomedical Imaging  
Yale School of Medicine  
Connecticut

#### Jason Talbott, MD, PhD

Associate Professor, Neuroradiology Section  
Department of Radiology and Biomedical Imaging  
University of California, San Francisco and  
Zuckerberg San Francisco General Hospital

### HEAD AND NECK IMAGING

#### Senior Editor

#### Amy Juliano, MD

Associate Professor of Radiology  
Massachusetts Eye and Ear  
Harvard Medical School

### Associate Editors

#### Burce Ozgen, MD

Clinical Professor of Radiology  
University of Illinois at Chicago

#### David Zander, MD

Assistant Professor, Radiology  
University of Colorado School of Medicine

### HEALTH POLICIES/QUALITY IMPROVEMENT/ EVIDENCE-BASED NEUROIMAGING

#### Senior Editor

#### Nadja Kadom, MD, FACR, FAAP

Professor, Department of Radiology and Imaging Sciences  
Emory University School of Medicine  
Pediatric Neuroradiologist, Department of Radiology  
Children's Healthcare of Atlanta

### Associate Editors

#### Melissa M. Chen, MD

Associate Professor,  
Department of Neuroradiology, Division of Diagnostic Imaging  
The University of Texas MD Anderson Center

#### Ajay Malhotra, MBBS, MD, MMM

Professor of Radiology and Biomedical Imaging and Neurosurgery  
Yale School of Medicine  
Connecticut

### MOLECULAR NEUROIMAGING/NUCLEAR MEDICINE

#### Senior Editor

#### Ana M. Franceschi, MD, PhD

Associate Professor of Radiology  
Donald and Barbara Zucker School of Medicine at Hofstra/Northwell  
The Feinstein Institutes for Medical Research  
Neuro-PET Imaging  
Lenox Hill Hospital  
New York

### Associate Editors

#### Nadya Pyatigorskaya, MD, PhD

Neuroradiology Department, Pitié-Salpêtrière Hospital  
Researcher, Brain Institute (ICM)  
France

#### Marc Daniel Benayoun, PhD, MD

Assistant Professor of Radiology  
Co-Section Head of Nuclear Medicine  
Medical Director of Nuclear Medicine and PET  
Vice Chair of Radiation Drug Research Committee  
Atrium Wake Forest Health  
North Carolina

### NEURODEGENERATIVE DISORDER IMAGING

#### Senior Editor

#### Gloria Chiang, MD

Associate Professor, Co-Director of the Brain Health Imaging Institute  
Department of Radiology  
Weill Cornell Medicine/NewYork-Presbyterian Hospital

### Associate Editors

#### Fang Frank Yu, MD

Assistant Professor of Radiology  
Division of Neuroradiology, Department of Radiology  
Advanced Imaging Research Center  
University of Texas Southwestern Medical Center



**Priya Rajagopalan, MD**

Assistant Professor of Radiology, Division of Neuroradiology  
Associate Program Director, Neuroradiology Fellowship  
Medical Director, Center for Image Acquisition Mark and Mary Stevens Neuroimaging and Informatics Institute  
Keck School of Medicine, University of Southern California

**NEUROIMAGING PHYSICS/FUNCTIONAL NEUROIMAGING/CT AND MRI TECHNOLOGY****Senior Editor****Hongyu An, DSc**

Professor, Mallinckrodt Institute of Radiology Neurology, Biomedical Engineering, Electrical and Systems Engineering, Division of Biology and Biomedical Sciences  
Director, Biomedical Magnetic Resonance Center  
Associate Director, Center for Clinical Imaging Research  
Washington University in St. Louis

**Associate Editors****Timothy J. Carroll, PhD**

Professor, Department of Radiology  
University of Chicago

**Hugo de Jong, PhD**

Professor of Medical Physics Radiology and Nuclear Medicine  
UMC Utrecht  
the Netherlands

**NEUROINTERVENTION****Senior Editor****Steven Hetts, MD, FACR**

Co-Chief, NeuroEndovascular Surgery Service Line  
Chief of Interventional Neuroradiology, Mission Bay Hospitals  
Professor of Radiology, Biomedical Imaging, and Neurological Surgery  
University of California, San Francisco

**Associate Editors****Kristine Blackham, MD**

Associate Professor  
Diagnostic and Interventional Neuroradiology  
Clinic for Radiology and Nuclear Medicine  
University Hospital of Basel

**Maksim Shapiro, MD**

Clinical Associate Professor  
Departments of Radiology, Neurosurgery, and Neurology  
Division of Neurointerventional Radiology  
NYU Langone Health and Bellevue NYCH + Hospitals  
New York

**NEUROPSYCHIATRIC IMAGING****Senior Editor****Jody Tanabe, MD**

Professor  
Chief of Neuroradiology  
University of Colorado-Anschutz Medical Campus

**Associate Editors****John-Paul J. Yu, MD, PhD**

Assistant Professor of Radiology, Psychiatry, and Biomedical Engineering  
University of Wisconsin School of Medicine and Public Health

**J. Eric Schmitt, MD, PhD**

Assistant Professor of Radiology and Psychiatry  
Division of Neuroradiology  
Perelman School of Medicine, University of Pennsylvania

**NEUROVASCULAR/STROKE IMAGING****Senior Editor****Ajay Gupta, MD, MS**

Alexander R. Margulis, MD, Distinguished Professor in Radiology  
Weill Cornell Medical College  
New York

**Associate Editors****Shalini Amukotuwa, MB BS, PhD, FRANZCR**

Head of Neuroradiology and Director of MRI, Monash Health  
Associate Professor of Radiology, Monash University  
Australia

**Mahmud Mossa-Basha, MD**

Professor of Radiology, Neurology and Electrical Engineering  
Vice Chair of Clinical Research and Clinical Transformation  
Co-Director of the Research Vascular Imaging Lab  
University of Washington School of Medicine

**PEDIATRIC NEUROIMAGING****Senior Editor****Caroline D. Robson, MBChB**

Division Chief & Endowed Chair, Neuroradiology  
Director, Head & Neck Imaging  
Department of Radiology  
Department of Otolaryngology  
Boston Children's Hospital  
Harvard Medical School

**Associate Editors****Anna Trofimova, MD, PhD**

Assistant Professor, Radiology and Imaging Sciences, Emory University  
Pediatric Neuroradiologist, Children's Healthcare of Atlanta

**Matthew Whitehead, MD**

Department of Radiology, Division of Neuroradiology  
Children's Hospital of Philadelphia  
Associate Professor of Radiology  
Perelman School of Medicine, University of Pennsylvania

**SPINE IMAGING AND SPINE IMAGE-GUIDED INTERVENTIONS****Senior Editor****J. Levi Chazen, MD**

Associate Professor, Neuroradiology  
Director, Spine Imaging  
Hospital for Special Surgery  
Weill Cornell Medicine  
New York

**Associate Editors****Jennifer McCarty, MD**

UTHealth Houston

**Vinil Shah, MD**

Associate Professor of Radiology Neuroradiology  
Division Chief  
University of California, San Francisco

**ULTRA-HIGH-FIELD MRI/IMAGING OF EPILEPSY/DEMYELINATING DISEASES/INFLAMMATION/INFECTION****Senior Editor****Erik Middlebrooks, MD**

Professor of Radiology  
Mayo Clinic Florida

**Associate Editors****Susie Y. Huang, MD, PhD**

Associate Professor of Radiology, Harvard Medical School  
Associate Chair, Faculty Affairs, Department of Radiology  
Director of Translational Neuro MR Imaging & Connectomics, Athinoula A. Martinos Center for Biomedical Imaging  
Massachusetts General Hospital

**Girish Bathla, MD, FRCR**

Associate Professor, Neuroradiology  
Mayo Clinic  
Minnesota

**OUTREACH AND EDUCATION****Senior Editor****Lea Alhilali, MD**

Radiology Partners, HonorHealth Research Institute  
Arizona

**DIGITAL MEDIA AND ENGAGEMENT****Senior Editor****Kevin Hsu, MD**

Clinical Assistant Professor  
Department of Radiology  
NYU Grossman School of Medicine  
New York

**Case Collection Editors****Matylda Machnowska, BMedSc, MD, FRCSC, ABR**

Assistant Professor of Radiology, University of Toronto  
Neuroradiologist, Sunnybrook Health Sciences Centre

**Anvita Pauranik, MD**

Clinical Assistant Professor of Radiology  
BC Children's Hospital  
University of British Columbia

**Sandy Cheng-Yu Chen, MD**

Chair, Translational Imaging Research Center  
Taipei Medical University Hospital  
Vice President of Taipei Medical University

**Podcast Editor****Kevin Hiatt, MD**

Assistant Professor, Radiology  
Wake Forest University School of Medicine  
North Carolina

**STATISTICS****Senior Editor****Bryan A. Comstock, MS**

Senior Biostatistician, Department of Biostatistics  
University of Washington

## **EDITORIAL FELLOWS**

### **Alexandre Boutet, MD, PhD**

Neuroradiologist  
Joint Department of Medical Imaging  
University of Toronto

### **Nicholas S. Cho, MD/PhD Candidate**

University of California, Los Angeles  
**Burak Berksu Ozkara, MD**  
Research Fellow  
Department of Neuroradiology  
The University of Texas MD Anderson Center

## **BOOK REVIEW EDITOR**

### **Robert Quencer, MD**

Professor Emeritus  
Department of Radiology  
University of Miami

---

*Founding Editor*  
**Juan M. Taveras**

*Editors Emeriti*  
Mauricio Castillo, Robert I. Grossman,  
Michael S. Huckman, Robert M. Quencer,  
Jeffrey S. Ross

---

*Managing Editor*  
**Karen Halm**

*Assistant Managing Editor*  
**Laura Wilhelm**  
*Executive Director, ASNR*  
**Mary Beth Hepp**

## A New Era Dawns at *AJNR*: Revamping the Editorial Board and Streamlining the Review Process

Max Wintermark, MD

Editor-in-Chief, *American Journal of Neuroradiology*

**A**t *AJNR*, we have a long tradition of continuously striving to improve the quality of our journal. In the months to come, based on the feedback of previous Chief and Deputy Editors, Editorial Board members, reviewers, and authors, the *AJNR* will see a series of transformative initiatives that will enhance the quality, speed, and diversity of the content it delivers to its readers. Today, after extensive consultations and advice, I am excited to share with all of you the first of these improvements, and I wish to express my gratitude to those who have been instrumental in bringing them to fruition.

First and foremost, I would like to extend our heartfelt thanks to Dr Jeff Ross and to the Senior Editors who dedicated their time, knowledge, and expertise to *AJNR* over the past years: Dr Harry Cloft, Dr Risto Filippi, Dr Thierry Huisman, Dr Nancy Fischbein, Dr Yvonne Lui, and Dr Doug Phillips, as well as Deputy Editor for AI, Dr Peter Chang. Their invaluable contributions helped shape the journal into what it is today. As these friends and colleagues step down, we recognize the lasting impact they have had on the journal and on our field. Dr Lubdha Shah will remain on board as the Deputy Editor. Bryan Comstock will remain our Senior Statistical Editor.

I also wish to thank the current members of the Editorial Board and the current reviewers for *AJNR* for their outstanding service, and we hope that they will continue to serve as reviewers for the Journal.

The new Editorial Board will ensure that the *AJNR* remains at the forefront of emerging trends and advances in neuroradiology. The new structure of the Editorial Board is expanded to encompass a broader range of expertise, with *14 teams each focusing on one specific area of neuroradiology*:

- Emergency Neuroradiology
- Neurovascular/Stroke Imaging
- Neurodegenerative Disorder Imaging
- Ultra-High-Field MRI/Imaging of Epilepsy/Demyelinating Diseases/Inflammation/Infection
- Brain Tumor Imaging

- Neuropsychiatric Imaging
- Pediatric Neuroimaging
- Head and Neck Imaging
- Spine Imaging and Spine Image-Guided Interventions
- Neurointervention
- Neuroimaging Physics/Functional Neuroimaging/CT and MRI Technology
- Molecular Neuroimaging/Nuclear Medicine
- Health Policies/Quality Improvement/Evidence-Based Neuroimaging
- Artificial Intelligence

The new Editorial Board reflects my commitment to diversity and inclusivity. I recognize that our field is rich with talent from across the globe, and I am proud to welcome editors with diverse perspectives and experiences to *AJNR*. This diversity will enrich the content of the Journal, making it more relevant to a global readership.

Along with a new Editorial Board will come a new review process that will leverage the expanded expertise of the new Editorial Board. The new review process is explained on our Web site (<https://www.ajnr.org/content/ajnr-academy-reviewers>). The goal of this new review process is to reduce the time from submission to editorial decision to *less than 3 weeks*. We understand the importance of timely dissemination of research findings and are committed to achieving this ambitious timeline.

To ensure a continuous flow of fresh ideas and expertise, we will limit the terms for Senior and Associate Editors (2 years, with a potential extension of 1 year). This approach will result in a regular rotation of editors, allowing us to tap into a wide pool of talent, as well as keeping the content of the Journal vibrant and up to date.

I invite individuals with expertise in neuroradiology to join our community of reviewers. I welcome anyone with relevant knowledge to participate and review a small number of articles (3–4 articles) each year, provided you can complete these reviews within 2 weeks of receiving them. This commitment to rapid reviews is instrumental in achieving our goal of expediting the editorial process and timely publishing.

Our readers need to trust that the *AJNR* is embracing change and innovation to better serve the neuroradiology community. Our revamped Editorial Board, commitment to diversity and international perspectives, and dedication to faster reviews are all aimed at elevating the quality, dissemination, and access of the Journal. We look forward to the exciting journey ahead, and we invite all neuroradiology enthusiasts to join us in this endeavor. Together, we will continue to push the boundaries of knowledge in our field.

# Ethical Considerations and Fairness in the Use of Artificial Intelligence for Neuroradiology

C.G. Filippi, J.M. Stein, Z. Wang, S. Bakas, Y. Liu, P.D. Chang, Y. Lui, C. Hess, D.P. Barboriak, A.E. Flanders, M. Wintermark, G. Zaharchuk, and O. Wu



## ABSTRACT

**SUMMARY:** In this review, concepts of algorithmic bias and fairness are defined qualitatively and mathematically. Illustrative examples are given of what can go wrong when unintended bias or unfairness in algorithmic development occurs. The importance of explainability, accountability, and transparency with respect to artificial intelligence algorithm development and clinical deployment is discussed. These are grounded in the concept of “primum no nocere” (first, do no harm). Steps to mitigate unfairness and bias in task definition, data collection, model definition, training, testing, deployment, and feedback are provided. Discussions on the implementation of fairness criteria that maximize benefit and minimize unfairness and harm to neuroradiology patients will be provided, including suggestions for neuroradiologists to consider as artificial intelligence algorithms gain acceptance into neuroradiology practice and become incorporated into routine clinical workflow.

**ABBREVIATION:** AI = artificial intelligence

Artificial intelligence (AI) is beginning to transform the practice of radiology, from order entry through image acquisition and reconstruction, workflow management, diagnosis, and treatment decisions. AI will certainly change neuroradiology practice across routine workflow, education, and research. Neuroradiologists are understandably concerned about how AI will affect their subspecialty and how they can shape its development. Multiple published consensus statements advocate the need for radiologists to play a primary role in ensuring that AI software used for clinical care is fair to and unbiased against specific groups of patients.<sup>1</sup> In this review, we focus on the need for developing and implementing

fairness criteria and how to balance competing interests that minimize harm and maximize patient benefits when implementing AI solutions in neuroradiology. The responsibility for promoting health care equity rests with the entire neuroradiology community, from academic leaders to private practitioners. We all have a stake in establishing best practices as AI enters routine clinical practice.

## Definitions

“Ethics,” in a strict dictionary definition, is a theory or system of values that governs the conduct of individuals and groups.<sup>2</sup> Ethical physicians should endeavor to promote fairness and avoid bias in their personal treatment of patients and with respect to the health care system at large. A biased object yields 1 outcome more frequently than statistically expected, eg, a 2-headed coin. Similarly, a biased algorithm systematically produces outcomes that are not statistically expected. One proposed definition for algorithmic bias in health care systems is “when the application of an algorithm compounds existing inequities in socioeconomic status, race, ethnic background, religion, sex, disability, or sexual orientation to amplify them and adversely impact inequities in health systems.”<sup>3</sup> This definition, while not ideal, is a request for developers and end users of AI algorithms in health care to be aware of the potential risk of poorly designed algorithms for not merely reflecting societal imbalances but also amplifying inequities.

“Fairness” can be defined as the absence of favoritism toward specific subgroups of populations.<sup>4</sup> Individual fairness is the principle that any 2 individuals who are similar should be treated equally.<sup>5</sup> In contrast, “group fairness,” ie, statistical or demographic

Received January 30, 2023; accepted after revision July 7.

From the Department of Radiology (C.G.F.), Tufts University School of Medicine, Boston, Massachusetts; Department of Radiology (J.M.S., S.B.), University of Pennsylvania, Philadelphia, Pennsylvania; Athinoula A. Martinos Center for Biomedical Imaging (Z.W., Y. Liu, O.W.), Department of Radiology, Massachusetts General Hospital, Boston, Massachusetts; Department of Radiological Sciences (P.D.C.), University of California, Irvine, California; Department of Neuroradiology (Y. Lui), NYU Langone Health, New York, New York; Department of Radiology and Biomedical Imaging (C.H.), University of California, San Francisco, San Francisco, California; Department of Radiology (D.P.B.), Duke University School of Medicine, Durham, North Carolina; Department of Neuroradiology/Otolaryngology (ENT) Radiology (A.E.F.), Thomas Jefferson University, Philadelphia, Pennsylvania; Department of Neuroradiology (M.W.), Division of Diagnostic Imaging, MD Anderson Cancer Center, Houston, Texas; and Department of Radiology (G.Z.), Stanford University, Stanford, California.

Please address correspondence to Christopher G. Filippi, MD, Tufts University School of Medicine, Department of Radiology, 800 Washington St, Box 299, Boston, MA 02111; e-mail: cfilippi@tuftsmedicalcenter.org; @sairaallapeikko

Indicates open access to non-subscribers at [www.ajnr.org](http://www.ajnr.org)

Indicates article with online supplemental data.

<http://dx.doi.org/10.3174/ajnr.A7963>



parity, is the principle that the demographics of the group receiving positive or negative treatment are the same as the population as a whole.<sup>5</sup> Considering harm caused by algorithmic bias, ie, allocational (denial of opportunities or resources<sup>6</sup>) or representational (reinforcement of negative stereotypes<sup>7</sup>) harm, may be more intuitive.

### Algorithmic Bias

We can quantify bias ( $\delta$ ) for AI models  $f(x)$  with regard to bias features,  $z$ , as

$$\delta = \hat{M}(f(x), f(x, z)),$$

for which  $\hat{M}$  is a distance metric that measures the difference between  $f(x)$  and  $f(x, z)$ . The formula intuitively corresponds to the dictionary definition of “bias” of AI models by measuring how much the model outcomes  $f(x, z)$  deviate from expected  $f(x)$ . Bias features  $z$  can be explicit (eg, sex, race, age, and so forth) or implicit (eg, data set imbalance, model architectures, poorly chosen learning metrics).<sup>8</sup>

### Algorithmic Fairness

Scientists and companies involved in designing and implementing AI solutions across various industries have recognized the importance of fairness and social responsibility in the software they create, embodied in the concept of fairness, accountability, transparency, and ethics in AI.<sup>9</sup> For commercial algorithms, there are regulatory considerations. For example, the Federal Trade Commission is empowered to prohibit “unfair or deceptive acts or practices in or affecting commerce,” which include racially biased algorithms.<sup>10</sup> A bill introduced in Congress (the Algorithmic Accountability Act) would go further by directing the Federal Trade Commission to require impact assessment around privacy, security, bias, and fairness from companies developing automated decision-making systems.<sup>11</sup>

Multiple ways to measure algorithmic fairness have been developed.<sup>12–15</sup> Corbett-Davies and Goel<sup>14</sup> proposed 3 definitions for algorithmic fairness: 1) anticlassification for which protected features (eg, sex, race) are explicitly excluded from the model, 2) classification parity for which model performance is equal across groups organized by protected features, and 3) calibration for which model outcomes are independent of protected attributes. However, the impossibility theorem shows that it is not possible to simultaneously equalize false-positive rates, false-negative rates, and positive predictive values across protected classes while maintaining calibration or anticlassification fairness.<sup>12</sup> If only 1 fairness criterion can be achieved, clinical and ethical reasoning will be required to determine which one is appropriate.<sup>16</sup>

Techniques have been developed to explain poor fairness scores in AI algorithms. One approach applied the decomposition method of “additive features”<sup>17</sup> to quantitative fairness metrics<sup>14,15</sup> (eg, statistical parity).<sup>18</sup> By means of simulation data for features which were purposefully manipulated to result in poor statistical parity, this method identified features that were most responsible for fairness disparities in the outputs of AI algorithms.

### AI Algorithms: What Could Possibly Go Wrong?

Prominent examples from outside of medicine can be instructive in understanding how particular problems in AI processes, namely lack of representative data sets and inadequate validation, may lead to unfair outcomes with the potential for serious consequences. A sparsity of training data from geographically diverse sources can lead to both representational harm (through bias amplification)<sup>19</sup> and allocational harm (from algorithms working less accurately).<sup>20,21</sup> A study of facial-recognition programs reported that while all software correctly identified white males (<1% error rate), the failure rate for women of color ranged from 21% to 35%.<sup>22</sup> A ProPublica<sup>23</sup> investigation of an AI algorithm that assessed the risk of recidivism showed that white defendants who re-offended were incorrectly classified as low risk almost twice as often as black offenders. In contrast, black defendants who did not re-offend were almost twice as likely as white defendants to be misclassified as at high risk of violent recidivism. These AI algorithms were inadvertently used to perpetuate institutional racism.<sup>24</sup> There are many theoretical reasons for the poor performance, with nonrepresentative training data being the most likely important factor.

### Primum No Nocere

Embedded in the Hippocratic Oath for physicians is the concept of “primum no nocere” (first, do no harm), which applies to technological advances in medicine, including neuroradiology and AI implementation. AI models deployed in health care can lead to unintended unfair patient outcomes and can exacerbate underlying inequity. Not surprising, given massive interest in applying AI to medical imaging, examples of bias specific to neuroradiology are emerging. In a study that analyzed >80 articles that used AI on head CT examinations, >80% of data sets were found to be from single-center sources, which increases the susceptibility of the models to bias and increases model error rates.<sup>25</sup> The prevalence of brain lesions in the training and testing data sets did not match real world prevalence, which will likely overinflate the performances of models.<sup>25</sup> In a meta-analysis of AI articles on intracranial aneurysm detection, the authors concluded that most studies had a high risk of bias with poor generalizability, with only one-quarter of studies using an appropriate reference standard and only 6/43 studies using an external or hold-out test set.<sup>26</sup> They found low-level evidence for using these AI algorithms and that none of the studies specifically tested for the possibility of bias in algorithm development.<sup>26</sup> In a study that used AI models to detect both intracranial hemorrhage and large-vessel occlusion, the algorithm showed similar excellent performance in diverse populations regardless of scanning parameters and geographic distribution, suggesting that it is unbiased.<sup>27</sup> This study did not use independent data sets to test that assertion formally.<sup>27</sup>

In the neuroradiology literature, there are currently few studies assessing how bias may affect AI algorithms developed for routine clinical use. In 1 study, training cohort bias in <sup>15</sup>O-Water PET CBF calculation was evaluated.<sup>28</sup> The study showed that predictions in patients with cerebrovascular disease were poorer if only healthy controls were used for training models. However, predictions for healthy controls were unaffected if the models were trained only on patient data.<sup>28</sup> Training with data including healthy controls and patients with cerebrovascular disease yielded

the best performance.<sup>28</sup> From these neuroradiology examples, incorporating diverse patient characteristics that reflect target patient populations in the training and validation sets may be a reasonable strategy for mitigating bias.

In health care, there are many potential sources of bias such as age, sex, ethnicity, cultural, geographic, environmental, and socioeconomic status along with additional confounders such as disease prevalence and comorbidities.<sup>1</sup> It is easy to imagine that physical characteristics present in neuroradiology images could affect algorithm performance if not sufficiently represented in training sets. Inadequate sampling or matching disease prevalence could impact performance for different populations. Population-based studies could have inadequate inclusion of diverse data. In neuroradiology, additional sources of bias include heterogeneity of scanners, scanner parameters, acquisition protocols, and postprocessing algorithms.

Other ethical issues in AI use center on clinical deployment. Will the use of algorithms be equitable across hospital systems, or will only large, urban academic hospitals have access to state-of-the-art tools? Other considerations include whether the AI model will perform robustly across time. Medicine, health care practices, and devices are constantly evolving. Models need to be periodically

validated on diverse populations and calibrated with data reflecting current clinical practices if they are expected to remain clinically relevant.<sup>29</sup> In medicine, interesting case studies that defy common medical knowledge can improve our understanding of disease and lead to practice changes. One such example is that of a patient who defied the odds of a severe motor vehicle crash to achieve complete recovery.<sup>30</sup> How to incorporate these outlier cases into AI algorithms is unclear. Overall, effective, fair, and ethical applications of AI to neuroradiology problems will require balancing competing demands across multiple domains (Online Supplemental Data).

### Mitigating Bias and Unfairness

Sources of bias in medical AI have been previously described.<sup>16</sup> In brief, there may be biases in the training data set construction, model training, clinician/patient interaction, and model deployment. It is incumbent on all stakeholders to do their part in mitigating bias and unfairness in the development, deployment, and use of AI models in neuroradiology.

### Integration of Fairness, Accountability, Transparency, and Ethics Principles in the AI Cycle

Fairness, accountability, transparency, and ethics principles should be integrated<sup>11,31,32</sup> into the AI development lifecycle (Fig 1, adapted from Cramer et al<sup>31</sup> and the Online Supplemental Data). Diverse stakeholder involvement is critical for all stages. For task definition, one should clearly define the intended long-term effects of the task and model. One should define processes for discovering unintended biases at this stage. This outcome can be achieved by defining fairness requirements.

Data collection that is ethical and transparent and allows sufficient representation of protected groups should be ensured. One should check for biases in data sources. Many neuroradiologic AI applications require labeled data, eg, subarachnoid hemorrhage versus subdural hemorrhage. How and by whom are labels generated? Does it match the expected clinical deployment context? One should check for biases in how data are collected, which could lead to underrepresentation of underserved populations. Data collection should preserve privacy. For example, the collection of high-resolution images enables reconstruction of faces that can potentially be cross-linked to the patient's real identity through face-recognition software<sup>33</sup> as demonstrated in a reconstruction of data from an anthropomorphic phantom (Fig 2).<sup>34</sup>

In a PET study for which CT and MR imaging data were collected for standard uptake value quantification, researchers showed that face-recognition software could match facial reconstructions from CT and MR imaging data to their actual face photographs with correct match rates ranging from 78% (CT) to 97%–98% (MR imaging), leading the researchers to advocate for the routine use of de-identification software.<sup>35</sup> When one uses de-identification software, the rates of recognition plummet to 5% for CT and 8% for MR



**FIG 1.** The AI algorithm development lifecycle.

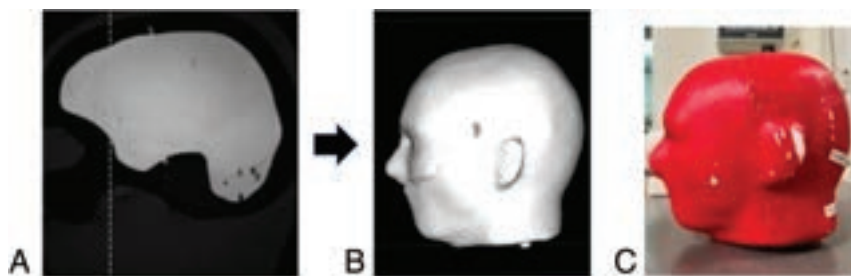


**FIG 2.** A 3D T1-weighted MR imaging scan (A) of an anthropomorphic phantom (B), which has no patient-identifying information. A 3D-rendered lifelike reconstruction (C) is possible, comparable with the original (photograph courtesy of Jacob C. Calkins, MGH Athinoula A. Martinos Center for Biomedical Imaging). The reconstruction was performed using open source software (Horos Version 3.3.6; Horos Project).

imaging, without impacting standard uptake value quantification.<sup>35</sup> A recent report used a novel de-identification software that deliberately distorted the ears, nose, and eyes that prevented facial recognition from CT and MR images,<sup>36</sup> which may be a viable solution for this privacy concern.

To address patient privacy concerns, many AI applications use synthetic data for training.<sup>37</sup> These synthetic data sets are typically produced using generative algorithms<sup>38</sup> and have the potential for promoting data-sharing (being unrestricted by regulatory agencies) and for the creation of diverse data sets.<sup>37</sup> However, the use of synthetic data can lead to nonrealistic scenarios<sup>39</sup> or inadvertently reinforce biases.<sup>40,41</sup>

For the model definition stage, model assumptions must be clearly defined, and potential biases, identified. Model architecture must be checked for introduction of biases and whether the cost function has unintended adverse effects.<sup>42</sup>

For the training stage, there are several online free resources to detect and mitigate bias<sup>43</sup> based on statistical definitions of fairness. Fairlearn<sup>44</sup> and AI Fairness 360<sup>45</sup> provide tools to detect and mitigate unfairness. Machine learning–Fairness–Gym takes a slightly different approach using simulation to evaluate the long-term fairness effects of learning agents in a specified environment.<sup>46</sup> The What-If Tool lets one visualize trained models to detect bias with minimal coding.<sup>47</sup> In addition, embedding learning methods that can debias AI models may help mitigate unfairness.<sup>8</sup> For example, Amini et al<sup>8</sup> proposed incorporating learning latent space structures for reweighting data during training to produce a less biased classifier.

For the testing stage, one should ensure that testing data have not leaked into the training data, match the expected deployed clinical context, and sufficiently represent the expected patient population. Potential issues with data-distribution discrepancies<sup>48</sup> can exacerbate unfairness. Variations among data sets can lead to biased learning of features from data sets collected from different sources (ie, domains) under different conditions.<sup>49</sup> Comparing differences between the source domain (where training data were collected) and the target domain (the test data for which the AI model will be used) may help explain any biases that are found. Many advanced domain-matching algorithms have been introduced to improve AI fairness by reducing the domain differences for cross-site data sets.<sup>50,51</sup>

In the deployment stage, continued surveillance of performance in terms of fairness and accuracy is needed. One should determine whether detected errors are one-off or systemic problems. There is no consensus yet on who bears this responsibility. Is it the end-users (radiologists/clinicians), the health care system/hospitals, or the vendors who make and sell the product? How will the algorithms be provided to the medical community? Will they be available equitably to diverse communities? One should ideally be able to explain how the trained AI model makes its decisions and predictions.

For the feedback stage, use and misuse of the system in the real world should be monitored and corrected in a transparent fashion. Fairness metrics<sup>14,15</sup> should be evaluated and then used to refine the model. Accountability for errors needs to be predefined.

### **Trust, Radiology, and AI: Guiding Principles**

Neuroradiologists need to become educated and involved to ensure that AI is used appropriately in the diagnosis, management,

and treatment of patients. For neuroradiologists to trust the use of AI in image interpretation, there needs to be greater transparency about the algorithm. Training data are foundationally critical to algorithm development, explaining why “good” data are so valuable. Therefore, trust-building for neuroradiology starts with the quality of data, its collection and management, its evaluation, the quality of its associated labels, and the protection of patient privacy. To many radiologists, the entire field of AI is opaque, where a “black box” takes images and spews out predictive analytics. For AI to gain widespread acceptance by patients and radiologists, everyone needs to comprehend how a particular trained AI model works.<sup>52</sup>

There are many unresolved issues around the development of AI in radiology. Large amounts of imaging data are needed, which are difficult to share among institutions because there is reticence to engage in data-sharing agreements when imaging data are financially valuable to industry. Additionally, there are data-use agreements and data-sharing agreements that stipulate noncommercial use. However, some might argue that excluding companies from developing products on the basis of de-identified, shared data is itself counterproductive and cannot be enforced in a meaningful way. Federated learning shows promise in disrupting this sharing-based landscape because it alleviates the need to share patient data by training models that gain knowledge from local data that are retained within the acquiring institution at all times.<sup>53,54</sup> However, security concerns<sup>54</sup> such as inferential attacks and “model poisoning” from corruption of the AI model and/or data from  $\geq 1$  site remain.<sup>55,56</sup> Unfairness in federated learning can be exacerbated by the challenge of simultaneously maintaining accuracy and privacy;<sup>57</sup> however, these potential limitations are being addressed.<sup>58</sup> Informed consent, ownership of data, privacy, and protection of data are major topics that remain in flux without clear best practice guidelines.<sup>59</sup>

For AI algorithm development in academic medical centers, new concepts are necessary. Should we assume that patients who enter a major academic medical center automatically opt-in to allow their anonymized imaging data to be used for research, including AI? Do patients need to explicitly opt-out in writing? If patient data are used to develop AI algorithms, should patients be financially compensated? One viewpoint is that “clinical data should be treated as a form of public good, to be used for the benefit of future patients” once its use for clinical treatment has ended.<sup>60</sup> These questions underscore the need to consider both the patient’s and society’s rights with respect to the use of such data.

The core principles of ethical conduct in patient research include beneficence (do only good), non-maleficence (do no harm), autonomy, and justice,<sup>61</sup> which must also guide AI development in neuroradiology. In the AI era of neuroradiology, there may be conflicts that evolve around how much decision-making is retained by the neuroradiologist and how much is willingly ceded to an AI algorithm. Floridi and Cowl<sup>52</sup> stated that the “autonomy of humans should be promoted and that the autonomy of machines should be restricted and made intrinsically reversible, should human autonomy need to be protected and re-established.” This statement is precisely the major problem that occurred when pilots were unable to override an automated, erroneous AI-driven

navigation system to prevent nosedives, leading to plane crashes with significant loss of life.<sup>62</sup> Justice is conceptually implicit throughout AI development in neuroradiology from the data chosen to train the model to its validation so that no harm or unfairness occurs to certain groups of patients.<sup>52</sup>

Some researchers have articulated the need for a new bioethical consideration specifically to address algorithm development of AI in neuroradiology. Explicability can include explainability (how does it work?) and accountability (who is responsible for how it works?).<sup>52,63,64</sup> It is important that both patients and neuroradiologists understand how imaging tools such as AI algorithms are used to render decisions that impact their health and well-being, particularly around potentially life-saving decisions in which neuroradiology has a clear role. For example, a visual saliency map that delineates on images where the AI algorithm focused its attention to arrive at a prediction (ie, intracranial metastatic lesion on a brain MR imaging examination) would be useful to drive its acceptance by both clinicians and patients.<sup>65</sup> Neuroradiologists need to think like patients and adopt patient-centered practices when AI is deployed. Neuroradiologists should establish a practice to address real or perceived grievances for any unintended harm attributable to AI use.<sup>52</sup> Fear, ignorance, and misplaced anxiety around novel technology can derail the best of scientific intentions and advances, so we need to be prudent as we develop AI and encode bioethical principles into its development and deployment. Transparency can build trust,<sup>66</sup> with both code and data sets made publicly available whenever possible. However, for AI applications involving medical images, one must also balance the need for open science with patient privacy.

Ideally, neuroradiologists should be able to explain in lay language how data are used to build an AI tool, how the AI algorithm rendered a particular prediction, what that prediction means to patient care, and how accurate and reliable those predictions are.<sup>64,65</sup> This explanation will require education in AI from residency through fellowship and a process of life-long learning. The American Society of Neuroradiology (ASNR) convened an AI Task Force to make recommendations around education, training, and research in AI so that the ASNR maintains its primacy as a leader in this rapidly evolving field.

### **Suggestions for Neuroradiologists in AI**

Academic neuroradiologists need to lead. It is our responsibility to establish the benchmarks for best practices in the clinical utility of AI in conjunction with our academic partners in imaging societies such as the American College of Radiology and the Radiological Society of North America, as well as federal stakeholders such as the National Institutes of Health, National Institute of Standards and Technology, the Advanced Research Projects Agency, and the Food and Drug Administration. Although guidelines have been published around the ethical implementation of AI code, more work is needed from all relevant stakeholders including neuroradiologists, clinicians, patients, institutions, and regulatory bodies so that consensus builds around best practices that include the new concepts of explainability and accountability while preserving patient privacy and protection against security breaches such as cyberattacks.<sup>1,52,61,65</sup> Quality assurance and quality improvement processes will be needed to detect potential biases in algorithms

used in clinical care. Additional processes are needed to redress any perceived grievances and to quantify how AI affects patient outcomes.<sup>67</sup> In the Online Supplemental Data, across the AI development lifecycle, guidelines are listed in the form of essential questions that should be considered and asked around task definition, data collection, model definition, training and testing, and deployment and feedback, particularly when neuroradiologists are asked to evaluate clinical AI tools for their practices.

### **Summary**

In a joint North American and European consortium white paper,<sup>1</sup> the authors made a recommendation that AI in radiology should “promote any use that helps individuals such as patients and providers and should block the use of radiology data and AI algorithms for irresponsible financial gains.” Additionally, all AI algorithms must be informed by bioethical principles in which the benefits of AI outweigh the risks and minimize the potential for harm or bad outcomes and minimize the chances that AI will lead to greater health care inequity. Neuroradiologists need to participate fully in this transformative technology and set best practice standards for fair, ethical, and nonbiased deployment of AI in routine neuroimaging practice.

### **ACKNOWLEDGMENTS**

We acknowledge Yilan Gu for assistance in literature research and Jacob Calkins for assistance with the phantom data.

Disclosure forms provided by the authors are available with the full text and PDF of this article at [www.ajnr.org](http://www.ajnr.org).

### **REFERENCES**

1. Geis JR, Brady AP, Wu CC, et al. **Ethics of Artificial Intelligence in Radiology: Summary of the Joint European and North American Multisociety Statement.** *Radiology* 2019;293:436–40 CrossRef Medline
2. “Ethics”. *Merriam-Webster.com Dictionary*. Merriam-Webster, Inc. <http://www.merriam-webster.com/dictionary/ethics>. Accessed January 3, 2023
3. Panch T, Mattie H, Atun R. **Artificial intelligence and algorithmic bias: implications for health systems.** *J Glob Health* 2019;9:010318 CrossRef Medline
4. “Fairness”. *Merriam-Webster.com Dictionary*. Merriam-Webster, Inc. <http://www.merriam-webster.com/dictionary/fairness>. Accessed January 3, 2023
5. Dwork C, Hardt M, Pitassi T, et al. **Fairness through awareness.** In: *Proceedings of the 3rd Innovations in Theoretical Computer Science Conference*, Cambridge, Massachusetts. January 8–10, 2012 CrossRef
6. Crawford K. **The trouble with bias.** *NIPS* 2017;10 [https://www.youtube.com/watch?v=fMym\\_BKWQzk](https://www.youtube.com/watch?v=fMym_BKWQzk). Accessed January 3, 2023
7. Abbasi M, Friedler SA, Scheidegger C, et al. **Fairness in representation: quantifying stereotyping as a representational harm.** In: *Proceedings of the 2019 SIAM International Conference on Data Mining*. SIAM, Calgary, Alberta, Canada, May 2–4, 2019
8. Amini A, Soleimany AP, Schwarting W, et al. **Uncovering and mitigating algorithmic bias through learned latent structure.** In: *Proceedings of the 2019 AAAI/ACM Conference on AI, Ethics, and Society* 2019;289–95 CrossRef
9. Association for Computing Machinery. **ACM Conference on Fairness, Accountability, and Transparency (ACM FAccT)**, Seoul, South Korea. June 21–24, 2022
10. Jillson E. **Aiming for truth, fairness, and equity in your company’s use of AI.** *Business Blog Federal Trade Commission*. April 19, 2021. <https://www.ftc.gov/business-guidance/blog/2021/04/aiming-truth-fairness-equity-your-companys-use-ai>. Accessed January 5, 2023



11. **Algorithmic Accountability Act of 2022.** HR 6580. 117th Congress, 2021–2022
12. Chouldechova A. **Fair prediction with disparate impact: a study of bias in recidivism prediction instruments.** *Big Data* 2017;5:153–63 CrossRef Medline
13. Kleinberg J, Mullainathan S, Raghavan M. **Inherent trade-offs in the fair determination of risk scores.** In: *Proceedings of the 8th Innovations in Theoretical Computer Science Conference (ITCS 2017)*, Berkeley, California. January 9–11, 2017. Schloss Dagstuhl-Leibniz-Zentrum fuer Informatik
14. Corbett-Davies S, Goel S. **The measure and mismeasure of fairness: a critical review of fair machine learning.** *arXiv* 2018 arXiv:180800023
15. Verma S, Rubin J. **Fairness definitions explained.** In: *Proceedings of the 2018 IEEE/ACM International Workshop on Software Fairness (Fairware)*. IEEE Xplore 2018;1–7 CrossRef
16. Rajkomar A, Hardt M, Howell MD, et al. **Ensuring fairness in machine learning to advance health equity.** *Ann Intern Med* 2018;169:866–72 CrossRef Medline
17. Lundberg SM, Lee SI. **A unified approach to interpreting model predictions.** *arXiv* 1705.07874 May 22, 2017
18. Lundberg SM. **Explaining quantitative measures of fairness.** In: *Proceedings of the Fair & Responsible AI Workshop. CHI '20: CHI Conference on Human Factors in Computing Systems*, Honolulu, Hawaii. April 25–30, 2020
19. Zhao J, Wang T, Yatskar M, et al. **Men also like shopping: reducing gender bias amplification using corpus-level constraints.** In: *Proceedings of the 2017 Conference on Empirical Methods in Natural Language Processing*, Copenhagen, Denmark. September 7–11, 2017
20. Zou J, Schiebinger L. **AI can be sexist and racist: it's time to make it fair.** *Nature* 2018;559:324–26 CrossRef Medline
21. Sweeney L. **Discrimination in online ad delivery.** *Communications of the ACM* 2013;56:44–54 CrossRef
22. Buolamwini J, Gebru T. **Gender shades: intersectional accuracy disparities in commercial gender classification.** In: *Proceedings of the Conference on Fairness, Accountability and Transparency*, New York, New York. February 23–24, 2018;77–91
23. Angwin J, Larson J, Matta S, et al. **Machine bias: there's software used across the country to predict future criminals. and it's biased against Blacks.** *ProPublica* May 23, 2016 <https://www.propublica.org/article/machine-bias-risk-assessments-in-criminal-sentencing>. Accessed January 6, 2023
24. Benjamin R. **The New Jim code: reimagining the default settings of technology & society.** *Race and technology: A Research Lecture Series*. May 1, 2021 to June 30, 2022. Virtual [https://www.youtube.com/watch?v=aMuD\\_LAy2zQ](https://www.youtube.com/watch?v=aMuD_LAy2zQ). Accessed July 24, 2022
25. Gunzer F, Jantscher M, Hassler EM, et al. **Reproducibility of artificial intelligence models in computed tomography of the head: a quantitative analysis.** *Insights Imaging* 2022;13:173 CrossRef Medline
26. Din M, Agarwal S, Grzeda M, et al. **Detection of cerebral aneurysms using artificial intelligence: a systematic review and meta-analysis.** *J Neurointerv Surg* 2023;15:262–71 CrossRef Medline
27. McLouth J, Elstrott S, Chaibi Y, et al. **Validation of a deep learning tool in the detection of intracranial hemorrhage and large vessel occlusion.** *Front Neurol* 2021;12:656112 CrossRef Medline
28. Guo J, Gong E, Fan AP, et al. **Predicting (15)O-Water PET cerebral blood flow maps from multi-contrast MRI using a deep convolutional neural network with evaluation of training cohort bias.** *J Cereb Blood Flow Metab* 2020;40:2240–53 CrossRef Medline
29. Gao MM, Wang J, Saposnik G. **The art and science of stroke outcome prognostication.** *Stroke* 2020;51:1358–60 Medline
30. Edlow BL, Giacino JT, Hirschberg RE, et al. **Unexpected recovery of function after severe traumatic brain injury: the limits of early neuroimaging-based outcome prediction.** *Neurocrit Care* 2013;19:364–75 CrossRef Medline
31. Cramer H, Holstein K, Vaughan J, et al. **Challenges of incorporating algorithmic fairness into industry practice.** *ACM FAT\* 2019 Translation Tutorial*. February 22, 2019 <https://www.youtube.com/watch?v=UickZv93SOY>, Accessed July 24, 2022
32. Barocas S, Hardt M. **Fairness in machine learning.** Tutorial. NIPS 2017. Long Beach, CA. December 4–9, 2017
33. Schwarz CG, Kremers WK, Therneau TM, et al. **Identification of anonymous MRI research participants with face-recognition software.** *N Engl J Med* 2019;381:1684–86 CrossRef Medline
34. Athinola A. **Martinos Center for Biomedical Imaging: Martinos Center Anthropomorphic Phantoms.** [https://phantoms.martinos.org/Main\\_Page](https://phantoms.martinos.org/Main_Page). Accessed May 21, 2023
35. Schwarz CG, Kremers WK, Lowe VJ, et al; Alzheimer's Disease Neuroimaging Initiative. **Face recognition from research brain PET: an unexpected PET problem.** *Neuroimage* 2022;258:119357 CrossRef Medline
36. Jeong YU, Yoo S, Kim YH, et al. **De-identification of facial features in magnetic resonance images: software development using deep learning technology.** *J Med Internet Res* 2020;22:e22739 CrossRef Medline
37. Arora A, Arora A. **Synthetic patient data in health care: a widening legal loophole.** *Lancet* 2022;399:1601–02 CrossRef Medline
38. Goodfellow I, Pouget-Abadie J, Mirza M, et al. **Generative adversarial nets; NIPS'14:** In: *Proceedings of the 27th International Conference on Neural Information Processing*, Montreal, Quebec, Canada. December 8–13, 2014
39. Ross C, Sweltitz I. **IBM's Watson supercomputer recommended 'unsafe and incorrect' cancer treatments, internal documents show.** *STAT+*. July 25, 2018 <https://www.statnews.com/wp-content/uploads/2018/09/IBMs-Watson-recommended-unsafe-and-incorrect-cancer-treatments-STAT.pdf>. Accessed July 19, 2022
40. Onder O, Yarasir Y, Azizova A, et al. **Errors, discrepancies and underlying bias in radiology with case examples: a pictorial review.** *Insights Imaging* 2021;12:51 CrossRef Medline
41. Choi K, Grover A, Singh T, et al. In: *Proceedings of the International Conference on Machine Learning*, Virtual. July 12–18, 2020;1887–98
42. Obermeyer Z, Powers B, Vogeli C, et al. **Dissecting racial bias in an algorithm used to manage the health of populations.** *Science* 2019;366:447–53 CrossRef Medline
43. Agarwal A, Beygelzimer A, Dudík M, et al. **A reductions approach to fair classification.** In: *Proceedings of the International Conference on Machine Learning*, Stockholm, Sweden. July 10–15, 2018;60–69
44. Fairlearn. **Improve fairness of AI systems.** <https://fairlearn.org/>. Accessed July 24, 2022
45. IBM Research. **AI Fairness 360.** <https://ibm.com/open-source/open-projects/ai-fairness-360>. Accessed July 24, 2022
46. Google. **The ML Fairness Gym.** <https://github.com/google/ml-fairness-gym>. Accessed July 24, 2022
47. **What-If Tool.** <https://pair-code.github.io/what-if-tool/>. Accessed July 24, 2022
48. Koh PW, Sagawa S, Marklund H, et al. **WILDS: a benchmark of in-the-wild distribution shifts.** In: Marina M, Tong Z, eds. In: *Proceedings of the 38th International Conference on Machine Learning* Virtual. July 18–21, 2021;5637–64
49. Yan W, Wang Y, Xia M, et al. **Edge-guided output adaptor: highly efficient adaptation module for cross-vendor medical image segmentation.** *IEEE Signal Process Lett* 2019;26:1593–97 CrossRef
50. Schumann C, Wang X, Beutel A, et al. **Transfer of machine learning fairness across domains.** *arXiv* 2019 arXiv:190609688
51. Joshi N, Burlina P. **AI fairness via domain adaptation.** *arXiv* 2021 arXiv:2104.01109
52. Floridi L, Cowls J. **A united framework of five principles for AI in society.** *Harvard Data Science Review* 2019;1 CrossRef
53. Sheller MJ, Edwards B, Reina GA, et al. **Federated learning in medicine: facilitating multi-institutional collaborations without sharing patient data.** *Sci Rep* 2020;10:12598 CrossRef Medline
54. Li T, Sahu AK, Talwalkar A, et al. **Federated learning: challenges, methods, and future directions.** *IEEE Signal Processing Magazine* 2020;37:50–60 CrossRef
55. Wang L, Xu S, Wang X, et al. **Eavesdrop the composition proportion of training labels in federated learning.** *arXiv* 2019 arXiv:1910.06044

56. Pejó B, Biczók G. **Quality inference in federated learning with secure aggregation.** *arXiv* 2020 arXiv:2007.06236
57. Abay A, Zhou Y, Baracaldo N, et al. **Mitigating bias in federated learning.** *arXiv* 2020 arXiv:2012.02447
58. Gu X, Tianqing Z, Li J, et al. **Privacy, accuracy, and model fairness trade-offs in federated learning.** *Computers & Security* 2022;122:102907 CrossRef
59. Mittelstadt BD, Floridi L. **The ethics of big data: current and foreseeable issues in biomedical contexts.** *Sci Eng Ethics* 2016;22:303–41 CrossRef Medline
60. Larson DB, Magnus DC, Lungren MP, et al. **Ethics of using and sharing clinical imaging data for artificial intelligence: a proposed framework.** *Radiology* 2020;295:675–82 CrossRef Medline
61. Varkey B. **Principles of clinical ethics and their application to practice.** *Med Princ Pract* 2021;30:17–28 CrossRef Medline
62. Mongan J, Kohli M. **Artificial intelligence and human life: five lessons for radiology from the 737 MAX Disasters.** *Radiol Artif Intell* 2020;2:e190111 CrossRef Medline
63. Floridi L, Taddeo M. **What is data ethics?** *Philos Trans A Math Phys Eng Sci* 2016;374:20160360 CrossRef
64. Floridi L, Cowls J, Beltrametti M, et al. **AI4People: an ethical framework for a good AI society—opportunities, risks, principles, and recommendations.** *Minds Mach (Dordr)* 2018;28:689–707 CrossRef Medline
65. Gilpin LH, Bau D, Yuan BZ, et al. **Explaining explanations: an overview of interpretability of machine learning.** In: *Proceedings of the 2018 IEEE 5th International Conference on Data Science and Advanced Analytics (DSAS)*, Turin, Italy. October 1–3, 2018;80–89 CrossRef
66. Haibe-Kains B, Adam GA, Hosny A, et al; Massive Analysis Quality Control (MAQC) Society Board of Directors. **Transparency and reproducibility in artificial intelligence.** *Nature* 2020;586:E14–16 CrossRef Medline
67. Kingston JKC. **Artificial intelligence and legal liability.** In: Bramer M, Petridis M, eds. *Research and Development in Intelligent Systems XXXIII*. Springer-Verlag International Publishing 2016:269–79

# Perfusion Collateral Index versus Hypoperfusion Intensity Ratio in Assessment of Collaterals in Patients with Acute Ischemic Stroke

● Brian Tsui, ● Iris E. Chen, ● May Nour, ● Shingo Kihira, ● Elham Tavakkol, ● Jennifer Polson, ● Haoyue Zhang, ● Joe Qiao, ● Meresedeh Bahr-Hosseini, ● Corey Arnold, ● Satoshi Tateshima, ● Noriko Salamon, ● J. Pablo Villablanca, ● Geoffrey P. Colby, ● Reza Jahan, ● Gary Duckwiler, ● Jeffrey L. Saver, ● David S. Liebeskind, and ● Kambiz Nael



## ABSTRACT

**BACKGROUND AND PURPOSE:** Perfusion-based collateral indices such as the perfusion collateral index and the hypoperfusion intensity ratio have shown promise in the assessment of collaterals in patients with acute ischemic stroke. We aimed to compare the diagnostic performance of the perfusion collateral index and the hypoperfusion intensity ratio in collateral assessment compared with angiographic collaterals and outcome measures, including final infarct volume, infarct growth, and functional independence.

**MATERIALS AND METHODS:** Consecutive patients with acute ischemic stroke with anterior circulation proximal arterial occlusion who underwent endovascular thrombectomy and had pre- and posttreatment MRI were included. Using pretreatment MR perfusion, we calculated the perfusion collateral index and the hypoperfusion intensity ratio for each patient. The angiographic collaterals obtained from DSA were dichotomized to sufficient (American Society of Interventional and Therapeutic Neuroradiology [ASITN] scale 3–4) versus insufficient (ASITN scale 0–2). The association of collateral status determined by the perfusion collateral index and the hypoperfusion intensity ratio was assessed against angiographic collaterals and outcome measures.

**RESULTS:** A total of 98 patients met the inclusion criteria. Perfusion collateral index values were significantly higher in patients with sufficient angiographic collaterals ( $P < .001$ ), while there was no significant ( $P = .46$ ) difference in hypoperfusion intensity ratio values. Among patients with good (mRS 0–2) versus poor (mRS 3–6) functional outcome, the perfusion collateral index of  $\geq 62$  was present in 72% versus 31% ( $P = .003$ ), while the hypoperfusion intensity ratio of  $\leq 0.4$  was present in 69% versus 56% ( $P = .52$ ). The perfusion collateral index and the hypoperfusion intensity ratio were both significantly predictive of final infarct volume, but only the perfusion collateral index was significantly ( $P = .03$ ) associated with infarct growth.

**CONCLUSIONS:** Results show that the perfusion collateral index outperforms the hypoperfusion intensity ratio in the assessment of collateral status, infarct growth, and determination of functional outcomes.

**ABBREVIATIONS:** AIS = acute ischemic stroke; ASITN = American Society of Interventional and Therapeutic Neuroradiology; AUC = area under the curve; HIR = hypoperfusion intensity ratio; IQR = interquartile range; mTICI = modified TICI; PCI = perfusion collateral index; ROC = receiver operating characteristic; Tmax = time-to-maximum

In patients with acute ischemic stroke (AIS), collateral status is considered a critical variable in determination of infarction growth and the success of thrombectomy.<sup>1–4</sup> Determining collateral status has the potential to extend endovascular treatment beyond the current timeline of 24 hours.<sup>5</sup> The latest American

Stroke Association guidelines state that collateral status may help to determine endovascular treatment eligibility in some candidates,<sup>6</sup> though no specific recommendations about the methodology to measure collaterals has been proposed.

DSA is the standard of reference for assessment of collaterals due to high spatial and temporal resolution. Noninvasive assessment of collaterals has been increasingly improving, though it remains a moving target with no concrete recommendations. Direct visualization of collateral vessels can be performed by CTA or MRA by taking into account the number, size, and density of these vessels,<sup>7–10</sup> with incremental added value of multiphase-over-single arterial phase imaging.<sup>11–13</sup>

By means of perfusion imaging, a multitude of methods for automated assessment of collateral status have been proposed,

Received May 14, 2023; accepted after revision August 20.

From the Departments of Radiological Sciences (B.T., I.E.C., M.N., S.K., E.T., J.Q., C.A., S.T., N.S., J.P.V., R.J., G.D., K.N.), Neurology (M.N., M.B.-H., J.L.S., D.S.L.), David Geffen School of Medicine, Bioengineering (J.P., H.Z., C.A.), and Neurosurgery (G.P.C.), University of California, Los Angeles, Los Angeles, California.

Please address correspondence to Kambiz Nael, MD, David Geffen School of Medicine at UCLA, Department of Radiological Sciences, 757 Westwood Plaza, Ste 1621, Los Angeles, CA, 90095-7532; e-mail: kambiznael@gmail.com; @kambiznael



Indicates article with online supplemental data.

<http://dx.doi.org/10.3174/ajnr.A8002>

including the hypoperfusion intensity ratio (HIR) and the perfusion collateral index (PCI).<sup>14-16</sup> The HIR was first investigated in the Diffusion-Weighted Imaging Evaluation for Understanding Stroke Evolution Study-2 (DEFUSE-2) cohort and is calculated by dividing the volume of tissue with a time-to-maximum (Tmax) delay of >10 seconds by the volume of tissue with Tmax of >6 seconds. The HIR has been used as a measure of collaterals, and HIR values > 0.4 have been associated with poor collaterals, infarction growth, and poor functional outcome.<sup>14,17</sup>

The PCI uses a multiparametric approach and is defined as the volume of moderately hypoperfused tissue (delay of 2–6 seconds) multiplied by its corresponding mean relative CBV.<sup>15</sup> Similar to the HIR, the PCI has been shown promising in the determination of collateral status. PCI values of >60 have been associated with good collaterals and outcome measures such as final infarct volume and functional outcomes.<sup>15,16</sup> The PCI was previously shown to have a diagnostic accuracy of 94% compared with DSA in the prediction of collateral status.<sup>15</sup>

The diagnostic accuracy of the HIR or PCI for the determination of collateral status remains to be investigated against each other in a single study. The central premise of this exploratory study was to evaluate the diagnostic performance of the HIR and PCI in the assessment of collateral status. The aims of this study were the following: 1) to assess the agreement of collateral status obtained from the HIR and PCI against DSA as the standard of reference; and 2) to perform a comparative analysis between the HIR and PCI in association with outcome measures, including final infarct volume, infarct growth, and functional outcome in patients with AIS.

## MATERIALS AND METHODS

### Patients

This retrospective study was approved by University of California Los Angeles (UCLA) institutional review board, and informed consent was waived. Consecutive patients with AIS were identified between January 1, 2010, and August 31, 2019, and they were included if they met the following inclusion criteria: 1) anterior circulation proximal arterial occlusion including the intracranial ICA or proximal MCA (M1), 2) pretreatment MRI with inclusion of MR perfusion, 3) DSA and endovascular treatment, and 4) the presence of follow-up MRI for the determination of final infarct volume.

Clinical data, including patient age, sex, time from stroke symptoms, NIHSS score, time of initial (pretreatment) imaging, and site of large-vessel occlusion, were collected. In addition, treatment type, including intravenous tPA, endovascular therapy, degree of reperfusion using the modified TICI (mTICI) scale,<sup>18</sup> and the mRS at 90 days were recorded when available.

### Image Analysis

**Collateral Assessment on DSA.** An interventional neuroradiologist with 8 years of postfellowship experience graded the collaterals using the American Society of Interventional and Therapeutic Neuroradiology (ASITN)/Society of Interventional Radiology collateral flow grading system (grades 0–4)<sup>19</sup> on baseline pretreatment DSA images. The interventional neuroradiologist was blinded to the clinical information and MRI findings. Patients were dichotomized to those with sufficient collaterals (grades 3

and 4) and insufficient collaterals (grades 0, 1, and 2). Patients were excluded if the baseline DSA was deemed inadequate to provide collateral assessment (ie, lack of an adequate number of phases, injections, or coverage).

### MR Imaging and Analysis

DWI was acquired using a single-shot spin-echo EPI sequence (TR/TE, 4300/78 ms; flip angle, 90°; FOV, 22 × 22 cm; matrix, 128 mm<sup>2</sup>; 26 slices × 5 mm). Diffusion gradients were applied along 6 noncollinear directions with b-values of 0 and 1000 s/mm<sup>2</sup>.

DSC perfusion was performed using a single-shot gradient-echo EPI sequence (TR/TE, 1450/30 ms; flip angle, 90°; FOV, 22 × 22 cm; matrix, 128 mm<sup>2</sup>; 24 slices × 5 mm). Sixty dynamic frames were obtained during a 90-second acquisition time.

From the perfusion data, the HIR (*Volume of Tmax >10 Seconds/Volume of Tmax >6 Seconds*) was calculated using RAPID software (Version 5.0.4; iSchemaView). Subsequently, MR perfusion data were processed using Olea Sphere (SP.23; Olea Medical) by applying a Bayesian probabilistic method.<sup>20</sup> The PCI (*Volume of Delay<sup>2-6 seconds</sup> × Relative CBV*) was calculated for each patient.

The baseline infarct volume was calculated automatically using ADC <600 × 10<sup>-6</sup> mm<sup>2</sup>/s from the pretreatment MRI. Final infarct volume was calculated from the follow-up MRI (obtained within 1–2 days from the pretreatment MRI). Due to the increase in ADC values following reperfusion,<sup>21</sup> final infarction volumes were segmented using hyperintensity on DWI (b=1000) by 1 neuroradiologist with >10 years of experience. The difference in infarction volumes between the second and first MRI was recorded as infarct growth.

### Statistical Analysis

Demographic characteristics and neuroimaging variables were presented as mean (SD) for continuous data and as median and interquartile range for categorical data. Statistical tests were performed using the Fisher *t* test or Wilcoxon rank-sum test as appropriate.

Receiver operating characteristic (ROC) curve analysis was performed, and the area under the curve (AUC) was calculated for the prediction of collateral status for both the HIR and PCI. The optimal cutoff point to identify collateral status was determined by the Youden index. Summary measures such as sensitivity and specificity were calculated on the basis of the optimal threshold to determine collateral status (sufficient-versus-insufficient). Furthermore, to test the effect of collaterals on measured outcomes with continuous values, including final infarct volume and infarct growth, a Mood median test was used. A  $\chi^2$  test was performed to compare the proportion of patients with good functional outcomes (mRS 0–2) among patients with sufficient and insufficient collaterals. All tests were 2-tailed and assumed significance at *P* < .05.

## RESULTS

Among 141 patients initially evaluated, a total of 98 met the study entry criteria. Fifteen patients were excluded due to nondiagnostic MR imaging (eg, severe motion artifacts, susceptibility distortion) and 28 patients due to baseline DSA deemed inadequate to provide collateral assessment (lack of an adequate number of phases and injections or coverage). Among the 98 patients included, 44.8% were women, mean age = 70.4 (SD, 13.6) years,

# Baseline and clinical data in patients with insufficient-versus-sufficient collateral flow

Variable	Overall (n = 98)	Sufficient Collaterals (n = 43)	Insufficient Collaterals (n = 55)	P Value
Age (mean) (SD)	70.4 (13.6)	69.6 (12.6)	71.2 (14.3)	.58
Sex, female (No.) (%)	44 (44.8%)	24 (55.8%)	20 (36.3%)	.55
Baseline NIHSS (median) (IQR)	15 (9–19)	14 (9–19)	15 (9–20)	.55
IV tPA (No.) (%)	10 (10%)	2 (5%)	8 (15%)	.11
Time from stroke onset (median) (IQR) (hr)	2.48 (1.27–4.98)	2.00 (1.38–4.57)	2.50 (1.24–5.31)	.90
Location of LVO (ICA/MCA) (No.)/(No.)	14/84	4/39	10/45	.80
Successful reperfusion (mTICI 2b–3) (No.) (%)	79 (80.6%)	38 (88.4%)	41 (74.5%)	.86

**Note:**—LVO indicates large-vessel occlusion; IQR, interquartile range.

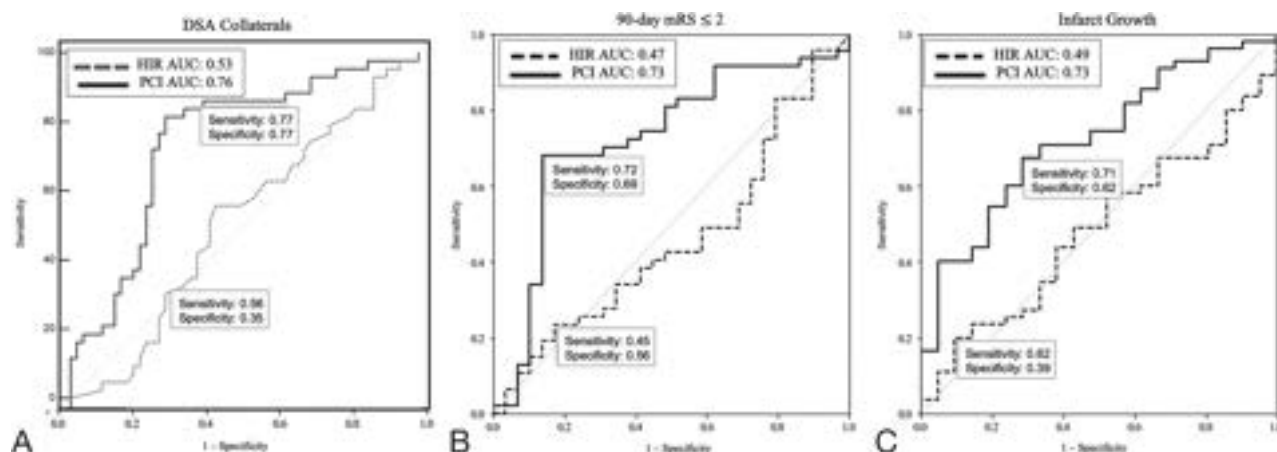


**FIG 1.** ROC curve analysis of the PCI and HIR in the prediction of DSA-based angiographic collaterals (A). In addition, ROC curves for PCI and HIR in the prediction of functional outcome (B) and infarct growth (C) are shown.

with NIHSS median = 15 (IQR, 9–19). Successful reperfusion (mTICI 2b–3) following mechanical thrombectomy was achieved in 79 patients (80.6%).

## Collateral Assessment

Using pretreatment DSA as the standard of reference, 55 patients (56%) had insufficient collaterals (ASITN < 3), and 43 patients (44%) had sufficient collaterals (ASITN ≥ 3). The baseline demographic and clinical data for the entire cohort and among patients with sufficient-versus-insufficient angiographic collaterals are summarized in the Table.

The HIR values were not significantly different between patients with sufficient-versus-insufficient collaterals, mean = 0.47 (SD, 0.44) versus 0.41 (SD, 0.21),  $P = 0.46$ . The mean PCI values were significantly higher in patients with sufficient collaterals versus insufficient collaterals, 106.1 (SD, 56.6) versus 58.3 (SD, 40.4),  $P < .001$ . ROC analysis for the HIR in determination of DSA-based collaterals resulted in AUC/sensitivity/specificity of 0.53/0.56/0.35 ( $P = .86$ ) at a 0.4 cutoff. ROC analysis for the PCI in determination of DSA-based collaterals showed an AUC/sensitivity/specificity of 0.76/0.77/0.77 ( $P < .001$ ) at a cutoff of 62. The ROC curves for the HIR and PCI are shown in Fig 1.

## Outcome Assessment

The 90-day mRS was used as the primary outcome measure to determine functional independence. Among 77 patients with 90-day mRS values available, 29 patients (38%) had good functional outcomes (mRS 0–2).

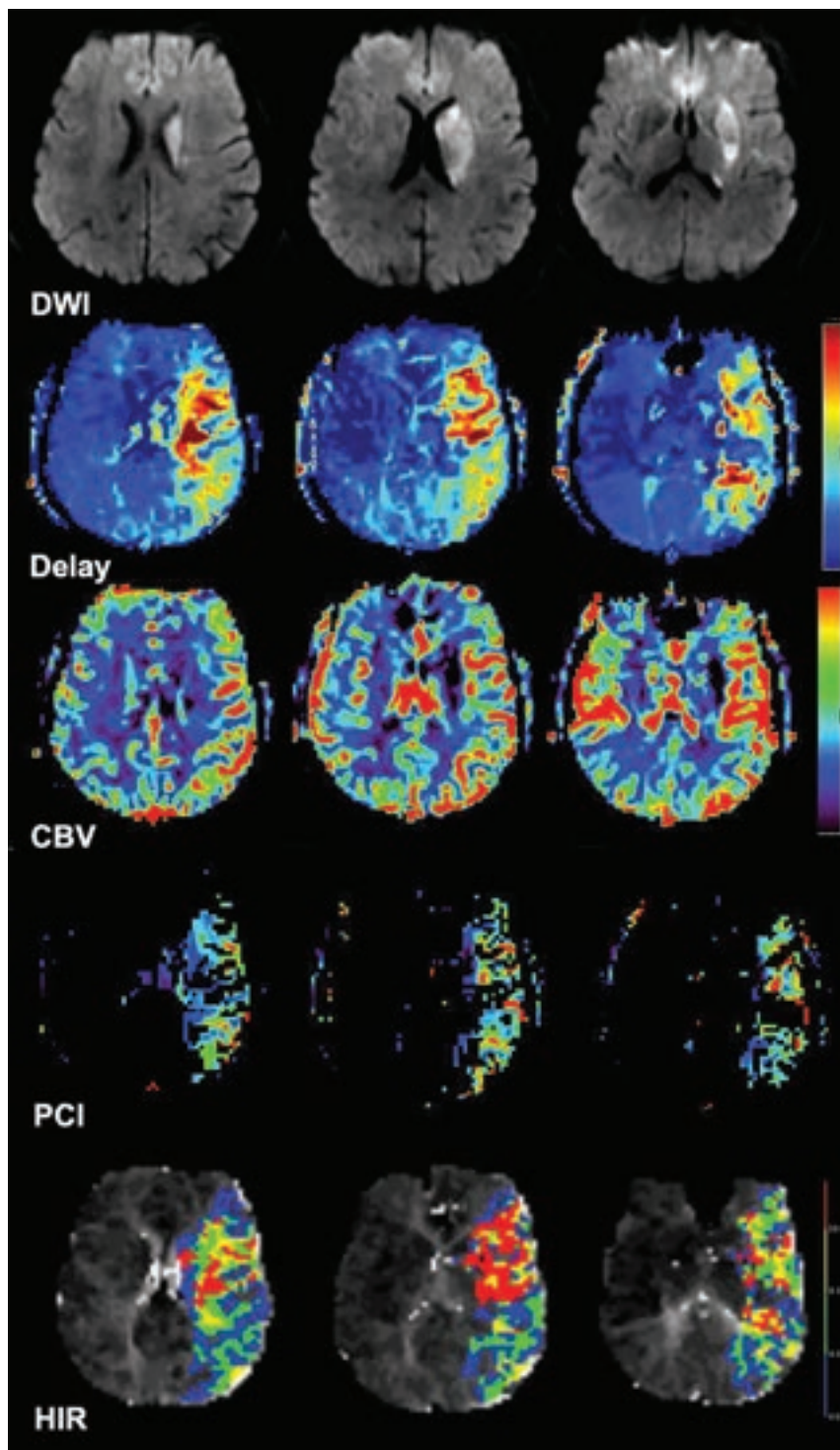
Comparative analysis of patients with good-versus-poor functional outcome showed a significantly younger age in patients with good outcome (mean = 63.9 [SD, 15.6] years versus 74.5 [SD, 11.1] years,  $P = .001$ ); significantly higher PCI values in patients with good outcome (mean = 106.3 [SD, 56.4] versus 68.8 [SD, 53.4],  $P = .005$ ); significantly smaller final infarct volumes in patients with good outcome (mean = 20.4 [SD, 20.1] mL versus 48.5 [SD, 43.1] mL,  $P = .002$ ); and significantly smaller mean values of infarct growth in patients with good outcomes (6.25 [SD, 8.7] mL versus 20.3 [SD, 28.9] mL,  $P = .001$ ). There was no significant difference between HIR values in patients with good-versus-poor outcome (mean = 0.45 [SD, 0.10] versus 0.49 [SD, 0.43],  $P = .70$ ).

Figure 1 shows the comparative ROC analysis between the PCI and HIR in relation to outcome measures, including 90-day mRS and infarct growth.

The diagnostic performance of collateral assessment on each method using dichotomized scores (ie, ASITN ≥ 3 on DSA, PCI ≥ 62, and HIR ≤ 0.4) are summarized in the Online Supplemental Data. Patients with good collaterals had statistically significantly smaller infarction volumes. Patients with PCI ≥ 62 had statistically significant lower infarct growth than patients with PCI < 62. PCI ≥ 62 was associated with better functional outcomes with an OR of 2.83 (Online Supplemental Data).

In 2 patients with good angiographic collaterals, an example of concordant PCI and HIR is shown in Fig 2, while Fig 3 demonstrates an example of discordant PCI and HIR. Figure 4 demonstrates an example of poor angiographic collaterals with a poor PCI and a discordant HIR.





**FIG 2.** Example of concordance between the PCI and HIR. Adult patient with right hemiparesis who underwent MR imaging approximately 10 hours after symptom onset. The patient has a left M1 occlusion (not shown). Aligned axial DWI, delay, CBV, PCI, and HIR maps from MR perfusion are shown. There is an ischemic core involving the left basal ganglia. The PCI value is estimated at 132, suggestive of sufficient collaterals. The estimated HIR is 0.36, also suggesting sufficient collaterals. Baseline catheter angiography (not shown) revealed good collaterals (ASITN 3).

## DISCUSSION

This study, to our knowledge, is the first to compare the diagnostic performance of HIR and PCI in predicting collateral status defined by DSA as the standard of reference. Results showed

superior performance of PCI over HIR in assessment of collateral status. We specifically highlight the following 2 findings:

First, the PCI provides a more accurate representation of true collaterals as measured by DSA compared with the HIR. At the threshold of 62, similar to what was previously reported,<sup>15</sup> the PCI provided a sensitivity and specificity of 77% and 77% in predicting sufficient angiographic collaterals. On the other hand, in our study, the HIR was not a significant predictor of DSA collaterals ( $AUC = 0.53$ ,  $P = .86$ ).

The PCI was developed on the basis of and in relation to DSA collaterals from its introduction.<sup>15</sup> This feature may explain the higher performance and correlation to DSA over HIR, which was developed initially as a surrogate of collateral status based on defining infarction core and growth rather than a direct correlation to DSA.<sup>14,22</sup> Recent studies have shown good correlation between HIR and CTA collaterals, including the work of Lyndon et al,<sup>23</sup> which showed an  $AUC$  of 0.86 for detection of good CTA collaterals using a CTP-estimated HIR  $< .45$ , and the work of Wang et al<sup>24</sup> with an  $AUC$  of 0.82 using an HIR  $< .68$ .

It was not until recently that the HIR relationship with DSA was shown in a study by Guenego et al.<sup>17</sup> In this study, HIR values  $< 0.4$  were associated with good angiographic collaterals with a specificity of 56% (compared with 35% in our study) and a sensitivity of 79% (compared with 56% in our study). Although the exact reason for the more modest results of the HIR in our study is unclear, our study included both ICA and M1 occlusions, while Guenego et al focused on patients with only M1 occlusions. It is plausible that inclusion of patients with ICA occlusion could have affected the sensitivity of the HIR in our study due to more proximal occlusion and its effect on upstream flow.

The second finding is that while both the PCI and HIR were significant in predicting the final infarction volume, only the PCI was predictive of infarct growth and functional independence. Collateral information in the HIR is obtained using Tmax only. The focus, therefore, is on arterial delay and the severity of hypoperfusion. Tissue with severe hypoperfusion

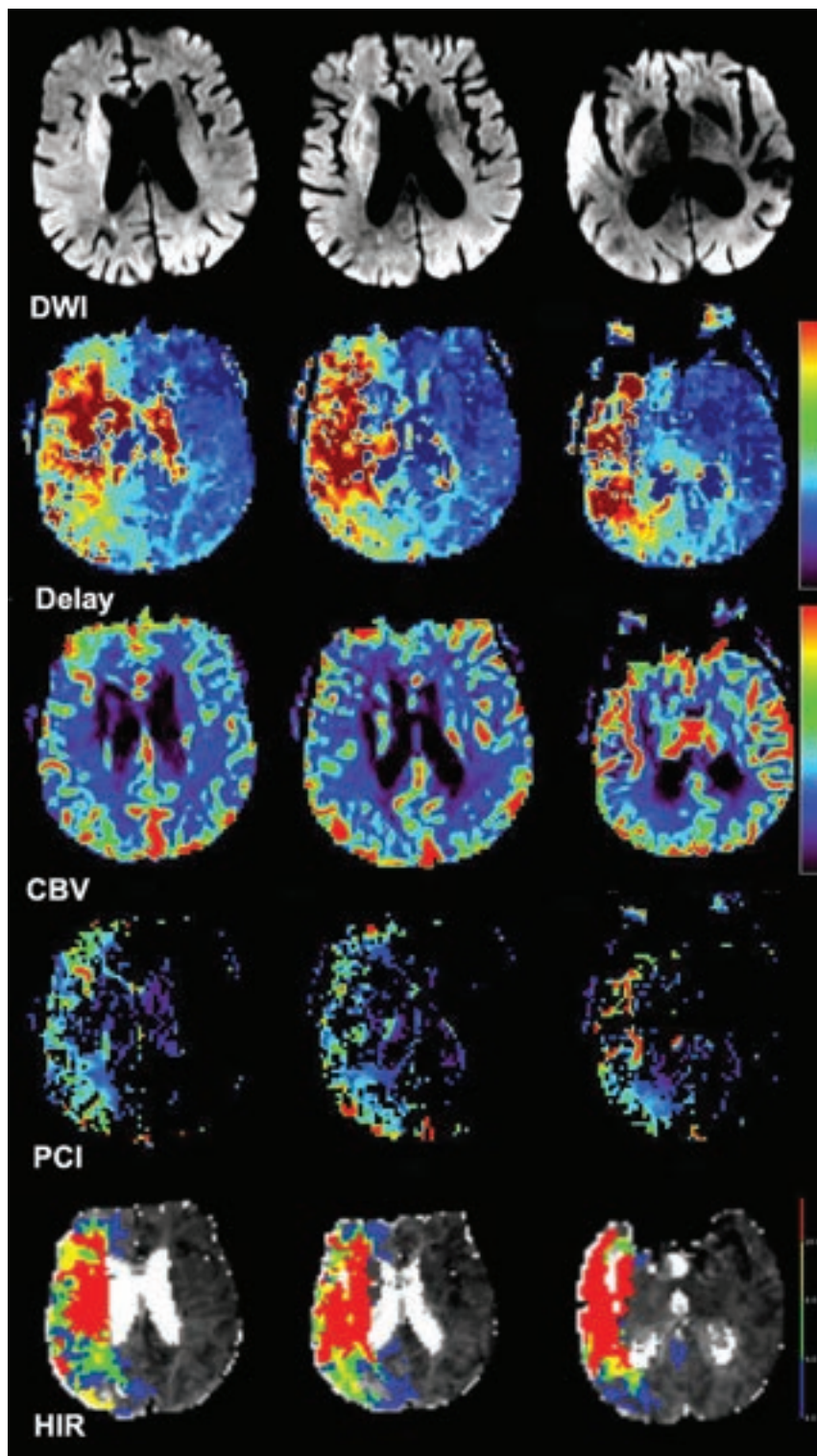


**FIG 3.** Example of discordance between the PCI and HIR in a patient with sufficient angiographic collaterals. Adult patient with left hemiparesis who underwent MR imaging approximately 4.5 hours after symptom onset. The patient has a right carotid terminus occlusion (not shown). Aligned axial DWI, delay, CBV, PCI, and HIR maps from MR perfusion are shown. There is an ischemic core involving the right basal ganglia, insula, and right temporal lobe. The PCI value is estimated at 130, suggestive of sufficient collaterals. The estimated HIR is 0.49, suggestive of poor collaterals. Baseline catheter angiography (not shown) revealed good collaterals (ASITN 3).

measured by Tmax of  $>10$  seconds is more likely to undergo infarction; hence, the HIR is a significant predictor of final infarct volume as shown by our study and other previous investigations.

However, in our study, the HIR was not a significant predictor of infarct growth or functional outcome, contrary to initial studies of the HIR.<sup>14,22</sup> In a follow-up study by Arenillas et al,<sup>25</sup> similar to our study, the HIR was not associated with infarct growth. Instead, the authors showed an association between infarct growth and the relative CBV index defined as the mean of normalized CBV values within the volume of tissue with a perfusion delay of Tmax  $> 6$  seconds.<sup>25,26</sup> This association is similar to what is incorporated into the PCI.

Evaluation of collaterals using perfusion imaging should consider both delay and dispersion.<sup>27</sup> By means of Tmax in the HIR and delay in the PCI, both measures likely evaluate the early arterial phase of collaterals, representing the delay component. The addition of CBV in the PCI, however, provides information regarding the amount of blood flow beyond the point of arterial occlusion (via dispersion), which is not evaluated in the HIR. Therefore, the PCI provides a more comprehensive assessment of collateral phases (both delay and dispersion components), similar to what has been shown by angiographic studies.<sup>28</sup> In our study, the PCI was able to predict infarct growth similar to DSA collaterals, in which combined arterial and venous phases of collaterals are considered,<sup>29</sup> reinforcing the importance of considering collaterals as a whole and not just focusing on the delay component.

The association between functional outcome and final infarct volume has been mixed in the literature.<sup>30-32</sup> Moreover, infarct growth rather than final infarct volume has been reported as a better predictor of functional outcomes.<sup>33</sup> In our study, the HIR was only associated with final infarct volume, while the PCI was a significant determinant of both infarct growth and functional outcome. Previous studies have shown that the extent of venous drainage can predict outcomes,<sup>28</sup> and again, it is plausible



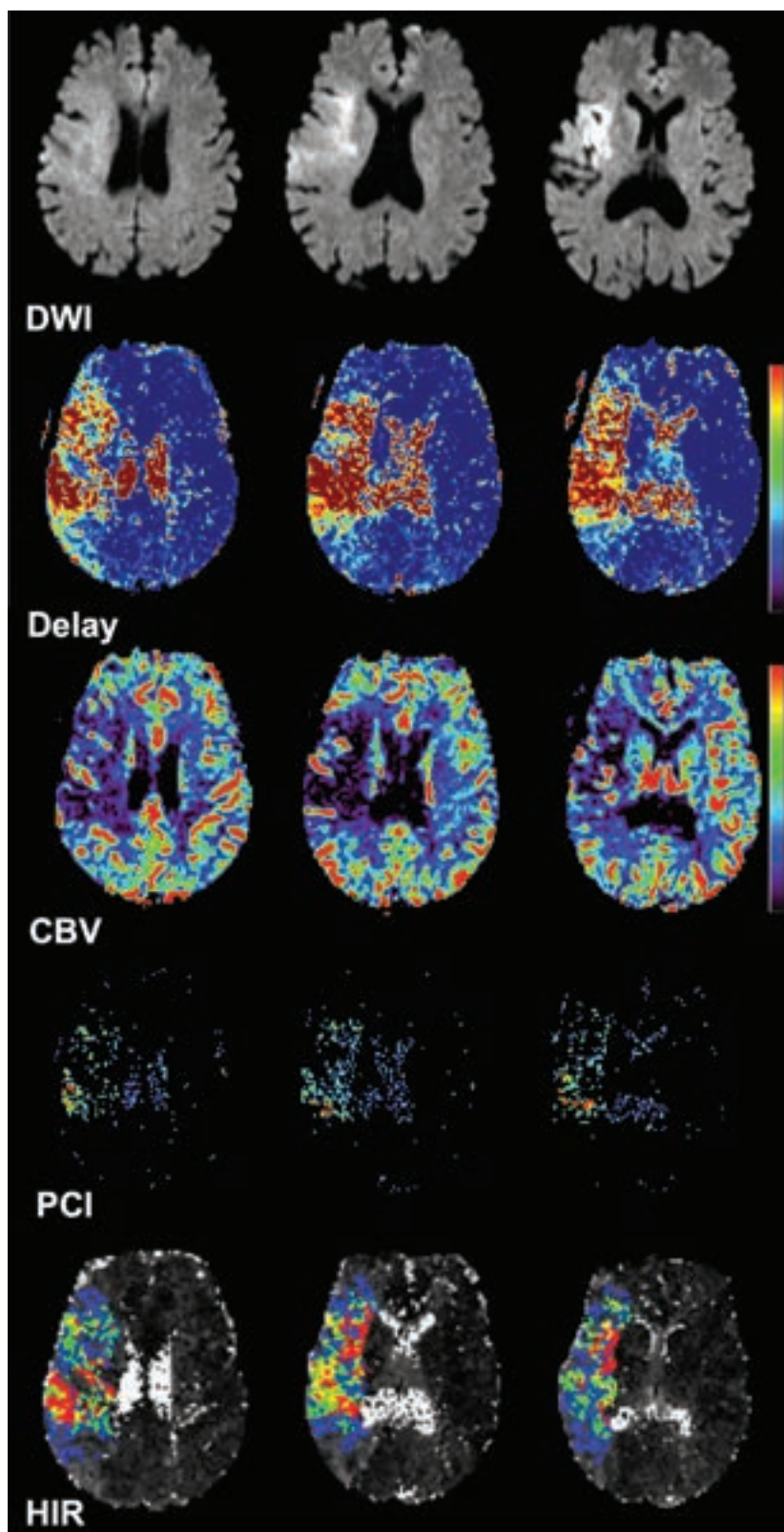


**FIG 4.** Example of discordance between the PCI and HIR in a patient with insufficient angiographic collaterals. Adult patient with left hemiparesis who underwent MR imaging approximately 1.3 hours after symptom onset. The patient has a right M1 occlusion (not shown). Aligned axial DWI, delay, CBV, PCI, and HIR maps from MR perfusion are shown. There is an ischemic core involving the right operculum, insula, and basal ganglia. There is low CBV in the region involved with PCI values estimated at 38, suggestive of insufficient collaterals. The estimated HIR is 0.30, suggestive of sufficient collaterals. Baseline catheter angiography (not shown) revealed poor collaterals (ASITN 1).

that when one incorporates relative CBV to evaluate late and venous phases of collaterals, the PCI captures some of this prognostic information that the Tmax alone does not provide. In our study, DSA-based collaterals were not a significant determinant of functional outcome, similar to the results of prior studies.<sup>34,35</sup>

### Limitations

Our study has several limitations. First, the retrospective nature introduces unknown biases. Despite looking into 8 years of data, the sample size remains relatively small due to strict inclusion criteria from a single institution. DSA collaterals were scored by 1 observer only, which precludes assessment of interobserver agreement. Another limitation is that the diagnostic performance of the PCI in determination of angiographic collaterals was lower in comparison with a prior report (accuracy of 76% versus 94% in the previous study).<sup>15</sup> This result may be due to inclusion of a larger data set in the present study and further supports the need for a more comprehensive and multi-center study to further validate and establish the PCI thresholds for broader clinical use.

### CONCLUSIONS

Results showed that the PCI outperforms the HIR in predicting of angiographic collaterals using DSA as the reference standard. In addition, while both the PCI and HIR are significant determinants of final infarct volume, only the PCI was significantly associated with infarct growth and functional independence. If its potential is realized in a larger study, the PCI, a quantitative index of collaterals derived from routinely performed perfusion imaging in patients with stroke, can be added as an extra imaging variable to provide a measure of baseline collateral status in patients with AIS. This information can be used for improved prognostication or treatment decision-making.

Disclosure forms provided by the authors are available with the full text and PDF of this article at [www.ajnr.org](http://www.ajnr.org).

## REFERENCES

- Sheth SA, Liebeskind DS. **Collaterals in endovascular therapy for stroke.** *Curr Opin Neurol* 2015;28:10–15 CrossRef Medline
- Liebeskind DS. **Collateral circulation.** *Stroke* 2003;34:2279–84 CrossRef Medline
- Christoforidis GA, Mohammad Y, Kehagias D, et al. **Angiographic assessment of pial collaterals as a prognostic indicator following intra-arterial thrombolysis for acute ischemic stroke.** *AJNR Am J Neuroradiol* 2005;26:1789–97 Medline
- Menon BK, Smith EE, Modi J, et al. **Regional leptomeningeal score on CT angiography predicts clinical and imaging outcomes in patients with acute anterior circulation occlusions.** *AJNR Am J Neuroradiol* 2011;32:1640–45 CrossRef Medline
- Jiang B, Ball RL, Michel P, et al. **Factors influencing infarct growth including collateral status assessed using computed tomography in acute stroke patients with large artery occlusion.** *Int J Stroke* 2019;14:603–12 CrossRef Medline
- Powers WJ, Rabinstein AA, Ackerson T, et al. **Guidelines for the early management of patients with acute ischemic stroke: 2019 Update to the 2018 Guidelines for the Early Management of Acute Ischemic Stroke—a Guideline for Healthcare Professionals from the American Heart Association/American Stroke Association.** *Stroke* 2019;50:e344–418 CrossRef Medline
- Menon BK, O'Brien B, Bivard A, et al. **Assessment of leptomeningeal collaterals using dynamic CT angiography in patients with acute ischemic stroke.** *J Cereb Blood Flow Metab* .2013;33:365–71 CrossRef Medline
- Lima FO, Furie KL, Silva GS, et al. **The pattern of leptomeningeal collaterals on CT angiography is a strong predictor of long-term functional outcome in stroke patients with large-vessel intracranial occlusion.** *Stroke* 2010;41:23160–22 CrossRef Medline
- Hernández-Pérez M, Puig J, Blasco G, et al. **Dynamic magnetic resonance angiography provides collateral circulation and hemodynamic information in acute ischemic stroke.** *Stroke* 2016;47:531–34 CrossRef Medline
- Ernst M, Forkert ND, Brehmer L, et al. **Prediction of infarction and reperfusion in stroke by flow- and volume-weighted collateral signal in MR angiography.** *AJNR Am J Neuroradiol* 2015;36:275–82 CrossRef Medline
- Menon BK, d'Esterre CD, Qazi EM, et al. **Multiphase CT angiography: a new tool for the imaging triage of patients with acute ischemic stroke.** *Radiology* 2015;275:510–20 CrossRef Medline
- Tsui B, Nour M, Chen I, et al. **MR angiography in assessment of collaterals in patients with acute ischemic stroke: a comparative analysis with digital subtraction angiography.** *Brain Sci* 2022;12:1181 CrossRef Medline
- Kim HJ, Lee SB, Choi JW, et al. **Multiphase MR angiography collateral map: functional outcome after acute anterior circulation ischemic stroke.** *Radiology* 2020;295:192–201 CrossRef Medline
- Olivot JM, Mlynash M, Inoue M, et al. **Hypoperfusion intensity ratio predicts infarct progression and functional outcome in the DEFUSE 2 cohort.** *Stroke* 2014;45:1018–23 CrossRef Medline
- Nael K, Doshi A, De Leacy R, et al. **MR perfusion to determine the status of collaterals in patients with acute ischemic stroke: a look beyond time maps.** *AJNR Am J Neuroradiol* 2018;39:219–25 CrossRef Medline
- Nael K, Sakai Y, Larson J, et al. **CT perfusion collateral index in assessment of collaterals in acute ischemic stroke with delayed presentation: comparison to single phase CTA.** *J Neuroradiol* 2022;49:1988–204 CrossRef Medline
- Guenego A, Fahed R, Albers GW, et al. **Hypoperfusion intensity ratio correlates with angiographic collaterals in acute ischaemic stroke with M1 occlusion.** *Eur J Neurol* 2020;27:864–70 CrossRef Medline
- Tomsick T, Broderick J, Carrozella J, et al. **Revascularization results in the Interventional Management of Stroke II trial.** *AJNR Am J Neuroradiol*. Mar 2008;29:582–87 CrossRef Medline
- Higashida RT, Furlan AJ, Roberts H, et al. **Trial design and reporting standards for intra-arterial cerebral thrombolysis for acute ischemic stroke.** *Stroke* 2003;34:e109–37 CrossRef Medline
- Boutelier T, Kudo K, Pautot F, et al. **Bayesian hemodynamic parameter estimation by bolus tracking perfusion weighted imaging.** *IEEE Trans Med Imaging* 2012;31:1381–95 CrossRef Medline
- An H, Ford AL, Vo K, et al. **Signal evolution and infarction risk for apparent diffusion coefficient lesions in acute ischemic stroke are both time- and perfusion-dependent.** *Stroke* 2011;42:1276–81 CrossRef Medline
- Guenego A, Mlynash M, Christensen S, et al. **Hypoperfusion ratio predicts infarct growth during transfer for thrombectomy.** *Ann Neurol* 2018;84:616–20 CrossRef Medline
- Lyndon D, van den Broek M, Niu B, et al. **Hypoperfusion index ratio correlates as a surrogate of collateral scoring on CT angiogram in large vessel stroke.** *AJNR Am J Neuroradiol* 2021;42:1380–86 CrossRef Medline
- Wang CM, Chang YM, Sung PS, et al. **Hypoperfusion index ratio as a surrogate of collateral scoring on CT angiogram in large vessel stroke.** *J Clin Med* 2021;10:1296 CrossRef Medline
- Arenillas JF, Cortijo E, García-Bermejo P, et al. **Relative cerebral blood volume is associated with collateral status and infarct growth in stroke patients in SWIFT PRIME.** *J Cereb Blood Flow Metab* 2018;38:1839–47 CrossRef Medline
- Mlynash M, Lansberg MG, Kemp S, et al. **Combination of Tmax and relative CBV perfusion parameters more accurately predicts CTA collaterals than a single perfusion parameter in DEFUSE 3.** *Stroke* 2019;50(Suppl) CrossRef
- Jerosch-Herold M, Hu X, Murthy NS, et al. **Time delay for arrival of MR contrast agent in collateral-dependent myocardium.** *IEEE Trans Med Imaging* 2004;23:881–90 CrossRef Medline
- Parthasarathy R, Kate M, Rempel JL, et al. **Prognostic evaluation based on cortical vein score difference in stroke.** *Stroke* 2013;44:2748–54 CrossRef Medline
- Parthasarathy R, Sohn SI, Jeerakathil T, et al. **A combined arterial and venous grading scale to predict outcome in anterior circulation ischemic stroke.** *J Neuroimaging* 2015;25:969–77 CrossRef Medline
- Wardlaw JM, Keir SL, Bastin ME, et al. **Is diffusion imaging appearance an independent predictor of outcome after ischemic stroke?** *Neurology* 2002;59:1381–87 CrossRef Medline
- Saver JL, Johnston KC, Homer D, et al. **Infarct volume as a surrogate or auxiliary outcome measure in ischemic stroke clinical trial: the RANTTAS Investigators.** *Stroke* 1999;30:293–98 CrossRef Medline
- Ganesh A, Ospel JM, Menon BK, et al. **Assessment of discrepancies between follow-up infarct volume and 90-day outcomes among patients with ischemic stroke who received endovascular therapy.** *JAMA Netw Open* 2021;4:e2132376 CrossRef Medline
- Deng W, Teng J, Liebeskind D, et al. **Predictors of infarct growth measured by apparent diffusion coefficient quantification in patients with acute ischemic stroke.** *World Neurosurg* 2019;123:e797–802 CrossRef Medline
- Kauw F, Dankbaar JW, Martin BW, et al. **Collateral status in ischemic stroke: a comparison of computed tomography angiography, computed tomography perfusion, and digital subtraction angiography.** *J Comput Assist Tomogr* 2020;44:984–92 CrossRef Medline
- Jansen IG, Berkhemer OA, Yoo AJ, et al. **Comparison of CTA- and DSA-based collateral flow assessment in patients with anterior circulation stroke.** *AJNR Am J Neuroradiol* 2016;37:2037–42 CrossRef Medline



# DWI-Detected Ischemic Lesions after Endovascular Treatment for Cerebral Aneurysms: An Updated Systematic Review and Meta-analysis

Abiel Berhe Habtezeghi, Sherief Ghozy, Cem Bilgin, Hassan Kobeissi, Ramanathan Kadirvel, and David F. Kallmes



## ABSTRACT

**BACKGROUND AND PURPOSE:** DWI-detected ischemic lesions are potential complications of endovascular procedures that are performed to treat intracranial aneurysms. We completed a systematic review and meta-analysis to identify the occurrence of DWI-detected ischemic lesions after endovascular treatment for intracranial aneurysms.

**MATERIALS AND METHODS:** A systematic literature search of PubMed, the Web of Science, EMBASE, and Scopus between January 2000 and June 2022 of post-endovascular procedures for intracranial aneurysm studies was conducted using the Nested Knowledge AutoLit software. The main outcome was DWI-detected ischemic lesions within 5 days of the procedures. Information regarding associated risk factors such as the type of procedure, patient demographics, and aneurysm characteristics was also collected.

**RESULTS:** Twenty-nine studies with 2686 patients were included. The overall incidence of DWI ischemic lesions was 47.0% (95% CI, 39.6%–55.8%). The highest rate of lesions was seen with flow diversion at 62.4% (95% CI, 48.4%–80.5%), followed by complex procedures at 49.3% (95% CI, 29.5%–82.1%), stent-assisted coiling at 47.5% (95% CI, 34.6%–65.3%), simple coiling at 47.1% (95% CI, 35.7%–62.3%), and balloon-assisted coiling at 37.0% (95% CI, 28.3%–48.4%). The differences among different techniques were not statistically significant; however, there was significant heterogeneity and a significant risk of publication bias among included studies.

**CONCLUSIONS:** Many patients who undergo endovascular procedures for intracranial aneurysms present with new postprocedural DWI-detected ischemic lesions, regardless of the endovascular procedure used. Future studies and meta-analyses are needed to investigate early and long-term outcomes of such small infarcts.

**ABBREVIATION:** APC = annual percentage change

Endovascular neurointerventional procedures have been used since the 1990s with the development of different techniques that obviate the need for a craniotomy. Endovascular techniques include simple coiling, stent-assisted coiling, balloon-assisted coiling, and flow diversion. Although less invasive than traditional surgery, these techniques have been associated with periprocedural complications ranging from aneurysmal rupture to different

thromboembolism presentations. DWI-identified ischemic lesions after endovascular procedures have been reported to be a common occurrence with unknown clinical significance.<sup>1–4</sup>

The overall incidence of DWI-positive lesions previously reported after endovascular procedures was 1 in 2 patients; however, previous literature was based on outdated studies, older devices and techniques.<sup>1</sup> We propose that the rates of DWI-detected lesions following endovascular procedures may vary with the introduction of new endovascular techniques and procedures. To determine the overall incidence of perioperative infarctions on DWI in patients undergoing endovascular treatment for intracranial aneurysms, we performed a systematic review and meta-analysis.

## MATERIALS AND METHODS

### Literature Search and Inclusion Criteria

In-depth article reviews were performed by A.B.H. and S.G. using keywords such “flow diverter,” “coiling,” “pipeline,” “endovascular,” “DWI-MR imaging,” “diffusion,” “restricted diffusion,” “MR imaging,” “diffusion-weighted imaging,” “cerebral aneurysm,” and “intracranial aneurysm.” During the review process, the last set of

Received February 23, 2023; accepted after revision September 8.

From the Departments of Radiology (A.B.H., S.G., C.B., H.K., R.K., D.F.K.), and Neurologic Surgery (R.K.), Mayo Clinic, Rochester, Minnesota.

Research reported in this publication was supported, in part, by the National Institute of Neurological Disorders and Stroke of the National Institutes of Health under award No. R01NS076491.

The content of this work is solely the responsibility of the authors and does not necessarily represent the official views of the National Institutes of Health.

Please address correspondence to Abiel Berhe Habtezeghi, MD, Department of Radiology, Mayo Clinic Rochester, MN, 200 First St SW, Rochester, MN 55905; e-mail: abielberhe7@gmail.com; @AbielHabtezeghi

Indicates open access to non-subscribers at [www.ajnr.org](http://www.ajnr.org)

Indicates article with online supplemental data.

<http://dx.doi.org/10.3174/ajnr.A8024>

Boolean traits found in the Online Supplemental Data were applied. On June 10, 2022, this search algorithm was used to search PubMed, the Web of Science, EMBASE, and Scopus.

The inclusion criteria were observational studies or randomized controlled trials between January 2000 and June 2022 that consisted of at least 10 consecutive patients treated for intracranial aneurysms by endovascular means with endovascular coiling or flow diversion and DWI examinations performed within 5 days of endovascular treatment in all patients. In addition, the reference lists from included studies were retrieved for possible inclusion of missed publications. Exclusion criteria were studies that had <10 patients, reported outcomes of parent artery occlusion, included only symptomatic patients who underwent postoperative DWI, used intrasaccular devices (such as the Woven EndoBridge [WEB]; Sequent Medical), and conference proceedings. In addition, studies that did not provide the number of patients who had no lesions on DWI and studies for which an English translation was not available were excluded.

The current study used a novel semiautomated software platform (AutoLit, Nested Knowledge; <https://wiki.nested-knowledge.com/doku.php?id=wiki:autolit>) for screening of studies and extraction of data. Two independent reviewers performed the screening, and a third reviewer arbitrated disagreements. Baseline characteristics of patients and aneurysm types such as aneurysmal size, location, and rupture status were extracted. During data extraction, whenever >2 means for subgroups were available, the formula found in the Online Supplemental Data from the Cochrane Guide for Systematic Reviews and Metaanalysis was used.<sup>5</sup> The guidelines provided by the Preferred Reporting Items for Systematic Reviews and Meta-Analyses (PRISMA) and Meta-analysis Of Observational Studies in Epidemiology (MOOSE) were followed, as well.

### Outcomes and Patient Groups

DWI-detected ischemic lesions within 5 days of the endovascular procedure were the primary end point. Treatment groups were stratified by the type of procedure: simple coiling, stent-assisted coiling, balloon-assisted coiling, and flow diversion. When  $\geq 2$  procedures and multiple catheters were used, it was termed a complex procedure. Patient sex (male versus female), aneurysm size (considered small if <10 mm, giant if >10 mm),<sup>6</sup> location (anterior or posterior circulation), and rupture status (ruptured or unruptured) were dichotomized.

### Risk of Bias Assessment

We selected items from the Newcastle-Ottawa Quality Assessment Scale to fit the type of included studies. In 3 domains with 8 criteria and a maximum score of 8, we queried the following study characteristics using a previous study by one of the authors: 1) patient groups clearly defined (1 point given if patient groups were clearly defined by the type of endovascular procedure, zero points given if not); 2) outcomes reported (1 point for reports taken from hospital data, 2 points for reports by radiologists for the study using DWI); 3) outcomes reported for each patient group studied (1 point given if an outcome was reported for each procedure, zero points given if not); 4) imaging interpreted by an independent reader or interpreted by the operator (1 point if independent readers read it, zero points given if not); 5) readers

blinded to the clinical status of the patient (1 point given if blinded, zero points given if not); 6) multiple readers used and interobserver agreement assessed (1 point given if interobserver agreement was assessed, zero points given if not); and 7) the study followed a specific study protocol in which all patients underwent MR imaging at the same time point (1 point given if the timing of the postprocedural MR imaging was provided, zero points given if not).<sup>1</sup>

### Statistical Analysis

The cumulative incidence rates with corresponding 95% CIs were calculated using R statistical and computing software, Version 4.2.2 (<http://www.r-project.org/>) and the package 'meta' (<https://cran.r-project.org/web/packages/meta/meta.pdf>). A random-effects model was used to pool the data due to methodologic heterogeneity among the included studies, and subgroup analysis was performed to obtain the estimate per year. Heterogeneity was assessed using the Cochran Q and  $I^2$  tests.  $P$  values < .05 for the Q statistic indicated statistical significance. An  $I^2$  of >50% suggested moderate-to-high heterogeneity. Whenever there were  $\geq 10$  studies included, the Egger regression test was used to assess publication bias. If publication bias existed, we used the trim-and-fill method to adjust for funnel plot asymmetry and calculate the bias-adjusted estimates.<sup>7,8</sup>

By means of the Joinpoint Regression Trend Analysis Software, Version 4.9.1.0 (<https://surveillance.cancer.gov/joinpoint/>), the pooled cumulative incidence rates and their standard errors were used to conduct a joinpoint regression analysis to explore any trends across the years.<sup>9,10</sup> This was conducted to calculate the average annual percentage change and annual percentage change (APC), selecting the best-fitting piecewise continuous log-linear model. The minimum number of "joinpoints" required to fit the data was determined using a permutation test.<sup>11,12</sup> The weighted Bayesian Information Criterion was the model adopted, and the empirical quantile methods were used to estimate confidence intervals.<sup>13</sup> The empirical method does not produce a test statistic or  $P$  value.<sup>13</sup>

## RESULTS

### Search Results and Patient Population

The literature search retrieved 491 studies, from which 209 duplicate studies were removed. From the remaining 282 studies, title and abstract screening resulted in 160 studies being excluded. Of the 122 studies remaining, full-text screening resulted in another 93 studies being excluded, as illustrated in Fig 1, which shows the process of identifying studies through databases and registers.

### Risk of Bias

Of the 29 studies included in this meta-analysis, 2 had a very high risk of bias with scores between 0 and 3 points, 22 had a high risk of bias with scores of 4–6 points, and 5 had a low risk of bias scoring 7–8 points, as determined by the Modified Newcastle Ottawa Scale.<sup>14</sup>

### Characteristics of the Included Studies

Twenty-nine studies with a total of 2686 patients presenting with 3687 intracranial aneurysms fulfilled our inclusion criteria and composed our analysis.<sup>15–43</sup> Endovascular procedures were simple coiling in 1184 patients, stent-assisted coiling in 662 patients, balloon-assisted coiling in 328 patients, flow diversion in 211 patients, and complex procedures in 301 patients. From studies that

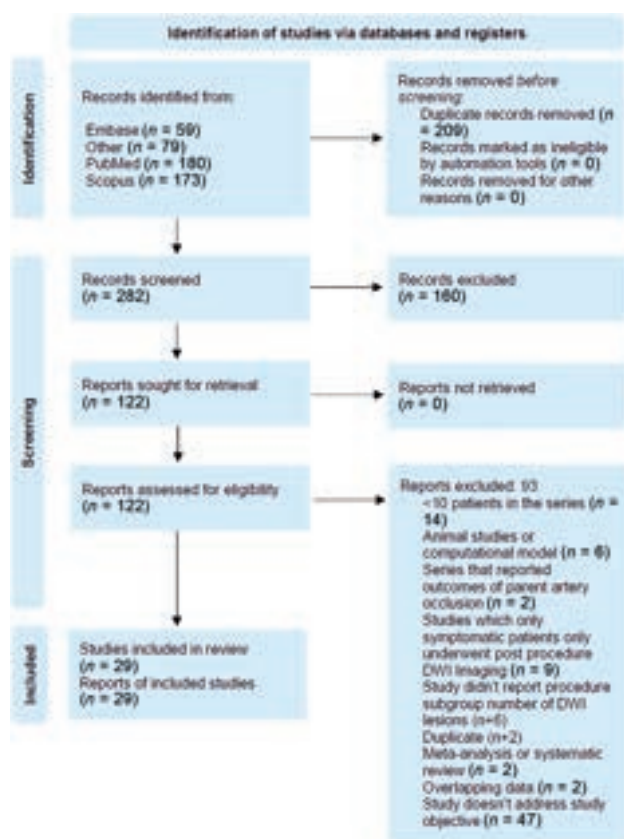


FIG 1. Identification of studies via databases and registers.

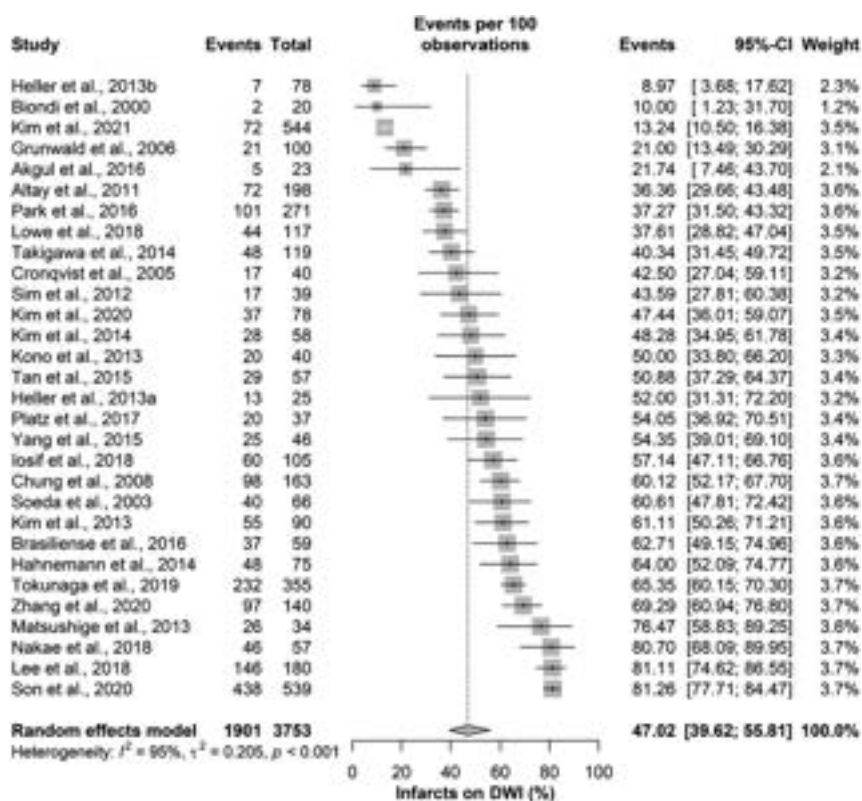


FIG 2. Infarcts on DWI.

reported aneurysm rupture status, 275 were ruptured during treatment, while 2552 were unruptured. Among the studies that reported the location of the aneurysms, 1624 were in the anterior circulation and 510 were in the posterior circulation.

### Study Outcomes

The overall incidence of DWI lesions was 47.0% (95% CI, 39.6%–55.8%), with significant heterogeneity among the included studies ( $I^2 = 95\%$ ;  $P$  value  $< .001$ ; Fig 2). Moreover, there was a significant risk of publication bias as assessed with the Egger regression test ( $P$  value  $< .001$ ; Fig 3).

On further subgrouping based on the treatment technique used, the highest rate of lesions was seen with flow diversion at 62.4% (95% CI, 48.4%–80.5%), complex procedures at 49.3% (95% CI, 29.5%–82.1%), stent-assisted coiling at 47.5% (95% CI, 34.6%–65.3%), simple coiling at 47.3% (95% CI, 35.5%–63.7%), and balloon-assisted coiling at 35.9% (95% CI, 25.5%–50.6%). The differences among different techniques were not statistically significant ( $P$  value = .139), with significant heterogeneity among the included studies in all subgroups (Fig 4).

For trend analysis, there was a significant reduction in DWI lesions through the full range of years from 2000 to 2022, with an average annual percent change of  $-5.0$  (95% CI,  $-7.6$  to  $-1.9$ ). Moreover, there was 1 joinpoint identified in 2019, with a significant reduction in detected ischemic lesions (APC =  $-50.0$ ; 95% CI,  $-63.1$  to  $-35.0$ ) after a relative stability in rates before that (APC =  $1.6$ ; 95% CI,  $-0.2$ – $5.0$ ; Online Supplemental Data).

### Impact of Aneurysm Characteristics and Sex

Aneurysms were more likely to be in the anterior circulation compared with the posterior circulation in DWI-detected lesions (OR = 8.56; 95% CI, 2.97–24.7,  $P$  value  $< .001$ ). Men were less likely than women to have aneurysms with DWI-detected lesions (OR = 0.15; 95% CI, 0.1–0.22,  $P$  value  $< .001$ ). Large-sized aneurysms were less common than small-sized aneurysms (OR = 0.05; 95% CI, 0.02–0.16,  $P$  value  $< .001$ ), while rupture status was comparable (OR = 0.25; 95% CI, 0.02–2.2,  $P$  value = 0.21). For all aneurysm characteristics and sex of patients, there was significant heterogeneity among the included studies (Fig 5).

### DISCUSSION

Our systematic review and meta-analysis found that the incidence of DWI-positive lesions after endovascular procedures for intracranial aneurysms was 47%. We found no statistically significant difference among techniques. These results highlight the high incidence of DWI-positive lesions, which are statistically similar among different endovascular treatments.

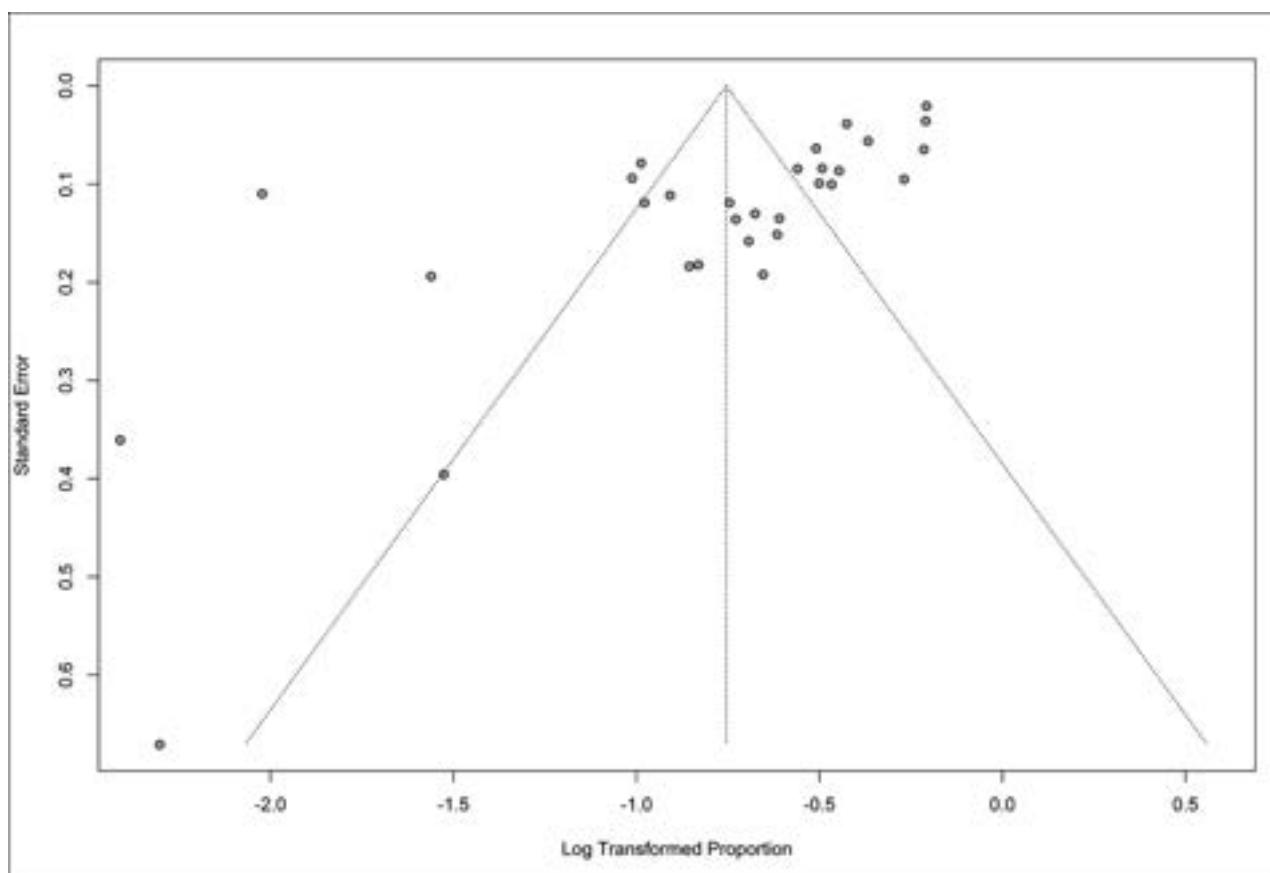


**FIG 3.** Publication bias as assessed with the Egger regression test.

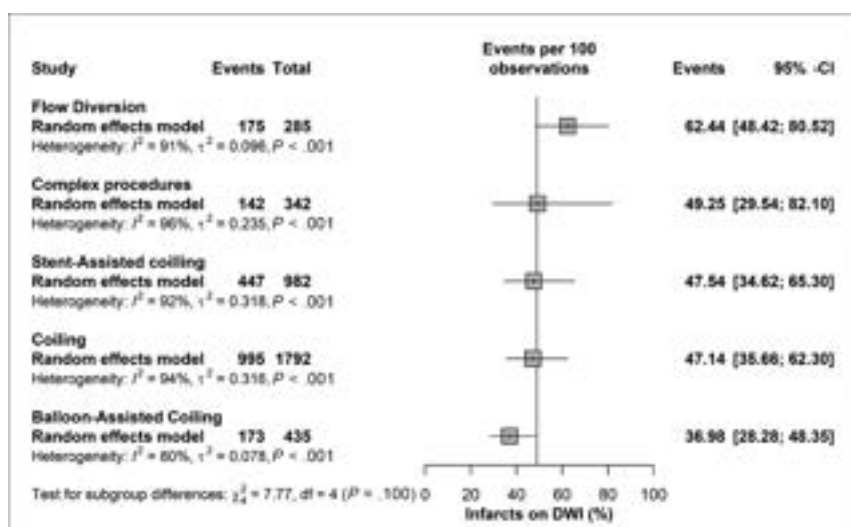


**FIG 4.** The subgroup of treatment technique used and DWI lesions.

Previous studies have examined the clinical impact of DWI-detected lesions. Almost half of these lesions are asymptomatic, and ischemic lesions have been shown to regress if their size is small ( $<5$  mm), resulting in favorable rates of good clinical outcomes.<sup>44</sup> Studies are needed to further validate these findings using clinical outcome measures such as a standardized method of assessing the

clinical relevance of lesions like the mRS. Other literature has evaluated the prevention of this postprocedural complication with remote ischemic preconditioning, which has been shown to be safe and effective.<sup>45</sup>

We found that the rate of silent infarcts in patients treated with flow diverters was higher than in those treated with coils alone, though this was not statistically significant. Flow diversion leads to more thromboembolic complications than coiling alone, despite the inherent thrombogenic properties of coils and flow diverters. Because flow diverters are high density and have large endoluminal surfaces, they have a high thrombosis risk in the parent arteries.

An embolized thrombus can occur from the shearing stress caused by blood flowing through the device. Because lower density coils are placed in the aneurysm sac outside the cerebral circulation, thrombi forming on them are less likely to embolize.<sup>1</sup>

Studies have shown that DWI-positive lesions are not significantly different between ruptured and unruptured aneurysms (as



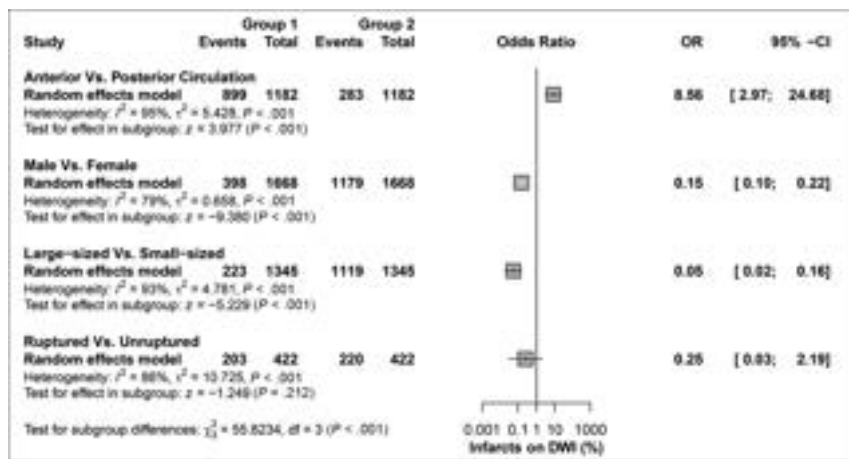


**FIG 5.** Risk factors and DWI lesions.

shown in Fig 5), are associated with long procedural times, and decrease in incidence with postprocedural anticoagulation, all of which are consistent with the results of our present analysis.<sup>46</sup> Additionally, previous literature has demonstrated that the presence or number of ischemic lesions on DWI is not related to cognitive changes following coil embolization.<sup>47</sup> Periprocedural thromboembolic events identified on DWI have been shown to be reduced with a dual-antiplatelet agent (for unruptured aneurysms), and patients are given preoperative low-molecular-weight heparin to prevent this complication.<sup>48</sup>

We could not identify a discernible trend in the incidence of DWI lesions with time. The absence of a notable temporal trend suggests that the occurrence of DWI lesions did not change before and after 2017 (Online Supplemental Data).

Our study has limitations. We included retrospective, non-randomized studies, and studies were inconsistent in their reporting of results. We did not consider the use of anticoagulants and individual antiplatelet therapy. We could not account for the differences among institutions performing endovascular procedures, the experience of the interventionalists who performed the procedures, and the radiologists who read the DWIs. There were associations between baseline characteristics such as female sex, anterior aneurysm, small aneurysm size, and the incidence of postprocedural DWI lesions. The studies included did not consistently report atherosclerotic risk factors, use of anticoagulants, and other aneurysmal characteristics.<sup>32</sup> Finally, we did not have access to individual patient data, limiting the data that could be analyzed. In our study, the presence or absence of DWI lesions was used as the primary criterion for determining their occurrence. However, we acknowledge that a more nuanced approach, considering the size, number, and distribution of DWI lesions, could provide a more comprehensive understanding of the ischemic risk and its clinical implications. Because these details are currently lacking in the literature, further studies are needed to address these concerns.

## CONCLUSIONS

In this systematic review and meta-analysis of 2686 patients, the rate of DWI-detected ischemic lesions was 47.0% (95% CI, 39.6%–

55.8%). Rates of lesions were statistically similar among all included endovascular treatments. Further prospective and randomized studies are needed to elucidate the DWI-detected ischemic lesion rate after endovascular procedures and their lasting complications.

## ACKNOWLEDGMENTS

The authors acknowledge Karl Holub, Stephen Mead, Jeffrey Johnson, and Darian Lehmann-Plantenberg for their design, development, and support of the Nested Knowledge meta-analytical software. The authors thank Desiree Lanzino, PhD, and Sonia Watson for their assistance in editing the manuscript.

**Disclosure forms** provided by the authors are available with the full text and PDF of this article at [www.ajnr.org](http://www.ajnr.org).

## REFERENCES

- Bond KM, Brinjikji W, Murad MH, et al. **Diffusion-weighted imaging-detected ischemic lesions following endovascular treatment of cerebral aneurysms: a systematic review and meta-analysis.** *AJNR Am J Neuroradiol* 2017;38:304–09 CrossRef Medline
- Choi SH, Na DL, Chung CS, et al. **Diffusion-weighted MRI in vascular dementia.** *Neurology* 2000;54:83–89 CrossRef Medline
- Ihn YK, Shin SH, Baik SK, et al. **Complications of endovascular treatment for intracranial aneurysms: management and prevention.** *Interv Neuroradiol* 2018;24:237–45 CrossRef Medline
- Zhao J, Lin H, Summers R, et al. **Current treatment strategies for intracranial aneurysms: an overview.** *Angiology* 2018;69:17–30 CrossRef Medline
- Higgins JPT, Thomas J, Chandler J, et al, eds. *Cochrane Handbook for Systematic Reviews of Interventions*. 2nd Edition. Chichester (UK): John Wiley & Sons; 2019
- Merritt WC, Berns HF, Ducruet AF, et al. **Definitions of intracranial aneurysm size and morphology: a call for standardization.** *Surg Neurol Int* 2021;12:506 CrossRef Medline
- Duval S, Tweedie R. **Trim and fill: A simple funnel-plot-based method of testing and adjusting for publication bias in meta-analysis.** *Biometrics* 2000;56:455–63 CrossRef Medline
- Shi L, Lin L. **The trim-and-fill method for publication bias: practical guidelines and recommendations based on a large database of meta-analyses.** *Medicine (Baltimore)* 2019;98:e15987 CrossRef Medline
- Dibas M, Doheim MF, Ghozy S, et al. **Incidence and survival rates and trends of skull base chondrosarcoma: a population-based study.** *Clin Neurol Neurosurg* 2020;198:106153 CrossRef Medline
- Ghozy S, Dibas M, Afifi AM, et al. **Primary cerebral lymphoma' characteristics, incidence, survival, and causes of death in the United States.** *J Neurol Sci* 2020;415:116890 CrossRef Medline
- Kim HJ, Fay MP, Feuer EJ, et al. **Permutation tests for joinpoint regression with applications to cancer rates.** *Stat Med* 2000;19:335–51 CrossRef Medline
- Politis M, Higuera G, Chang LR, et al. **Trend analysis of cancer mortality and incidence in Panama, using joinpoint regression analysis.** *Medicine (Baltimore)* 2015;94:e970 CrossRef Medline
- Kim HJ, Chen HS, Midthune D, et al. **Data-driven choice of a model selection method in joinpoint regression.** *J Appl Stat* 2023;50:1992–2013 CrossRef Medline
- Wells GA, Shea B, O'Connell D, et al. **The Newcastle-Ottawa Scale (NOS) for assessing the quality of nonrandomised studies in meta-analyses.** *Clin Epidemiol* 2000 [https://www.ohri.ca/programs/clinical\\_epidemiology/oxford.asp](https://www.ohri.ca/programs/clinical_epidemiology/oxford.asp). Accessed July 21, 2022

15. Akgul E, Onan HB, Akpınar S, et al. **The DERIVO Embolization Device in the treatment of intracranial aneurysms: short- and mid-term results.** *World Neurosurg* 2016;95:229–40 CrossRef Medline
16. Biondi A, Oppenheim C, Vivas E, et al. **Cerebral aneurysms treated by Guglielmi detachable coils: evaluation with diffusion-weighted MR imaging.** *AJNR Am J Neuroradiol* 2000;21:957–63 Medline
17. Bräslinse LB, Stanley MA, Grewal SS, et al. **Silent ischemic events after Pipeline Embolization Device: a prospective evaluation with MR diffusion-weighted imaging.** *J Neurointerv Surg* 2016;8:1136–39 CrossRef Medline
18. Cronqvist M, Wirestam R, Ramgren B, et al. **Diffusion and perfusion MRI in patients with ruptured and unruptured intracranial aneurysms treated by endovascular coiling: complications, procedural results, MR findings and clinical outcome.** *Neuroradiology* 2005;47:855–73 CrossRef Medline
19. Grunwald IQ, Papanagiotou P, Politi M, et al. **Endovascular treatment of unruptured intracranial aneurysms: occurrence of thromboembolic events.** *Neurosurgery* 2006;58:612–18 CrossRef Medline
20. Heller RS, Dandamudi V, Calnan D, et al. **Neuroform intracranial stenting for aneurysms using simple and multi-stent technique is associated with low risk of magnetic resonance diffusion-weighted imaging lesions.** *Neurosurgery* 2013;73:582–90; discussion 590–91 CrossRef Medline
21. Heller RS, Dandamudi V, Lanfranchi M, et al. **Effect of antiplatelet therapy on thromboembolism after flow diversion with the Pipeline Embolization Device.** *J Neurosurg* 2013;119:1603–10 CrossRef Medline
22. Iosif C, Lecomte JC, Pedrolo-Silveira E, et al. **Evaluation of ischemic lesion prevalence after endovascular treatment of intracranial aneurysms, as documented by 3-T diffusion-weighted imaging: a 2-year, single-center cohort study.** *J Neurosurg* 2018;128:982–91 CrossRef Medline
23. Kim JK, Choi JH, Kim BS, et al. **Association of anterior cerebral artery variants and cerebral infarction in patients with balloon-assisted coil embolization for unruptured internal carotid artery aneurysms.** *World Neurosurg* 2021;147:e69–77 CrossRef Medline
24. Kim MJ, Lim YC, Oh SY, et al. **Thromboembolic events associated with electrolytic detachment of Guglielmi detachable coils and target coils: comparison with use of diffusion-weighted MR imaging.** *J Korean Neurosurg Soc* 2013;54:19–24 CrossRef Medline
25. Kim MS, Jo KI, Yeon JY, et al. **Association between postprocedural infarction and antiplatelet drug resistance after coiling for unruptured intracranial aneurysms.** *AJNR Am J Neuroradiol* 2016;37:1099–105 CrossRef Medline
26. Kim SH, Lee H, Kim SB, et al. **Differences in thromboembolism after stent-assisted coiling for unruptured aneurysms between aspirin plus clopidogrel and ticagrelor.** *J Clin Neurosci* 2020;82:128–33 CrossRef Medline
27. Kono K, Shintani A, Yoshimura R, et al. **Triple antiplatelet therapy with addition of cilostazol to aspirin and clopidogrel for Y-stent-assisted coil embolization of cerebral aneurysms.** *Acta Neurochir (Wien)* 2013;155:1549–57 CrossRef Medline
28. Lee SH, Jang MU, Kang J, et al. **Impact of reducing the procedure time on thromboembolism after coil embolization of cerebral aneurysms.** *Front Neurol* 2018;9:1125 CrossRef Medline
29. Lowe SR, Bhalla T, Tillman H, et al. **A comparison of diffusion-weighted imaging abnormalities following balloon remodeling for aneurysm coil embolization in the ruptured vs unruptured setting.** *Neurosurgery* 2018;82:516–24 CrossRef Medline
30. Matsushige T, Kiura Y, Sakamoto S, et al. **Multiple antiplatelet therapy contributes to the reversible high signal spots on diffusion-weighted imaging in elective coiling of unruptured cerebral aneurysm.** *Neuroradiology* 2013;55:449–57 CrossRef Medline
31. Nakae R, Nagaishi M, Kawamura Y, et al. **Microhemorrhagic transformation of ischemic lesions on T2\*-weighted magnetic resonance imaging after Pipeline Embolization Device treatment.** *J Neurosurg* 2018 May 1 [Epub ahead of print] CrossRef Medline
32. Park JC, Lee DH, Kim JK, et al. **Microembolism after endovascular coiling of unruptured cerebral aneurysms: incidence and risk factors.** *J Neurosurg* 2016;124:777–83 CrossRef Medline
33. Petrov A, Rentsenkhuu G, Nota B, et al. **Initial experience with the novel p64MW HPC flow diverter from a cohort study in unruptured anterior circulation aneurysms under dual antiplatelet medication.** *Interv Neuroradiol* 2021;27:42–50 CrossRef Medline
34. Pikis S, Mantziaris G, Mamalis V, et al. **Diffusion weighted image documented cerebral ischemia in the postprocedural period following Pipeline Embolization Device with shield technology treatment of unruptured intracranial aneurysms: a prospective, single center study.** *J Neurointerv Surg* 2020;12:407–11 CrossRef Medline
35. Platz J, Wagner M, Güresir E, et al. **Early diffusion-weighted MRI lesions after treatment of unruptured intracranial aneurysms: a prospective study.** *J Neurosurg* 2017;126:1070–78 CrossRef Medline
36. Sim SY, Shin YS. **Silent microembolism on diffusion-weighted MRI after coil embolization of cerebral aneurysms.** *Neurointervention* 2012;7:77–84 CrossRef Medline
37. Soeda A, Sakai N, Sakai H, et al. **Thromboembolic events associated with Guglielmi detachable coil embolization of asymptomatic cerebral aneurysms: evaluation of 66 consecutive cases with use of diffusion-weighted MR imaging.** *AJNR Am J Neuroradiol* 2003;24:127–32 Medline
38. Son W, Kang DH. **Risk factor analysis of delayed intracerebral hemorrhage after coil embolization of unruptured cerebral aneurysms.** *Front Neurol* 2020;11:584596 CrossRef Medline
39. Takigawa T, Suzuki K, Sugiura Y, et al. **Thromboembolic events associated with single balloon-, double balloon-, and stent-assisted coil embolization of asymptomatic unruptured cerebral aneurysms: evaluation with diffusion-weighted MR imaging.** *Neuroradiology* 2014;56:1079–86 CrossRef Medline
40. Tan LA, Keigher KM, Munich SA, et al. **Thromboembolic complications with Pipeline Embolization Device placement: impact of procedure time, number of stents and pre-procedure P2Y12 reaction unit (PRU) value.** *J Neurointerv Surg* 2015;7:217–21 CrossRef Medline
41. Tokunaga K, Hatano T, Nakahara I, et al. **Factors associated with postprocedural diffusion-weighted imaging-positive lesions in endovascular treatment for unruptured cerebral aneurysms.** *World Neurosurg* 2019;130:e457–62 CrossRef Medline
42. Yang H, Li Y, Jiang Y, et al. **Thromboelastography for monitoring platelet function in unruptured intracranial aneurysm patients undergoing stent placement.** *Interv Neuroradiol* 2015;21:61–68 CrossRef Medline
43. Altay T, Kang HI, Woo HH, et al. **Thromboembolic events associated with endovascular treatment of cerebral aneurysms.** *J Neurointerv Surg* 2011;3:147–50 CrossRef Medline
44. Iosif C, Camilleri Y, Saleme S, et al. **Diffusion-weighted imaging-detected ischemic lesions associated with flow-diverting stents in intracranial aneurysms: safety, potential mechanisms, clinical outcome, and concerns.** *J Neurosurg* 2015;122:627–36 CrossRef Medline
45. Mohammad Seyedasadat S, Rangel Castilla L, Lanzino G, et al. **Remote ischemic preconditioning for elective endovascular intracranial aneurysm repair: a feasibility study.** *Neuroradiol J* 2019;32:166–72 CrossRef Medline
46. Lee SH, Kim SH, Jang JH, et al. **Diffusion-weighted imaging-positive lesions following endovascular treatment for ruptured and unruptured aneurysms: its incidence according to antithrombotic drugs.** *J Cerebrovasc Endovasc Neurosurg* 2022;24:249–56 CrossRef Medline
47. Kang DH, Kim BM, Kim DJ, et al. **MR-DWI-positive lesions and symptomatic ischemic complications after coiling of unruptured intracranial aneurysms.** *Stroke* 2013;44:789–91 CrossRef Medline
48. Edwards NJ, Jones WH, Sanzgiri A, et al. **Antiplatelet therapy for the prevention of peri-coiling thromboembolism in high-risk patients with ruptured intracranial aneurysms.** *J Neurosurg* 2017;127:1326–32 CrossRef Medline

# Mesoscopic Assessment of Microstructure in Glioblastomas and Metastases by Merging Advanced Diffusion Imaging with Immunohistopathology

Urs Würtemberger, Daniel Erny, Alexander Rau, Jonas A. Hosp, Veysel Akgün, Marco Reisert, Valerij G. Kiselev, Jürgen Beck, Sonja Jankovic, Peter C. Reinacher, Marc Hohenhaus, Horst Urbach, Martin Diebold, and Theo Demerath



## ABSTRACT

**BACKGROUND AND PURPOSE:** Glioblastomas and metastases are the most common malignant intra-axial brain tumors in adults and can be difficult to distinguish on conventional MR imaging due to similar imaging features. We used advanced diffusion techniques and structural histopathology to distinguish these tumor entities on the basis of microstructural axonal and fibrillar signatures in the contrast-enhancing tumor component.

**MATERIALS AND METHODS:** Contrast-enhancing tumor components were analyzed in 22 glioblastomas and 21 brain metastases on 3T MR imaging using DTI-fractional anisotropy, neurite orientation dispersion and density imaging–orientation dispersion, and diffusion microstructural imaging–micro-fractional anisotropy. Available histopathologic specimens (10 glioblastomas and 9 metastases) were assessed for the presence of axonal structures and scored using 4-level scales for Bielschowsky staining (0: no axonal structures, 1: minimal axonal fragments preserved, 2: decreased axonal density, 3: no axonal loss) and glial fibrillary acid protein expression (0: no glial fibrillary acid protein positivity, 1: limited expression, 2: equivalent to surrounding parenchyma, 3: increased expression).

**RESULTS:** When we compared glioblastomas and metastases, fractional anisotropy was significantly increased and orientation dispersion was decreased in glioblastomas (each  $P < .001$ ), with a significant shift toward increased glial fibrillary acid protein and Bielschowsky scores. Positive associations of fractional anisotropy and negative associations of orientation dispersion with glial fibrillary acid protein and Bielschowsky scores were revealed, whereas no association between micro-fractional anisotropy with glial fibrillary acid protein and Bielschowsky scores was detected. Receiver operating characteristic curves revealed high predictive values of both fractional anisotropy (area under the curve = 0.8463) and orientation dispersion (area under the curve = 0.8398) regarding the presence of a glioblastoma.

**CONCLUSIONS:** Diffusion imaging fractional anisotropy and orientation dispersion metrics correlated with histopathologic markers of directionality and may serve as imaging biomarkers in contrast-enhancing tumor components.

**ABBREVIATIONS:** AD = axial diffusivity; AMICO = Accelerated Microstructure Imaging Via Convex Optimization; AUC = area under the curve; DMI = diffusion microstructure imaging; FA = fractional anisotropy; GBM = glioblastoma; GFAP = glial fibrillary acidic protein; ICVF = intracellular volume fraction; MD = mean diffusivity; NODDI = neurite orientation dispersion and density imaging; OD = orientation dispersion; RD = radial diffusivity; ROC = receiver operating characteristic; V-CSF = free water/CSF volume fraction; V-intra = intra-axonal volume fraction; V-ISO = isotropic volume

**G**lioblastomas (GBMs) and metastases are the most common malignant intra-axial brain tumors in adults. Because these entities require distinct clinical management, differentiation is important.

Received June 8, 2023; accepted after revision August 30.

From the Department of Neuroradiology (U.W., A.R., V.A., H.U., T.D.), Institute of Neuropathology (D.E., M.D.), Department of Diagnostic and Interventional Radiology (A.R.), Department of Neurology and Neurophysiology (J.A.H.), Department of Medical Physics (M.R., V.G.K.), Department of Stereotactic and Functional Neurosurgery (M.R., P.C.R.), and Department of Neurosurgery (J.B., M.H.), Faculty of Medicine, Medical Center—University of Freiburg, University of Freiburg, Freiburg, Germany; Department of Radiology (S.J.), Faculty of Medicine, University Clinical Center Nis, University of Nis, Nis, Serbia; Fraunhofer Institute for Laser Technology (P.C.R.), Aachen, Germany; IMM-PACT Clinician Scientist Program (M.D.), and Berta-Ottenstein-Program for Advanced Clinician Scientists (D.E.), Faculty of Medicine, University of Freiburg, Freiburg, Germany.

Martin Diebold and Theo Demerath contributed to this work equally and share last authorship.

While the definite diagnosis is based on histopathology, MR imaging is the technique of choice for the noninvasive assessment of cerebral neoplasms. The differentiation of GBM and metastases in MR imaging is challenging though because features such as central necrosis, irregular contrast-enhanced margins, and peripheral edema may be present in both entities.<sup>1</sup> The distinction is particularly important when solitary intracerebral lesions are present.

Because metastases represent secondary brain tumors displacing normal brain tissue and GBMs are brain-derived tumors with

Please address correspondence to Urs Würtemberger, MD, Department of Neuroradiology, Breisacher Straße 64, 79106 Freiburg, Germany; e-mail: urs.wuertemberger@uniklinik-freiburg.de



Indicates article with online supplemental data.  
<http://dx.doi.org/10.3174/ajnr.A8022>

infiltrative growth, axonal components, and defined structural proteins (eg, glial fibrillary acidic protein [GFAP]), microstructural differences are conceivable within contrast-enhancing tumor areas.<sup>2</sup> Moreover, both tumor entities are histomorphologically well-distinguished by the presence of glial structural proteins such as GFAP, being highly abundant in GBM, but sporadic or absent in metastases,<sup>3,4</sup> and the extent of axonal remnants, which are frequently observed in diffusely growing gliomas but rarely in solid metastases.<sup>5</sup>

Current diffusion-weighted MR imaging provides the opportunity to noninvasively study the microstructure in vivo in a mesoscopic approach.<sup>6</sup> Our study aims to bridge the gap between the millimeter resolution of MR imaging at the voxel level and the histopathologically comprehensible structural changes at the subvoxel or micrometer level.<sup>7</sup> DTI is the most established technique for in vivo investigations of the brain microstructure<sup>8</sup> and allows graduating the directionality of diffusion, which is expressed in fractional anisotropy (FA). Numerous previous studies have shown an increase in FA within the central tumor component in GBM compared with metastases,<sup>9–13</sup> whereas some studies have shown inconclusive results<sup>14,15</sup> or even a decrease in FA in GBM.<sup>16</sup> FA is sensitive to anisotropic cell structures such as axons, and several studies have suggested that FA correlates with the extent of GFAP-positive astrocytes<sup>17–19</sup> but is also sensitive to their orientation dispersion (OD).<sup>20</sup> This finding is a major limitation for the use of FA as a biomarker of tissue integrity, especially in regions with complex microarchitecture. Further investigation of contrast-enhancing tumor components is also of interest because proliferative tumor components are expected there and correlation with histopathology is still lacking.

Novel, biophysically motivated advanced multicompartamental imaging techniques such as neurite orientation dispersion and density imaging (NODDI) or diffusion microstructure imaging (DMI) allow a more specific approximation of the microstructure, for example by quantifying free water<sup>21</sup> or the axonal density in white matter.<sup>7</sup> Furthermore, microFA better reflects the underlying microstructure compared with FA in areas with increased OD, independent of, for example, increased axonal fiber crossings.<sup>20</sup> Therefore, we aimed to additionally investigate the OD and microFA in comparison with FA.

On the basis of the distinct histologic characteristics of GBM and metastases, we hypothesized that microstructural differences between the 2 entities within the proliferative, contrast-enhancing tumor components are traceable with directionality-based diffusion metrics such as DTI-FA, NODDI-OD, and DMI-microFA and are associated with histopathology in terms of the presence of axonal and fibrillary microstructure and/or GFAP expression.

## MATERIALS AND METHODS

### Patient and Imaging Characteristics

This retrospective study was approved by the local institutional review board of Medical Center–University of Freiburg (EK:400/20). All procedures performed in studies involving human participants were in accordance with the ethics standards of the institutional and national research committee and with the 1964 Helsinki declaration

### Patient characteristics and ROI (contrast-enhancing tumor area) derived diffusion metrics<sup>a</sup>

	GBM	Metastasis	P Value (GBM vs Met)
No.	22	21	
Sex (male/female)	11/11	12/9	<i>P</i> = .82
Age (yr)	65.6 (12.7)	66.6 (11.8)	<i>P</i> = .99
FA	0.16 (0.04)	0.11 (0.02)	<i>P</i> < .001
OD	0.43 (0.08)	0.56 (0.10)	<i>P</i> < .001
microFA	0.29 (0.10)	0.27 (0.10)	<i>P</i> = .56

**Note:**—Met indicates Metastasis.

<sup>a</sup>Data are given as mean and standard deviation (SD).

and its later amendments. Informed written consent was waived by the local ethics committee due to the purely retrospective analysis.

Within 4 years (January 2018 to February 2022), a total of 43 patients with newly diagnosed brain metastases (*n* = 21) and GBMs (*n* = 22) were enrolled. Patients with relevant small-vessel disease (Fazekas > 1), concomitant vascular lesions (eg, vascular malformations), or imaging features of neurodegenerative disorders (eg, Alzheimer disease, frontotemporal lobar degeneration, cerebral amyloid angiopathy) were excluded. Similarly, previous tumor resections and brain biopsies, prior radiation therapy, and poor image quality led to study exclusion. Patient demographics and clinical details are summarized in the Table.

Imaging was conducted with 3T MR imaging scanners (Magnetom Prisma and Magnetom Prisma FIT; Siemens) using a 64-channel head and neck coil. Diffusion MR imaging sequences were acquired with the following parameters: axial orientation, 42 slices, voxel size = 1.5 × 1.5 × 3 mm<sup>3</sup>, TR = 2800 ms, TE = 88 ms, bandwidth = 1778 Hz, flip angle = 90°, simultaneous multiband acceleration factor = 2, generalized autocalibrating partially parallel acquisition factor = 2, 65 diffusion-encoding gradient directions, 15 non-diffusion-weighted images, 2 × 58 images with b-factors = 1000 and 2000 s/mm<sup>2</sup>. Acquisition time was 6 minutes and 22 seconds. High-resolution isotropic T1WI postcontrast sequences were acquired 4–5 minutes after IV injection of 0.1 mmol/kg of gadoteridol (Gd) (ProHance; Bracco Imaging) with 3D magnetization-prepared 180° radiofrequency pulses and a rapid gradient-echo (MPRAGE) sequence (TR = 2500 ms, TE = 2.82 ms, flip angle = 7°, TI = 1100 ms, generalized autocalibrating partially parallel acquisition factor = 2, 1.0-mm isotropic voxels, 192 contiguous sagittal slices).

A portion of the data sets (19 in the GBM, 17 in the metastases group) was used in a previous project on peritumoral diffusion measures.<sup>22,23</sup>

**Image Postprocessing.** Data processing was performed on a local instance of the postprocessing platform NORA ([www.nora-imaging.org](http://www.nora-imaging.org); last accessed on March 4, 2023). T1WI data sets were automatically segmented into white matter, gray matter, and CSF (with SPM12; <http://www.fil.ion.ucl.ac.uk/spm/software/spm12>).

Preprocessing of diffusion MR imaging data included denoising,<sup>24</sup> Gibbs-ringing artifacts correction,<sup>25</sup> and up-sampling to an isotropic resolution of 1.5 mm<sup>3</sup>.<sup>26</sup> DTI measures were obtained from *b* = 0 and 1000 s/mm<sup>2</sup> images using a publicly available open-source toolbox (Fibertools; <https://www.uniklinik-freiburg.de/mr-en/research-groups/diffperf/fibertools.html>) using the ordinary



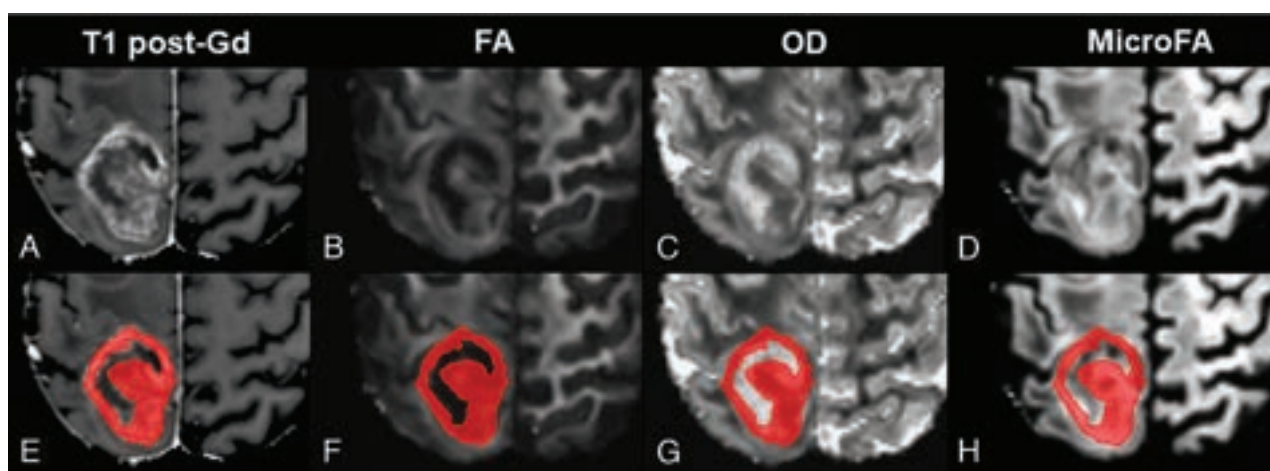


**FIG 1.** Presurgical (3T) MR imaging in a patient with a right parietal GBM. Representative axial images are shown in the *upper row* (A–D) with the corresponding ROI (of contrast-enhancing tumor components based on A) overlaid sections in the *lower row* (E–H). Gd indicates Gadoteridol.

log-linear fitting and calculating the FA and also mean, radial, and axial diffusivity. NODDI-derived OD and the intracellular and isotropic volume fractions were calculated with the Accelerated Microstructure Imaging Via Convex Optimization (AMICO) method, a regularized version of NODDI with faster processing times due to the linearization of fitting procedures.<sup>27</sup> DMI-based microFA and the intra-axonal (V-intra) and free water (V-CSF) volume fractions were estimated using a Bayesian approach.<sup>20</sup>

Image postprocessing and manual segmentation of contrast-enhancing tumor components was performed by 2 neuroradiologists (with 5 and 7 years of clinical neuroimaging experience) on 3D T1WI postcontrast data sets in coregistration with isotropic 3D T2-weighted FLAIR images to avoid erroneous segmentation of nonenhancing tumor components. First, the image data sets were checked for motion artifacts. Then, regular coregistrations of the MPRAGE and diffusion data sets were checked. Increased motion artifacts were found in 2 patients (1 per group), which led to exclusion. In addition, the coregistration was manually corrected in 1 patient (GBM group). To account for potential partial volume effects, we carefully excluded non-contrast-enhancing outer tumor margins and adjacent gray matter (Fig 1E).

**Histopathology.** Histologic analysis of contrast-enhancing tumors was performed by standardized protocols of the local institute of neuropathology. The samples analyzed in this study were obtained from radical removal surgeries of contrast-enhancing tumor portions in close temporal correlation with the analyzed MR imaging; stereotactic biopsies were not considered due to minimal/unrepresentative tissue availability. Therefore, usable histopathologic tissue samples could not be obtained for all tumors studied. A total of 19 samples (9 metastases and 10 GBMs) were processed by established diagnostic procedures for fixation in 4% paraformaldehyde, paraffin embedding, staining, and immunohistochemistry. Sections of 4- $\mu$ m thickness underwent Bielschowsky silver staining to demonstrate axonal fibers, as well as immunohistochemical labeling for glial fibrillary acidic protein (GFAP) in combination with hematoxylin staining. Immunohistochemistry was performed on an Autostainer Link 48 (Agilent), according to the manufacturer's instructions with a primary antibody against

GFAP (IR524; Agilent DAKO) and a corresponding secondary goat anti-rabbit immunoglobulin G4 (4050-08; SouthernBiotech).

Both readout measures were analyzed in a semiquantitative fashion by a 4-step scale regarding Bielschowsky staining (0: no axonal structures in tumor, 1: minimal axonal fragments maintained in the tumor, 2: decreased axonal density in the tumor, 3: no axonal loss in the tumor) and GFAP immunohistochemistry (0: no GFAP positivity in the tumor, 1: restricted expression in the tumor, 2: equivalent to surrounding parenchyma, 3: increased expression in the tumor). Representative images were acquired using a BX40 microscope (Olympus) and a DFC450 camera (Leica Microsystems). Figure 2 shows 1 example each of GBM and metastasis with anatomic and parametric MR imaging maps and histopathologic imaging.

**Statistical Analysis.** Normal data distribution was tested with the Shapiro-Wilk test. Patient age and histologic outcomes were compared between GBM and metastases using the Mann-Whitney *U* test. Sex was compared with the  $\chi^2$  test between GBM and metastases groups. A one-way ANOVA was performed between contrast-enhancing areas comparing GBM and metastases groups, and a Bonferroni correction was used to account for multiple comparisons. Linear regression modeling with the Spearman rank correlation coefficient was used to relate diffusion metrics FA, OD, and microFA to semiquantitative histopathology metrics. The receiver operating characteristic (ROC) and logistic regression curves of FA, OD, and microFA of GBMs and metastases were plotted using a simple logistic regression analysis of ranked outcomes for each measure. An  $\alpha$ -level of .05 was considered statistically significant. All statistical analyses were performed using Graphpad Prism (Version 9.3.1; GraphPad Software).

## RESULTS

### Study Population

A total of 43 patients (with 22 GBMs and 21 brain metastases; mean age, 65.6 and 66.6 years; 11 and 12 women, respectively) were included in this study. Of those, histopathology confirmed an *IDH* wild-type GBM in 22 patients (11 women; mean age, 65.6

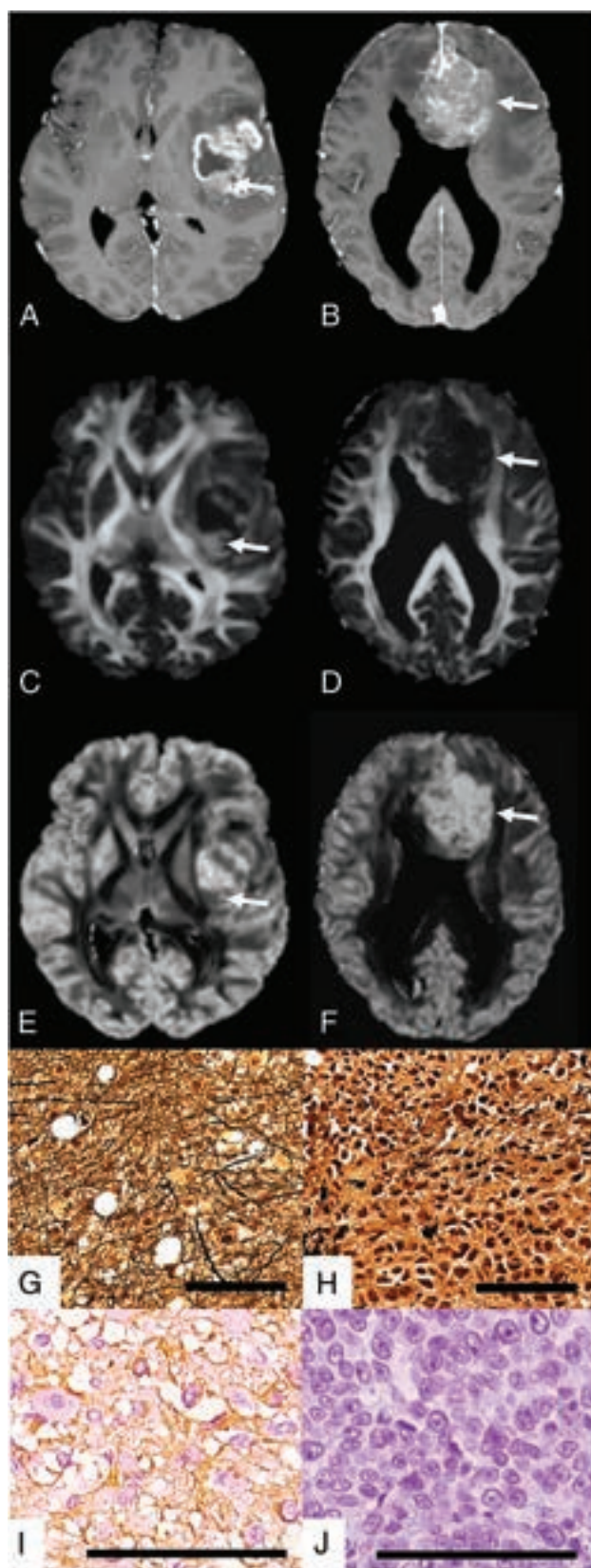


**FIG 2.** Representative MR images of patients with left insular GBM (A, T1WI post-Gd; C, FA; E, OD) and a large callosal melanoma metastasis (B, T1 post-Gd; D, FA; F, OD). Representative Bielschowsky silver staining to demonstrate nerve fibers and neurofibrillary tangles (G and H) and immunohistochemical labeling for GFAP (I and J). Scale bar = 100  $\mu$ m.

[SD, 12.7] years; range, 41.8–88.0 years), whereas 21 patients (12 women; mean age, 66.6 [SD, 11.8] years; range, 46.5–87.2 years) had brain metastases. Primary tumors in patients with brain metastases comprised non-small-cell lung cancer ( $n = 10$ ), small-cell lung cancer ( $n = 1$ ), melanoma ( $n = 5$ ), breast cancer ( $n = 1$ ), urothelial carcinoma ( $n = 1$ ), colorectal carcinoma ( $n = 1$ ), esophageal carcinoma ( $n = 1$ ), and thymus carcinoma ( $n = 1$ ). There was no significant difference in age ( $P = .96$ ) or sex ( $P = .86$ ) between groups. Among these, 10 patients in the metastases cohort and 12 patients in the GBM cohort had received corticosteroids before imaging, but none of the patients had received chemotherapy or radiation therapy before imaging. Within the metastases cohort, there were 2 patients with 1 lesion, 4 patients with 2 lesions, 1 patient with 3 lesions, 1 patient with 4 lesions, 3 patients with 5 lesions, and 10 patients with 6 lesions.

### Diffusion Metrics in Contrast-Enhancing Areas of Brain Metastasis and GBM

Comparison of DTI, DMI, and NODDI parameters of contrast-enhancing tumor areas revealed significantly higher FA in GBM compared with metastasis, ( $F [2, 89] = 548.8, P < .001$ ) with a simultaneous significant decrease in OD ( $F [2, 89] = 173.8, P < .001$ ). In contrast, no significant differences in microFA between GBM and metastasis were found, whereas both microFA in GBM and metastasis was lower compared with normal-appearing white matter ( $F [2, 89] = 92.2, P < .001$ ). There was no significant difference in intracellular volume fraction (ICVF), V-intra, mean diffusivity (MD), radial diffusivity (RD), or axial diffusivity (AD) (all  $P > .1$ ). There was in metastases, however, a significant increase in isotropic volume (V-ISO) ( $P = .0025$ ) and a tendency toward increased V-CSF ( $P = .077$ ). Group-related metrics and ranges are presented in the Table. The distribution of the individual values is shown in Fig 3 and the Online Supplemental Data.

**Histopathology.** Semiquantitative histopathologic readout scores regarding the presence of axonal structures in the tumor (Bielschowsky silver stain) and the presence of GFAP revealed distinct differences between GBM and metastases samples. In GBM samples, we visually recognized the presence of axonal structures ranging from minimal maintained axonal structures to widely intact axonal structures, whereas in tumor areas of all except 1 case with metastases, no axonal structures were found. Exemplary images are shown in the Online Supplemental Data, with detailed histology and comparison of semiquantitative assessment scores.

**Correlation Analysis.** Results of the Spearman correlation test revealed a positive association between the Bielschowsky score and FA ( $r = 0.6761, P = .0053$ ) as well as between GFAP score and FA ( $r = 0.6253; P = .015$ ). Furthermore, we identified a negative

As illustrated by parametric maps for FA (C and D, arrows) and OD (E and F, arrows), values in contrast-enhancing solid tumor components (A and B, arrows) approximate normal-appearing white matter in GBM. This finding is accompanied by abundant axonal structures visualized by Bielschowsky silver staining (G) and high GFAP expression (I) in GBM compared with melanoma metastasis (H and J). Scale = 100  $\mu$ m.



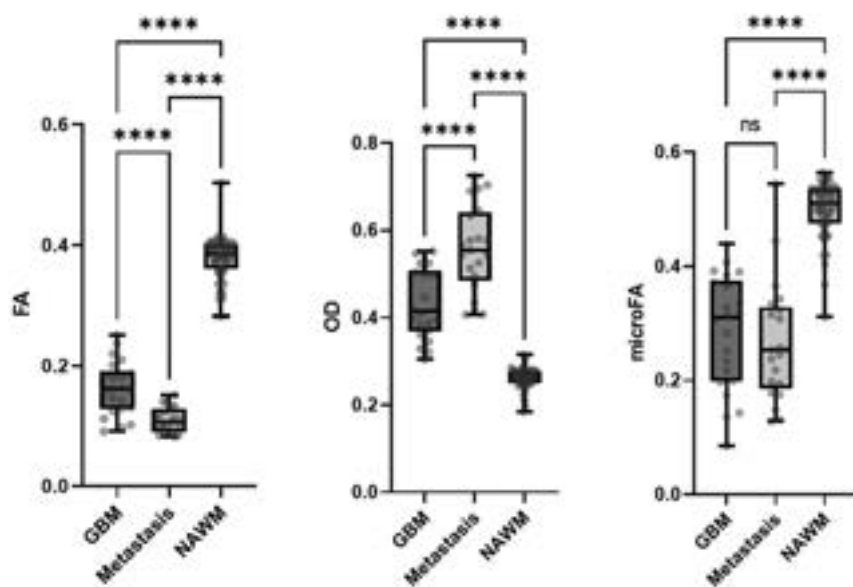


**FIG 3.** DTI, NODDI, and DMI metrics in contrast-enhancing tumor areas in patients with GBM ( $n = 22$ ) and metastases ( $n = 21$ ). Compared with metastases, GBM showed a significant shift toward increased FA and decreased OD, whereas no significant differences were found regarding microFA. Four asterisks indicate  $P \leq .001$ . NAWM indicates normal-appearing white matter.

correlation between the Bielschowsky score and OD ( $r = -0.7084$ ,  $P = .003$ ) and between the GFAP score and OD ( $r = -0.6468$ ,  $P = .0085$ ). In contrast, no significant correlations were observed between histomorphologic features and microFA (Bielschowsky score and microFA:  $r = -0.08317$ ,  $P = .7581$ ; GFAP score and microFA:  $r = -0.1155$ ,  $P = .6655$ ). Correlation plots are presented in Fig 4.

### ROC and Linear Regression Analysis

Building on the systematic differences regarding FA and OD values within contrast-enhancing tumor components between GBM and metastases, we conducted an ROC analysis defining FA, OD, or microFA as dependent variables and GBM and metastases groups as class variables. This model supported the affiliation of GBM cases with higher FA values (area under the curve [AUC] = 0.8463; 95% CI, 0.73–0.96;  $P < .001$ ). The inverse of OD appeared comparably sensitive and specific (AUC = 0.8398; 95% CI, 0.72–0.96;  $P < .001$ ). The curve of microFA did not significantly deviate from the random classifier (AUC = 0.5736; 95% CI, 0.40–0.75;  $P = .40$ ). ROC and logistic regression curves are presented in Fig 5.

### DISCUSSION

Advanced DWI revealed distinct microstructural alterations within the contrast-enhancing tumor in GBM and metastasis regarding preserved directional diffusion in GBMs, which correlated with increased GFAP expression and axonal density in GBM. On the basis of the pattern of microstructural changes, GBM and metastases could be distinguished with sufficient accuracy.

Within the contrast-enhancing tumor area, a significant increase in FA was observed in GBM compared with metastasis. Conversely, there was a significant reduction in OD in GBM. Histopathologic assessment revealed a significant increase in GFAP expression and the presence of axonal structures in GBM,

corresponding to a positive overall correlation of FA with GFAP and Bielschowsky scores and a significant negative correlation of OD with these histopathology scores in the tumor tissue. Of note, there was no significant difference in microFA between groups.

While GBMs diffusely infiltrate the brain parenchyma, spreading around a partially conserved axonal framework, metastases typically form distinct tumor masses with virtually no remnants of neuronal structures. For example, in 1 study, the peritumoral edema of GBMs was found to have a higher relative content of viable tumor cells and comparable cellularity compared with contrast-enhancing tumor,<sup>28</sup> whereas infiltrative growth into the tumor microenvironment up to 450  $\mu\text{m}$  from the main tumor was also described in some metastases.<sup>29</sup> In diffuse gliomas, tumor cells have been described to extend far beyond, into macroscopically healthy brain tissue.<sup>30,31</sup>

Previous works have suggested that quantification of free water in the peritumoral area may reflect the diffusely infiltrative nature in GBM compared with metastases,<sup>32,33</sup> and FA has also been used to differentiate these entities, with most studies indicating a rather low diagnostic potential of peritumoral FA<sup>12,14,16</sup> and only a few studies indicating increased FA within the peritumoral edema in GBM.<sup>13</sup> However, increased edematization of the surrounding tissue in metastases may also cause alterations in FA. Therefore, more specific parameters are required.

The contrast-enhancing solid tumor component was subject to several studies that investigated possible correlations of histopathologic parameters with MR imaging features in GBM or metastases. Increased “architectural disruption” in contrast-enhancing tumor was noted by indirectly assessing the presence of axonal structures on the basis of antibodies, though correlation of this finding with FA was lacking.<sup>32</sup> Even though most DTI-based studies also reported increased FA levels in contrast-enhancing tumor components in GBM compared with metastases,<sup>9–13</sup> there are a few studies that did not find any<sup>14,15</sup> or even contradictory results.<sup>16</sup> FA is known to be sensitive to anisotropic cell structures such as axons but also to their orientation dispersion, possibly leading to reduced FA due to increased crossing fiber tracts.<sup>20</sup> Therefore, the role of FA as a marker of tissue integrity may also be hampered in regions of complex microarchitecture such as in contrast-enhancing tumor.

Thus, we also examined OD and microFA. Here, we observed an inverse relationship between FA and OD, with evidence of increased OD in metastatic tissue, a plausible finding because metastases, depending on the degree of differentiation, frequently consist of unstructured cell clusters or fragmented and heterotopic tissue structures. In contrast to DTI, NODDI-based studies comparing these 2 common tumor groups are scarce to date. In

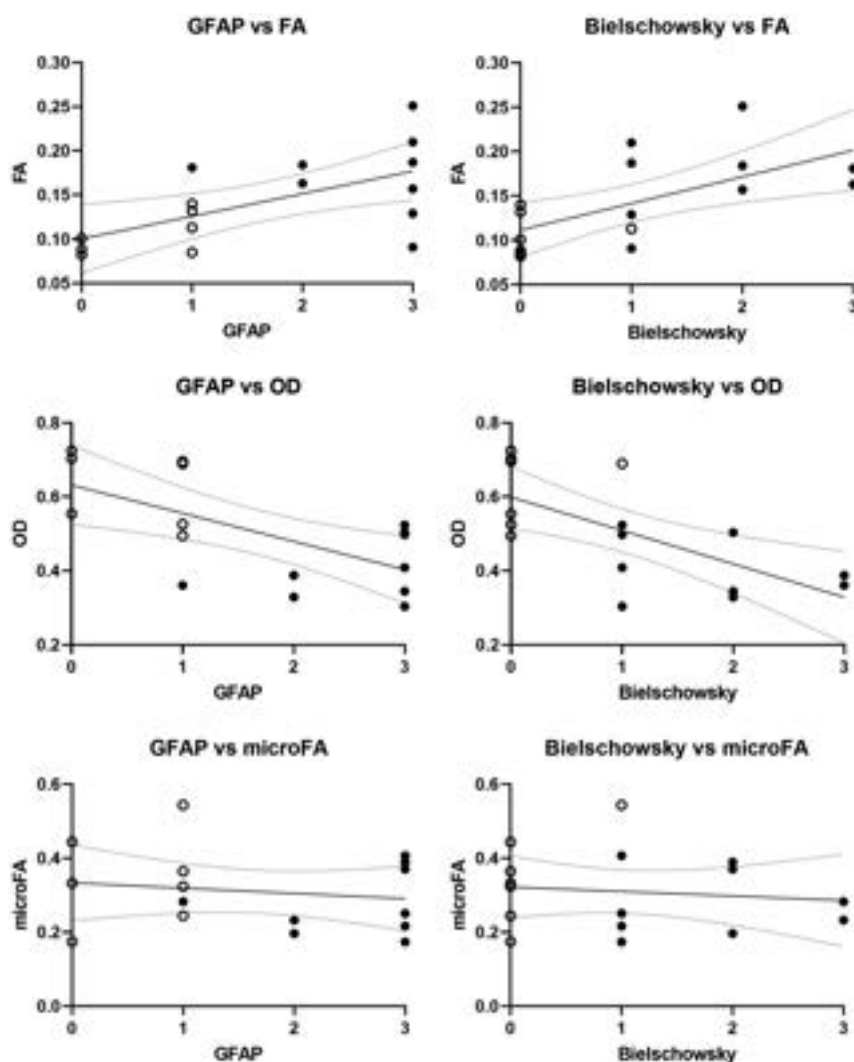


**FIG 4.** The Spearman rank correlation demonstrates a positive association of FA with GFAP and Bielschowsky scores (*upper row*) and a negative association of OD with GFAP and Bielschowsky scores (*middle row*). No association between microFA with GFAP and Bielschowsky scores can be detected (*lower row*). *Open circles indicate metastasis cases; filled circles, GBM cases.*

line with our results, lower OD was observed in high-grade gliomas,<sup>12</sup> whereas another NODDI-based study did not report OD.<sup>15</sup> Within the white matter, increased OD is thought to reflect increased axonal dispersion and degeneration, whereas a decrease in OD in gray matter may indicate dendritic thinning.<sup>33</sup> Therefore, the opposing signal changes of OD and FA in GBM and metastases can be well-reconciled because the presence of residual axonal structures in the contrast-enhancing tumor may tend to condition some diffusional directionality in GBM. This tendency is also supported by the significant negative correlations of OD with the increase in the Bielschowsky score, which does indeed classify the presence of axonal structures.

Because GBM and brain metastases differ with respect to the presence of axonal structures in contrast-enhancing tumor areas and OD is altered, the question arises as to why these entities do not differ in microscopic anisotropy. First, the literal interpretation of microFA represents an anticipated oversimplification. Because microFA quantifies only a single feature of microstructure

(namely, the ratio of diffusivities in the principal and secondary directions), it would only coincide with FA if all microscopic tissue elements in a voxel were aligned with the parallel principal diffusion directions. Hence, FA is smaller than microFA, the higher the OD is. Moreover, as any mean value, microFA does not reflect the underlying variance. Specifically, the formal microFA values may be identical in tissue with sufficiently homogeneous microstructure and a tissue consisting of islands with high and low microFA. Such islands may further be spatially separated or related to different cellular populations, eg, axons and astrocytes. In summary, stratification of cellular morphology through microFA is limited in the diffusely growing and heterogeneous tissues assessed in this study.

In our subsequent analysis of ICVF and V-intra, we did not detect any significant difference in these estimated axonal volume fractions between the entities, even though we clearly observed histopathologic features for the presence of axons in GBM. We acknowledge that these NODDI and DMI model assumptions limit the application in intratumoral environments. The local microstructural blocks are less orientationally ordered than in normal-appearing white matter according to the significant increase in OD in tumors. Because FA summarizes the voxel-averaged microFA, the decrease in

FA is fully compatible with the increase in OD; both effects are quantitatively larger in metastases. On the other hand, the work of Zhang et al<sup>34</sup> clearly demonstrated that there is a strong inverse relationship between FA and OD, not only in white but also gray matter, with FA also being more strongly influenced by OD than by neurite density, at least in healthy brain tissues. However, we do not disagree that optimization of advanced diffusion models to the tumor microenvironment is warranted, as already shown in the works of Panagiotaki et al<sup>35</sup> and Zaccagna et al,<sup>36</sup> applying the Vascular, Extracellular, and Restricted Diffusion for Cytometry in Tumor (VERDICT) model.

We did not find differences for MD, RD, and AD in the contrast-enhancing tumor component between GBM and metastases. The available literature is inconsistent in this regard, with 1 study also describing no differences in MD,<sup>10</sup> whereas another study measured lower MD and RD in high-grade gliomas.<sup>12</sup>

Some tentative conclusions can be drawn from our results: 1) FA of the solid tumor component may be useful as a diagnostic



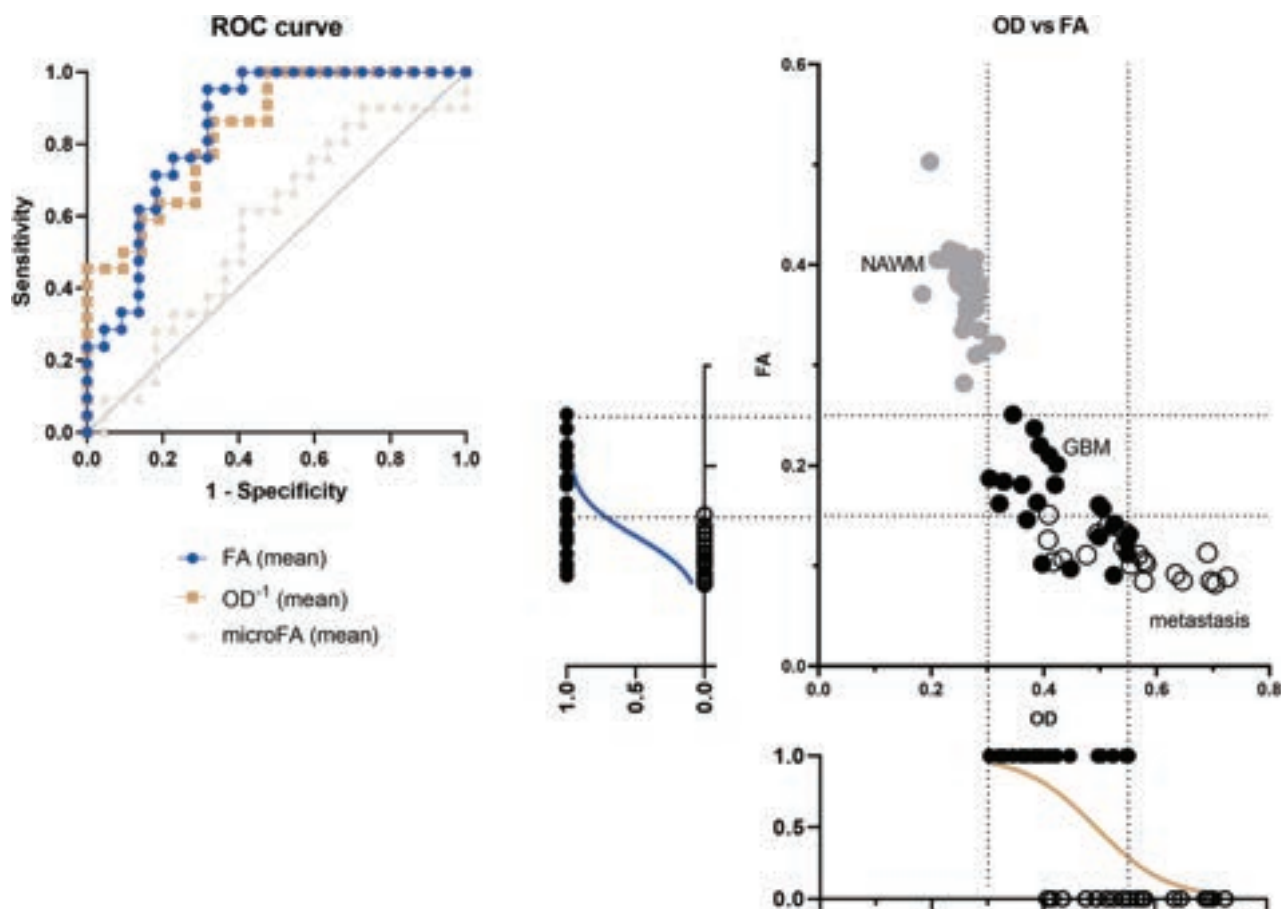


**FIG 5.** ROC curves of 22 patients with GBM and 21 with cerebral metastases showing a high predictive value of both FA (AUC = 0.8463) and OD (AUC = 0.8398) regarding the presence of GBM versus metastasis (*left panel*) and a scatterplot of OD and FA values for each sample (normal-appearing white matter controls = gray filled circles, GBM = black filled circles, metastasis = open circles) with arbitrary cutoff values of 0.3 and 0.55 for OD and 0.15 and 0.25 for FA. Logistic regression indicates the probability of GBM diagnosis compared with metastasis diagnosis at each individual OD or FA value (*right panel*).

indicator for differentiating GBM and metastases, the most common malignant neoplasms of the adult human brain. 2) In the preoperative setting, FA-based tractography is used to assess the extension of tumor components to eloquent white matter tracts such as the corticospinal or optical tract, thus anticipating risks in relation to surgically approachable lesions. The definition of these findings regarding functional relevance should be the aim of future studies.

Besides the obvious intrinsic limitations of a retrospective study, our study is further limited by the rather small patient population, and biopsies for histopathologic evaluation were available for only a subset of the cohort. Even though in the metastases cohort, almost one-half of the histopathologic primary tumors were non-small-cell lung cancer (10/21), there was still relevant heterogeneity with a total of 8 different primary tumors. Because of the additional heterogeneity between the GBM and metastasis groups due to lesion number, the aspect of differentiation based on solitary lesions was not directly addressed in the present work. However, we assume that the findings obtained can be applied to solitary (nonoverlapping) metastatic lesions.

Also, defining the contrast-enhancing tumor areas remains methodologically challenging because they can be thin, especially

in GBM, and often located around a central necrotic core. To achieve the most accurate segmentation of solid tumor portions, with exclusion of necrosis, gray matter, and CSF space, we performed manual segmentation.

We assume congruence between histologic tumor specimens and MR imaging-based ROIs, which requires that tumor specimens represent contrast-enhancing components. Accidental incongruence represents a potential limitation of this study. To minimize this aspect, we used established practices with navigated techniques for resection (both in GBM and metastases) as well as necrotic areas easily identified histologically.

## CONCLUSIONS

Our study reconciles the significant differences in diffusion metrics between contrast-enhanced areas in GBM and brain metastases with semiquantitatively assessed histopathologic features. Our approach demonstrates that well-established histopathologic features of axonal and glial tumor microstructure correlate with directionality-driven diffusion metrics, indicating the potential of DTI- and NODDI-based diffusion metrics for tumor discrimination.

Disclosure forms provided by the authors are available with the full text and PDF of this article at [www.ajnr.org](http://www.ajnr.org).

## REFERENCES

- Young RJ, Knopp EA. **Brain MRI: tumor evaluation.** *J Magn Reson Imaging* 2006;24:709–24 CrossRef Medline
- Louis DN, Perry A, Wesseling P, et al. **The 2021 WHO Classification of Tumors of the Central Nervous System: a summary.** *Neuro Oncol* 2021;23:1231–51 CrossRef Medline
- Jacque CM, Vinner C, Kujas M, et al. **Determination of glial fibrillary acidic protein (GFAP) in human brain tumors.** *J Neurol Sci* 1978;35:147–55 CrossRef Medline
- Eng LF, Vanderhaeghen JJ, Bignami A, et al. **An acidic protein isolated from fibrous astrocytes.** *Brain Res* 1971;28:351–54 CrossRef Medline
- Seker-Polat F, Pinarbasi Degirmenci N, Solaroglu I, et al. **Tumor cell infiltration into the brain in glioblastoma: from mechanisms to clinical perspectives.** *Cancers (Basel)* 2022;14:443 CrossRef Medline
- Novikov DS, Jensen JH, Helpert JA, et al. **Revealing mesoscopic structural universality with diffusion.** *Proc Natl Acad Sci U S A* 2014;111:5088–93 CrossRef Medline
- Demerath T, Donkels C, Reisert M, et al. **Gray-white matter blurring of the temporal pole associated with hippocampal sclerosis: a microstructural study involving 3 T MRI and ultrastructural histopathology.** *Cereb Cortex* 2022;32:1882–93 CrossRef Medline
- Basser PJ, Pierpaoli C. **Microstructural and physiological features of tissues elucidated by quantitative-diffusion-tensor MRI.** 1996. *J Magn Reson* 2011;213:560–70 CrossRef Medline
- Wang S, Kim S, Chawla S, et al. **Differentiation between glioblastomas and solitary brain metastases using diffusion tensor imaging.** *Neuroimage* 2009;44:653–60 CrossRef Medline
- Wang S, Kim SJ, Poptani H, et al. **Diagnostic utility of diffusion tensor imaging in differentiating glioblastomas from brain metastases.** *AJNR Am J Neuroradiol* 2014;35:928–34 CrossRef Medline
- Bette S, Huber T, Wiestler B, et al. **Analysis of fractional anisotropy facilitates differentiation of glioblastoma and brain metastases in a clinical setting.** *Eur J Radiol* 2016;85:2182–87 CrossRef Medline
- Mao J, Zeng W, Zhang Q, et al. **Differentiation between high-grade gliomas and solitary brain metastases: a comparison of five diffusion-weighted MRI models.** *BMC Med Imaging* 2020;20:124 CrossRef Medline
- Nguyen DH, Le TD, Nguyen HV, et al. **Discriminating glioblastoma from solitary brain metastases on 3 Tesla magnetic resonance imaging: the roles of fractional anisotropy and mean diffusivity.** *Eur Rev Med Pharmacol Sci* 2022;26:8823–31 CrossRef Medline
- Tsougos I, Svolos P, Kousi E, et al. **Differentiation of glioblastoma multiforme from metastatic brain tumor using proton magnetic resonance spectroscopy, diffusion and perfusion metrics at 3 T.** *Cancer Imaging* 2012;12:423–36 CrossRef Medline
- Kadota Y, Hirai T, Azuma M, et al. **Differentiation between glioblastoma and solitary brain metastasis using neurite orientation dispersion and density imaging.** *J Neuroradiol* 2020;47:197–202 CrossRef Medline
- Wang W, Steward CE, Desmond PM. **Diffusion tensor imaging in glioblastoma multiforme and brain metastases: the role of p, q, L, and fractional anisotropy.** *AJNR Am J Neuroradiol* 2009;30:203–08 CrossRef Medline
- Preziosa P, Kiljan S, Steenwijk MD, et al. **Axonal degeneration as substrate of fractional anisotropy abnormalities in multiple sclerosis cortex.** *Brain* 2019;142:1921–37 CrossRef Medline
- Galbusera R, Bahn E, Weigel M, et al. **Postmortem quantitative MRI disentangles histological lesion types in multiple sclerosis.** *Brain Pathol* 2022 Dec 8. [Epub ahead of print] CrossRef Medline
- Lee JK, Liu D, Jiang D, et al. **Fractional anisotropy from diffusion tensor imaging correlates with acute astrocyte and myelin swelling in neonatal swine models of excitotoxic and hypoxic-ischemic brain injury.** *J Comp Neurol* 2021;529:2750–70 CrossRef Medline
- Szczepankiewicz F, Lasic S, van Westen D, et al. **Quantification of microscopic diffusion anisotropy disentangles effects of orientation dispersion from microstructure: applications in healthy volunteers and in brain tumors.** *Neuroimage* 2015;104:241–52 CrossRef Medline
- Rau A, Reisert M, Kellner E, et al. **Increased interstitial fluid in periventricular and deep white matter hyperintensities in patients with suspected idiopathic normal pressure hydrocephalus.** *Sci Rep* 2021;11:19552 CrossRef Medline
- Würtemberger U, Diebold M, Erny D, et al. **Diffusion microstructure imaging to analyze perilesional T2 signal changes in brain metastases and glioblastomas.** *Cancers (Basel)* 2022;14:1155 CrossRef Medline
- Würtemberger U, Rau A, Reisert M, et al. **Differentiation of perilesional edema in glioblastomas and brain metastases: comparison of diffusion tensor imaging, neurite orientation dispersion and density imaging and diffusion microstructure imaging.** *Cancers (Basel)* 2022;15:129 CrossRef Medline
- Veraart J, Novikov DS, Christiaens D, et al. **Denoising of diffusion MRI using random matrix theory.** *Neuroimage* 2016;142:394–406 CrossRef Medline
- Kellner E, Dhital B, Kiselev VG, et al. **Gibbs-ringing artifact removal based on local subvoxel-shifts.** *Magn Reson Med* 2016;76:1574–81 CrossRef Medline
- Reisert M, Kellner E, Dhital B, et al. **Disentangling micro from mesostructure by diffusion MRI: a Bayesian approach.** *Neuroimage* 2017;147:964–75 CrossRef Medline
- Daducci A, Canales-Rodriguez EJ, Zhang H, et al. **Accelerated Microstructure Imaging via Convex Optimization (AMICO) from diffusion MRI data.** *Neuroimage* 2015;105:32–44 CrossRef Medline
- Eidel O, Burth S, Neumann JO, et al. **Tumor infiltration in enhancing and non-enhancing parts of glioblastoma: a correlation with histopathology.** *PLoS One* 2017;12:e0169292 CrossRef Medline
- Berghoff AS, Rajky O, Winkler F, et al. **Invasion patterns in brain metastases of solid cancers.** *Neuro Oncol* 2013;15:1664–72 CrossRef Medline
- Sahm F, Capper D, Jeibmann A, et al. **Addressing diffuse glioma as a systemic brain disease with single-cell analysis.** *Arch Neurol* 2012;69:523–26 CrossRef Medline
- Venkataramani V, Schneider M, Giordano FA, et al. **Disconnecting multicellular networks in brain tumours.** *Nat Rev Cancer* 2022;22:481–91 CrossRef Medline
- Barajas RF, Phillips JJ, Parvataneni R, et al. **Regional variation in histopathologic features of tumor specimens from treatment-naïve glioblastoma correlates with anatomic and physiologic MR imaging.** *Neuro Oncol* 2012;14:942–54 CrossRef Medline
- Zhang H, Hubbard PL, Parker GJM, et al. **Axon diameter mapping in the presence of orientation dispersion with diffusion MRI.** *Neuroimage* 2011;56:1301–15 CrossRef Medline
- Zhang H, Schneider T, Wheeler-Kingshott CA, et al. **NODDI: practical in vivo neurite orientation dispersion and density imaging of the human brain.** *Neuroimage* 2012;61:1000–16 CrossRef Medline
- Panagiotaki E, Walker-Samuel S, Siow B, et al. **Noninvasive quantification of solid tumor microstructure using VERDICT MRI.** *Cancer Res* 2014;74:1902–12 CrossRef Medline
- Zaccagna F, Riemer F, Priest AN, et al. **Non-invasive assessment of glioma microstructure using VERDICT MRI: correlation with histology.** *Eur Radiol* 2019;29:5559–66 CrossRef Medline

# Radiogenomics Provides Insights into Gliomas Demonstrating Single-Arm 1p or 19q Deletion

Arian Lasocki, Michael E. Buckland, Tahlia Molinaro, Jing Xie, and Frank Gaillard



## ABSTRACT

**BACKGROUND AND PURPOSE:** *IDH*-mutant gliomas are further divided on the basis of 1p/19q status: oligodendroglioma, *IDH*-mutant and 1p/19q-codeleted, and astrocytoma, *IDH*-mutant (without codeletion). Occasionally, testing may reveal single-arm 1p or 19q deletion (unideletion), which remains within the diagnosis of astrocytoma. Molecular assessment has some limitations, however, raising the possibility that some undeleted tumors could actually be codeleted. This study assessed whether undeleted tumors had MR imaging features and survival more consistent with astrocytomas or oligodendrogliomas.

**MATERIALS AND METHODS:** One hundred twenty-one *IDH*-mutant grade 2–3 gliomas with 1p/19q results were identified. Two neuroradiologists assessed the T2-FLAIR mismatch sign and calcifications, as differentiators of astrocytomas and oligodendrogliomas. MR imaging features and survival were compared among the undeleted tumors, codeleted tumors, and those without 1p or 19q deletion.

**RESULTS:** The cohort comprised 65 tumors without 1p or 19q deletion, 12 undeleted tumors, and 44 codeleted. The proportion of undeleted tumors demonstrating the T2-FLAIR mismatch sign (33%) was similar to that in tumors without deletion (49%;  $P = .39$ ), but significantly higher than codeleted tumors (0%;  $P = .001$ ). Calcifications were less frequent in undeleted tumors (0%) than in codeleted tumors (25%), but this difference did not reach statistical significance ( $P = .097$ ). The median survival of patients with undeleted tumors was 7.8 years, which was similar to that in tumors without deletion (8.5 years;  $P = .72$ ) but significantly shorter than that in codeleted tumors (not reaching median survival after 12 years;  $P = .013$ ).

**CONCLUSIONS:** *IDH*-mutant gliomas with single-arm 1p or 19q deletion have MR imaging appearance and survival that are similar to those of astrocytomas without 1p or 19q deletion and significantly different from those of 1p/19q-codeleted oligodendrogliomas.

**ABBREVIATIONS:** codelet = codeleted; FISH = fluorescence in situ hybridization;  $IDH^{mut}$  = *IDH*-mutant;  $IDH^{WT}$  = *IDH*-wild-type; WHO = World Health Organization

The molecular status of tumors of the CNS is of increasing importance in their classification. The 2016 update to the World Health Organization Classification of Tumors of the Central Nervous System (henceforth WHO 2016) introduced molecular status into the diagnosis of intracranial gliomas.<sup>1</sup> Some of the key changes related to grade 2–3 gliomas, which were

divided into 3 subtypes based on *IDH* and 1p/19q status: oligodendroglioma, *IDH*-mutant ( $IDH^{mut}$ ) and 1p/19q-codeleted (demonstrating combined loss of the short arm of chromosome 1 and the long arm of chromosome 19 [1p/19q<sup>codelet</sup>]); astrocytoma,  $IDH^{mut}$  (without 1p/19q-codeletion); and astrocytoma, *IDH*-wild-type (without an *IDH* mutation [ $IDH^{WT}$ ]).<sup>1</sup> The 2021 WHO classification (henceforth WHO 2021) increased the importance of molecular status in tumor diagnosis.<sup>2</sup> For example, CDKN2A/B copy number status has become important in the grading of  $IDH^{mut}$  astrocytomas, with CDKN2A/B homozygous deletion allowing the diagnosis of a grade 4 tumor even in the absence of the classic histologic features of microvascular proliferation and necrosis.<sup>2</sup>

Occasionally, testing for 1p/19q status may reveal a single-arm 1p or 19q deletion (unideletion), without 1p/19q-codeletion. Such tumors (provided they are  $IDH^{mut}$ ) remain within the diagnosis of astrocytoma,  $IDH^{mut}$ . Despite being the criterion standard, molecular assessment can have some limitations. For example, 1p/19q fluorescence in situ hybridization (FISH) can produce false-

Received April 27, 2023; accepted after revision September 15.

From the Department of Cancer Imaging (A.L.), Department of Medical Oncology (T.M.), and Centre for Biostatistics and Clinical Trials (J.X.), Peter MacCallum Cancer Centre, Melbourne, Victoria, Australia; Sir Peter MacCallum Department of Oncology (A.L.) and Department of Radiology (A.L., F.G.), The University of Melbourne, Parkville, Victoria, Australia; Department of Neuropathology (M.E.B.), Royal Prince Alfred Hospital, Camperdown, New South Wales, Australia; School of Medical Sciences (M.E.B.), University of Sydney, Camperdown, New South Wales, Australia; and Department of Radiology (F.G.), The Royal Melbourne Hospital, Parkville, Victoria, Australia.

This study was supported by a RANZCR research grant in 2018.

Please address correspondence to Arian Lasocki, MD, Department of Cancer Imaging, Peter MacCallum Cancer Centre, Grattan St, Melbourne, Victoria 3000, Australia; e-mail: arian.lasocki@petermac.org

<http://dx.doi.org/10.3174/ajnr.A8034>

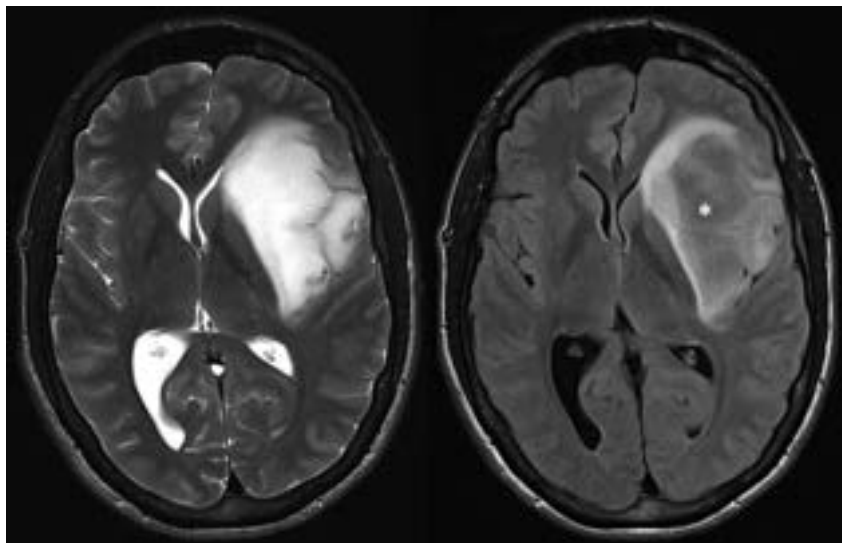


**FIG 1.** T2-weighted (left) and FLAIR (right) MR images of a left fronto-insular glioma show that much of the tumor has substantially lower signal on FLAIR (asterisk) than on T2-weighted imaging, consistent with the T2-FLAIR mismatch sign, which is characteristic of astrocytoma, *IDH*<sup>mut</sup>. This tumor had a single-arm 19q deletion.



**FIG 2.** This unenhanced CT image demonstrates calcifications in an oligodendroglioma (*IDH*<sup>mut</sup> and 1p/19q<sup>codelet</sup>) involving the left insula.

positive results in the presence of partial deletions.<sup>3</sup> In addition, sequencing can provide false-negative results if there are relatively few tumor cells within the sample,<sup>4</sup> particularly relevant to gliomas from which only a small sample can be safely obtained. The possibility of sampling error is also particularly relevant to intracranial diffuse gliomas, given their inherent heterogeneity.<sup>5</sup> This raises the likelihood that some tumors diagnosed as having 1p- or 19q-unideletion could actually be 1p/19q codeleted (1p/19q<sup>codelet</sup>),

which has implications not only for formal diagnosis but also for grading and treatment.

The field of radiogenomics aims to predict glioma genotype on the basis of imaging features, most commonly using MR imaging, and a variety of features have been studied.<sup>6</sup> The T2-FLAIR mismatch sign, strongly predictive of an *IDH*<sup>mut</sup> astrocytoma in the case of histologic grade 2–3 gliomas, is the most distinctive feature across all diffuse glioma grades and genotypes.<sup>6–10</sup> Calcification has long been reported as a feature of oligodendrogliomas based on the histologic criteria before WHO 2016, and it has also been more recently confirmed as a predictor of oligodendroglioma, *IDH*<sup>mut</sup> and 1p/19q<sup>codelet</sup>.<sup>8,11,12</sup> Additional features can be helpful in distinguishing 2 of the 3 glioma genotypes, but they are less predictive when all 3 are included.<sup>6</sup>

For example, a frontal lobe location predicts an *IDH* mutation but has less predictive value for determining 1p/19q status.<sup>6</sup>

Radiogenomics has the potential to overcome some of the limitations of histologic assessment.<sup>13</sup> For example, Patel et al<sup>14</sup> demonstrated that MR imaging features were able to identify some tumors incorrectly classified as 1p/19q<sup>codelet</sup> based on FISH. We sought to use radiogenomics to provide additional insight into gliomas demonstrating 1p- or 19q-unideletion, by determining whether their MR imaging features were more consistent with astrocytomas (*IDH*<sup>mut</sup> but without 1p/19q<sup>codelet</sup>) or oligodendrogliomas (*IDH*<sup>mut</sup> and 1p/19q<sup>codelet</sup>), by using the T2-FLAIR mismatch sign (Fig 1) and the presence of calcifications (Fig 2), because the literature<sup>6</sup> suggests these features as the best differentiators of the 2 tumor types. The survival associated the different tumor types was also compared.

## MATERIALS AND METHODS

Results from 2 previous radiogenomics studies were combined to identify *IDH*<sup>mut</sup> grade 2–3 gliomas with available 1p/19q testing results.<sup>8,12</sup> All were adult patients. In the earlier study, 1p/19q status had been determined by FISH,<sup>8</sup> while in the later study, next-generation sequencing was used unless FISH results were already available as part of routine clinical practice or earlier research.<sup>12</sup> MR imaging had been performed on a variety of scanners, including at external institutions, and included, at least, T2WI, FLAIR, and pre- and postcontrast T1WI.<sup>8,12</sup> The T2-FLAIR mismatch sign and the presence of calcifications on preoperative imaging were assessed by 2 neuroradiologists with subspecialty expertise in neuro-oncology, blinded to the molecular diagnosis. Discrepancies were resolved by consensus. Identification of the T2-FLAIR mismatch sign was based on the definition originally presented by Patel et al,<sup>9</sup> namely an area of non-contrast-enhancing tumor demonstrating high T2 signal and relatively hypointense FLAIR signal. The T2-FLAIR mismatch sign was considered positive

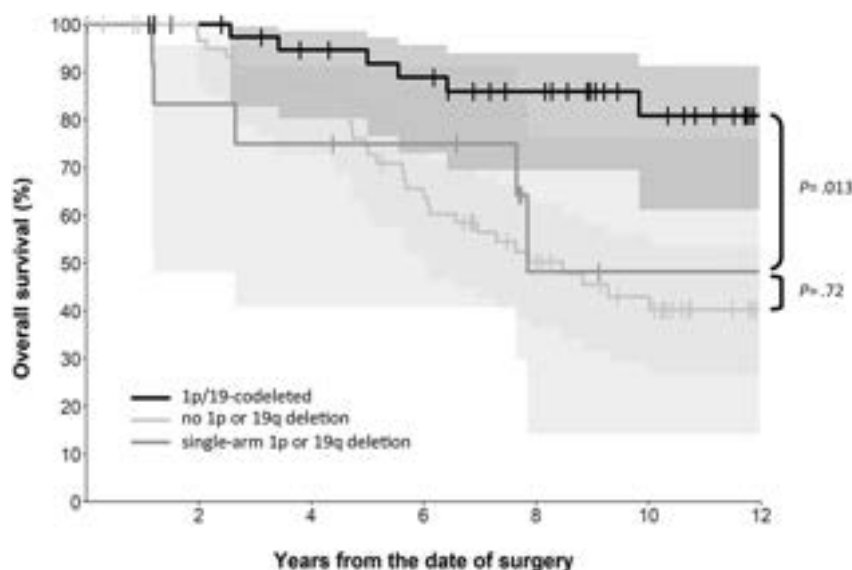


**Table 1: Patient demographics for the 3 tumor genotypes and the overall cohort**

	No Deletion	Unideletion	Co-Deletion	Total
No. (%)	65 (54%)	12 (10%)	44 (36%)	121
Age (yr)				
Range	17–70	23–61	17–72	17–72
Median	37	34	39	37
Sex				
Male	42 (65%)	7 (58%)	24 (55%)	73 (60%)
Female	23 (35%)	5 (42%)	20 (45%)	48 (40%)

**Table 2: Comparison of imaging features and median survival across the 3 tumor genotypes**

	No Deletion	Unideletion	Co-Deletion
T2-FLAIR mismatch			
Present	32 (49%)	4 (33%)	0 (0%)
Absent	33 (51%)	8 (67%)	44 (100%)
P value	$P = .39$	Reference	$P = .0013$
Calcifications			
Present	2 (3%)	0 (0%)	11 (25%)
Absent	63 (97%)	12 (100%)	33 (75%)
P value	$P = 1$	Reference	$P = .097$
Survival			
Median (yr)	8.5	7.8	>12
P value	$P = .72$	Reference	$P = .013$

**FIG 3.** Kaplan-Meier survival curves of all 3 groups of tumors, demonstrating that the undeleted tumors in the cohort had survival that was significantly shorter than that of 1p/19q<sup>codelet</sup> tumors ( $P = .013$ ), but similar to that in tumors without 1p or 19q deletion ( $P = .72$ ).

if >50% mismatch was present.<sup>8,12</sup> Assessment for calcifications also used susceptibility-sensitive sequences and relevant CT studies, when available.<sup>8,12</sup> If magnetic susceptibility on MR imaging or precontrast hyperdensity on CT or both were present but could not be confidently attributed to calcification as opposed to hemorrhage, this feature was considered negative for calcification. Good interobserver agreement has already been reported, with  $\kappa > 0.6$  for both features across both cohorts.<sup>8,12</sup>

The presence of the 2 MR imaging features was considered across 3 tumor groups (all being *IDH*<sup>mut</sup>): no 1p or 19q deletion, single-arm 1p or 19q deletion (unideletion), and 1p/19q<sup>codelet</sup>.

Statistical correlations were performed using the Fisher exact test. Survival was assessed using Kaplan-Meier curves. The multivariate model included patient age, sex, and histologic tumor grade (2 or 3). A  $P$  value < .05 was considered statistically significant. All statistical analyses were performed with R statistical and computing software (Version 4.0.3; <http://www.r-project.org/>) using standard and validated statistical procedures.

## RESULTS

One hundred twenty-one patients with an *IDH*<sup>mut</sup> grade 2–3 gliomas with available 1p/19q results were identified across the 2 studies. These comprised 65 tumors without 1p or 19q deletion, 12 tumors with unideletion (11 with 19q-unideletion and 1 with 1p-unideletion), and 44 1p/19q<sup>codelet</sup> tumors. Most tumors were WHO grade 2 (103 of 121, or 85%); the remainder were grade 3. The median age across the cohort was 37 years (range, 17–72 years), with a slightly greater proportion of males (73 of 121, or 60%). The demographics of the patients across the 3 genotypes and the overall cohort are summarized in Table 1.

T2-FLAIR mismatch was identified in 4 (33%) of the 12 tumors with unideletion, 32 (49%) of 65 tumors without deletion, and none (0%) of the 44 codeleted tumors. There was a significant difference in the frequency of T2-FLAIR mismatch when comparing the undeleted and codeleted tumors ( $P = .001$ ), but there was no significant difference when comparing the undeleted tumors and those without deletion ( $P = .39$ ). Calcifications were demonstrated in none (0%) of the undeleted tumors, 2 (3%) of the tumors without deletion, and 11 (25%) of the codeleted tumors. There was a trend ( $P = .097$ ) toward a difference in the frequency of calcifications when comparing the undeleted and codeleted tumors, but no significant difference was found when comparing the undeleted tumors and those without deletion ( $P = 1$ ). Of note, the tumor with 1p-unideletion demonstrated neither T2-FLAIR mismatch nor calcifications. The above results are summarized in Table 2.

The median survival of patients with undeleted tumors was 7.8 years, which was similar to the median survival of 8.5 years for those with tumors without deletion ( $P = .72$ ). In contrast, the median survival was not reached for the codeleted tumors after 12 years of follow-up, and there was a statistically significant difference in survival between those with undeleted and codeleted tumors ( $P = .013$  on multivariate analysis). Kaplan-Meier survival curves for all 3 tumor groups are shown in Fig 3, and median survival data are also included in Table 2.

## DISCUSSION

Both our imaging and survival data strongly support that tumors with single-arm 1p or 19q deletion are equivalent to *IDH*<sup>mut</sup>

astrocytomas, rather than oligodendrogliomas, in line with the WHO classification.<sup>2</sup> This finding provides reassurance to pathologists and treating clinicians that tumors with 1p- or 19q-unideletion should indeed be considered astrocytomas, rather than having a reason to question the 1p/19q result or repeat testing on a different part of the tumor. Our results are also concordant with our understanding of the underlying biology: 1p/19q-codeletion is thought to occur due to a translocation between chromosomes 1 and 19, with loss of the resulting derivative chromosome,<sup>15,16</sup> accounting for the simultaneous deletion of both chromosome arms. In turn, this implies that single-arm 1p or 19q deletion occurs through different mechanisms, which then manifest as different MR imaging appearances and clinical behavior compared with those of an oligodendroglioma.

Despite the large amount of research into glioma radiogenomics, more recently incorporating artificial intelligence, clinical translation of these techniques has been limited and should be a priority for future research.<sup>17,18</sup> We see radiogenomics as complementary to the criterion standard histologic/molecular assessment, rather than a competing technique. As noted before, radiogenomics can be used to question a molecular testing result, prompting additional genetic testing and hence refinement of the diagnosis.<sup>14</sup> We have demonstrated another potential role of radiogenomics through this work, namely using MR imaging to support the molecular diagnosis and provide additional insight into the underlying tumor biology.

We deliberately assessed only 2 of the radiogenomic features described in grade 2–3 tumors, because these features are the most specific predictors of genotype when *IDH* status is unknown.<sup>6</sup> As we sought to identify features that might potentially question the molecular testing result, it was important to select features with high specificity,<sup>13</sup> rather than necessarily those with the highest sensitivity or overall accuracy. Some other features can help distinguish astrocytomas and oligodendrogliomas if the tumor is known to be *IDH*<sup>mut</sup>—ie, predicting whether the tumor is 1p/19q<sup>codelet</sup>—but are less helpful discriminators if an *IDH*<sup>wt</sup> tumor is also a consideration. For example, oligodendrogliomas tend to be more ill-defined and demonstrate lower ADC values than *IDH*<sup>mut</sup> astrocytomas,<sup>19–22</sup> but *IDH*<sup>wt</sup> tumors are also usually ill-defined, with generally even lower ADC values than oligodendrogliomas.<sup>6,23–26</sup> Similarly, oligodendrogliomas can demonstrate elevated CBV even when low-grade,<sup>27</sup> but CBV elevation is also a feature of *IDH*<sup>wt</sup> tumors.<sup>28</sup> It can be challenging to confidently distinguish calcification and hemorrhage, especially if a preoperative CT scan is not available, so it is possible that calcification could have been underdiagnosed among the unideleted tumors. However, this issue is also true of the oligodendrogliomas, so if optimal characterization had been possible for all tumors, we consider it more likely that calcification would have been identified in additional oligodendrogliomas. If so, a statistically significant difference in the frequency of calcifications between the unideleted and codeleted tumors may have been found. Despite these limitations, we think that our results show quite conclusively that the MR imaging features of unideleted tumors are equivalent to those of *IDH*<sup>mut</sup> astrocytomas rather than oligodendrogliomas.

It was not feasible to correct for treatment in the survival analysis, because the use of chemotherapy and/or radiation therapy was often prompted by evidence of tumor progression, thus could not be considered an independent variable. We did not consider it appropriate to correct for the 2 imaging features assessed in our survival analysis because none of the 1p/19q<sup>codelet</sup> tumors demonstrated T2-FLAIR mismatch and none of the unideleted tumors exhibited calcifications. Additionally, the survival of patients with *IDH*<sup>mut</sup> astrocytomas with and without T2-FLAIR mismatch has already been compared for part of this cohort, with no significant difference in survival found.<sup>29</sup>

We note that there was only one 1p-unideleted tumor in our cohort; thus, it is not possible to assess any potential differences in the MR imaging appearance between 1p- and 19q-unideleted tumors. This is in line with earlier research demonstrating a larger (albeit still small) number of tumors with single-arm 19q deletion than 1p-unideletion.<sup>16,30</sup> Given that 1p- or 19q-unideletion does not alter the molecular diagnosis, it is possible that such findings were under-reported (predominantly for the minority of 1p/19q testing in this cohort that was performed as standard of care), though the numbers seem to be broadly consistent with those in previous studies.<sup>16,30</sup> The rarity of 1p-unideleted tumors implies that if only chromosome 1 were to be assessed, most tumors with 1p deletion would actually be 1p/19q<sup>codelet</sup>. This possibility likely accounts for earlier research showing that 1p deletion predicts a better response to chemotherapy and longer survival.<sup>31</sup>

We acknowledge that the number of unideleted tumors in our cohort is small, but these tumors are uncommon, representing a small proportion of *IDH*-mutant histologic grade 2–3 gliomas (10% in our cohort), which themselves comprise a minority of all adult-type diffuse gliomas. Although these relatively small numbers invite further validation, ultimately our results are themselves providing validation for the existing WHO guidelines, utilizing the unique and complementary ability of imaging to assess the entire tumor. This feature increases confidence that an *IDH*<sup>mut</sup> glioma shown to have single-arm 1p or 19q deletion can truly be considered an astrocytoma, in turn increasing confidence regarding the appropriate management.

## CONCLUSIONS

We have shown that *IDH*<sup>mut</sup> gliomas demonstrating single-arm 1p or 19q deletion have MR imaging appearances and survival similar to those of astrocytomas without 1p or 19q deletion and significantly different from those of 1p/19q<sup>codelet</sup> oligodendrogliomas. This result supports the existing WHO classification that such tumors lie within the spectrum of astrocytomas.























Disclosure forms provided by the authors are available with the full text and PDF of this article at [www.ajnr.org](http://www.ajnr.org).

## REFERENCES

1. Louis DN, Perry A, Reifenberger G, et al. **The 2016 World Health Organization Classification of Tumors of the Central Nervous System: a summary.** *Acta Neuropathol* 2016;131:803–20 CrossRef Medline
2. Louis DN, Perry A, Wesseling P, et al. **The 2021 WHO Classification of Tumors of the Central Nervous System: a summary.** *Neuro Oncol* 2021;23:1231–51 CrossRef Medline

3. Horbinski C, Nikiforova MN, Hobbs J, et al. **The importance of 10q status in an outcomes-based comparison between 1p/19q fluorescence in situ hybridization and polymerase chain reaction-based microsatellite loss of heterozygosity analysis of oligodendrogliomas.** *J Neuropathol Exp Neurol* 2012;71:73–82 CrossRef Medline
4. Horbinski C. **What do we know about IDH1/2 mutations so far, and how do we use it?** *Acta Neuropathol* 2013;125:621–36 CrossRef Medline
5. Lasocki A, Tsui A, Tacey MA, et al. **MRI grading versus histology: predicting survival of World Health Organization grade II–IV astrocytomas.** *AJNR Am J Neuroradiol* 2015;36:77–83 CrossRef Medline
6. Lasocki A, Anjari M, Örs Kokurcan S, et al. **Conventional MRI features of adult diffuse glioma molecular subtypes: a systematic review.** *Neuroradiology* 2021;63:353–62 CrossRef Medline
7. Broen MPG, Smits M, Wijnenga MMJ, et al. **The T2-FLAIR mismatch sign as an imaging marker for non-enhancing IDH-mutant, 1p/19q-intact lower grade glioma: a validation study.** *Neuro Oncol* 2018;20:1393–99 CrossRef Medline
8. Lasocki A, Gaillard F, Gorelik A, et al. **MRI features can predict 1p/19q status in intracranial gliomas.** *AJNR Am J Neuroradiol* 2018;39:687–92 CrossRef Medline
9. Patel SH, Poisson LM, Brat DJ, et al. **T2-FLAIR mismatch, an imaging biomarker for IDH and 1p/19q status in lower-grade gliomas: a TCGA/TCIA project.** *Clin Cancer Res* 2017;23:6078–85 CrossRef Medline
10. Park SI, Suh CH, Guenette JP, et al. **The T2-FLAIR mismatch sign as a predictor of IDH-mutant, 1p/19q-noncodeleted lower-grade gliomas: a systematic review and diagnostic meta-analysis.** *Eur Radiol* 2021;31:5289–99 CrossRef Medline
11. Saito T, Muragaki Y, Maruyama T, et al. **Calcification on CT is a simple and valuable preoperative indicator of 1p/19q loss of heterozygosity in supratentorial brain tumors that are suspected grade II and III gliomas.** *Brain Tumor Pathol* 2016;33:175–82 CrossRef Medline
12. Lasocki A, Buckland ME, Drummond KJ, et al. **Conventional MRI features can predict the molecular subtype of adult grade 2-3 intracranial diffuse gliomas.** *Neuroradiology* 2022;64:2295–305 CrossRef Medline
13. Lasocki A, Rosenthal MA, Roberts-Thomson SJ, et al. **Neuro-oncology and radiogenomics: time to integrate?** *AJNR Am J Neuroradiol* 2020;41:1982–88 CrossRef Medline
14. Patel SH, Batchala PP, Mrachek EK, et al. **MRI and CT identify isocitrate dehydrogenase (IDH)-mutant lower-grade gliomas misclassified to 1p/19q codeletion status with fluorescence in situ hybridization.** *Radiology* 2020;294:160–67 CrossRef Medline
15. Brandner S, McAleenan A, Jones HE, et al. **Diagnostic accuracy of 1p/19q codeletion tests in oligodendroglioma: a comprehensive meta-analysis based on a Cochrane systematic review.** *Neuropathol Appl Neurobiol* 2022;48:e12790 CrossRef Medline
16. Jenkins RB, Blair H, Ballman KV, et al. **A t(1;19)(q10;p10) mediates the combined deletions of 1p and 19q and predicts a better prognosis of patients with oligodendroglioma.** *Cancer Res* 2006;66:9852–61 CrossRef Medline
17. Bhandari AP, Liong R, Koppen J, et al. **Noninvasive determination of IDH and 1p19q status of lower-grade gliomas using MRI radiomics: a systematic review.** *AJNR Am J Neuroradiol* 2021;42:94–101 CrossRef Medline
18. Kalarooan D, Lasocki A. **MRI-based deep learning techniques for the prediction of isocitrate dehydrogenase and 1p/19q status in grade 2-4 adult gliomas.** *J Med Imaging Radiat Oncol* 2023;67:492–98 CrossRef Medline
19. Johnson DR, Diehn FE, Giannini C, et al. **Genetically defined oligodendroglioma is characterized by indistinct tumor borders at MRI.** *AJNR Am J Neuroradiol* 2017;38:678–84 CrossRef Medline
20. Kim JW, Park CK, Park SH, et al. **Relationship between radiological characteristics and combined 1p and 19q deletion in World Health Organization grade III oligodendroglial tumours.** *J Neurol Neurosurg Psychiatry* 2011;82:224–27 CrossRef Medline
21. Cui Y, Ma L, Chen X, et al. **Lower apparent diffusion coefficients indicate distinct prognosis in low-grade and high-grade glioma.** *J Neurooncol* 2014;119:377–85 CrossRef Medline
22. Thust SC, Hassanein S, Bisdas S, et al. **Apparent diffusion coefficient for molecular subtyping of non-gadolinium-enhancing WHO grade II/III glioma: volumetric segmentation versus two-dimensional region of interest analysis.** *Eur Radiol* 2018;28:3779–88 CrossRef Medline
23. Darlix A, Deverdun J, Menjot de Champfleury N, et al. **IDH mutation and 1p19q codeletion distinguish two radiological patterns of diffuse low-grade gliomas.** *J Neurooncol* 2017;133:37–45 CrossRef Medline
24. Delfanti RL, Piccioni DE, Handwerker J, et al. **Imaging correlates for the 2016 update on WHO classification of grade II/III gliomas: implications for IDH, 1p/19q and ATRX status.** *J Neurooncol* 2017;135:601–09 CrossRef Medline
25. Hyare H, Rice L, Thust S, et al. **Modelling MR and clinical features in grade II/III astrocytomas to predict IDH mutation status.** *Eur J Radiol* 2019;114:120–27 CrossRef Medline
26. Park YW, Han K, Ahn SS, et al. **Prediction of IDH1-mutation and 1p/19q-codeletion status using preoperative MR imaging phenotypes in lower grade gliomas.** *AJNR Am J Neuroradiol* 2018;39:37–42 CrossRef Medline
27. Lev MH, Ozsunar Y, Henson JW, et al. **Glial tumor grading and outcome prediction using dynamic spin-echo MR susceptibility mapping compared with conventional contrast-enhanced MR: confounding effect of elevated rCBV of oligodendrogliomas [corrected].** *AJNR Am J Neuroradiol* 2004;25:214–21 Medline
28. Xing Z, Yang X, She D, et al. **Noninvasive assessment of IDH mutational status in World Health Organization grade II and III astrocytomas using DWI and DSC-PWI combined with conventional MR imaging.** *AJNR Am J Neuroradiol* 2017;38:1138–44 CrossRef Medline
29. Lasocki A, Buckland ME, Molinaro T, et al. **Correlating MRI features with additional genetic markers and patient survival in histological grade 2-3 IDH-mutant astrocytomas.** *Neuroradiology* 2023;65:1215–23 CrossRef Medline
30. Vogazianou AP, Chan R, Bäcklund LM, et al. **Distinct patterns of 1p and 19q alterations identify subtypes of human gliomas that have different prognoses.** *Neuro Oncol* 2010;12:664–78 CrossRef Medline
31. Thiessen B, Maguire JA, McNeil K, et al. **Loss of heterozygosity for loci on chromosome arms 1p and 10q in oligodendroglial tumors: relationship to outcome and chemosensitivity.** *J Neurooncol* 2003;64:271–78 CrossRef Medline

# Impact of Balloon Guide Catheters in Elderly Patients Treated with Mechanical Thrombectomy: Insights from the ROSSETTI Registry

 Mikel Terceño,  Saima Bashir,  Josep Puig,  Josep Daunis-I-Estadella, Eduardo Murias, Jose María Jiménez,  Eva González Díaz, Jon Fondevila Monso, Isabel Bravo-Rey,  Veredas Romero,  Mariano Werner,  Antonio López-Rueda,  Luis San Román,  Jordi Blasco Anadaluz,  Antonio Doncel-Moriano,  Santiago Rosati,  Carlos Pérez-García,  Sebastian Remollo,  Isabel Rodríguez Caamaño, Sonia Aixut,  Oscar Sabino Chirife Chaparro,  Juan Manuel Sanchis Garcia,  Jacobo Porto-Álvarez, Jose Carlos Mendez-Cendón,  Jose Carlos Rayon-Aledo,  Yeray Aguilar,  Guillermo Parrilla, Miguel Castaño, Joaquín Serena, and  Yolanda Silva



## ABSTRACT

**BACKGROUND AND PURPOSE:** Several nonrandomized studies have demonstrated the effectiveness of balloon guide catheters in treating patients with anterior circulation large-vessel occlusion. However, their impact on the elderly populations has been under-reported. We aimed to analyze the effect of balloon guide catheters in a cohort of elderly patients (80 years of age or older) with anterior circulation large-vessel occlusion.

**MATERIALS AND METHODS:** Consecutive patients from June 2019 to June 2022 were collected from the ROSSETTI Registry. Demographic and clinical data, angiographic endovascular technique, and clinical outcome were compared between balloon guide catheter and non-balloon guide catheter groups. We studied the association between balloon guide catheters and the rate of complete recanalization after a single first-pass effect modified TICI 2c–3, as well as their association with functional independence at 3 months.

**RESULTS:** A total of 808 patients were included during this period, 465 (57.5%) of whom were treated with balloon guide catheters. Patients treated with balloon guide catheters were older, had more neurologic severity at admission and lower baseline ASPECTS, and were less likely to receive IV fibrinolytics. No differences were observed in terms of the modified first-pass effect between groups (45.8 versus 39.9%,  $P = .096$ ). In the multivariable regression analysis, balloon guide catheter use was not independently associated with a modified first-pass effect or the final modified TICI 2c–3, or with functional independence at 3 months.

**CONCLUSIONS:** In our study, balloon guide catheter use during endovascular treatment of anterior circulation large-vessel occlusion in elderly patients did not predict the first-pass effect, near-complete final recanalization, or functional independence at 3 months. Further studies, including randomized clinical trials, are needed to confirm these results.

**ABBREVIATIONS:** BGC = balloon guide catheter; ET = endovascular thrombectomy; EVT = endovascular treatment; GPTR = groin puncture to first run; GTR = groin puncture to revascularization time; LVO = large-vessel occlusion; mFPE = modified first-pass effect; mTICI = modified TICI; sICH = symptomatic intracranial hemorrhage

The efficacy of endovascular treatment (EVT) in elderly patients with anterior circulation large-vessel occlusion (LVO) has been proven in several studies,<sup>1–5</sup> though the proportion of elderly patients included in clinical trials (around 15%)

has been low and likely unrepresentative of the real-life situation.<sup>6</sup>

Additionally, the use of the balloon guide catheter (BGC) has been widely associated with higher reperfusion rates in anterior

Received May 5, 2023; accepted after revision August 17.

From the Stroke Unit, Department of Neurology (M.T., S.B., J.S., Y.S.), Hospital Universitari Doctor Josep Trueta de Girona, Girona Biomedical Research Institute, Girona, Spain; Department of Radiology (J.P.), Hospital Universitari de Girona Doctor Josep Trueta, Girona, Catalunya, Spain; Department of Computer Science (J.D.-I.-E.), Applied Mathematics and Statistics, University of Girona, Girona, Catalunya, Spain; Department of Radiology (E.M., J.M.J.), Hospital Universitario Central de Asturias, Oviedo, Asturias, Spain; Department of Interventional Neuroradiology (E.G.D., J.F.M.), Department of Radiology, Cruces University Hospital, Barakaldo, País Vasco, Spain; Diagnostic and Therapeutic Neuroradiology Unit (I.B.-R., V.R.), Reina Sofia University Hospital, Córdoba, Andalucía, Spain; Neurointerventional Department, Centro de Diagnóstico por la Imagen (CDI) (M.W.)

and Department of Neurology (A.D.-M.), Hospital Clinic de Barcelona, Barcelona, Spain; Department of Interventional Neuroradiology (A.L.-R., L.S.R., J.B.A.), Clinic University Hospital, Barcelona, Barcelona, Spain; Department of Interventional Neuroradiology (S. Rosati, C.P.-G.), Department of Radiology, Hospital Universitario Clínico San Carlos, Madrid, Spain; Department of Interventional Neuroradiology (S. Remollo, I.R.C.), Hospital Universitari Germans Trias i Pujol, Badalona, Spain; Department of Interventional Neuroradiology (S.A., O.S.C.C.), Hospital Universitari de Bellvitge, L'Hospitalet de Llobregat, Barcelona, Spain; Neuroradiology Unit (J.M.S.G.), Hospital Universitario y Politécnico La Fe, Valencia, Spain; Department of Neuroradiology (J.P.-A.), Complejo Hospitalario Universitario de Santiago de Compostela, Galicia, Spain; Interventional Neuroradiology Unit (J.C.M.-C.), Department of Radiology, Hospital Ramón y Cajal, Madrid, Spain; Department of Interventional Neuroradiology (J.C.R.-A.),



circulation LVO and better clinical outcomes.<sup>7-11</sup> However, the efficacy of the BGC in the elderly population is uncertain and poorly reported; consequently, its potential benefit in this population has yet to be proven.

The aim of the study was to determine the effect of BGC use on the rates of modified first-pass effect (mFPE) in a large cohort of elderly patients with anterior circulation LVO, due to the paucity of available data and the ongoing debate over the optimal endovascular approach to achieve complete reperfusion.

## MATERIALS AND METHODS

The Registry of Combined vs Single Thrombectomy Techniques (ROSSETTI) (ClinicalTrials.gov Identifier: NCT04886687) is an ongoing investigator-initiated prospective study recruiting deidentified consecutive patients with acute ischemic stroke secondary to anterior circulation LVO treated with endovascular thrombectomy (ET) across 15 comprehensive stroke centers in Spain.

For this study, conducted according to the Strengthening the Reporting of Observational Studies in Epidemiology (STROBE) guidelines, we included patients treated from June 2019 to June 2022. The study inclusion criteria were the following: 80 years of age or older with confirmed LVO in the anterior circulation (intracranial ICA, M1, proximal M2); time from last seen well to treatment up to 24 hours; baseline NIHSS score  $\geq 2$ ; and a premorbid mRS score  $\leq 2$ . The presence of multiterritory arterial embolisms and tandem occlusions was the main exclusion criterion for this study. The type of ET approach and technique was at the discretion of the operator, including the use of BGC or conventional guide catheters.

Qualifying patients were categorized according to whether BGC was used. The primary outcome was the rate of mFPE defined as achieving near-complete/complete revascularization (modified TICI [mTICI 2c-3]) after a single-device and single-pass approach.

The secondary outcome was the rate of near-complete reperfusion at the end of the procedure. We also analyzed the association between BGC use and the rate of functional independence, defined as an mRS score of 0-2 at 3-month follow-up.

Demographic and clinical data, the mTICI reperfusion scores, symptomatic intracranial hemorrhage (sICH) (according to the Second European Cooperative Acute Stroke Study [ECASS-II] definition), rates of mFPE defined as achieving mTICI 2b-3 after a single-device and single-pass approach, final rates of successful (mTICI 2b-3) and near-complete (mTICI 2c-3) reperfusion, and rates of functional independence at 3 months were assessed for the BGC and non-BGC subgroups. Groin puncture to revascularization time (GTR) was subcategorized into groin puncture to first run (GPTFR) and first run to final revascularization (ET time) and was also compared between the 2 groups. Reperfusion scores and sICH evaluation were center-adjudicated by experienced interventionists and neuroradiologists, and functional outcome at 3 months was assessed by stroke neurologists blinded to the imaging data.

## Statistical Analysis

Demographic and clinical data, procedural details, and angiographic and clinical outcomes were compared in non-BGC-treated versus BGC-treated patients, FPE versus non-FPE events, and independent (mRS  $\leq 2$ ) versus dependent functional outcome (mRS  $> 2$ ) at 3 months.  $\chi^2$  and Fisher exact tests were used for categorical variables; the Student *t* test/*F*-test, for continuous variables; and the  $\chi^2$  test, for categorical variables. Continuous variables are shown as mean (SD) or median (interquartile intervals) and were compared using the Student *t* test, ANOVA, Mann-Whitney, or Kruskal-Wallis tests as appropriate. Categorical variables were reported as proportions. Variables with a *P* value  $< .1$  in the univariate analyses were entered into the multivariable models. Using binary logistic regression models in multivariate analysis, we evaluated the use of BGC as an independent factor contributing to first-pass effect and/or final near-complete recanalization.

All statistical analyses were performed using R statistical and computing software (Version 3.6.1; <http://www.r-project.org/>).

## Ethics

All participating centers received institutional review board approval from their respective ethical committees and patients or their representatives signed the corresponding informed consent. The ROSSETTI Registry has been approved by the Independent Ethics Committee of the Hospital (Clinic of Barcelona HCB/2019/0152).

## RESULTS


From 1728 patients included in the registry, a total of 808 patients met the inclusion criteria. The median age was 85 years, 521 (64.5%) were women, and 303 patients (37.5%) achieved functional independence at 3 months (Table 1). Patients treated with BGC (465 patients, 57.5%) were significantly older (86 versus 85 years of age,  $P < .001$ ), had better ASPECTS at baseline (9 versus 8,  $P < .008$ ), and had better neurologic status at admission (NIHSS 16 versus 18,  $P = .035$ ).

The primary outcome (mFPE) was achieved in 45.8% of patients in the BGC group and in 39.9% of patients in the non-BGC group, with no statistical differences ( $P = .096$ ). Furthermore, the rates of FPE were also similar between groups (55.9% versus 51%,  $P = .168$ ).

Both successful and near-complete recanalizations were significantly higher in patients treated with BGC (93.8% versus 89.8%,  $P = .039$ , and 77.4% versus 66.2%,  $P = .001$ , respectively), with no statistical differences observed in the number of passes, final mTICI 0, or emboli to a new territory. Technical modification was less frequent in the BGC group (21.9% versus 35.4%,  $P = .001$ ), and procedural times were shorter in this group (30 minutes versus 42 minutes,  $P = .001$ ). Figure 1 summarizes the results of the final mTICI by BGC use. NIHSS score at 24 hours was significantly lower (7 versus 10.5,  $P = .002$ ), but no differences

Hospital General Universitario de Alicante, Alicante, Valenciana, Spain; Department of Radiology (Y.A.), Hospital Universitario Insular de Gran Canaria, Las Palmas de Gran Canaria, Spain; Department of Interventional Neuroradiology (G.P.), Department of Radiology, Hospital Clínico Universitario Virgen de la Murcia, Spain; and Department of Interventional Neuroradiology (M.C.), Hospital Clínico Universitario de Salamanca, Salamanca, Spain.

Please address correspondence to Saima Bashir, MD, Unitat d'Ictus, Servei de Neurologia, Hospital Universitari Doctor Josep Trueta de Girona, Av de França s/n 17007 Girona; e-mail: sbashir.girona.ics@gencat.cat; @MikelTerceno; @SaimaBV; @Ictus\_Girona; @jordiblascoa; @AntonioLR81; @Sremollo

 Indicates article with online supplemental data.  
<http://dx.doi.org/10.3174/ajnr.A8003>

**Table 1: Demographics, clinical and neurologic characteristics by BGC use**

	Overall Patients ≥80 Years (n = 808)	Non-BGC Use (n = 343, 42.5%)	BGC Use (n = 465, 57.5%)	P Value
Age (median) (IQR) (yr)	85 (83–88)	85 (82–88)	86 (83–89)	.001
Female sex (No.) (%)	521 (64.5)	217 (63.3)	304 (65.4)	.535
NIHSS score at admission (median) (IQR)	17 (12–21)	18 (13–21)	16 (11–21)	.035
ASPECTS at admission (median) (IQR)	9 (7–10)	8 (7–10)	9 (8–10)	.008
Time from stroke onset to diagnosis (median) (IQR) (min)	280 (180.75–589.25)	300 (196.5–564)	261 (172–609)	.069
IV tPA administered (No.) (%)	212 (26.2)	114 (33.2)	98 (21.1)	<.001
General anesthesia during EVT (No.) (%)	262 (32.4)	120 (35)	142 (30.5)	.142
Right-sided occlusion (No.) (%)	388 (48)	157 (45.8)	231 (49.7)	.272
Level of vessel occlusion (No.) (%)				.002
Carotid terminus	157 (19.5)	79 (23)	78 (16.8)	
MCA-M1	425 (52.7)	189 (55.1)	236 (50.9)	
MCA-M2	225 (27.9)	75 (21.9)	150 (32.3)	
GPTFR (median) (IQR) (min)	7 (5–12)	9 (5–16)	6 (4–10)	<.001
ET time (median) (IQR) (min)	25 (12–43)	30 (16–49)	22 (11–39)	<.001
GTR (median) (IQR) (min)	35 (22–57)	42 (27–66.5)	30 (19–49.25)	<.001
SR use	790 (97.8)	335 (97.7)	455 (97.8)	.863
Distal aspiration catheter use (No.) (%)	422 (52.2)	406 (51.4)	16 (88.9)	.002
Combined technique use (CA + SR)	406 (50.2)	292 (85.1)	114 (24.5)	<.001
FPE (mTICI 3) (No.) (%)	293 (36.3)	112 (32.7)	181 (38.9)	.067
mFPE (mTICI 2c–3) (No.) (%)	350 (43.3)	137 (39.9)	213 (45.8)	.096
FPE (mTICI 2b–3) (No.) (%)	435 (53.8)	175 (51)	260 (55.9)	.168
Final No. of passes (No.) (%)				.991
1	380 (47)	161 (46.9)	219 (47.1)	
2	192 (23.8)	81 (23.6)	111 (23.9)	
>2	236 (29.2)	101 (29.4)	135 (29)	
Technique modification	134 (27.9)	75 (35.4)	59 (21.9)	.001
mTICI 0 after first pass	256 (31.7)	118 (34.4)	138 (29.7)	.154
Final mTICI 0	29 (3.6)	17 (5)	12 (2.6)	.073
Final mTICI ≥ 2b (No.) (%)	744 (92.1)	308 (89.8)	436 (93.8)	.039
Final mTICI ≥ 2c (No.) (%)	587 (72.6)	227 (66.2)	360 (77.4)	<.001
Emboli to new territory	129 (16)	59 (17.2)	70 (15.1)	.410
sICH (No.) (%)	53 (6.6)	36 (10.5)	17 (3.7)	<.001
Complications				.692
Perforation	11 (29.7)	5 (29.4)	6 (30)	
Dissection	15 (40.5)	8 (47.1)	7 (35)	
NIHSS score at 24 hr (median) (IQR)	8 (3–16)	10.5 (4–17)	7 (2–15)	.002
Early neurologic deterioration (No.) (%)	52 (6.4)	26 (7.5)	26 (5.6)	.071
mRS 0–1 at 3 mo	191 (23.6)	81 (23.6)	110 (23.7)	.989
mRS 0–2 at 3 mo	303 (37.5)	136 (39.7)	167 (35.9)	.278
Mortality at 3 mo (No.) (%)	225 (27.8)	107 (31.2)	118 (25.4)	.068

**Note:**—IQR indicates interquartile range; SR, stent retriever; CA, contact aspiration.

were observed in functional independence or mortality at 3 months (Table 1 and Fig 2).

No endovascular technique, including BGC use, was associated with higher rates of mFPE (Table 2). Baseline ASPECTS, BGC use, distal aspiration catheter use, IV recombinant tPA, GTR, and endovascular time were statistically associated with final mTICI 2c–3. However, in the multivariate analysis, BGC use was not identified as an independent predictor of mFPE or final mTICI 2c–3 (Table 3). The univariate analyses for final mTICI2c–3 and endovascular techniques are available in the Online Supplemental Data. Finally, no differences were observed in functional outcome by BGC use (Fig 2).

## DISCUSSION

Our study shows that in a large cohort of consecutive elderly patients treated endovascularly, there was no evidence of benefit of BGC use in terms of early near-complete reperfusion (mFPE TICI 2c–3) or final near-complete reperfusion (mTICI 2c–3) compared with classic guide catheters or on clinical outcome.

Despite the low representation of elderly patients in clinical trials, several nonrandomized studies have demonstrated the benefit of EVT in elderly patients with anterior circulation LVO stroke. Although the efficacy is likely lower than in younger patients, it remains cost-effective for patients older than 80 years of age.<sup>1–5</sup> A subanalysis of the Highly Effective Reperfusion evaluated in Multiple Endovascular Stroke Trials (HERMES) meta-analysis showed a benefit of EVT in patients 85 years of age or older compared with conservative treatment (adjusted OR, 0.20 [95% CI, 0.13–0.33]).<sup>11</sup> Likewise, in the Multicenter Randomized Clinical Trial of Endovascular Treatment for Acute Ischemic Stroke in the Netherlands (MR CLEAN) Registry, an association between successful recanalization and good clinical outcome was also observed in patients 80 years of age or older.<sup>12</sup>

The reported rates of successful recanalization in the elderly population range from 75% to 88%, whereas functional independence at 3 months (defined by the presence of mRS 0–2) ranges from 18.2% to 27%, depending on the series,<sup>14,11</sup> considerably

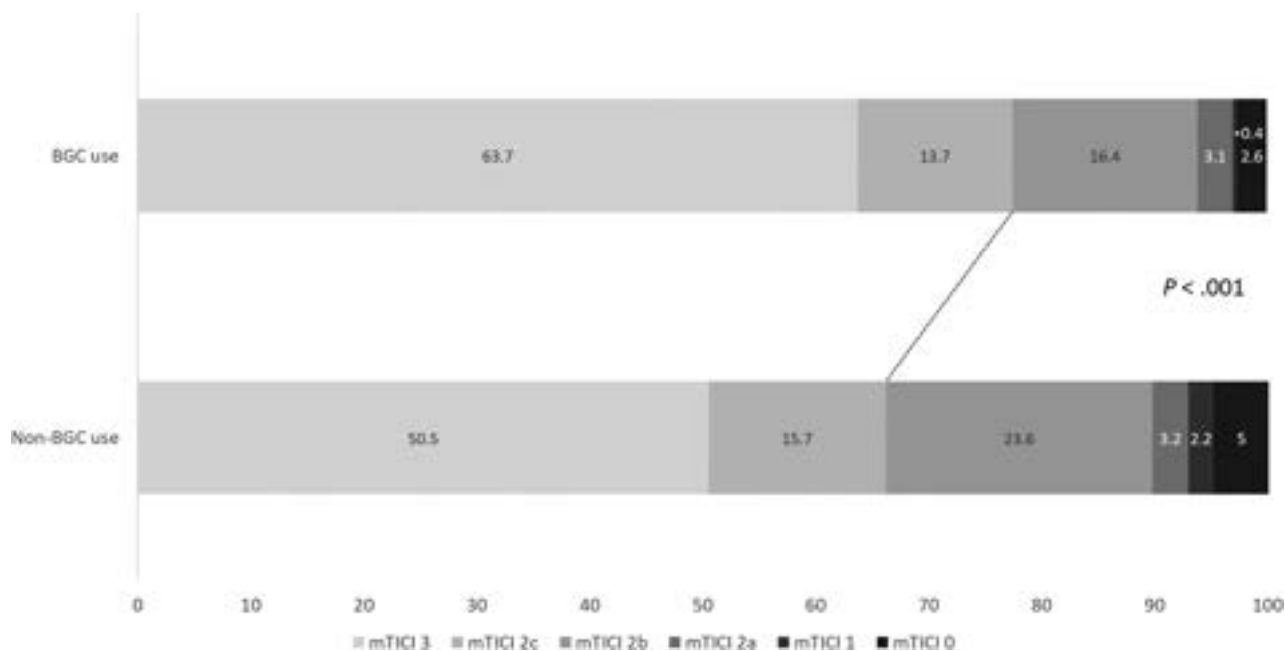


**FIG 1.** Distribution of the final mTICI according to BGC versus non-BGC use.

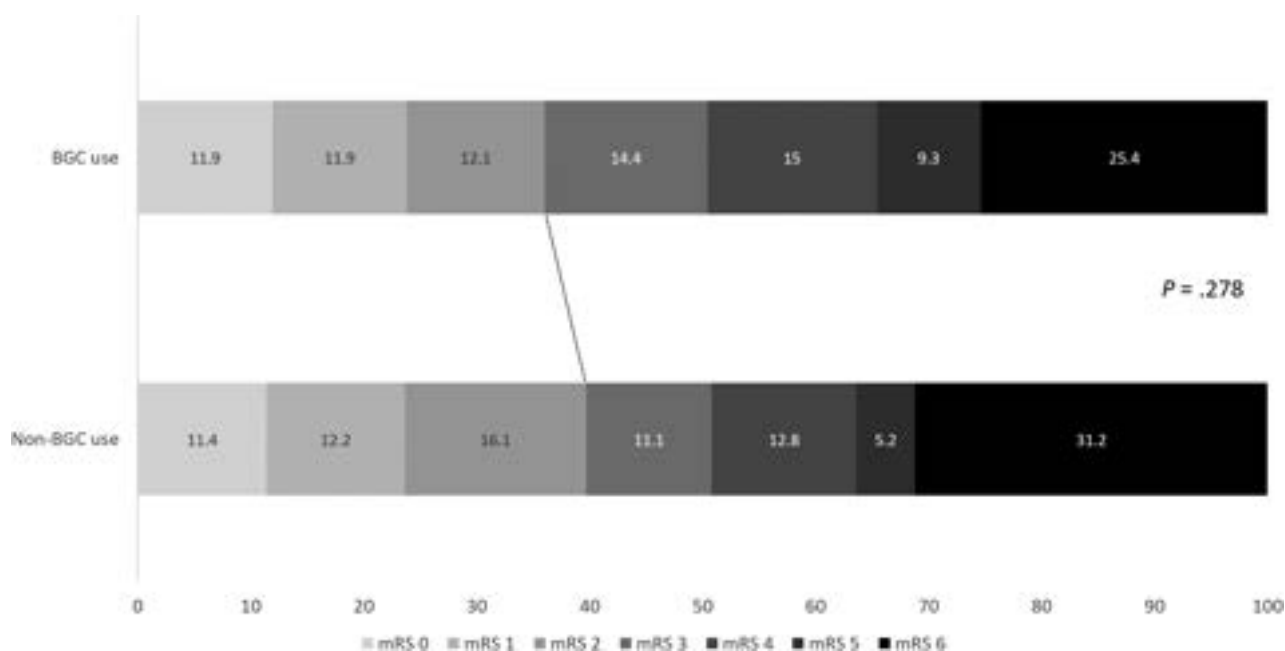


**FIG 2.** Distribution of mRS at 3 months according to BGC versus non-BGC use.

lower than that reported in the overall population of the HERMES meta-analysis (46%). Mehta et al<sup>13</sup> published what may be the largest series from a nationwide sample with 1547 elderly patients (80 years of age or older) admitted between 2014 and 2016 without ET and a functional independence at 3 months of 9%.

Unfortunately, there is a lack of data regarding endovascular approaches in elderly patients, and there is no evidence regarding the efficacy of BGC due to the absence of specific studies in this population.

Since Nguyen et al<sup>14</sup> reported, in 2014, the benefit of BGC in revascularization and outcome results for the first time, several

studies have confirmed the efficacy of BGC in anterior circulation LVO as an independent factor associated with successful recanalization and functional independence.<sup>7-11,15-19</sup>

On the other hand, a small number of studies found that BGC did not improve angiographic or clinical outcomes compared with conventional guide catheters. A recent meta-analysis involving 2091 patients reported no benefit of BGC use in terms of near-complete recanalization, FPE, or functional independence at 3 months. In addition, the authors concluded that the combined technique (contact aspiration plus stent retriever) did not improve reperfusion rates.<sup>20</sup> Bourcier et al<sup>21</sup> published their experience with

**Table 2: Univariate analysis for mFPE (mTICI 2c–3)**

	Overall Patients ≥80 Years (n = 808)	No mFPE (n = 458, 56.7%)	mFPE (n = 350, 43.3%)	P Value
Age (median) (IQR) (yr)	85 (83–88)	85 (83–88)	85 (83–88.75)	.294
Female sex (No.) (%)	521 (64.5)	293 (56.2)	228 (43.8)	.731
NIHSS score at admission (median) (IQR)	17 (12–21)	17 (12–21)	17 (12–20)	.323
ASPECTS at admission (median) (IQR)	9 (7–10)	9 (7–10)	9 (8–10)	.002
Last time seen well (median) (IQR) (min)	280 (180.75–589.25)	280 (183–608)	280 (178–568.5)	.478
IV tPA administered (No.) (%)	212 (26.2)	125 (27.3)	87 (24.9)	.459
General anesthesia (No.) (%)	262 (32.4)	138 (30.1)	124 (35.4)	.123
Local anesthesia (No.) (%)	160 (19.8)	87 (19)	73 (20.9)	
Conscious sedation (No.) (%)	386 (47.8)	233 (50.9)	153 (43.7)	
Right-sided occlusion (No.) (%)	388 (48)	226 (49.3)	162 (46.3)	.388
Level of vessel occlusion (No.) (%)				.564
Carotid terminus	157 (19.5)	94 (20.6)	63 (18)	
MCA-M1	425 (52.7)	234 (51.2)	191 (54.6)	
MCA-M2	225 (27.9)	129 (28.2)	96 (27.4)	
GPTFR (median) (IQR) (min)	7 (5–12)	7 (5–13)	7 (5–12)	.202
ET time (median) (IQR) (min)	25 (12–43)	37 (25–54.5)	12 (8–20)	<.001
GTR (median) (IQR) (min)	35 (22–57)	48 (35–71)	22 (15–31)	<.001
BGC use (No.) (%)	465 (57.5)	252 (55)	213 (60.9)	.096
SR (No.) (%)	790 (97.8)	446 (97.4)	344 (98.3)	.387
Combined technique use (CA + SR)	406 (50.2)	241 (52.6)	165 (47.1)	.123
Distal aspiration catheter use (No.) (%)	422 (52.2)	251 (54.8)	171 (48.9)	.094
Technique modification	134 (27.9)	130 (31.1)	4 (6.3)	<.001
siCH (No.) (%)	53 (6.6)	37 (8.1)	16 (4.6)	.134
Complications				.548
Perforation	11 (29.7)	10 (33.3)	1 (14.3)	
Dissection	15 (40.5)	12 (40)	3 (42.9)	
NIHSS score at 24 hr (median) (IQR)	8 (3–16)	12 (5–18)	5 (2–12)	<.001
mRS score 0–2 at 3 mo (No.) (%)	303 (37.5)	146 (31.9)	157 (44.9)	<.001
Mortality at 3 mo (No.) (%)	225 (27.8)	154 (33.6)	71 (20.3)	<.001

**Note:**—SR indicates stent retriever; CA, contact aspiration.

**Table 3: Multivariate analysis for FPE (mTICI 2c–3) and final mTICI 2c–3**

Variable	P Value	aOR	95% CI
Model 1: mFPE (mTICI 2c–3) <sup>a</sup>			
AUC = 0.845			
BGC use	.459	0.851	0.556–1.303
Distal aspiration catheter use	.333	1.230	0.809–1.872
ASPECTS	.102	0.981	0.981–1.236
Model 2: final mTICI 2c–3 <sup>b</sup>			
AUC = 0.765			
BGC use	.772	0.938	0.607–1.449
Distal aspiration catheter use	.013	0.570	0.366–0.888
SR use	.004	1.225	1.282–1.619
GTR	<.001	0.979	0.974–0.984
ASPECTS	.004	1.190	1.057–1.340
NIHSS admission	.549	.991	0.961–1.022
IV tPA administered	.014	.494	0.281–0.869
Right-sided occlusion	.020	0.652	0.456–0.934

**Note:**—BGC indicates balloon guide catheter and distal aspiration catheter use; aOR, adjusted OR; SR, stent retriever.

<sup>a</sup> Variables included in model 1 with a *P* value < .1 in the univariate analysis for FPE (mTICI2c–3).

<sup>b</sup> Variables included in model 2 with *P* value < .1 in the univariate analysis for final mTICI 2c–3.

607 patients recorded in the Endovascular Treatment of Ischemic Stroke (ETIS) Registry, including an analysis of 190 matched pairs. After adjusting for potential confounders, the use of BGC did not improve reperfusion and clinical outcomes when the combined technique was used. In addition, a recent propensity score corresponded to analyses that reached similar conclusions.<sup>22</sup> Unfortunately, no randomized clinical trials have been conducted

to date to explore the benefit of BGC use over conventional guide catheters, so observational studies provide the only available data at this time.

In our study, patients treated with BGC had higher rates of successful (mTICI 2b–3) and near-complete recanalization (mTICI 2c–3) on concluding EVT. There was a trend towards statistical significance in terms of mFPE (mTICI 2c–3) (45.8 versus 39.9%, *P* = .096), but there were no statistical differences in terms of safety and clinical outcomes at 3 months. However, the use of BGC was not independently associated with improved early or final recanalization rates after adjusting by confounder effects. Our results are consistent with those already published in the recent meta-analysis<sup>20</sup> and with the propensity score matching analysis published by Chen et al,<sup>22</sup> in which no differences in recanalization, favorable outcome, or complications were observed between patients treated with or without BGC independent of age.

In our recently published global cohort of 426 patients, from the ROSSETTI Registry, with a median age of 76 years, BGC use was identified as an independent factor associated with FPE and functional outcome at 3 months.<sup>8</sup> On the basis of this result, we can hypothesize that the age of patients undergoing ET may have a significant impact on angiographic and clinical outcomes. In these patients, arterial tortuosity may play an important role. In elderly patients, arterial tortuosity and the difficulty in reaching the target location to inflate the balloon and achieve flow arrest may compromise the efficacy of the BGC in terms of successful recanalization.<sup>23,24</sup> Velasco Gonzalez et al<sup>24</sup> studied the impact of



arterial tortuosity in the FPE in 200 consecutive patients treated endovascularly with BGC. FPE can range from 30% to 70%, depending on anatomic factors, and the BGC distal position was independently associated with FPE, highlighting the importance of optimizing the BGC technique.

### Limitations and Strengths

Our study has several limitations. As an observational study, the use of BGC or other techniques was not randomized because operator preference was respected. Moreover, there was no independent evaluation of the angiographic results for each patient, but blinded investigators reported functional outcome at 3 months and NIHSS scores at 24 hours.

On the other hand, this is the largest cohort of elderly patients studied in a multicenter prospective registry with a maintained database exploring the effect of BGC use.

### CONCLUSIONS

In our study, the use of BGC during endovascular treatment of elderly patients with anterior circulation LVO did not predict FPE or near-complete recanalization. Further studies and randomized trials are needed to confirm these results.

### ACKNOWLEDGMENTS

We thank all patients and their relatives and also all ROSSETTI investigators: Eva González, Ion Labayen, Jon Fondevila, Xavier Manso, Pedro Vega, Eduardo Murias, José María Jiménez, Juan Chaviano, María Castañón, Elena Lopez, Rafael Oteros, Elvira Jiménez, Isabel Bravo Rey, Veredas Romero, Fernando Delgado, Luis San Román, Antonio López Rueda, JM Macho Fernandez, Napoleón Macías, Federico Zarco, Arturo Renú, Jordi Blasco, Mariano Werner, Manuel Moreu, Carlos Perez García, Santiago Rosati, Alfonso López-Frias, Oscar Chirife, Sonia Aixut, Isabel Rodríguez Caamaño, María Ángeles de Miquel, Roger Barranco, Lucía Aja, Víctor Cuba, Mikel Terceño, Saima Bashir, Laura Paul, Carlos Castaño, Sebastian Remollo, Manel Pumar, Antonio Mosqueira, Yeray Aguilar, Daniel Cubillo, Alexis Bravo de Laguna Toboada, Jose Carlos Méndez, Isabel Bermúdez-Coronel, Eduardo Fandiño, Jose Ignacio Gallego, Nicolas López Hernandez, Sarai Moliner, José Carlos Rayon, Juan Carlos Llibre, José Antonio de las Heras García, Miguel Ángel Castaño, Joaquín Zamarró, Mariano Espinosa de Rueda, Guillermo Parrilla, Blanca García Villalba-Navaridas, Jose Diaz Pérez, Gonzalo de Paco Tudela, Isabel Vielba, Fernando Aparici.

The ROSSETTI Registry has been approved by the Independent Ethics Committee of the Hospital (Clinic of Barcelona HCB/2019/0152).

Disclosure forms provided by the authors are available with the full text and PDF of this article at [www.ajnr.org](http://www.ajnr.org).

### REFERENCES

1. Meyer L, Alexandrou M, Flottmann F, et al. **Endovascular treatment of very elderly patients aged  $\geq 90$  with acute ischemic stroke.** *J Am Heart Assoc* 2020;9:e014447 CrossRef Medline
2. Kunz WG, Hunink MG, Dimitriadis K, et al. **Cost-effectiveness of endovascular therapy for acute ischemic stroke: a systematic review of the impact of patient age.** *Radiology* 2018;288:518–26 CrossRef Medline
3. Zhao W, Ma P, Zhang P, et al. **Mechanical thrombectomy for acute ischemic stroke in octogenarians: a systematic review and meta-analysis.** *Front Neurol* 2020;10:1355 CrossRef Medline
4. Alawieh A, Starke RM, Chatterjee AR, et al. **Outcomes of endovascular thrombectomy in the elderly: a 'real-world' multicenter study.** *J Neurointerv Surg* 2019;11:545–53 CrossRef Medline
5. Hilditch CA, Nicholson P, Murad MH, et al. **Endovascular management of acute stroke in the elderly: a systematic review and meta-analysis.** *AJNR Am J Neuroradiol* 2018;39:887–91 CrossRef Medline
6. Goyal M, Menon BK, van Zwam WH, et al. **Endovascular thrombectomy after large-vessel ischaemic stroke: a meta-analysis of individual patient data from five randomised trials.** *Lancet* 2016;387:1723–31 CrossRef Medline
7. Baek JH, Kim BM, Kang DH, et al. **Balloon guide catheter is beneficial in endovascular treatment regardless of mechanical recanalization modality.** *Stroke* 2019;50:1490–96 CrossRef Medline
8. Blasco J, Puig J, Daunis-I-Estadella P, et al. **Balloon guide catheter improvements in thrombectomy outcomes persist despite advances in intracranial aspiration technology.** *J Neurointerv Surg* 2021;13:773–78 CrossRef Medline
9. Nguyen TN, Castonguay AC, Nogueira RG, et al. **Effect of balloon guide catheter on clinical outcomes and reperfusion in Trevo thrombectomy.** *J Neurointerv Surg* 2019;11:861–65 CrossRef Medline
10. Pederson JM, Reiersen NL, Hardy N, et al. **Comparison of balloon guide catheters and standard guide catheters for acute ischemic stroke: a systematic review and meta-analysis.** *World Neurosurg* 2021;154:144–53.e21 CrossRef Medline
11. McDonough RV, Ospel JM, Campbell BC, et al. **Functional outcomes of patients  $\geq 85$  years with acute ischemic stroke following EVT: a HERMES substudy.** *Stroke* 2022;53:2220–26 CrossRef Medline
12. Groot AE, Treurniet KM, Jansen IG, et al. **Endovascular treatment in older adults with acute ischemic stroke in the MR CLEAN Registry.** *Neurology* 2020;95:e131–39 CrossRef Medline
13. Mehta A, Fifi JT, Shoirah H, et al. **National trends in utilization and outcome of endovascular thrombectomy for acute ischemic stroke in elderly.** *J Stroke Cerebrovasc Dis* 2021;30:105505 CrossRef Medline
14. Nguyen TN, Malisch T, Castonguay AC, et al. **Balloon guide catheter improves revascularization and clinical outcomes with the Solitaire device: analysis of the North American Solitaire Acute Stroke Registry.** *Stroke* 2014;45:141–45 CrossRef Medline
15. Brinjikji W, Starke RM, Murad MH, et al. **Impact of balloon guide catheter on technical and clinical outcomes: a systematic review and meta-analysis.** *J Neurointerv Surg* 2018;10:335–39 CrossRef Medline
16. Zaidat OO, Castonguay AC, Linfante I, et al. **First pass effect: a new measure for stroke thrombectomy devices.** *Stroke* 2018;49:660–66 CrossRef Medline
17. Zaidat OO, Mueller-Kronast NH, Hassan AE, et al. **Impact of balloon guide catheter use on clinical and angiographic outcomes in the STRATIS Stroke Thrombectomy Registry.** *Stroke* 2019;50:697–704 CrossRef Medline
18. Ahn JH, Cho SS, Kim SE, et al. **The effects of balloon-guide catheters on outcomes after mechanical thrombectomy in acute ischemic strokes: a meta-analysis.** *J Korean Neurosurg Soc* 2019;62:389–97 CrossRef Medline
19. Podlasek A, Dhillon PS, Jewett G, et al. **Clinical and procedural outcomes with or without balloon guide catheters during endovascular thrombectomy in acute ischemic stroke: a systematic review and meta-analysis with first-line technique**

- subgroup analysis.** *AJNR Am J Neuroradiol* 2021;42:1464–71 CrossRef Medline
20. Teo YN, Sia CH, Tan BY, et al. **Combined balloon guide catheter, aspiration catheter, and stent retriever technique versus balloon guide catheter and stent retriever alone technique: a systematic review and meta-analysis.** *J Neurointerv Surg* 2023;15:127–32 CrossRef Medline
  21. Bourcier R, Marnat G, Labreuche J, et al. **Balloon guide catheter is not superior to conventional guide catheter when stent retriever and contact aspiration are combined for stroke treatment.** *Neurosurgery* 2020;88:E83–90 CrossRef Medline
  22. Chen Z, Liu Y, Li B, et al. **Comparing the conventional and balloon-guided catheter-assisted SWIM technology for the treatment of acute ischemic stroke.** *Front Neurol* 2022;13:86667 CrossRef Medline
  23. Jeong DE, Kim JW, Kim BM, et al. **Impact of balloon-guiding catheter location on recanalization in patients with acute stroke treated by mechanical thrombectomy.** *AJNR Am J Neuroradiol* 2019;40:840–44 CrossRef Medline
  24. Velasco Gonzalez A, Görlich D, Buerke B, et al. **Predictors of successful first-pass thrombectomy with a balloon guide catheter: results of a decision tree analysis.** *Transl Stroke Res* 2020;11:900–09 CrossRef Medline

# Considering Psychological and Cognitive Factors in Interventional Neuroradiology: A Systematic Literature Review

Chiara Riccietti, Silvia Schiavolin, Valentina Caldiera, Giuseppe Ganci, Annalisa Sgoifo, Giorgia Camarda, Matilde Leonardi, and Elisa Ciceri



## ABSTRACT

**BACKGROUND:** Interventional neuroradiology is a relatively recent discipline that diagnoses and treats cerebral vascular diseases. However, specific literature on cognitive and psychological domains of patients undergoing interventional neuroradiology procedures is limited.

**PURPOSE:** Our aim was to review the existent literature on cognitive and psychological domains in patients undergoing interventional neuroradiology procedures to raise clinicians' awareness of their mental status.

**DATA SOURCES:** Articles were searched in PubMed, EMBASE, and Scopus from 2000 to 2022 using terms such as "interventional neuroradiology," "psychology," and "cognition" according to Preferred Reporting Items for Systematic Reviews and Meta-Analyses (PRISMA) guidelines.

**STUDY SELECTION:** Of 1483 articles in English, 64 were included and analyzed. Twelve focused on psychological aspects; 52, on cognitive ones.

**DATA ANALYSIS:** Regarding psychological aspects, it appears that early psychological consultations and "nonpharmacologic" strategies can impact the anxiety and depression of patients undergoing endovascular procedures. Regarding cognitive aspects, it appears that endovascular treatment is safe and generates similar or even fewer cognitive deficits compared with analogous surgical procedures.

**DATA SYNTHESIS:** Among the 12 articles on psychological aspects, 6/12 were retrospective with one, while 6/12 were prospective. Among the 52 articles on cognitive aspects, 7/54 were retrospective, while 45/52 were prospective.

**LIMITATIONS:** The main limitation derives from the inhomogeneity of the cognitive and psychological assessment tools used in the articles included in our analysis.

**CONCLUSIONS:** Our review highlights the need to include cognitive and psychological assessments in clinical practice in case patients eligible for interventional neuroradiology procedures. In the future, much more research of and attention to cognitive and psychologic aspects of neurovascular disease is needed. Systematic incorporation of strategies and tools to access and address pre-, peri-, and postprocedural psychological and cognitive components could have major benefits in patient satisfaction, recovery, and the success of endovascular practice.

**ABBREVIATIONS:** CAS = carotid artery stent placement; DAVF = dural arteriovenous fistula; EC = endovascular coiling; INR = interventional neuroradiology; QoL = quality of life; RCT = randomized control trial; RIA = ruptured intracranial aneurysm; SC = surgical clipping; UIA = unruptured intracranial aneurysm

The number of patients with vascular disease undergoing diagnostic and therapeutic neuroangiography procedures has increased during the past decades.<sup>1</sup> Studies of neurovascular interventions have focused primarily on morbidity/mortality,

clinical deficiency, and disability. However, it is increasingly recognized that many neurovascular patients may have cognitive and psychological impairments that contribute to a decrease in their quality of life (QoL). It is a common experience that patients who have undergone neurovascular procedures do not feel a "real

Received May 3, 2023; accepted after revision August 30.

From the Imaging Radiology and Interventional Neuroradiology Unit (C.R., V.C., G.G., E.C.), Department of Neurosurgery, and Department of Neurology (S.S., G.C., M.L.), Public Health and Disability Unit, Fondazione Istituto di Ricovero e Cura a Carattere Scientifico Istituto Neurologico Carlo Besta, Milan, Italy; and Department of Neurology and Stroke Unit (A.S.), ASST Grande Ospedale Metropolitano Niguarda, Milan, Italy.

This work was supported by the Italian Ministry of Health Ricerca Corrente (Current Research).

Please address correspondence to Silvia Schiavolin, MD, Neurology, Public Health and Disability Unit, Fondazione IRCSS Istituto Neurologico Carlo Besta, Via Celoria 11, 20133 Milan, Italy; e-mail: [silvia.schiavolin@istituto-besta.it](mailto:silvia.schiavolin@istituto-besta.it)

Indicates open access to non-subscribers at [www.ajnr.org](http://www.ajnr.org)

Indicates article with online supplemental data.

<http://dx.doi.org/10.3174/ajnr.A8007>

recovery,”<sup>2</sup> even when they achieve complete anatomic cure. Unfortunately, these difficulties are not adequately assessed by standard clinical scales (ie, mRS, Glasgow Outcome Scale).<sup>3,4</sup>

We believe that a review of the existent literature can be helpful in raising clinicians’ awareness of a patient’s mental status and to recognize possible related psychological and cognitive changes.<sup>5,6</sup>

Being hospitalized is an unpleasant situation for most patients. Besides their illness, they must deal with several stressful experiences, including invasive vascular procedures.<sup>7</sup> Among these procedures, angiography is the criterion standard test for visualizing the neurovascular anatomy and understanding the complexity of cerebral circulation. However, due to its invasive nature and the risk of catheter-related injury, it represents a triggering experience causing anxiety. Furthermore, the level of anxiety and the ability to cope with it can influence the patient’s physiologic status (eg, respiratory and heart rates, blood pressure).<sup>8</sup> In addition, excessive stress during cerebral angiography could limit the patient’s ability to follow instructions during critical phases of the procedure.<sup>8</sup> Consequently, physiologic and psychological reactions may even increase the length of the procedure and the amount of sedation required. Moreover, even in the presence of favorable clinical outcomes and technically successful treatments, the mere presence of a CBV disease often results in some mental health impairment due to CBV symptoms or maladaptive coping with diagnostic tests and treatments.<sup>5,9,10</sup> Therefore, all these aspects should be seriously considered because they influence not only the patient’s well-being and compliance with future follow-up but also the safety and efficacy of the procedure.

Unfortunately to date, patients with CBV disease rarely receive adequate psychological consultation as a standard medical service.<sup>11</sup>

When a vascular disease involves eloquent neuronal areas or determines specific hemodynamic changes, it can affect cognitive functions such as language, attention, information-processing speed, memory and executive and visuospatial abilities. These capacities are not always clinically detectable by simple routine functional scales, as mentioned above.<sup>12-14</sup>

Beyond the neurocognitive deficits caused by the illness itself, such as in SAH and vasospasm, a preventive treatment (endovascular or surgical) of an unruptured intracranial aneurysm (UIA) may carry risks of cognitive morbidities.<sup>15,16</sup>

Moreover, in case of cerebral arteriovenous shunt diseases, such as AVMs or dural arteriovenous fistulas (DAVFs), cognitive impairment is part of the natural clinical presentation of the disease, due to long-standing cerebral venous engorgement and edema. Clinical improvement can be achieved by solving cerebral vascular congestion, though the cognitive aspects of this process are often not adequately investigated.<sup>17-19</sup>

## MATERIALS AND METHODS

### Search Strategy

The review was conducted according to the latest available Preferred Reporting Items for Systematic Reviews and Meta-Analyses (PRISMA) guidelines.<sup>20</sup> PubMed, EMBASE, and Scopus were searched from January 2000 to July 2022 using medical subject headings and free text related to cerebrovascular diseases (ie,

“aneurysm,” “AVM,” “DAVF,” “interventional neuroradiology,” and “psychology”). Specific search terms and strings are listed in the Online Supplemental Data.

We included studies in English with an abstract, which were indexed by at least one of the websites. Selection was based on the following eligibility criteria: 1) clinical studies; 2) a sample composed of patients with neurovascular disease; 3) patients undergoing a neuroradiology procedure, both diagnostic and therapeutic; 4) assessment of cognitive or psychological outcomes related to the procedure; and 5) no limitation on the duration of postprocedural outcome assessment.

Articles that considered only clinical or medical outcomes or only age as a sociodemographic variable and treatment other than interventional neuroradiology (INR) were not accepted. Exclusion criteria were the following: 1) not related to the addressed topic, such as not considering a neurovascular or cerebrovascular population; 2) psychological or cognitive variables not related to the INR procedure; 3) neuro- or radiosurgical procedure only; 4) merely medical variables taken into consideration; and 5) considered variables related only to general QoL measurements, not specifically cognitive or psychological ones.

### Article Selection and Data Extraction

All abstracts were assessed by 1 researcher to check the inclusion criteria, and 20% of them were double-checked by other researchers who were unaware of the first one’s conclusion. By means of the same process, the full texts were screened. All points of contention among the reviewers were discussed to obtain a consensus. The following information was obtained from each study: study design, study population characteristics, postoperative outcome data collected (sociodemographic, cognitive, and psychological), as well as the appropriate assessment scales, timing of the outcome assessment and follow-up, and pertinent study findings. The methodologic quality of all the selected studies was evaluated using the Newcastle-Ottawa Scale,<sup>21</sup> a well-established quality-assessment tool. All selected studies were high-quality articles based on the criteria and cutoff of the Newcastle-Ottawa Scale. Consistent with other literature,<sup>2,6</sup> a study was evaluated as high quality if at least 60% of the criteria were met (total score of  $\geq 5$  of 8).

## RESULTS

The results of the study selection are shown in a study flow chart (Figure). Of 1483 records, 873 studies were removed because they were duplicates or case studies or reviews or not fully published in English. Thus, we screened 610 abstracts. Most of the articles ( $n = 404$ ) were excluded during the abstract screening because they did not deal with the aim of the review; for instance, the population studied was not affected by a neurovascular or cerebrovascular pathology (reason 1). Thus, 206 records were sought for retrieval, and 15 were excluded because the full text was not available. One hundred ninety-one full-text articles were assessed for eligibility, of which 127 articles were excluded at the full-text screening for the following reasons: 39 because the outcomes/variables of interest were not evaluated in relation to neuroradiologic interventions or procedures (reason 2); 24 because the procedures were surgical or radiosurgical only (reason 3); 51 because they



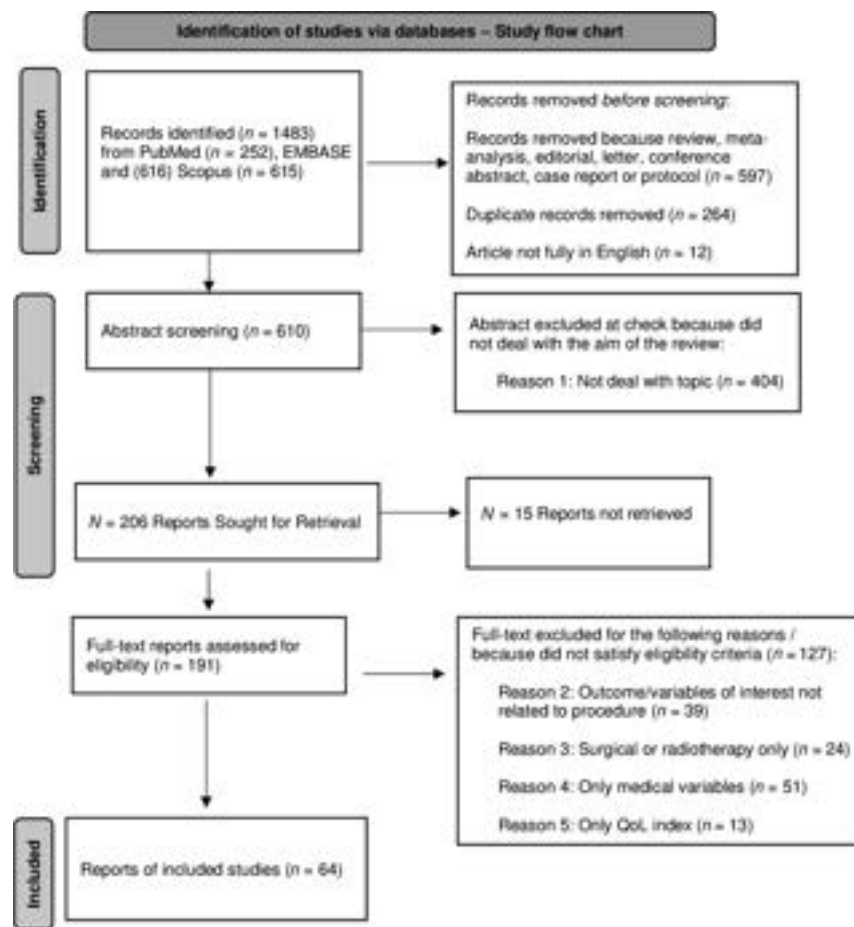


**FIGURE.** PRISMA study selection diagram. Study flow chart.

used only medical variables (reason 4); and 13 because only general variables on QoL were taken into account (reason 5). Finally, a total of 64/1483 (4%) articles met our inclusion criteria.

Of the 64 articles, 12 investigated only psychological variables, particularly depression, anxiety, and stress symptoms, while 4 also contained QoL measures.<sup>6,7,9,11,21-27</sup> Moreover, 52 articles evaluated cognitive domains: general cognitive functioning, language, attention, processing speed, executive function, and learning and memory and visual construction. Each study could evaluate >1 type of outcome.

The included articles were grouped into 2 different tables. The Online Supplemental Data Table S1 list the articles<sup>6,7,9-11,21-27</sup> focused on psychological outcomes ( $n = 12$ ), whereas the Online Supplemental Data Table S2 list the articles focused on cognitive investigation ( $n = 52$ ). The second table is split into subgroups according to the different neurovascular procedures and conclusions. The Online Supplemental Data Table S2a include articles ( $n = 9/52$ ) that do not report cognitive differences in outcomes of cerebral aneurysm procedures treated by endovascular coiling (EC) versus surgical clipping (SC).<sup>13,28-35</sup> The Online Supplemental Data Table S2b include articles ( $n = 11/52$ ) that find a better cognitive outcome after EC versus SC.<sup>3,36-45</sup> The Online Supplemental Data Table S2c include articles ( $n = 15/52$ ) that simply examine endovascular treatment outcomes without any comparison with other invasive techniques (eg, aneurysm,

acute stroke, vascular malformation).<sup>4,17,46-58</sup> Finally, the Online Supplemental Data Table S2d include articles ( $n = 17/52$ ) that specifically consider carotid stent placement or endarterectomy in patients with vessel stenosis.<sup>12,59-74</sup>

Of the 12 articles that explored psychological aspects (Online Supplemental Data Table S1), 6/12 were retrospective with one focused on MR imaging, while 6/12 were prospective with 2 randomized control trials (RCTs). Overall, anxiety and depression were the most considered symptoms, mainly measured with the State and Traits Anxiety Inventory and the Hamilton Anxiety and Depression Scale.<sup>7,9,10,22-24</sup>

In general terms, the main result from retrospective studies focused on UIAs (3/6:1/3 INR and SC treated versus untreated, and 2/3 EC or SC versus controls) is the good acceptance of a psychological consultation in case of severe psychological symptoms. From the retrospective studies on ruptured aneurysms (RIAs) (2/6 INR versus SC), the main result is that finding a new aneurysm in recently treated patients with RIAs does not affect their level of anxiety and depression. In the only retrospective observational MR imaging study in which patients with RIAs treated with SC versus EC were compared, the former presented with a higher occurrence of mood disorders, associated with hippocampal neuronal loss on MR imaging-DTI.<sup>9</sup>

The last of the retrospective studies, focusing on various CBV diseases, surgically or endovascularly treated, demonstrates

mental health impairment within 30 days of the procedure, with normalization at 6-month follow-up.

Among the 6 prospective studies included, 1/5 was an RCT,<sup>24</sup> and 5/6 discussed the effect of nonpharmacologic interventions before and during diagnostic angiography.<sup>7,23-26</sup> Only in 3 of them did discussing multimedia-based information, room-orientation tour, and music before the procedure demonstrate a reduction in the patient's anxiety.

The main results obtained from our analysis of the 54 articles focused on cognitive aspects are listed below.

The first cluster (Online Supplemental Data Table S2a) comprises articles showing similar cognitive outcomes in patients, regardless of treatment (EC or SC).<sup>13,28-35</sup> In 9/54 studies, one was retrospective<sup>28</sup> and 8 were prospective, including 1 RCT. All 9 studies dealt with patients with RIAs, except for 1 prospective study involving patients with UIAs.<sup>35</sup> The only retrospective study on patients with RIAs did not show any clear differences between EC versus SC at the 2-year follow-up.<sup>28</sup> Regarding the prospective analysis of patients with RIAs, 4/8 studies<sup>13,30,32,33</sup> demonstrated no score differences at 12-month postprocedural evaluation, even in patients with a good clinical recovery. Similar conclusions emerged from the more recent studies assessing cognitive outcome at 6-month postintervention.<sup>13,29</sup> Similarly, no cognitive differences between the SC and EC groups were demonstrated in patients with UIAs.<sup>35</sup>

The second cluster (Online Supplemental Data Table S2b) comprises articles showing better cognitive outcomes in patients with EC versus SC. In 11/54 studies, one was retrospective,<sup>36</sup> while 10 were prospective<sup>3,37-45</sup> and 2 of them were randomized.<sup>41,42</sup> All the studies included patients with RIAs, despite 3 prospective studies that involved patients with UIAs.<sup>43,45,47</sup> The only retrospective article demonstrated that patients undergoing EC had fewer cognitive deficits at 12 months, probably due to the more invasive nature of SC. In the 10 prospective studies, 7 following SAH showed worse performance of SC compared with the EC group on auditory-verbal/visuospatial memory,<sup>37</sup> frontal functions,<sup>38</sup> and general cognitive status.<sup>2</sup> The better cognitive outcome of the EC group was more evident in the acute phase after treatment (within 2 weeks) than in the long term (6 months).<sup>39</sup> The only study that compared the pre- and posttreatment assessment, also confirmed this result.<sup>40</sup> The same outcome emerged from the 2 RCTs performed on 181 patients with RIAs, with follow-up at 3 and 12 months. In 1 RCT, an additional investigation with voxel-based morphometry, MR imaging was performed, which showed significant gray matter atrophy in the SC group at 1 year.<sup>41</sup> Among the 3 prospective studies on UIAs, the largest available study was the neuropsychological substudy (474 patients) of the International Subarachnoid Trial (ISAT), which confirmed a greater cognitive impairment in the SC group at 12 months, also intriguingly evident in patients not disabled at mRS (Modified Ranking Scale).<sup>43</sup>

The third cluster (Online Supplemental Data Table S2c) includes 15 studies on patients treated by endovascular means only, for cerebral aneurysm, acute stroke, or vascular malformation (7/15 with EC, 1/15 with a flow diverter, 1/15 with various devices such as coils, stents, flow diverters and intrasaccular web, 4/15 with endovascular mechanical thrombectomies, 2/15 using glue in

AVMs or DAVFs). Among them, 11/15 studies included prospective analysis, and in 5/11, a pre- and posttreatment cognitive status assessment was performed.<sup>50,51,53,54,58</sup> Only 1/15 was an RCT.<sup>5-7</sup> The 4 retrospective studies<sup>17,49,52,56</sup> involved patients with RIAs (1/4)<sup>49</sup> and patients with UIAs (1/4),<sup>52</sup> patients with endovascular treatment (1/4),<sup>56</sup> and patients with AVMs (1/4).<sup>17</sup> In this cluster, 3 studies implemented additional imaging investigations (DWI, fMRI, resting-state fMRI).<sup>17,50,58</sup>

Among the 6/15 studies on patients undergoing EC, 4/6 focused on RIAs,<sup>29,47-49</sup> while 2/6 focused on patients with UIAs.<sup>50,51</sup> In the first group, memory functions resulted in less impairment than executive functions,<sup>47</sup> and mild cognitive impairment, this was independently associated with aneurysm location.<sup>48</sup> In addition, SAH may cause cognitive impairment as a late outcome for decades, even after a successful treatment and a good mRs at discharge.<sup>49</sup> Bründl et al,<sup>46</sup> in 2018, suggested that an excessive release of endogenous neuropeptide Y in the CSF can be responsible for this phenomenon. Regarding patients with UIAs, endovascular coiling results to be safe, without any significant impact on neurocognitive functioning,<sup>51</sup> even when new devices such as flow divertors (1/15) or other hypothetically highly thrombogenic devices (1/15) are used.<sup>54</sup>

In general terms, carefully monitored anesthesia contributes to improved postoperative cognitive outcomes.<sup>52,53</sup>

The 4/15 articles investigating patients with acute stroke treated by mechanical thrombectomy, alone or in combination with thrombolysis,<sup>3,56</sup> demonstrated that mechanical thrombectomy improves cognitive performance.<sup>55,57</sup>

The 2/15 articles in this group using advanced fMRI highlighted possible rearrangements of the neuronal network related to cognitive decline and potential recovery after treatment in patients with cerebrovascular malformations (AVMs and DAVFs).<sup>17,58</sup>

The fourth cluster (Online Supplemental Data Table S2d) includes 17 studies focused on the neuropsychological changes after carotid artery stent placement (CAS) or endarterectomy; only one was retrospective.<sup>59</sup> Among the prospective ones, 4/17 had additional imaging assessment.<sup>59,60,71,72</sup> Cases of chronic ICA occlusion revascularization were considered in 2/16 prospective studies, while 4 cases of intracranial stent placement were included in the retrospective study.

All the studies, except for 1 prospective study,<sup>63</sup> agreed on the evidence of a cognitive improvement after CAS, due to a global cerebral perfusion amelioration.<sup>12,59,62,65,68,70,74,75</sup>

Remarkably, in the studies comparing CAS and endarterectomy, no significant differences in cognitive outcomes between groups were detected.<sup>64,70,72,73</sup> Even the only RCT study in this group demonstrated no differences between CAS and endarterectomy groups in verbal and nonverbal memory, attention, and executive functioning.<sup>73</sup>

Two of 4 imaging studies revealed that cognitive improvement after CAS could be related to a perfusion amelioration.<sup>59,72</sup> However, Corriere et al<sup>60</sup> reported in their series that 2/8 patients with CAS who had undergone MR imaging presented with cognitive deficits despite increased perfusion values without detectable microembolization. The last imaging study, which correlated enhancing atherosclerotic plaques with intraprocedural cerebral ischemic lesions and cognitive impairment, revealed that

enhancing unstable plaque was strongly associated with new lesions on DWI, even without any cognitive deficit.<sup>71</sup>

## DISCUSSION

In this section, we discuss salient results and research gaps in the literature reviewed.

For ease of reading, this section is divided according to the content of the Tables (Online Supplemental Data Tables S1 and S2a–d).

### Articles Focused on Psychological Factors

Interestingly enough, the level of anxiety and depression was not significantly different in the articles comparing the psychological impact in patients with treated-versus-untreated aneurysms (Online Supplemental Data Table S1).<sup>10,22</sup>

When different CBV diseases are studied, patients who self-reported high levels of depression and anxiety generally reverted to the normal range at 6-month follow-up.<sup>21</sup> These results suggest that an early psychological consultation can be relevant in improving patients' short-term outcomes.<sup>11</sup>

A strong limitation of the retrospective studies included in this section is a lack of preoperational baseline evaluations. This omission can explain the low level of QoL found in retrospective studies, which may have been pre-existing and not related to diagnosis or treatment.<sup>6</sup>

Instead, the patients' baseline statuses were always assessed in the prospective analyses. Among these, studies on nonpharmacologic interventions give the general impression that the multimedia information session,<sup>23,24</sup> orientation in the room,<sup>2,6</sup> or musical intervention<sup>7,25</sup> positively interfered with anxiety and physiologic stress reduction. Nevertheless, due to the inhomogeneity of the samples in terms of pathology, timing, and treatment methods, some results remain conflicting.

In practice, these management strategies are difficult to implement because they are highly time- and resource-consuming. Further investigations in this field of INR are advisable, similar to what has already widely occurred in cardiovascular research.<sup>75</sup>

In the only prospective RCT comparing endovascular treatment versus IVT in patients with acute stroke, the distribution of depression scores in patients receiving endovascular therapy was significantly better than that in the medical arm. However, the authors themselves hypothesized that survival of a potentially lethal neurologic event following a new endovascular therapy could have positively influenced the outcome of these patients per se.

In summary, all the studies included in our research agree that early psychological consultations<sup>6,11,21</sup> and behavioral interventions<sup>7,23–26</sup> can potentially impact the management of anxiety and depression in subjects undergoing diagnostic or therapeutic procedures.<sup>10</sup> Remarkably, although treatment for anxiety and depression will not alleviate functional deficits, it still improves QoL.<sup>76</sup> This outcome should be remembered in developing strategies for psychological care.<sup>77</sup>

From a methodologic point of view, we noted several limitations mainly related to the inhomogeneity in the CBV sample and in the controls, which were often pathologic (eg, spinal diseases). These limitations add confounding variables when trying to draw conclusions.<sup>6,7,11,23–26</sup>

Additionally, we observed that very few studies compared the psychological statuses of INR patients with surgical patients:<sup>6,9,22</sup> This gap should be addressed in future studies.

Only 1 study in this section made an additional observation associating anxiety and depression with neuroimaging findings (MR imaging-DTI).<sup>9</sup> Further investigations are needed to investigate the correlation between neuroimaging and psychological outcome.

Finally, from our review, we found that the most commonly used questionnaire to evaluate QoL was the 36-item Short Form Health Survey (SF-36), which has been recommended to study vascular disease<sup>78</sup> due to its simplicity and quick self-administration.<sup>10</sup> However, we believe that given the general nature of the SF-36 tool, neurovascular patients would benefit from the most specific neuro-QoL questionnaire.<sup>22</sup>

### Articles Focused on Cognitive Factors

After treatment, some patients may experience varying degrees of cognitive changes in different domains, such as memory, attention, language, executive functions, and general cognition (Online Supplemental Data Table S2). Cerebral perfusion and blood flow modifications are part of the pathophysiologic basis of the altered cognitive status, with an impact on QoL and thus on work, family, and social interaction.<sup>42</sup>

These factors partly explain the divergent results obtained from the analysis of the first 2 clusters of articles, both focused on EC-versus-SC treatment outcomes (Online Supplemental Data Table S2a–b).

For instance in subjects with RIAs, the SAH grade, the occurrence of vasospasm, or the need for a ventricular shunt are all independent predictors of clinical recovery, but they are not always systematically considered.<sup>30</sup> Furthermore, the preoperational assessment is often missing (15/20), though it is fundamental for determining cognitive changes after an intervention and for correctly comparing different groups (EC versus SC). The few studies enrolling only subjects with UIAs with pretreatment controls showed similar results in both groups at 1-year follow-up, suggesting that the cognitive differences are prevalent in the short term after treatment, favoring the EC approach.<sup>29,35,45</sup> In the RIA group, pretreatment assessment was performed in only 2 studies of the second cluster (EC better than SC); therefore, confrontation with the first cluster was inherently limited.<sup>40,42</sup> Additionally, the time of follow-up assessment was inhomogeneous among different studies even inside the same clusters, adding difficulty to the interpretation of the results. The randomization of EC or SC samples would have partially overcome these limitations. Unfortunately, only 3/20 studies were RCTs, and even if all 3 focused on patients with SAH, they again were not totally comparable because of the different timing of assessments and the different neuropsychological tests used.<sup>34,41,42</sup>

We consider it reasonable, as some authors have suggested, to pre-alert surgical patients that total cognitive recovery can be delayed, on the basis of the observations reported in the second cluster of studies.<sup>45</sup>

Because some cognitive deficits are associated with lesions of the frontal lobes, we find it interesting that aneurysms in the anterior circulation, specifically in the anterior communicating artery, were present in similar percentages between the 2 clusters.<sup>3,28,30,37,38</sup>

The third cluster (Online Supplemental Data Table S2c) includes 15 studies analyzing groups of patients undergoing various INR treatments. Most of them (9/15) studied patients with RIAs or ischemic stroke, in whom the same acute events strongly influence the results. Indeed, neuropsychological sequelae after INR procedures are difficult to disentangle from the ones caused by the pathology itself, particularly when preoperative assessment is absent. Thus, we believe it is important to broaden knowledge about elective procedures, in which underlying conditions and other confounding factors can be better analyzed than in an emergency context.

The situation described above, calls for future investigations with larger samples and longer follow-up, including patients implanted with more recent devices, such as flow divertors.

The fourth cluster (Online Supplemental Data Table S2d) demonstrates that stent placement of the cervical segment of the ICA may offer more than just a reduced risk of stroke, contributing to improved cognition measured with the Mini-Mental State Examination, particularly in patients with highly impaired cerebral perfusion.<sup>12,68</sup> The clinical advantage was specifically detected in the verbal memory,<sup>55</sup> attention, and psychomotor processing speed,<sup>65</sup> more often in younger patients with the worst cognitive performance before the procedure.<sup>70</sup>

This last cluster, compared with the other ones, is less prone to bias and misinterpretation. In fact, the studies were mostly prospective, focused on the same pathology (vessel stenosis), with baseline cognitive function assessment frequently available.

In our research, globally, we found very few articles (8/65) that explored a possible relationship between neuroimaging and cognitive and/or psychological factors in patients undergoing neurointerventional procedures. The results reported are limited by various factors, including the restricted number of patients, the uneven CBV pathologies, and the different techniques used (MR imaging, PWI, DWI, and fMRI). Also in this area, further studies are needed to better understand the correlation among neuroimaging, neuropsychology, and cerebrovascular treatments.

The Online Supplemental Data Table S3 summarizes a list of points that we believe should be further investigated regarding psychological and cognitive variables of cerebrovascular patients undergoing INR procedures.

### Limitations

The first limitation of this review is the poor standardization of the measurement of cognitive and psychological factors, which makes it difficult to compare data among studies. Additionally, the poor collection of data on psychiatric history limits the interpretations of results.

A second limitation is the strong influence of pathologic events and their related stress on the psychological and cognitive outcomes as well as the effect of the treatment procedure such as in the case of SAH or vasospasm in patients with RIA.

A third intrinsic limitation of our review is the inhomogeneity of the samples in terms of pathology and treatment.

However, our goal was not to investigate the cognitive and psychological factors of a single pathology or treatment but to consider these aspects in the everyday practice of interventional neuroradiology, raising awareness on the complexity of this crucial topic. Ideally, one should consider psychological and

cognitive variables together, due to their mutual conditioning, without excluding psychophysiologic aspects such as fatigue and sleep.<sup>6</sup>

Finally, the research criteria may have limited this review because they may have excluded some articles dealing with similar topics.

### CONCLUSIONS

Despite the numerous limitations that emerged from the analysis of the literature, our review highlights some important aspects regarding psychological and cognitive factors in INR.

The first message is that early psychological consultations<sup>6,11,21</sup> and behavioral interventions<sup>7,23-26</sup> can impact the management of anxiety and depression in subjects undergoing diagnostic or therapeutic procedures.<sup>10</sup> Even if treatment for anxiety and depression does not address functional deficits, it does contribute to improved QoL (Online Supplemental Data Table S1).<sup>76</sup> Possible differences in the cognitive outcome of patients undergoing EC versus SC remain debatable (Online Supplemental Data Table S2a-b), first and second clusters). In patients with RIA, without a preoperative assessment, it is almost impossible to distinguish damage caused by the disease from damage due to the treatment.<sup>47,49</sup> This limitation is overcome when preoperative testing is feasible, such as in patients with UIA, in whom endovascular treatment demonstrates no impact on cognitive functioning (Online Supplemental Data Table S2c, 3rd cluster).<sup>51,54</sup> Finally, all studies on the cognitive outcome of patients undergoing carotid stent placement agree in demonstrating cognitive improvement after the procedure, mainly due to a better redistribution of cerebral perfusion (Online Supplemental Data Table S2d, fourth cluster).

In accordance with other authors, we strongly believe that a better understanding of the relationship between the curative approach and the patient's cognitive and psychosocial profile could optimize the care of patients affected by cerebrovascular diseases.<sup>49</sup> Thus, a greater awareness of the importance of this relationship is needed to encourage its investigation in INR research and its integration into INR standard treatment protocols. To proceed, however, it is essential to identify a minimum set of neuropsychological and psychological tests, specifically designed for patients undergoing INR procedures, as recently implemented for the neurosurgical setting.<sup>79</sup> This identification would make the data shareable and comparable even independent of pathologies and treatments, overcoming the many limitations that we have encountered when reviewing the specific literature (Online Supplemental Data Table S3).

Finally, to our knowledge, this is the first comprehensive review considering all cognitive and psychological aspects in all types of INR procedures, diagnostic and therapeutic.

Disclosure forms provided by the authors are available with the full text and PDF of this article at [www.ajnr.org](http://www.ajnr.org).

### REFERENCES

1. Rodesch G, Picard L, Berenstein A, et al. "Editorial Interventional Neuroradiology: A Neuroscience Sub-Specialty?" *Interv Neuroradiol* 2013;19:263-70 CrossRef Medline
2. Dai RQ, Bai WX, Gao BL, et al. Internal carotid artery occlusion may affect long-term quality of life in patients with high-flow



- carotid cavernous fistulas. *Interv Neuroradiol* 2020;26:83–89 CrossRef Medline
3. Chan A, Ho S, Poon WS. Neuropsychological sequelae of patients treated with microsurgical clipping or endovascular embolization for anterior communicating artery aneurysm. *Eur Neurol* 2002;47:37–44 CrossRef Medline
4. Lattanzi S, Coccia M, Pulcini A, et al. Endovascular treatment and cognitive outcome after anterior circulation ischemic stroke. *Sci Rep* 2020;10:18524 CrossRef Medline
5. Clarke RE, Jelen MB, Jones B, et al. Letter: “How to Defuse a Ticking Time Bomb?” Considering psychosocial factors in patients with small unruptured intracranial aneurysms. *Neurosurgery* 2022;90:e45–46 CrossRef Medline
6. Fontana J, Wenz R, Groden C, et al. The preinterventional psychiatric history as a major predictor for a reduced quality of life after treatment of unruptured intracranial aneurysms. *World Neurosurg* 2015;84:1215–22 CrossRef Medline
7. Schneider N, Schedlowski M, Schürmeyer TH, et al. Stress reduction through music in patients undergoing cerebral angiography. *Neuroradiology* 2001;43:472–76 CrossRef Medline
8. Buffum MD, Sasso C, Sands LP, et al. A music intervention to reduce anxiety before vascular angiography procedures. *J Vasc Nurs* 2006;24:68–73; quiz 74 CrossRef Medline
9. Wostrack M, Friedrich B, Hammer K, et al. Hippocampal damage and affective disorders after treatment of cerebral aneurysms. *J Neurol* 2014;261:2128–35 CrossRef Medline
10. Van Der Schaaf IC, Wermer MJH, Velthuis BK, et al. Psychosocial impact of finding small aneurysms that are left untreated in patients previously operated on for ruptured aneurysms. *J Neurol Neurosurg Psychiatry* 2006;77:748–52 CrossRef Medline
11. Wenz H, Wenz R, Maros ME, et al. The neglected need for psychological intervention in patients suffering from incidentally discovered intracranial aneurysms. *Clin Neurol Neurosurg* 2016;143:65–70 CrossRef Medline
12. Grunwald IQ, Supprian T, Politi M, et al. Cognitive changes after carotid artery stenting. *Neuroradiology* 2006;48:319–23 CrossRef Medline
13. Zabyhian S, Mousavi-Bayegi SJ, Baharvahdat H, et al. Cognitive function, depression, and quality of life in patients with ruptured cerebral aneurysms. *Curr J Neurol* 2019 Jan 20. [Epub ahead of print] CrossRef
14. Dammann P, Wittek P, Darkwah Oppong M, et al. Relative health-related quality of life after treatment of unruptured intracranial aneurysms: long-term outcomes and influencing factors. *Ther Adv Neurol Disord* 2019;12:1756286419833492 CrossRef Medline
15. Zaki Ghali MG, Srinivasan VM, Wagner K, et al. Cognitive sequelae of unruptured and ruptured intracranial aneurysms and their treatment: modalities for neuropsychological assessment. *World Neurosurg* 2018;120:537–49 CrossRef Medline
16. Bonares MJ, Egeto P, De Oliveira Manoel AL, et al. Unruptured intracranial aneurysm treatment effects on cognitive function: a meta-analysis. *J Neurosurg* 2016;124:784–90 CrossRef Medline
17. Korno NV, Ivanova NE, Ivanov AY, et al. Clinical value of functional MRI in the diagnosis of cognitive disorders in patients with arteriovenous malformations. In: *Proceedings of the International Joint Conference on Biomedical Engineering Systems and Technologies, BIOSTEC 2020*, February 24–26, 2020. Valletta, Malta CrossRef
18. Berra LV, Armocida D, D’Angelo L, et al. Vascular intracranial malformations and dementia: an under-estimated cause and clinical correlation: clinical note. *Cereb Circ Cogn Behav* 2022;3:100146 CrossRef Medline
19. de Souza Coelho D, de Oliveira Santos BF, da Costa MD, et al. Cognitive performance in patients with cerebral arteriovenous malformation. *J Neurosurg* 2019;132:1548–55 CrossRef Medline
20. Page MJ, Moher D, Bossuyt PM, et al. PRISMA 2020 explanation and elaboration: updated guidance and exemplars for reporting systematic reviews. *BMJ* 2021;372:n160 CrossRef Medline
21. Lombardo L, Shaw R, Sayles K, et al. Anxiety and depression in patients who undergo a cerebrovascular procedure. *BMC Neurol* 2020;20:124 CrossRef Medline
22. Buijs JE, Greebe P, Rinkel GJ. Quality of life, anxiety, and depression in patients with an unruptured intracranial aneurysm with or without aneurysm occlusion. *Neurosurgery* 2012;70:868–72 CrossRef Medline
23. Choi H, Kim J. Effects of multimedia-based information on anxiety, discomfort and satisfaction with care among patients undergoing cerebral angiography: a quasi-experimental study. *J Clin Nurs* 2022;31:949–57 CrossRef Medline
24. Sayadi L, Varaei S, Faghihzadeh E, et al. The effects of multimedia education on anxiety and physiological status among patients with cerebral angiography: a randomized controlled clinical trial. *Nurs Pract Today* 2018;5:375–84 CrossRef
25. Vanderboom TL, Arcari PM, Duffy ME, et al. Effects of a music intervention on patients undergoing cerebral angiography: a pilot study. *J Neurointerv Surg* 2012;4:229–33 CrossRef Medline
26. Kolahi Z, Zandi M, Esmaeili R, et al. Effect of angiography room orientation tour on anxiety of patients awaiting cerebrovascular angiography. *Advances in Nursing & Midwifery* 2020;29:7–11
27. Polding LC, Tate WJ, Mlynash M, et al; DEFUSE 3 Investigators. Quality of life in physical, social, and cognitive domains improves with endovascular therapy in the DEFUSE 3 Trial. *Stroke* 2021;52:1185–91 CrossRef Medline
28. Ma N, Feng X, Wu Z, et al. Cognitive impairments and risk factors after ruptured anterior communicating artery aneurysm treatment in low-grade patients without severe complications: a multicenter retrospective study. *Front Neurol* 2021;12:613785 CrossRef Medline
29. Brundl E, Schodel P, Bele S, et al. Treatment of spontaneous subarachnoid hemorrhage and self-reported neuropsychological performance at 6 months: results of a prospective clinical pilot study on good-grade patients. *Turk Neurosurg* 2018;28:369–88 CrossRef Medline
30. Koivisto T, Vanninen R, Hurskainen H, et al. Outcomes of early endovascular versus surgical treatment of ruptured cerebral aneurysms: a prospective randomized study. *Stroke* 2000;31:2369–77 CrossRef Medline
31. Mukerji N, Holliman D, Baisch S, et al. Neuropsychologic impact of treatment modalities in subarachnoid hemorrhage: clipping is no different from coiling. *World Neurosurg* 2010;74:129–38 CrossRef Medline
32. Preiss M, Koblihova J, Netuka D, et al. Ruptured cerebral aneurysm patients treated by clipping or coiling: comparison of long-term neuropsychological and personality outcomes. *Zentralbl Neurochir* 2007;68:169–75 CrossRef Medline
33. Proust F, Martinaud O, Gérardin E, et al. Quality of life and brain damage after microsurgical clip occlusion or endovascular coil embolization for ruptured anterior communicating artery aneurysms: neuropsychological assessment: clinical article. *J Neurosurg* 2009;110:19–29 CrossRef Medline
34. Proust F, Bracard S, Lejeune JP, et al; FASHE Investigators. A randomized controlled study assessing outcome, cognition, autonomy and quality of life in over 70-year-old patients after aneurysmal subarachnoid hemorrhage. *Neurochirurgie* 2018;64:395–400 CrossRef Medline
35. Preiss M, Netuka D, Koblihová J, et al. Cognitive functions before and 1 year after surgical and endovascular treatment in patients with unruptured intracranial aneurysms. *Br J Neurosurg* 2012;26:514–16 CrossRef Medline
36. Latimer SF, Wilson FC, McCusker CG, et al. Subarachnoid haemorrhage (SAH): long-term cognitive outcome in patients treated with surgical clipping or endovascular coiling. *Disabil Rehabil* 2013;35:845–50 CrossRef Medline
37. Beeckmans K, Crunelle CL, Van den Bossche J, et al. Cognitive outcome after surgical clipping versus endovascular coiling in patients with subarachnoid hemorrhage due to ruptured anterior communicating artery aneurysm. *Acta Neurol Belg* 2020;120:123–32 CrossRef Medline

38. Fontanella M, Perozzo P, Ursone R, et al. **Neuropsychological assessment after microsurgical clipping or endovascular treatment for anterior communicating artery aneurysm.** *Acta Neurochir (Wien)* 2003;145:867–72; discussion 872 CrossRef Medline
39. Frazer D, Ahuja A, Watkins L, et al. **Coiling versus clipping for the treatment of aneurysmal subarachnoid hemorrhage: a longitudinal investigation into cognitive outcome.** *Neurosurgery* 2007;60:434–42 CrossRef Medline
40. Vieira AC, Azevedo-Filho HR, Andrade G, et al. **Cognitive changes in patients with aneurysmal subarachnoid hemorrhage before and early posttreatment: differences between surgical and endovascular.** *World Neurosurg* 2012;78:95–100 CrossRef Medline
41. Bendel P, Koivisto T, Niskanen E, et al. **Brain atrophy and neuropsychological outcome after treatment of ruptured anterior cerebral artery aneurysms: a voxel-based morphometric study.** *Neuroradiology* 2009;51:711–22 CrossRef Medline
42. Gao P, Jin Z, Wang P, et al. **Effects of intracranial interventional embolization and intracranial clipping on the cognitive and neurologic function of patients with intracranial aneurysms.** *Arch Clin Neuropsychol* 2022;37:1688–98 CrossRef Medline
43. Scott RB, Eccles F, Molyneux AJ, et al. **Improved cognitive outcomes with endovascular coiling of ruptured intracranial aneurysms: neuropsychological outcomes from the International Subarachnoid Aneurysm Trial (ISAT).** *Stroke* 2010;41:1743–47 CrossRef Medline
44. Bründl E, Böhm C, Lürding R, et al. **Treatment of unruptured intracranial aneurysms and cognitive performance: preliminary results of a prospective clinical trial.** *World Neurosurg* 2016;94:145–56 CrossRef Medline
45. Caveney AF, Langenecker SA, Pandey AS, et al. **Neuropsychological changes in patients undergoing treatment of unruptured intracranial aneurysms.** *Clin Neurosurg* 2019;84:581–87 CrossRef Medline
46. Bründl E, Proescholdt M, Schödel P, et al. **Excessive release of endogenous neuropeptide Y into cerebrospinal fluid after treatment of spontaneous subarachnoid haemorrhage and its possible impact on self-reported neuropsychological performance: results of a prospective clinical pilot study on good-grade patients.** *Neurol Res* 2018;40:1001–13 CrossRef Medline
47. Manning L, Pierot L, Dufour A. **Anterior and non-anterior ruptured aneurysms: Memory and frontal lobe function performance following coiling.** *Eur J Neurol* 2005;12:466–74 CrossRef Medline
48. Shen Y, Dong Z, Pan P, et al. **Risk factors for mild cognitive impairment in patients with aneurysmal subarachnoid hemorrhage treated with endovascular coiling.** *World Neurosurg* 2018;119:e527–33 CrossRef Medline
49. Sousa L, Antunes A, Mendes T, et al. **Long-term neuropsychiatric and neuropsychological sequelae of endovascularly treated aneurysmal subarachnoid hemorrhage.** *Acta Med Port* 2019;32:706–13 CrossRef Medline
50. Kang DH, Hwang YH, Kim YS, et al. **Cognitive outcome and clinically silent thromboembolic events after coiling of asymptomatic unruptured intracranial aneurysms.** *Neurosurgery* 2013;72:638–45; discussion 645 CrossRef Medline
51. Srivatsan A, Mohanty A, Saleem Y, et al. **Cognitive outcomes after unruptured intracranial aneurysm treatment with endovascular coiling.** *J Neurointerv Surg* 2021;13:430–33 CrossRef Medline
52. Pang J, Zhao C, Zhang A, et al. **Impact of different surgical methods for endovascular embolization of intracranial wide-necked aneurysms on patient prognosis and cognitive function.** *Int J Clin Exp Med* 2020;13:3630–36
53. Ishii D, Zanaty M, Roa JA, et al. **Postoperative cognitive dysfunction after endovascular treatments for unruptured intracranial aneurysms: a pilot study.** *Interv Neuroradiol* 2022;28:439–43 CrossRef Medline
54. Wagner K, Srivatsan A, Mohanty A, et al. **Cognitive outcomes after unruptured intracranial aneurysm treatment with flow diversion.** *J Neurosurg* 2019;134:1–6 CrossRef
55. López-Cancio E, Millán M, Muñoz L, et al. **Endovascular treatment improves cognition after stroke: a secondary analysis of REVASCAT trial.** *Neurology* 2017;88:245–51 CrossRef Medline
56. Strambo D, Bartolini B, Beaud V, et al. **Thrombectomy and thrombolysis of isolated posterior cerebral artery occlusion: cognitive, visual, and disability outcomes.** *Stroke* 2020;51:254–61 CrossRef Medline
57. Xu G, Dong X, Niu X, et al. **Cognitive function and prognosis of multimodal neuroimage-guided thrombectomy on mild to moderate anterior circulation infarction patients with broadened therapeutic window: a prospective study.** *Eur Neurol* 2017;78:257–63 CrossRef Medline
58. Sekar S, Kannath SK, Ramachandran S, et al. **Alterations in resting-state functional MRI connectivity related to cognitive changes in intracranial dural arteriovenous fistulas before and after embolization treatment.** *J Magn Reson Imaging* 2022;55:1183–99 CrossRef Medline
59. Moftakhar R, Turk AS, Niemann DB, et al. **Effects of carotid or vertebralbasilar stent placement on cerebral perfusion and cognition.** *AJNR Am J Neuroradiol* 2005;26:1772–80 Medline
60. Corriere MA, Edwards MS, Geer CP, et al. **Longitudinal evaluation of neurobehavioral outcomes after carotid revascularization.** *Ann Vasc Surg* 2014;28:874–81 CrossRef Medline
61. Fan YL, Wan JQ, Zhou ZW, et al. **Neurocognitive improvement after carotid artery stenting in patients with chronic internal carotid artery occlusion: a prospective, controlled, single-center study.** *Vasc Endovascular Surg* 2014;48:305–10 CrossRef Medline
62. Gupta AN, Bhatti AA, Shah MM, et al. **Carotid artery stenting and its impact on cognitive function: a prospective observational study.** *Neurointervention* 2020;15:74–78 CrossRef Medline
63. Hitchner E, Baughman BD, Soman S, et al. **Microembolization is associated with transient cognitive decline in patients undergoing carotid interventions.** *J Vasc Surg* 2016;64:1719–25 CrossRef Medline
64. Kim JJ, Schwartz S, Wen J, et al. **Comparison of neurocognitive outcomes after carotid endarterectomy and carotid artery stenting.** *Am Surg* 2015;81:1010–14
65. Lin MS, Chiu MJ, Wu YW, et al. **Neurocognitive improvement after carotid artery stenting in patients with chronic internal carotid artery occlusion and cerebral ischemia.** *Stroke* 2011;42:2850–54 CrossRef Medline
66. Piegza M, Jaworska I, Piegza J, et al. **Cognitive functions after carotid artery stenting: 1-year follow-up study.** *J Clin Med* 2022;11:3019 CrossRef Medline
67. Raabe RD, Burr RB, Short R. **One-year cognitive outcomes associated with carotid artery stent placement.** *J Vasc Interv Radiol* 2010;21:983–88; quiz 989 CrossRef Medline
68. Song LP, Zhang WW, Gu YQ, et al. **Cognitive improvement after carotid artery stenting in patients with symptomatic internal carotid artery near-occlusion.** *J Neurol Sci* 2019;404:86–90 CrossRef Medline
69. Tanashyan MM, Medvedev RB, Lagoda OV, et al. **The state of cognitive functions after angioreconstructive operations on the carotid arteries.** *Immuno-Oncology* 2019;5:65–71 CrossRef
70. Turowicz A, Czapiaga A, Malinowski M, et al. **Carotid revascularization improves cognition in patients with asymptomatic carotid artery stenosis and cognitive decline. Greater improvement in younger patients with more disordered neuropsychological performance.** *J Stroke Cerebrovasc Dis* 2021;30:105608 CrossRef Medline
71. Varetto G, Gibello L, Faletti R, et al. **Contrast-enhanced ultrasound to predict the risk of microembolization during carotid artery stenting.** *Radiol Med* 2015;120:1050–55 CrossRef Medline
72. Whooley JL, David BC, Woo HH, et al. **Carotid revascularization and its effect on cognitive function: a prospective nonrandomized multicenter clinical study.** *J Stroke Cerebrovasc Dis* 2020;29:104702 CrossRef Medline
73. Witt K, Börsch K, Daniels C, et al. **Neuropsychological consequences of endarterectomy and endovascular angioplasty with stent placement for treatment of symptomatic carotid stenosis: a prospective randomised study.** *J Neurol* 2007;254:1524–32 CrossRef Medline
74. Xu G, Liu X, Meyer JS, et al. **Cognitive performance after carotid angioplasty and stenting with brain protection devices.** *Neurol Res* 2007;29:251–55 CrossRef Medline

75. Eastwood JA, Doering LV, Dracup K, et al. **Health-related quality of life: the impact of diagnostic angiography.** *Heart Lung* 2011;40:147–55 CrossRef Medline
76. King JT Jr, Kassam AB, Yonas H, et al. **Mental health, anxiety, and depression in patients with cerebral aneurysms.** *J Neurosurg* 2005;103:636–41 CrossRef Medline
77. Lemos M, Román-Calderón JP, Calle G, et al. **Personality and anxiety are related to health-related quality of life in unruptured intracranial aneurysm patients selected for non-intervention: a cross sectional study.** *PLoS One* 2020;15:e0229795 CrossRef Medline
78. Beattie DK, Golledge J, Greenhalgh RM, et al. **Quality of life assessment in vascular disease: towards a consensus.** *Eur J Vasc Endovasc Surg* 1997;13:9–13 CrossRef Medline
79. Schiavolin S, Mariniello A, Broggi M, et al. **Patient-reported outcome and cognitive measures to be used in vascular and brain tumor surgery: proposal for a minimum set.** *Neurol Sci* 2022;43:5143–51 CrossRef Medline

# 4D-DSA for Assessment of the Angioarchitecture and Grading of Cranial Dural AVF

P.F. Samp, F. Keil, R. du Mesnil, A. Birkhold, M. Kowarschik, E. Hattingen, and J. Berkefeld



## ABSTRACT

**BACKGROUND AND PURPOSE:** Time-resolved 3D rotational angiography (4D-DSA) has been used to demonstrate details of the angioarchitecture of AVM, whereas it has rarely been used to describe features of dural AVF. In this exploratory study, we analyzed dural AVFs with a novel 4D software prototype, developed and provided by Siemens, to determine whether identification of the location of the fistulous point, grading, and treatment planning were feasible.

**MATERIALS AND METHODS:** 4D-DSA volumes were calculated from existing 3D rotational angiography data sets of patients with dural AVFs. The 4D-DSA volumes were displayed in a virtual DSA mode and MPR or MIP in 3 orthogonal planes and compared with 2D-DSA by 2 experienced neuroradiologists. Fusions with unenhanced CT or MR images were used to improve visualization of adjacent anatomic structures.

**RESULTS:** Comparison with 2D-DSA showed that evaluation of the fistulous point and grading according to the classification of Borden, Cognard, or Barrow was feasible in 26 of 27 cases. In 8 of 27 cases, 4D-DSA was considered advantageous for determining the fistulous point and the course of the draining vein in the dural AVF with cortical venous drainage, especially in the frontoethmoidal and frontoparietal regions. In 6 cases, the display of angioarchitecture was considered inferior to that of 2D-DSA due to motion artifacts, suboptimal selection of the injected vessel, and lack of temporal resolution.

**CONCLUSIONS:** Detailed analysis of dural AVFs according to the standardized display of 4D-DSA volumes was feasible and helpful in understanding the angioarchitecture in selected cases. Further improvement and validation of the 4D software should solidify the complementary role of 4D-DSA to conventional 2D-DSA series.

**ABBREVIATIONS:** DAVF = dural AVF; 3DRA = 3D rotational angiography; 4D-DSA = time-resolved 3D rotational angiography; ECA = external carotid artery; fpCBCTA = flat panel conebeam CTA

2D-DSA remains the standard for diagnosis, grading, and treatment planning of patients with dural AVFs (DAVFs). Although noninvasive imaging techniques such as MRA and CTA have improved in this regard,<sup>1-3</sup> their spatial and temporal resolution is still inferior to that of angiographic imaging with modern flat panel DSA equipment. 3D rotational angiography (3DRA) is frequently used in addition to DSA projection images for optimal visualization of the shunt zone in any projection or through the generation of flat panel conebeam CTA (fpCBCTA) cross-sectional images.<sup>4</sup>

It has been demonstrated that time-resolved 3D rotational angiography (4D-DSA) with its combination of high spatial and temporal resolution could be favorable for detailed analysis of the microvasculature of the shunt zone of an AVM.<sup>4-9</sup> Previous studies have included only a limited number of DAVF cases.<sup>4,6,10</sup> Furthermore, 4D-DSA volumes and 4D-fpCBCTA reconstructions were not systematically evaluated for identifying the fistulous point and grading or planning of endovascular or surgical treatment of DAVF.

Within this exploratory study, we used a novel software prototype, developed and provided by Siemens, to calculate 4D-DSA from existing 3DRA data sets. By comparing 4D-DSA in a standardized display with virtual DSA and cross-sectional images with 2D-DSA, we aimed to obtain a first impression of the potential diagnostic value for pretherapeutic assessment of patients with DAVFs.

## MATERIALS AND METHODS

We reviewed the records of patients with cranial DAVFs between 2016 and 2021. We included all cases of DAVFs that had DSA

Received June 5, 2023; accepted after revision August 30.

From the Institute of Neuroradiology (P.F.S., F.K., R.d.M., E.H., J.B.), University Hospital Frankfurt, Goethe University Frankfurt, Frankfurt am Main, Germany; and Siemens Healthcare (A.B., M.K.), Forchheim, Germany.

Please address correspondence to Patrick F. Samp, MD, Institute of Neuroradiology, University Hospital Frankfurt, Goethe University Frankfurt, Schleusenweg 2-16, 60528 Frankfurt am Main, Germany; e-mail: patrickf.samp@kgu.de

Indicates open access to non-subscribers at www.ajnr.org

Indicates article with online supplemental data.

<http://dx.doi.org/10.3174/ajnr.A8008>



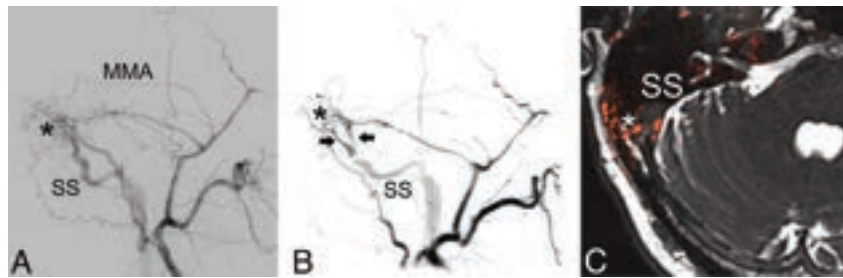


**FIG 1.** A DAVF between the middle meningeal artery (MMA), occipital artery and venous channels in the wall of the right lateral sinus with postthrombotic changes. Comparison of a standard lateral projection in 2D-DSA (A) and a slightly modified oblique projection of a virtual DSA-reconstruction (B) as well as an axial fusion image (C) derived from a 4D-DSA data set fused with a CISS MR imaging sequence. The possibility to choose an optimized projection on 4D-DSA improves the visualization of the arterial network at the fistulous point (*asterisk*) with connections to 2 venous channels (*arrows*) with Y-shaped convergence to a single venous channel in the wall of the sigmoid sinus (SS) with postthrombotic changes.

and 3DRA for treatment planning, being part of our routine protocol. We excluded patients without 3DRA. Our local ethics committee approved the study protocol. No additional patient consent was required.

2D-DSA series and 3DRA were obtained on a modified Axiom Artis zee biplane angiography system (Siemens) using an acquisition with a 260° rotation angle and a scan duration of 12 seconds. More recently, we used a new Artis icono biplane system (Siemens) with the same scan parameters. The interventionalist selected the DAVF-supplying artery from which 3DRA was performed. For the external carotid artery (ECA), 20 mL of nonionic contrast, iopromide (Ultravist 300; Bayer HealthCare), was injected by hand to reduce patient movement due to irritating heat sensations in the viscerocranium. For the ICA or the vertebral artery, we used an automatic injector with a flow rate of 3 mL/s.

4D-DSA volumes and 4D-fpCBCTA cross-sectional images were calculated from the 3DRA data sets on a dedicated research workstation (syngo X Workplace VD20; Siemens). A novel software prototype with an improved algorithm for 4D-DSA reconstructions, developed and provided by Siemens, was used. Compared with the commercially available syngo Dyna4D product (Siemens), the 4D-DSA software prototype adds a streak artifact removal method during the reconstruction of the initial 3D-DSA image. This is intended to reduce image-quality issues of 4D-DSA based on inconsistent 2D projection data due to noise and contrast agent dynamics. Multiplicative back-projection of 2D projection images into a static 3D image can lead to implausible vessel enhancement because contrast information from overlapping vessel segments cannot be entirely separated. Therefore, a physically motivated, plausibility-based flow constraint is applied to the 4D reconstruction process to prevent the appearance of incorrect or nonphysiologic vessel filling. This temporal artifact-reduction method takes into account that a particular vessel segment can be contrast-enhanced only under certain conditions. A recent study demonstrated these advantages when using the software prototype for an AVM compared with the commercially available syngo Dyna4D product.<sup>11</sup>

In our study, the 4D volumes were presented in a virtual DSA mode to allow direct comparison with conventional 2D-DSA

(Figs 1 and 2). For visualization of arterial feeders, the fistulous point, and draining veins, we selected the time point with the best filling of the DAVF and a projection with minimal overlay from adjacent vessels. 4D-fpCBCTA images were displayed in 3 orthogonal planes with variable section thickness between 1 and 10 mm, either as MPR or MIP, as well as Volume Rendering Technique (VRT). 2D-DSA was acquired at variable frame rates up to 6 frames/s in posteroanterior and lateral projections and, in selected cases, in additional oblique projections.

4D-DSA in a virtual DSA mode and 2D-DSA were rated by 2 independent reviewers. Furthermore, the added

value of 4D-fpCBCTA reconstructions and fusions between unenhanced fpCBCTA and MR images was assessed.

The rating was performed on a scale of 0 to 4:

- 0 = Not evaluable (no grading possible)
- 1 = Poor (grading uncertain, limited image quality)
- 2 = Acceptable (grading possible, limited quality in several features)
- 3 = Good (grading possible, limited quality in a single feature)
- 4 = Very good (grading possible, high quality in all features).

The criteria for the analysis were the following:

- 1) Detection of arterial feeders
- 2) Location of the fistulous point or fistulous zone
- 3) Course and direction of flow in the draining sinus or vein
- 4) Grading of the fistula according to the classifications of Cognard and Borden, as well as Barrow in the case of carotid cavernous fistula
- 5) Suitability of arterial or venous vessels as access for endovascular therapy
- 6) Anatomic neighborhood of the arteriovenous shunt.

The results were summarized in a table, and we illustrated the main features of 4D in a case series. We calculated the interrater agreement using a linearly weighted Cohen  $\kappa$  coefficient within SPSS, Version 29.0 (IBM).

## RESULTS

We included data sets from 27 DAVFs in 26 patients, 21 men and 5 women. Table 1 shows the patient and DAVF characteristics.

The largest group ( $n = 9$ , 33%) had DAVFs located at the distal transverse sinus, in whom pulsatile tinnitus was the most frequent clinical symptom. A small number of cases ( $n = 5$ , 18%) presented with intracranial hemorrhage. Focal neurologic deficits occurred in 5 cases. Twenty-six percent of cases ( $n = 7$ ) had low-grade DAVFs (Borden I, Cognard I and IIa), 63% ( $n = 17$ ) had high-grade DAVFs (Borden II and III, Cognard IIb, III, and IV), and 11% ( $n = 3$ ) had symptomatic carotid cavernous fistulas (Barrow A and D), with ocular symptoms such as chemosis and proptosis, as well as various cranial nerve deficits.

**Table 1: Patient overview with DAVF grading according to Cognard or Barrow**

Age (yr)	Sex	Location	Type	Symptoms	Therapy
62	Male	Frontoethmoidal	III	None	Transvenous coiling
64	Male	Frontoethmoidal	IV	None	Transvenous coiling
72	Male	Frontoethmoidal	IV	None	Transvenous coiling
51	Female	Frontoethmoidal	IV	None	Surgery
48	Male	Frontal	IV	Headache, vertigo	Transarterial Onyx
43	Male	Frontal	III	None	Transarterial Onyx
45	Male	Frontal	III	Visual field loss	Transarterial Onyx
66	Male	Frontal	III	Acute cerebral hemorrhage	Surgery
69	Male	Infratentorial	III	None	Transarterial Onyx
54	Male	Infratentorial	III	Acute cerebral hemorrhage	Surgery
57	Male	Infratentorial	IV	Acute cerebral hemorrhage	Surgery
75	Female	Occipital	Ila	Pulsatile tinnitus	Transarterial Onyx
47	Male	Occipital	I	Pulsatile tinnitus	Transarterial Onyx
77	Male	Occipital	Ila	Pulsatile tinnitus	Transarterial Onyx
79	Male	Occipital	IV	Acute cerebral hemorrhage	Transarterial Onyx
72	Male	Occipital	I	Pulsatile tinnitus	None
64	Male	Occipital	Ila	Pulsatile tinnitus	Transarterial Onyx
70	Male	Occipital	I	Pulsatile tinnitus	Transvenous coiling
84	Female	Occipital	Ilb	Pulsatile tinnitus	None
59	Male	Occipital	I	Pulsatile tinnitus	None
31	Male	Temporo-occipital	III	Acute cerebral hemorrhage	Transarterial Onyx
31	Male	Temporo-occipital	III	None	Surgery
62	Male	Tentorial	IV	Headache	Transarterial Onyx
53	Male	Tentorial	IV	Hemiparesis	Radisurgery
62	Male	Carotid cavernous	A	Cranial nerve deficit (II)	Transarterial coiling
68	Female	Carotid cavernous	A	Cranial nerve deficit (III+IV)	Transarterial coiling
67	Female	Carotid cavernous	D	Cranial nerve deficit (IV)	Transvenous coiling

**Table 2: Advantages and disadvantages of 4D-DSA compared with 2D-DSA**

	No.	%
4D considered equal to 2D	13	48.1
4D considered advantageous to 2D	8	29.7
Improved projection	6	22.2
Reduction of vessel overlay	4	14.8
Display of adjacent anatomic structures	4	14.8
4D considered inferior to 2D	6	22.2
Incorrect grading	2	7.4
Endovascular access not displayed	2	7.4
Contrast injection too early	1	3.7
Incomplete display of arterial feeders	4	18.5
Pseudoretrograde display of small vessels	2	7.4
Motion artifacts	4	14.8

All patients with intracranial hemorrhage and neurologic deficits presented with higher DAVF grades with drainage via the cortical veins, or carotid cavernous fistulas with drainage via orbital veins.

Most patients ( $n = 24$ , 89%) received treatment after angiography. Only 3 cases remained untreated. Endovascular treatment was the preferred treatment option with either transarterial embolization with Onyx ( $n = 11$ ; Covidien) or transvenous embolization with detachable coils ( $n = 5$ ). Neurosurgical treatment was performed in 5 patients with fistulas inaccessible to superselective catheterization. A single patient with a recurrent cortical DAVF was treated with radiosurgery after declining surgery.

The diagnosis of a DAVF and identification of the fistulous point based on 4D-DSA were feasible in 26 of 27 cases. Grading according to the classifications of Cognard or Barrow was identical to that of 2D-DSA in 25 of 27 cases. The rating of the image

quality for grading by 2 independent reviewers resulted in a linearly weighted Cohen  $\kappa$  coefficient of 0.653, indicating adequate and significant interrater agreement ( $P < .001$ ).

In terms of visualization quality, 4D-DSA was comparable with 2D-DSA in 21 of 27 cases. In 6 of 27 cases, 4D-DSA was considered inferior to 2D-DSA due to a combination of factors: incomplete filling of small arterial feeders ( $n = 4$ ), incorrect or “pseudoretrograde” visualization of flow direction in feeding arteries or draining veins ( $n = 2$ ), image degradation due to motion artifacts ( $n = 4$ ), or missing visualization of potential access for endovascular treatment ( $n = 2$ ). This issue resulted in incorrect grading in 2 cases, one primarily due to motion artifacts and the other due to missing visualization of retrograde flow in the transverse sinus, therefore leading to incorrect grading of a Cognard Ila DAVF as Cognard I.

However, in 8 of 27 data sets, analysis of virtual DSA and 4D-fpCBCTA provided additional information regarding the exact location of the fistulous point and the course of the initial segment of the draining vein as targets for treatment. The main advantages (Table 2) in these 8 cases were improved visualization of the arteriovenous transition due to free selection of an optimal projection ( $n = 6$ ), less overlay of veins due to selection of an optimal time point of the 4D-DSA ( $n = 4$ ), and the possibility of displaying the adjacent anatomic structures ( $n = 4$ ). These advantages were especially found in high-grade DAVFs with cortical venous drainage (Fig 2), most notably in the frontoethmoidal and frontoparietal regions.

## DISCUSSION

The use of 4D-DSA volumes and 4D-fpCBCTA reconstructions for detailed analysis of the angioarchitecture and grading of cranial DAVFs was feasible and mostly comparable with 2D-DSA.

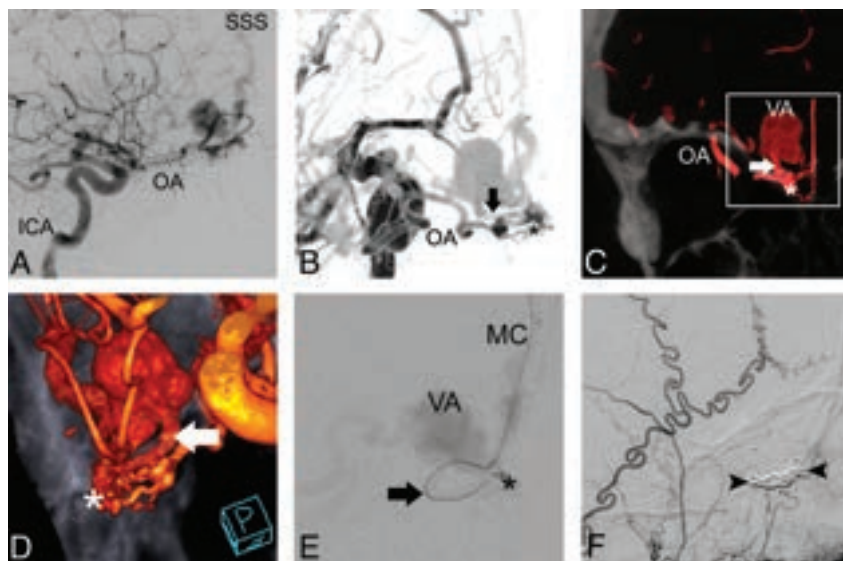


**FIG 2.** Comparison of a lateral standard projection in 2D-DSA (A) with an oblique projection in virtual DSA derived from 4D-DSA (B) and 4D-DSA coronal CT MIP (C) and volume rendering with an overlay of skull in an oblique zoomed-in projection (D). The 2D-DSA standard projection shows the frontoethmoidal DAVF supplied by the ophthalmic artery (OA) with drainage into the cortical veins and then the superior sagittal sinus (SSS). 4D-DSA images offer better visualization of the frontoethmoidal fistulous point (*asterisk*) and its anatomic relation to the draining vein (*arrow*), which is obscured in the standard projection of 2D-DSA, and the following venous aneurysm (VA). Note that the fistulous point is located within the olfactory groove. For endovascular therapy, a transvenous approach is selected with superselective positioning of the microcatheter (MC) in the draining vein past the VA (E), close to the fistulous point. After coiling (*arrowheads*) of the draining vein (F), we achieved complete embolization of the DAVF, as seen in the control angiogram of the ECA.

Correct grading, according to the classifications of Cognard or Barrow, was possible, except in 2 cases.

In selected cases, the new 4D method was considered advantageous in identifying the fistulous point and the initial segment of the draining vein as the main targets for treatment. The ability to visualize the shunt zone in any projection and at any time point of the scan was especially advantageous in cases with drainage into cortical veins or venous channels in the wall of a sinus. This ability may influence the decision as to whether the initial segment of the draining vein is suitable for transarterial penetration of Onyx without balloon protection of the adjacent sinus or for transvenous placement of coils. The 4D data may also be valuable for the planning of surgical or radiosurgical treatment. Fusion images with unenhanced fpCBCTA or MR images were used to demonstrate the relationship between the fistulous point and adjacent anatomic structures.

The question remains as to whether 4D is superior to 3DRA reconstructions without temporal resolution. In most cases, 3DRA may provide the same information. However, in cases with rapid flow or massive overlay by enlarged draining veins, the selection of a time point with the best visualization of the arteriovenous transition was helpful.

The main disadvantage of 4D-DSA was the limited suitability for planning of transarterial embolization with Onyx. In cases with multiple arterial feeders, the visualization of small-caliber meningeal arteries as the preferred access for the microcatheter was often incomplete or inferior to the superior spatial resolution of 2D DSA. Overlapping angiographic

phases continue to pose a relevant obstacle, requiring further improvement of the software prototype to enhance the validity of subsequent filling of small tortuous vessels.

We used a comparatively lengthy contrast bolus and scan duration to achieve sufficient filling of small vessels. Hand injection in ECA angiograms could also contribute to inconsistent vessel filling and bolus timing. We used hand injections to adapt the contrast volume and flow to the flow in the ECA branches and to minimize patient movement due to heat sensations associated with ECA contrast injection. Further systematic studies with different injection and scan protocols and use of an automatic injector may be necessary to optimize the filling of vessels with varying caliber and flow.

3DRA was acquired with an injection in only 1 feeding artery, whereas most DAVFs had several feeding arteries from multiple vascular territories. The interventionalist's selection was not always optimal for treatment planning. The accessibility of arteries and veins for superselective catheterization, especially as potential therapeutic

endovascular access, was not always considered during the diagnostic angiography.

We avoided repeat 3DRA acquisitions from different feeders for radiation protection. The modification of the scan angle (260° for 4D-DSA compared with 200° for standard 3D-DSA) and longer scan duration (12 seconds compared with 5 seconds) led to an increase in the radiation dose, which was still within reported doses for standard 3DRA and significantly less compared with 4D-CTA.<sup>12,13</sup> Future studies will use protocols with a reduction of the scan duration to 6 seconds, which should significantly decrease the radiation dose.

A complete display of all feeding arteries can be obtained through noninvasive CTA or MRA.

The main advantage of DSA and especially fpCBCTA is the unique spatial resolution, which greatly improves the visualization of the angioarchitecture compared with CTA or contrast-enhanced MRA.<sup>14</sup> The spatial and temporal resolution of 4D-DSA is notably superior to that of current time-resolved contrast-enhanced MRA, which was deemed insufficient for the grading of DAVFs.<sup>15</sup> In the future, new, time-resolved CTA and MRA techniques may further increase the value of the noninvasive imaging of DAVF.<sup>2,12,16,17</sup>

An important limitation of our study is its retrospective design with a small number of cases in a single center. Further multicenter studies are necessary to evaluate the usefulness and validity of 4D-DSA and 4D-fpCBCTA.

The interrater agreement was adequate considering the complexity of evaluating 4D-DSA and 4D-fpCBCTA. In our opinion,

the differences in ratings were minor and limited to the assessment of image quality. There were no major differences in rater opinions in terms of whether grading or identification of the fistulous point was possible.

We aimed to standardize the reconstruction parameters to improve postprocessing efficiency. Due to numerous manual steps, the average time for postprocessing was approximately 45 minutes. However, automated display of predefined reconstructions with optimal vessel contrast and window settings could substantially improve postprocessing, particularly for independent reviewers.

## CONCLUSIONS

Detailed analysis of the angioarchitecture of DAVFs with 4D-DSA volumes and fpCBCTA images is feasible and helpful for treatment planning in selected cases. At the current stage of development, 4D-DSA should be considered as complementary to 2D-DSA, and not as a substitute. Further validation of the method requires improvement of examination protocols and the 4D software.








**Disclosure forms** provided by the authors are available with the full text and PDF of this article at [www.ajnr.org](http://www.ajnr.org).

## REFERENCES

1. Ye X, Wang H, Huang Q, et al. **Four-dimensional computed tomography angiography is valuable in intracranial dural arteriovenous fistula diagnosis and fistula evaluation.** *Acta Neurol Belg* 2015;115:303–09 CrossRef Medline
2. In 't Veld M, Fronczek R, Dos Santos MP, et al. **High sensitivity and specificity of 4D-CTA in the detection of cranial arteriovenous shunts.** *Eur Radiol* 2019;29:5961–70 CrossRef Medline
3. Nishimura S, Hirai T, Sasao A, et al. **Evaluation of dural arteriovenous fistulas with 4D contrast-enhanced MR angiography at 3T.** *AJNR Am J Neuroradiol* 2010;31:80–85 CrossRef Medline
4. Lescher S, Gehrisch S, Klein S, et al. **Time-resolved 3D rotational angiography: display of detailed neurovascular anatomy in patients with intracranial vascular malformations.** *J Neurointerv Surg* 2017;9:887–94 CrossRef Medline
5. Keil F, Bergkemper A, Birkhold A, et al. **4D flat panel conebeam CTA for analysis of the angioarchitecture of cerebral AVMs with a novel software prototype.** *AJNR Am J Neuroradiol* 2022;43:102–09 CrossRef Medline
6. Lang S, Göltz P, Struffert T, et al. **4D DSA for dynamic visualization of cerebral vasculature: a single-center experience in 26 cases.** *AJNR Am J Neuroradiol* 2017;38:1169–76 CrossRef Medline
7. Sandoval-Garcia C, Royalty K, Yang P, et al. **4D DSA a new technique for arteriovenous malformation evaluation: a feasibility study.** *J Neurointerv Surg* 2016;8:300–04 CrossRef Medline
8. Ognard J, Magro E, Caroff J, et al. **A new time-resolved 3D angiographic technique (4D DSA): description, and assessment of its reliability in Spetzler-Martin grading of cerebral arteriovenous malformations.** *J Neuroradiol* 2018;45:177–85 CrossRef Medline
9. Chen KK, Guo WY, Yang HC, et al. **Application of time-resolved 3D digital subtraction angiography to plan cerebral arteriovenous malformation radiosurgery.** *AJNR Am J Neuroradiol* 2017;38:740–46 CrossRef Medline
10. Srinivasan VM, Chintalapani G, Duckworth EA, et al. **Application of 4-dimensional digital subtraction angiography for dural arteriovenous fistulas.** *World Neurosurg* 2016;96:24–30 CrossRef Medline
11. Xiang W, Yan L, Zhao Y, et al. **Four-dimensional digital subtraction angiography to assess cerebral arteriovenous malformations.** *J Neuroimaging* 2023;33:67–72 CrossRef Medline
12. Radon MR, Chandran A, Bhojak M, et al. **Radiation dose reduction in 4D cerebral CT angiography by individualized estimation of cerebral circulation time.** *AJNR Am J Neuroradiol* 2016;37:2189–94 CrossRef Medline
13. Huizinga N, Keil F, Birkhold A, et al. **4D flat panel conebeam CTA for in vivo imaging of the microvasculature of the human cortex with a novel software prototype.** *AJNR Am J Neuroradiol* 2020;41:976–79 CrossRef Medline
14. Davis B, Royalty K, Kowarschik M, et al. **4D digital subtraction angiography: implementation and demonstration of feasibility.** *AJNR Am J Neuroradiol* 2013;34:1914–21 CrossRef Medline
15. Dissaux B, Eugène F, Ognard J, et al. **Assessment of 4D MR angiography at 3T compared with DSA for the follow-up of embolized brain dural arteriovenous fistula: a dual-center study.** *AJNR Am J Neuroradiol* 2021;42:340–46 CrossRef Medline
16. Balasubramanian AP, Kannath SK, Rajan JE, et al. **Utility of silent magnetic resonance angiography in the evaluation and characterisation of intracranial dural arteriovenous fistula.** *Clin Radiol* 2021;76:712.e1–e8 CrossRef Medline
17. Denby CE, Chatterjee K, Pullicino R, et al. **Is four-dimensional CT angiography as effective as digital subtraction angiography in the detection of the underlying causes of intracerebral haemorrhage: a systematic review.** *Neuroradiology* 2020;62:273–81 CrossRef Medline



# Blunt Cerebrovascular Injury: Are We Overscreening Low-Mechanism Trauma?

 Kevin D. Hiatt,  Raghav Agarwal,  Chesney S. Oravec, Erica C. Johnson,  Nishk P. Patel,  Carol P. Geer,  Stacey Q. Wolfe, and  Michael E. Zapadka



## ABSTRACT

**BACKGROUND AND PURPOSE:** Screening patients with trauma for blunt cerebrovascular injury with neck CTA is a common practice, but there remains disagreement regarding which patients should be screened. We reviewed adult blunt cerebrovascular injury data from a level I trauma center to investigate whether screening is warranted in low-mechanism trauma.

**MATERIALS AND METHODS:** We reviewed all neck CTAs performed on adult trauma patients in the emergency department during the 2019 calendar year. Clinical and imaging risk factors for blunt cerebrovascular injury, trauma mechanism, initial neck CTA interpretations, results from subsequent CTA and DSA studies, antiplatelet and anticoagulant treatments, and outcome data were recorded.

**RESULTS:** One thousand one hundred thirty-six neck CTAs met the inclusion criteria, of which 965 (85%) were interpreted as having negative findings; 125, as having indeterminate findings (11%); and 46, as having positive findings (4%). Review of subsequent imaging and clinical documentation led to classification of 40 indeterminate studies (32%) as true-positives and 85 (68%) as false-positives. Blunt cerebrovascular injury was identified in 77 (12.6%) cases meeting and in 9 (1.7%) cases not meeting the expanded Denver criteria. The subset of 204 low-mechanism trauma cases (ground-level falls, blunt assaults, and low-impact motor vehicle collisions) not meeting the expanded Denver criteria (18% of the entire data set) could have been excluded from screening with 1 questionable injury and 0 ischemic strokes missed and 12 false-positive cases prevented.

**CONCLUSIONS:** We advocate reservation of blunt cerebrovascular injury screening in low-mechanism trauma for patients meeting the expanded Denver criteria. Further research is needed to determine the behavior of indeterminate cases and to establish criteria for separating true-positive from false-positive findings.

**ABBREVIATIONS:** BA = blunt assault; BCVI = blunt cerebrovascular injury; FP = false-positive; GLF = ground-level fall; MVC = motor vehicle collision; TP = true-positive

**B**lunt cerebrovascular injury (BCVI) is a rare but increasingly recognized injury to the carotid or vertebral arteries, which may lead to ischemic stroke in trauma patients. These injuries are estimated to occur in 0.2%–3% of blunt trauma cases<sup>1–6</sup> and are most often asymptomatic at the time of presentation.<sup>3,5,7</sup> The risk of ischemic stroke may be as high as 30%,<sup>8</sup> though this risk significantly decreases with antiplatelet therapy.<sup>3,5,6,8,9</sup> The large

percentage of asymptomatic cases and the margin for preventable morbidity and mortality make appropriate screening for BCVI a critical component of trauma evaluation.

Since Biffl et al,<sup>3</sup> in 1998, raised awareness of BCVI, it has been consistently demonstrated that a standardized approach to screening improves detection and patient outcomes, with CTA widely accepted as the preferred screening modality.<sup>3,6,10,11</sup> Screening criteria generally rely on clinical risk factors, such as soft-tissue injuries to the neck and neurologic symptoms worrisome for ischemic stroke, and imaging risk factors such as skull base and cervical spine fractures.<sup>10</sup> However, recent research has shown that accepted screening paradigms such as the expanded Denver and Memphis criteria miss 20%–50% of cases of BCVI. Therefore, more liberal and even universal screening for BCVI has been implemented at many institutions.<sup>12–15</sup> At our institution (Atrium Health Wake Forest Baptist), a more liberal approach to screening including all patients with “above the clavicle” injuries was implemented in 2010.<sup>16</sup>

Received March 4, 2023; accepted after revision August 21.

From the Wake Forest School of Medicine (K.S.H., R.A., C.S.O., N.P.P., C.P.G., S.Q.W., M.E.Z.), Winston-Salem, North Carolina; Departments of Radiology (K.D.H., C.P.G., S.Q.W., M.E.Z.), and Neurological Surgery (C.S.O., S.Q.W.), Atrium Health Wake Forest Baptist, Winston-Salem, North Carolina; and Department of General Surgery (E.C.J.), Virginia Commonwealth University Health, Richmond, Virginia.

Please address correspondence to Kevin D. Hiatt, MD, Atrium Health Wake Forest Baptist, Medical Center Blvd, Winston-Salem, NC 27157; e-mail: kehiatt@wakehealth.edu; @kdhiatt



Indicates article with online supplemental data.

<http://dx.doi.org/10.3174/ajnr.A8004>

**Table 1: The expanded Denver criteria<sup>a</sup>**

Signs/Symptoms	Risk Factors
Potential arterial hemorrhage from face or neck Cervical bruit in patient <50 yr Expanding cervical hematoma Neurologic deficit inconsistent with head CT Stroke on CT or MRI	High-energy trauma mechanism with: LeFort II or III facial fracture Mandible fracture Complex skull or skull base fracture Severe TBI with GCS < 6 Cervical spine fracture, subluxation, or ligamentous injury at any level Near hanging with anoxic brain injury Clothesline type injury or seat belt abrasion with significant swelling, pain, or altered mental status TBI with thoracic injuries Scalp degloving Thoracic vascular injury Blunt cardiac rupture Upper rib fractures

**Note:**—TBI indicates traumatic brain injury; GCS, Glasgow Coma Scale.

<sup>a</sup> Adapted from Nagpal et al.<sup>37</sup>

**Table 2: Additional clinical risk factors recorded specific to trauma mechanism**

Mechanism-Specific Risk Factors	
MVC	Motorcycle/ATV
Vehicle speed	Vehicle speed
Head-on collision	Head-on collision
Ejection	No helmet
Rollover	
No seat belt	
Air bags deployed	

**Note:**—ATV indicates all-terrain vehicle.

Inclusive screening approaches have been shown to be clinically advantageous and cost-effective<sup>17</sup> if the injuries identified are true injuries. However, in the case of BCVI, there is a recognized risk for false-positive (FP) results using screening CTA,<sup>18</sup> meaning that screening more patients may lead to more unnecessary treatment. Digital subtraction angiography (DSA) is the criterion standard test for diagnosing BCVI, but it is not performed on most trauma patients due to risk and cost;<sup>18</sup> therefore, neck CTA is widely relied on to determine the presence or absence of BCVI in clinical practice and in the existing literature.<sup>10,11,19</sup> To date, there has been little discussion of the potential for CTA findings to be ambiguous or misleading, particularly in the push for universal screening. Concerned by the frequency of CTAs ordered for low-mechanism trauma and of indeterminate CTA findings in our practice, we reviewed all adult trauma neck CTAs performed at our institution for 1 calendar year to investigate the occurrence, management, and outcomes of BCVI among patients with low-mechanism trauma and the rate at which CTA yielded ambiguous and FP results.

## MATERIALS AND METHODS

We retrospectively reviewed all neck CTAs performed for traumatic indications on adult patients in the emergency department at a level 1 academic trauma center during the 2019 calendar year. This study was written in accordance with Strengthening the Reporting of Observational Studies in Epidemiology (STROBE) guidelines.<sup>20</sup> Our institutional review board approved a waiver of informed consent for this study,

given its deidentified nature. Patient age and sex, study time and date, the CT scanner used, the name of the interpreting radiologist, and the times and dates of additional CT and MR imaging studies performed for the trauma evaluation were recorded for each patient. Clinical documentation and imaging reports were searched to determine whether each of the expanded Denver criteria was met (Table 1). In addition, trauma mechanism and mechanism-specific risk factors were recorded (Table 2).

For more precise classification of the mechanism of injury, we divided the ground-level fall (GLF), blunt assault (BA), and motor vehicle collision (MVC) groups into subgroups that met (GLF+, BA+, MVC+) and did not meet (GLF-, BA-, MVC-) the expanded Denver criteria. An additional, “low risk” MVC subgroup (MVC<sub>low</sub>) was created, including patients who did not meet the expanded Denver criteria or other high-risk trauma attributes (vehicle speed  $\geq$  40 miles per hour, head-on collision, rollover, patient ejection, air bag deployment, or lack of appropriate seat belt use).

Each initial CTA was classified as negative, indeterminate, or positive on the basis of the radiology report. Indeterminate studies were further classified as having FP or true-positive (TP) findings on the basis of the interpretation of subsequent imaging studies and review of the clinical documentation. On the basis of imaging reports, an indeterminate study was labeled FP if a subsequent study determined the initially described findings unlikely to represent an acute BCVI (eg, if the finding resolved or if it persisted but the appearance favored an alternate diagnosis such as atherosclerotic disease, fibromuscular dysplasia, or remote injury) and if the report resulted in the clinical team resolving the BCVI as an active patient problem. On the basis of clinical documentation, an indeterminate study was labeled FP if the clinical team decided against assigning or treating for a diagnosis of BCVI, citing either clinical suspicion or a neurosurgery overread as grounds for reaching this decision. Studies with positive and indeterminate findings were classified using the Biffl grading system as grades I, II, III, IV, or V. For each study with indeterminate or positive findings, the timing and results of subsequent CTA and catheter angiography studies were recorded. Follow-up imaging findings were classified as improved, the same, or worse in comparison with the initial study.

**Table 3. Classification of trauma mechanisms**

Trauma Mechanism	No.	%
MVC	443	39.0
GLF	149	13.1
Fall down stairs	101	8.9
BA	93	8.2
MVC	88	7.8
Fall from higher than ground level	61	5.4
Penetrating injury	52	4.6
Pedestrian struck by motor vehicle	50	4.4
All-terrain vehicle or dirt bike	22	1.9
Hanging	8	0.7
Other	69	6.1

For each indeterminate and positive CTA finding, treatment and outcome data were also recorded. The starting date, dose, and duration of therapy were recorded for each antiplatelet or anticoagulant medication administered. Outcome data included notation of neurologic deficits on the discharge summary or follow-up clinic visits, the detection of emboli on transcranial Doppler ultrasound, new or worsening intracranial hemorrhage after initiation of drug therapy, extracranial bleeding complications after initiation of drug therapy (eg, gastrointestinal hemorrhage), ischemic stroke, and death.

Statistical analysis was performed using JMP software (JMP Pro Version 15; SAS Institute) with pair-wise data mean comparison performed using the Student *t* test. Statistical significance was defined as  $P < .05$ .

## RESULTS

One thousand one hundred ninety-six neck CTAs were performed on adult patients in the emergency department during the 2019 calendar year, of which 1136 (95.0%) were performed for traumatic indications and were included in the analysis. Four hundred eighteen patients were women (36.8%), and the mean patient age was 51.6 years. The most common trauma mechanism was MVC ( $n = 450$ , 38.9%) followed by GLF ( $n = 152$ , 13.1%). Trauma mechanisms are further detailed in Table 3. Neck CTA was ordered as part of the initial trauma imaging bundle in 809 (71.2%) patients and was ordered after the imaging report was available for other cross-sectional imaging studies in the remainder of cases.

Neck CTAs were interpreted by a total of 12 subspecialty neuroradiologists, with each interpreting at least 50 studies. The individual rates of reporting studies with positive findings ranged from 2.0% to 7.4%, and the rates of reporting indeterminate studies ranged from 6.2% to 18.5%.

Nine hundred sixty-five neck CTAs were interpreted as having negative findings (85.0%); 125, as having indeterminate findings (11.0%); and 46, as having positive findings (4.0%) for BCVI. Of the indeterminate studies, 40 (32.0%) were classified as TPs and 85 (68.0%) were classified as FPs. The determination of a study with FP findings was made by a subsequent imaging study interpretation in 67 of 85 cases (78.9%), clinical documentation in 13 cases (15.3%), and neurosurgery overread in 5 cases (5.9%). Including the indeterminate TP cases, grade I injuries were most common, followed by grade II (Table 4).

In the 171 cases with positive and indeterminate findings, an ICA injury was reported in 114 (66.7%) and a vertebral artery injury

**Table 4: Number of Biffl grade I–V injury assignments in patients with positive and indeterminate findings on neck CTAs**

Group	I	II	III	IV	V
Positive studies	9	16	10	8	3
Indeterminate studies	114	6	1	3	0
TP	36	3	0	1	0
FP	78	3	1	2	0
Positive + TP	45	19	10	9	3

was reported in 82 (48%). Injury to 1 vessel was reported in 96 (56.1%), to 2 vessels in 60 (35.1%), to 3 vessels in 11 (6.4%), and to all 4 vessels in 4 (2.3%) cases. Sixty-four of the ICA injuries (56.1%) and 29 of the vertebral artery injuries (35.4%) were subsequently classified as FPs. ICA injuries were more likely to be reclassified as FPs than vertebral artery injuries ( $P < .005$ ). There was no significant correlation between the number of vessel injuries reported in a patient and the likelihood of the patient being classified as a having FP findings.

Five hundred twenty-three cases (46%) did not meet expanded Denver criteria. Within these, 9 BCVIs (positive and indeterminate TP findings) were identified (1.7%), in addition to 30 indeterminate FPs (5.7%). Among the 613 cases meeting expanded Denver criteria, 77 BCVIs were identified (12.6%), in addition to 55 indeterminate FP findings (9%). Subgroup analysis of the GLF, BA, and MVC low-risk groups revealed 0 BCVIs and 7 indeterminate FPs in the GLF group, 1 BCVI and 2 indeterminate FPs in the BA group, and 0 BCVIs and 3 indeterminate FPs in the MVC<sub>low</sub> group. The single BCVI identified in the BA group was interpreted as indeterminate and had no follow-up imaging or treatment because the patient was lost to follow-up. The patient re-emerged about 1 year later, at which time neuroimaging showed no evidence of prior ischemic infarct. Repeat vascular imaging was not performed. Due to the case ambiguity and the documented intent to treat the patient, it was classified as a TP, but it remains unclear whether this was a true injury. Altogether, 204 of 1136 cases (18%) or 39% of the cases not meeting the expanded Denver criteria could have been excluded from screening neck CTA with only 1 questionable injury missed and 12 indeterminate FPs prevented (Online Supplemental Data).

At least 1 follow-up CTA was performed for 130 of the 171 studies with positive and indeterminate findings (76%), with the first follow-up CTA performed at a median of 2.1 days following the initial study. Seventy-nine studies (60.8%) showed improvement in the initial imaging finding, 49 (37.7%) demonstrated no change, and 2 (1.5%) showed progression. The 2 cases demonstrating progression were both initially classified as having grade IV injuries. DSA was performed in 13 cases (7.6%), with stenting performed in 4, angioplasty in 1, and vessel sacrifice in 2 cases.

Fifty-seven of the 86 cases with positive and TP findings (66.3%) were treated with aspirin (28 with 81 mg daily, 11 with 162 mg daily, and 18 with 325 mg daily) and 9 (10.5%) were additionally treated with clopidogrel (75 mg daily). Eighteen of the 85 indeterminate FP cases (21.2%) were treated with aspirin, and zero were treated with clopidogrel, with aspirin typically discontinued once the injury was determined to be a FP unless aspirin was required for a separate indication. The median duration of aspirin therapy in the cases in which it was discontinued was 3 days.

In the 86 cases with positive and TP findings, ischemic stroke occurred 3 times (3.5%) compared with 0 times in the cases with 85 FP findings ( $P = .08$ ). Death occurred in 18 of the patients with positive and TP findings (20.9%) and in 3 of the cases with FP findings (3.5%;  $P < .005$ ). Worsening intracranial hemorrhage after admission was observed in 5 patients with positive and TP findings (5.8%) and in 2 patients with FP findings (2.4%;  $P = .26$ ). No instances of bleeding outside the CNS (eg, gastrointestinal bleeding) were reported to have developed after initiation of antiplatelet therapy in any of the patients studied.

## DISCUSSION

High-sensitivity screening for BCVI is important in adult trauma patients because of the high percentage of patients who are initially asymptomatic and the potential to decrease the rates of ischemic stroke, permanent disability, and death with appropriate management.<sup>3-6,8,9,11</sup> The reported high rate of BCVI missed by established screening algorithms such as the expanded Denver criteria has led many to advocate for universal screening.<sup>12-15,17,21,22</sup> In our data set, 10.5% of BCVIs were not captured by the expanded Denver criteria, even after excluding cases determined to be FPs. However, the potential benefit from expanded screening should be balanced against the risks, which include the potential adverse effects of antiplatelet or anticoagulant treatment, extended hospital stays, iodinated contrast material-related reactions and renal injuries, radiation exposure, and increased cost to patients and health care systems.<sup>23-26</sup>

Trauma mechanism is a useful consideration in the selection of patients for BCVI screening because high-mechanism trauma portends an increased risk for BCVI, even in the absence of other identifiable injuries.<sup>7,27,28</sup> Conversely, low-mechanism trauma confers a very low risk for BCVI, particularly in the absence of other risk factors. We focused on GLF, BA, and low-impact MVC as low mechanism injuries due to concern from our practice that patients presenting with these mechanisms are overscreened. First, we defined low-risk GLF injuries as those not meeting the expanded Denver criteria. In a retrospective review of >1.2 million trauma cases in elderly patients (65 years of age or older), Anto et al<sup>29</sup> discovered the overall incidence of BCVI among patients with GLFs to be 0.15%. Among the subset of patients with  $\geq 1$  risk factor, the incidence was significantly higher at 0.86%. Although not directly reported, the incidence of BCVI among elderly patients with GLFs with no risk factors calculated from their data set was 0.07%. Anto et al and others have reported low rates of screening in elderly patients with GLFs as well as increased morbidity and mortality in elderly compared with young patients with GLFs with BCVI,<sup>29-32</sup> but there is little justification for screening patients with GLFs without risk factors for BCVI in the existing literature. Second, in the absence of a literature precedent for uniquely classifying BA injuries to define BCVI risk, we chose to define low-risk BA injuries as those not meeting the expanded Denver criteria. Finally, stratifying MVCs into high and low impact can be challenging, particularly when history is lacking, but when possible, we defined low-impact MVCs as those with a vehicle speed of <40 miles per hour, no airbag deployment, appropriate seatbelt use, and no head-on collision, rollover, or patient ejection, mirroring the criteria outlined

by Farhat-Sabet et al<sup>27</sup> (though we selected 40 miles per hour instead of 40 km/hour as our speed threshold).

In support of trauma mechanism as a useful discriminator in selecting patients for BCVI screening, we identified 204 cases of low-mechanism trauma (GLF, BA, and low-impact MVC) not meeting the expanded Denver criteria, among which 1 questionably TP and 12 FP BCVIs were encountered. In other words, 18% of our data set could have been excluded from BCVI screening with only 1 questionable injury missed. The cost savings of excluding these 204 studies would have been \$51,571.20 US dollars (at our calculated institution-specific price for performing and interpreting a neck CTA of \$252.80), though the savings are likely much greater when considering the elimination of unnecessary follow-up imaging studies, neurosurgical consultations, patient treatment, and prolonged in-hospital patient evaluation. A future dedicated cost analysis would be useful to better determine the expense of overscreening.

The existing literature largely accepts confirmation of BCVI on CTA, given that catheter angiography is not commonly performed. However, the weaknesses of CTA are well-established in studies comparing CTA with DSA. Several have reported a mediocre sensitivity of CTA in comparison with DSA ranging from 51% to 74%.<sup>33-35</sup> While the same studies have reported the high specificity of CTA for BCVI ranging from 86% to 95%, a separate study by Grandhi et al<sup>18</sup> reported a CTA FP rate of 48% compared with DSA. Because DSA was not available for most of our data set and was only performed to further evaluate or treat cases with positive findings, we cannot determine our CTA false-negative rate. However, 68% of CTA studies interpreted as indeterminate in our study were determined to be FPs based on clinical documentation and follow-up imaging results. Certainly, the reporting of indeterminate BCVI may vary widely among institutions, across levels of radiologists' experience and training, and even in the same interpreting radiologist across time. Reporting variability is demonstrated by the approximately 3-fold variability in rates of reporting cases positive for BCVI (2%–7.4%) and indeterminate for BCVI (6.2%–18.5%) among our 12 neuroradiologists. The importance of indeterminate interpretations is in the subsequent practice of repeating a follow-up neck CTA to confirm resolution or the need for ongoing treatment, which doubles the cost and risk exposure to contrast material and radiation.

There is, unfortunately, a paucity of literature addressing indeterminate BCVI. Crawford et al<sup>36</sup> identified 59 indeterminate BCVIs from a set of 138 non-negative neck CTAs obtained for trauma (43%). Of these indeterminate cases, 23 resolved, 21 remained indeterminate, and 15 were reclassified as true BCVIs on subsequent imaging, though it is unclear from their research whether this reclassification necessarily resulted from a worsening of imaging findings. Our rate of indeterminate studies was higher than what they reported (73% of our non-negative cases were indeterminate), highlighting a likely wide variability in the reporting of BCVI among radiologists. The new implementation of standardized wording for indeterminate BCVI at our institution just prior to the time period of the data set we studied may have also led to an increased rate of reporting indeterminate injuries. None of our indeterminate cases demonstrated progression



on follow-up imaging studies, with at least 1 follow-up CTA obtained in 76% of cases.

Ischemic infarct and death are commonly reported outcome measures in patients with BCVI. The stroke rate among patients with positive and TP findings in our study of 3.5% is comparable with rates reported in the literature.<sup>1,5,8,9</sup> Among patients with FP findings, the stroke rate was 0%. The mortality rate among patients with positive and TP findings in our study of 20.9% represents an all-cause mortality rather than mortality directly attributable to BCVI. There was a significantly lower mortality rate in patients with FP compared with those with positive/TP findings, though the small number of observed ischemic infarcts and deaths in this data set limits cross-group comparisons.

Our study has several limitations. Due to its retrospective nature, the set of cases obtained reflects the ordering biases of a heterogeneous group of emergency and trauma surgery physicians. Although standardized algorithms aim to make practice more uniform, differing approaches among ordering physicians breed heterogeneity. Additionally, the interpreting radiologists had access to data about the trauma mechanism and were aware of the presence or absence of injuries predisposing to BCVI, such as cervical spine fractures. These data likely impacted study interpretation. Unfortunately, even in a blinded study environment, it would be difficult to shield interpreting radiologists from imaging risk factors for BCVI including cervical, skull base, facial, and upper rib and thoracic vertebral fractures because these are often apparent on the neck CTA. Finally, our division of indeterminate cases into TP and FP relied on the opinions of interpreting radiologists and clinical teams, which are not immune to error. However, all cases benefited from subspecialty neuroradiologists' interpretations and patient assessment by a dedicated trauma surgery service at a level 1 trauma center.

## CONCLUSIONS

More inclusive approaches to BCVI screening offer greater sensitivity at the expense of increased cost to the medical system, increased radiation and contrast media exposure to patients, and an increased number of FP results leading to unnecessary treatment. Within a liberal screening system using "above the clavicle" injuries as the inclusion criterion, we identified 204 low-mechanism trauma cases not meeting the expanded Denver criteria during 1 calendar year, among which only 1 questionable BCVI and 12 studies with FP findings were identified and no ischemic strokes occurred. We, therefore, advocate reservation of BCVI screening for low-mechanism trauma patients (including GLFs, BAs, and low-impact MVCs) to those meeting the expanded Denver criteria, meaning that neck CTA should not be routinely included as part of the initial trauma imaging bundle in these patients. Additionally, we found a high rate of indeterminate studies (73% of all non-negative studies in our data set), among which 68% had FP findings. More research is needed to better elucidate the behavior of indeterminate injuries and to establish standards for distinguishing studies with TP from those with FP findings.

**Disclosure forms** provided by the authors are available with the full text and PDF of this article at [www.ajnr.org](http://www.ajnr.org).

## REFERENCES

1. Azad TD, Raj D, Ahmed K, et al. **Predictors of blunt cerebrovascular injury, stroke, and mortality in patients with cervical spine trauma.** *World Neurosurg* 2023;169:e251–59 CrossRef Medline
2. Berne JD, Cook A, Rowe SA, et al. **A multivariate logistic regression analysis of risk factors for blunt cerebrovascular injury.** *J Vasc Surg* 2010;51:57–64 CrossRef Medline
3. Biffi WL, Moore EE, Ryu RK, et al. **The unrecognized epidemic of blunt carotid arterial injuries: early diagnosis improves neurologic outcome.** *Ann Surg* 1998;228:462–70 CrossRef Medline
4. Burlew CC, Biffi WL. **Imaging for blunt carotid and vertebral artery injuries.** *Surg Clin North Am* 2011;91:217–31 CrossRef Medline
5. Murphy PB, Severance S, Holler E, et al. **Treatment of asymptomatic blunt cerebrovascular injury (BCVI): a systematic review.** *Trauma Surg Acute Care Open* 2021;6:e000668 CrossRef Medline
6. Tso MK, Lee MM, Ball CG, et al. **Clinical utility of a screening protocol for blunt cerebrovascular injury using computed tomography angiography.** *J Neurosurg* 2017;126:1033–41 CrossRef Medline
7. Bensch FV, Varjonen EA, Pyhältö TT, et al. **Augmenting Denver criteria yields increased BCVI detection, with screening showing markedly increased risk for subsequent ischemic stroke.** *Emerg Radiol* 2019;26:365–72 CrossRef Medline
8. Hundesmarck D, Slooff WM, Homans JF, et al. **Blunt cerebrovascular injury: incidence and long-term follow-up.** *Eur J Trauma Emerg Surg* 2021;47:161–70 CrossRef Medline
9. Esposito EC, Kufera JA, Wolff TW, et al. **Factors associated with stroke formation in blunt cerebrovascular injury: an EAST multicenter study.** *J Trauma Acute Care Surg* 2022;92:347–54 CrossRef Medline
10. Brommeland T, Helseth E, Aarhus M, et al. **Best practice guidelines for blunt cerebrovascular injury (BCVI).** *Scand J Trauma Resusc Emerg Med* 2018;26:90 CrossRef Medline
11. Kim DY, Biffi W, Bokhari F, et al. **Evaluation and management of blunt cerebrovascular injury: a practice management guideline from the Eastern Association for the Surgery of Trauma.** *J Trauma Acute Care Surg* 2020;88:875–87 CrossRef Medline
12. Black JA, Abraham PJ, Abraham MN, et al. **Universal screening for blunt cerebrovascular injury.** *J Trauma Acute Care Surg* 2021;90:224–31 CrossRef Medline
13. Bruns BR, Tesoriero R, Kufera J, et al. **Blunt cerebrovascular injury screening guidelines: what are we willing to miss?** *J Trauma Acute Care Surg* 2014;76:691–95 CrossRef Medline
14. Jacobson LE, Ziemba-Davis M, Herrera AJ. **The limitations of using risk factors to screen for blunt cerebrovascular injuries: the harder you look, the more you find.** *World J Emerg Surg* 2015;10:46 CrossRef Medline
15. Leichtle SW, Banerjee D, Schrader R, et al. **Blunt cerebrovascular injury: the case for universal screening.** *J Trauma Acute Care Surg* 2020;89:880–86 CrossRef Medline
16. McCullough MA, Cairns AL, Shin J, et al. **Above the clavicle: a simplified screening method for asymptomatic blunt cerebral vascular injury.** *Am Surg* 2023;89:79–83 CrossRef Medline
17. Ali A, Broome JM, Tatum D, et al. **Cost effectiveness of universal screening for blunt cerebrovascular injury: a Markov analysis.** *J Am Coll Surg* 2023;236:468–75 CrossRef Medline
18. Grandhi R, Weiner GM, Agarwal N, et al. **Limitations of multidetector computed tomography angiography for the diagnosis of blunt cerebrovascular injury.** *J Neurosurg* 2018;128:1642–47 CrossRef Medline
19. Zeineddine HA, King N, Lewis CT, et al. **Blunt traumatic vertebral artery injuries: incidence, therapeutic management, and outcomes.** *Neurosurgery* 2022;90:399–406 CrossRef Medline
20. Elm Ev, Altman DG, Egger M, et al. **Strengthening the Reporting of Observational Studies in Epidemiology (STROBE) statement: guidelines for reporting observational studies.** *BMJ* 2007;335:806 CrossRef Medline
21. Geddes AE, Burlew CC, Wagenaar AE, et al. **Expanded screening criteria for blunt cerebrovascular injury: a bigger impact than anticipated.** *Am J Surg* 2016;212:1167–74 CrossRef Medline

22. Harper PR, Jacobson LE, Sheff Z, et al. **Routine CTA screening identifies blunt cerebrovascular injuries missed by clinical risk factors.** *Trauma Surg Acute Care Open* 2022;7:e000924 CrossRef Medline
23. Du PZ, Barton D, Bridge N, et al. **Cervical fracture patterns associated with blunt cerebrovascular injuries when utilizing computed tomographic angiography: a systematic review and meta-analysis.** *Spine J* 2022;22:1716–25 CrossRef Medline
24. Fourman MS, Shaw JD, Vaudreuil NJ, et al. **Cervical spine fractures: who really needs CT angiography?** *Spine (Phila Pa 1976)* 2019;44:1661–67 CrossRef Medline
25. Jordan RW Jr, Breland DM, Zhang X, et al. **The utility of a screening neck computed tomographic angiogram in blunt trauma patients presenting with a seat belt sign in the absence of associated risk factors.** *J Comput Assist Tomogr* 2020;44:941–46 CrossRef Medline
26. Saqib R, Madhavan A, Thornber E, et al. **The value of performing cerebrovascular CT angiography in major trauma patients: a 5-year retrospective review.** *Clin Radiol* 2023;78:e190–96 CrossRef Medline
27. Farhat-Sabet A, Lauerma M, Chavez A, et al. **Blunt cerebrovascular injury screening criteria should include motor vehicle crash characteristics.** *Am Surg* 2021;87:390–95 CrossRef Medline
28. Hanna K, Okumura K, Shnaydman I. **Improving blunt cerebrovascular injury screening in motor vehicle collision patients: does airbag deployment matter?** *Am J Surg* 2022;224:1393–97 CrossRef Medline
29. Anto VP, Brown JB, Peitzman AB, et al. **Blunt cerebrovascular injury in elderly fall patients: are we screening enough?** *World J Emerg Surg* 2018;13:30 CrossRef Medline
30. Flashburg E, Ong AW, Muller A, et al. **Fall downs should not fall out: blunt cerebrovascular injury in geriatric patients after low-energy trauma is common.** *J Trauma Acute Care Surg* 2019;86:1010–14 CrossRef Medline
31. Le DT, Barhorst KA, Castiglione J, et al. **Blunt cerebrovascular injury in the geriatric population.** *Neurosurg Focus* 2020;49:E10 CrossRef Medline
32. Page PS, Josiah DT. **Traumatic vertebral artery injuries in the geriatric population: a retrospective cohort study.** *J Neurosurg Spine* 2020 Jan 17 [Epub ahead of print] CrossRef Medline
33. Kik CC, Slooff WM, Moayeri N, et al. **Diagnostic accuracy of computed tomography angiography (CTA) for diagnosing blunt cerebrovascular injury in trauma patients: a systematic review and meta-analysis.** *Eur Radiol* 2022;32:2727–38 CrossRef Medline
34. Malhotra AK, Camacho M, Ivatury RR, et al. **Computed tomographic angiography for the diagnosis of blunt carotid/vertebral artery injury: a note of caution.** *Ann Surg* 2007;246:632–42; discussion 642–33 CrossRef Medline
35. Paulus EM, Fabian TC, Savage SA, et al. **Blunt cerebrovascular injury screening with 64-channel multidetector computed tomography: more slices finally cut it.** *J Trauma Acute Care Surg* 2014;76:279–83; discussion 28479–85 CrossRef Medline
36. Crawford JD, Allan KM, Patel KU, et al. **The natural history of indeterminate blunt cerebrovascular injury.** *JAMA Surg* 2015;150:841–47 CrossRef Medline
37. Nagpal P, Policeni BA, Bathla G, et al. **Blunt cerebrovascular injuries: advances in screening, imaging, and management trends.** *AJNR Am J Neuroradiol* 2017;39:406–14 CrossRef Medline

# Specificity of Quantitative Functional Brain Mapping with Arterial Spin-Labeling for Preoperative Assessment

Giannina R. Iannotti, Isaure Nadin, Vladimira Ivanova, Quentin Tourdot, Agustina M. Lascano, Shahan Momjian, Karl L. Schaller, Karl O. Lovblad, and Frederic Grouiller



## ABSTRACT

**BACKGROUND AND PURPOSE:** Arterial spin-labeling is a noninvasive MR imaging technique allowing direct and quantitative measurement of brain perfusion. Arterial spin-labeling is well-established in clinics for investigating the overall cerebral perfusion, but it is still occasionally employed during tasks. The typical contrast for functional MR imaging is blood oxygen level-dependent (BOLD) imaging, whose specificity could be biased in neurologic patients due to altered neurovascular coupling. This work aimed to validate the use of functional ASL as a noninvasive tool for presurgical functional brain mapping. This is achieved by comparing the spatial accuracy of functional ASL with transcranial magnetic stimulation as the criterion standard.

**MATERIALS AND METHODS:** Twenty-eight healthy participants executed a motor task and received a somatosensory stimulation, while BOLD imaging and arterial spin-labeling were acquired simultaneously. Transcranial magnetic stimulation was subsequently used to define hand somatotopy.

**RESULTS:** Functional ASL was found more adjacent to transcranial magnetic stimulation than BOLD imaging, with a significant shift along the inferior-to-superior direction. With respect to BOLD imaging, functional ASL was localized significantly more laterally, anteriorly, and inferiorly during motor tasks and pneumatic stimulation.

**CONCLUSIONS:** Our results confirm the specificity of functional ASL in targeting the regional neuronal excitability. Functional ASL could be considered as a valid supplementary technique to BOLD imaging for presurgical mapping when spatial accuracy is crucial for delineating eloquent cortex.

**ABBREVIATIONS:** ASL = arterial spin-labeling; BOLD = blood oxygen level-dependent; CMRO<sub>2</sub> = cerebral metabolic rate of oxygen; CoG = center of gravity; ESI = electrical source imaging; fASL = functional ASL; MAX = global maximum of activation; TMS = transcranial magnetic stimulation

fMRI is a noninvasive imaging technique for studying cerebral functions in healthy, clinical populations. Blood oxygen level-dependent (BOLD)<sup>1</sup> imaging relies on the complex interplay between neuronal activity and associated blood changes (CBF, CBV, and the cerebral metabolic rate of oxygen [CMRO<sub>2</sub>]). Therefore, BOLD imaging offers an indirect and nonquantitative measure of neuronal activity. Moreover, BOLD specificity can be

biased by the presence of draining veins<sup>2</sup> or in the case of pathologic neurovascular coupling, as with brain tumors,<sup>3,4</sup> epilepsy,<sup>5,6</sup> and cerebrovascular diseases.<sup>7</sup>

Previous studies compared BOLD localization with other imaging modalities, particularly in sensory and motor experiments. During finger movement, anterior-to-posterior and medial-to-lateral shifts of BOLD imaging with respect to electrical source imaging (ESI) have been found.<sup>8</sup> Inuggi et al<sup>9</sup> showed that BOLD activation of a tapping thumb localized more posteriorly with respect to transcranial magnetic stimulation (TMS). Similarly, during pneumatic stimulation of the thumb, BOLD imaging localized significantly more laterally and posteriorly than ESI.<sup>10</sup>

The limitations of BOLD imaging have motivated the development of quantitative MR imaging to characterize the hyperemic (CBF, CBV) and metabolic responses (CMRO<sub>2</sub>) triggered by neuronal spiking.<sup>11,12</sup> Arterial spin-labeling (ASL) is one of the most established MR imaging techniques for absolute quantification of CBF: The perfusion map is obtained by the averaged pair-wise subtraction of brain images acquired alternately in conditions of blood-sensitized (labeled) and static (control) tissue.<sup>13,14</sup> Alternatively,

Received April 11, 2023; accepted after revision August 28.

From the Division of Neuroradiology, Diagnostic Department (G.R.I., K.O.L.), Department of Neurosurgery (G.R.I., I.N., V.I., S.M., K.L.S.), and Division of Neurology (A.M.L.), Department of Clinical Neuroscience, Geneva University Hospitals and University of Geneva, Geneva, Switzerland; Faculty of Pharmacy (Q.T.), University of Montpellier, Montpellier, France; Swiss Centre for Affective Sciences (F.G.) and Laboratory of Neurology and Imaging of Cognition (F.G.), Department of Basic Neurosciences, University of Geneva, Geneva, Switzerland; and CIBM Center for Biomedical Imaging (F.G.), Geneva, Switzerland.

This study was supported by the Louis-Jeantet Foundation.

Please address correspondence to Frédéric Grouiller, PhD, CIBM MRI HUG-UNIGE, Service de Radiologie, Boulevard de la Tour 8, 1211 Geneva 14, Switzerland; e-mail: Frederic.Grouiller@unige.ch; @GrouillerF

Indicates article with online supplemental data.

<https://dx.doi.org/10.3174/ajnr.A8006>

from the succession of pair-wise subtractions, the functional time course of perfusion can be extracted,<sup>15</sup> implying that ASL can be used as a functional MR imaging technique (functional ASL [fASL]) to quantify the arterial blood delivered to the brain tissue during tasks.

Given the variety of MR imaging sequences,<sup>16</sup> the intrinsic low SNR and temporal resolution, and the lack of standardized pipelines,<sup>17,18</sup> ASL is slowly emerging in the clinical setting as a functional tool. Nevertheless, ASL has remarkable advantages with respect to BOLD imaging: 1) quantitative measurement relevant for longitudinal<sup>19</sup> or pharmacologic studies,<sup>20</sup> 2) unaffected by venous contamination,<sup>21</sup> and 3) insensitive to slow drift.<sup>22</sup> Moreover, ASL has a higher intra- and intersubject stability compared with BOLD imaging.<sup>23,24</sup>

fASL has been investigated in various tasks<sup>25–27</sup> and for functional connectivity,<sup>28,29</sup> but few publications tackled localization specificity compared with other techniques. Noteworthy, most studies have compared fASL and BOLD imaging using different sessions or relying on the BOLD imaging extracted by the ASL sequence.<sup>25,26,30,31</sup> For an appropriate comparison with BOLD imaging in task-based imaging, the selection of the ASL sequence is fundamental.<sup>16</sup> Recently, dual-echo pseudocontinuous ASL sequences have been developed, enabling simultaneous acquisition of BOLD imaging and ASL with optimal parameters for both contrasts.<sup>27–29,32,33</sup>

The translation of fASL into the clinical routine requires a systematic characterization of the advantages and potential disadvantages with respect to the standard BOLD imaging.

In this context, the current work aims to assess the performance of fASL for the delineation of the functional cortex during motor and somatosensory tasks in a cohort of healthy subjects. We used dual-echo pseudocontinuous ASL to obtain, simultaneously, perfusion-based and BOLD images, avoiding intersession variability.<sup>34</sup> Also, we attributed our results to the individual hand somatotopy obtained during TMS and linked the information driven by the 2 MR imaging modalities with the motor neuron excitability. In line with previous findings, we hypothesized a significant shift in the localization between BOLD imaging and fASL. Moreover, given the quantitative nature of fASL, targeting the blood flow changes directly associated with the neuronal activity, we expect that fASL activation would be in closer proximity to the actual neuronal sites compared to BOLD activation.

## MATERIALS AND METHODS

Our experiments followed international guidelines and were approved by the local ethics committee. Twenty-eight right-handed healthy volunteers (14 women; 18–56 years of age; mean age, 33 years) were enrolled in this study and gave informed consent for their participation. All subjects had normal or corrected visual acuity and had no psychiatric or neurologic symptoms.

### Experimental Design

Subjects underwent an MR imaging session (Magnetom Trio 3T; Siemens, 32-channel-head coil) with motor and somatosensory tasks, followed by a neuronavigated TMS examination on a different day (1–7 days later).

The motor task consisted of seven 35-second alternations between hand-clenching and rest. The somatosensory stimulation

included ten 35-second blocks of rest and stimulation, during which the right or left thumb received nonpainful air wisps at 2.14 Hz using MR imaging-compatible pneumatic equipment. Participants were asked to look at a fixation cross during rest periods. Hand order was counterbalanced across participants.

During tasks, BOLD imaging and fASL were acquired simultaneously, with a dual-echo pseudocontinuous ASL sequence having the following parameters: TR = 3500 ms, TE1/TE2 = 10/25 ms, label duration = 1500 ms, post-labeling delay = 1000 ms, FOV = 205 × 205 mm, 3-mm-thickness slices with a 0.6-mm gap, in-plane resolution = 3.2 × 3.2 mm, 20 slices. The FOV covered the top half of the brain, and the labeling plane was positioned, with the help of a sagittal angiography sequence, 14 cm below the center of the image slab perpendicular to the carotids. Structural imaging included a high-resolution 3D T1 (multiecho MPRAGE: TR = 2530 ms, TI = 1100 ms, TE1/TE2/TE3/TE4 = 1.64/3.5/5.36/7.22 ms, 1-mm isotropic).

Individual MR imaging was used for neuronavigated TMS to map the motor cortex associated with both hands. TMS recordings were performed using the Navigated Brain Stimulation System from Nexstim (<https://www.nexstim.com/>), following standard stimulation guidelines.<sup>35</sup> Two pairs of electrodes were placed on the abductor pollicis brevis and the first dorsal interosseus muscles on each hand, and a ground-reference electrode was placed on the right wrist. Motor-evoked potentials were recorded throughout the entire stimulation. The anatomic hotspot in the precentral gyrus was visually identified for each hemisphere. The resting motor threshold for the first dorsal interosseus muscles was found by delivering single-pulse stimulations and recording the lowest intensity capable of eliciting 50- $\mu$ V motor-evoked potentials in at least 50% of the stimulations, within a 20-ms latency range.<sup>36</sup> The subject-specific stimulation intensity above the resting motor threshold (105%) was used for stimulation, while moving the coil medially and laterally around the predefined anatomic hotspot. Stimulation toward the postcentral and precentral sulci defined the boundaries of the somatotopy. Significant stimulation points associated with suprathreshold motor-evoked potentials (50- $\mu$ V, peak-to-peak) were collected for further analysis.

### Data Analysis

MR imaging data-preprocessing and analysis were performed using customized scripts in Matlab (MathWorks), SPM12 (IBM), and the open-source toolbox ASLtbx (<https://www.cfn.upenn.edu/zewang/ASLtbx.php>).<sup>37</sup> Preprocessing consisted of realignment and coregistration to 3D T1 spatial smoothing using an isotropic Gaussian kernel (6 mm for BOLD imaging and 5 mm for fASL). For fASL data, label and control images were realigned separately and then coregistered to the 3D T1. Pair-wise subtraction between the label and control was considered to estimate the perfusion-weighted images.<sup>38</sup> 3D T1 was segmented, and a brain mask was created for further analysis.

Individual activation of BOLD imaging and fASL for the clenching task and the somatosensory stimulation was obtained with the independent FSL General Linear Model (<http://fsl.fmrib.ox.ac.uk/fsl/fslwiki/GLM>) for each hand.

In clenching task, the threshold for significant BOLD activation was established at a family-wise error rate  $P < .001$ , with a



**Table 1: Difference between fASL and BOLD in terms of Euclidean distance**

	fASL-BOLD (mean [SD]) mm			
	X: Left→Right	Y: Anterior→Posterior	Z: Inferior→Superior	Euclidean Distance
MAX				
Right hand	−2.41 (SD, 6.03) <sup>a</sup>	3.10 (SD, .21) <sup>a</sup>	−12.76 (SD, 5.19) <sup>b</sup>	15.45 (SD, 6.36) <sup>b</sup>
Left hand	0.37 (SD, 6.12)	2.67 (SD, 6.65) <sup>a</sup>	−13.51 (SD, 5.56) <sup>b</sup>	16.62 (SD, 5.01) <sup>b</sup>
CoG				
Right hand	−2.58 (SD, 4.26) <sup>a</sup>	3.02 (SD, 5.29) <sup>a</sup>	−6.90 (SD, 6.78) <sup>b</sup>	10.51 (SD, 6.69) <sup>b</sup>
Left hand	2.91 (SD, 6.10) <sup>a</sup>	0.61 (SD, 3.41) <sup>a</sup>	−7.51 (SD, 4.10) <sup>b</sup>	10.10 (SD, 5.21) <sup>b</sup>

<sup>a</sup>  $P < .05$ .<sup>b</sup>  $P < .001$ .

requirement for a minimum extent of 30 contiguous voxels. Due to the known low SNR of fASL and because the total number of volumes was halved with respect to BOLD imaging, we considered  $P < .001$  with a 10-voxel extent threshold for fASL. Activations associated with somatosensory stimulation are very focal and less robust than motor responses. Different thresholds were then explored to detect significant activations.

Systematic shifts of BOLD and fASL localization between them and versus TMS were analyzed at an individual level. For each activation map derived from BOLD imaging and fASL, coordinates of the global maximum of activation (MAX) were collected in the individual MR imaging space. In parallel, the coordinates of the TMS point exhibiting the maximal motor-evoked potential amplitude for each hemisphere were considered and projected in the MR imaging individual space. To complement the information of the activation strength expressed by the MAX, we calculated the center of gravity (CoG)<sup>39</sup> for each subject, hand, and technique. Indeed, the CoG allows accounting for the distribution of significant points, being defined as

$$CoG = \frac{\sum_{i=1}^N V_i L_i}{\sum_{i=1}^N V_i},$$

where  $i$  is the index of the point,  $L$  is the location ( $x, y, z$ ), and  $V$  is the  $t$  value for fASL/BOLD maps and motor-evoked potential amplitude for the TMS at position  $L_i$ .

For fASL and BOLD imaging, CoG calculation was restricted to the cluster containing the MAX. For TMS, all significant points were included to account for the different neuronal excitability of the stimulated pericentral region.<sup>40</sup>

For each hand and alternatively for MAX and CoG, BOLD-fASL comparison was assessed in the subject's individual MR imaging space by calculating the Euclidean distance. Paired  $t$  tests were applied for all directions: left-to-right ( $x$ ), posterior-to-anterior ( $y$ ), and inferior-to-superior ( $z$ ). Similarly, the proximity of fASL and BOLD imaging to TMS was assessed by paired  $t$  tests of the Euclidean distance.

Second-level analyses were also conducted after normalization into the Montreal Neurological Institute space to compare fASL and BOLD activation maps at the group level.

## RESULTS

Two participants withdrew from the study due to claustrophobia during the MR imaging session. For 3 subjects, the coregistration between TMS and MR imaging failed due to an unresolved issue

of the Nexstim software. Consequently, for the motor task, statistical assessment and group analysis between MR imaging modalities and TMS were conducted on 26 and 23 subjects, respectively. For the somatosensory stimulation, an additional participant was excluded due to incomplete task execution, and the analysis was performed on 25 subjects.

The Euclidean distances between fASL and BOLD imaging for each hand and in terms of MAX and CoG were significantly ( $P < .001$ ) different from zero (Online Supplemental Data). The average values ranged between 10.12 and 16.61 mm, depending on the selection of MAX or CoG. Concordance of values (in 1 SD) was found between the right and left hand (Table 1).

This spatial difference was mainly driven by the inferior-superior ( $z$ ) direction, where fASL was found significantly ( $P < .001$ ) more inferior than BOLD imaging, following the anatomy of the central sulcus (Online Supplemental Data).

The distance along the  $z$ -axis varied from 6.94 to 12.91 mm, depending on the selection of MAX and CoG. Along the other anatomic directions, fASL localized between 0.62 and 3.10 mm more lateral than BOLD imaging ( $P < .05$ , except when considering the MAX during the clenching of the left hand) and between 0.41 and 2.93 mm more anterior than BOLD imaging ( $P < .05$ , except for the left clenching when the CoG was considered). The overview of the intra-MRI modality variability across participants is given in Figure 1 and in terms of the relative difference between fASL and BOLD imaging in Table 1.

By comparing the Euclidean distances between fASL and TMS and between BOLD imaging and TMS, we observed a shift between 9.0 and 14.5 mm between MR imaging modalities and TMS (Table 2), in line with the literature.<sup>31,41</sup> Moreover, only for the MAX and in the case of the left hand, was fASL significantly more proximal than BOLD to TMS (Online Supplemental Data and Table 2).

By investigating the difference along each orientation, we found that fASL was significantly more proximal to TMS than BOLD imaging along the inferior-superior direction ( $P < .001$ ) for MAX in each hand condition and additionally along the left-right for the CoG ( $P < .05$ ) in the left hand condition, as shown in the Online Supplemental Data. The shift among the 3 different mapping techniques can be observed in the Figure 2, which depicts the CoG of each hand, subject, and technique, projected on a Montreal Neurological Institute template.

For the somatosensory stimulation of the thumb, though a flexible threshold of  $P < .001$  was chosen, it was difficult to select the most representative localization between the MAX or secondary local maxima even for the BOLD imaging. For fASL, in which

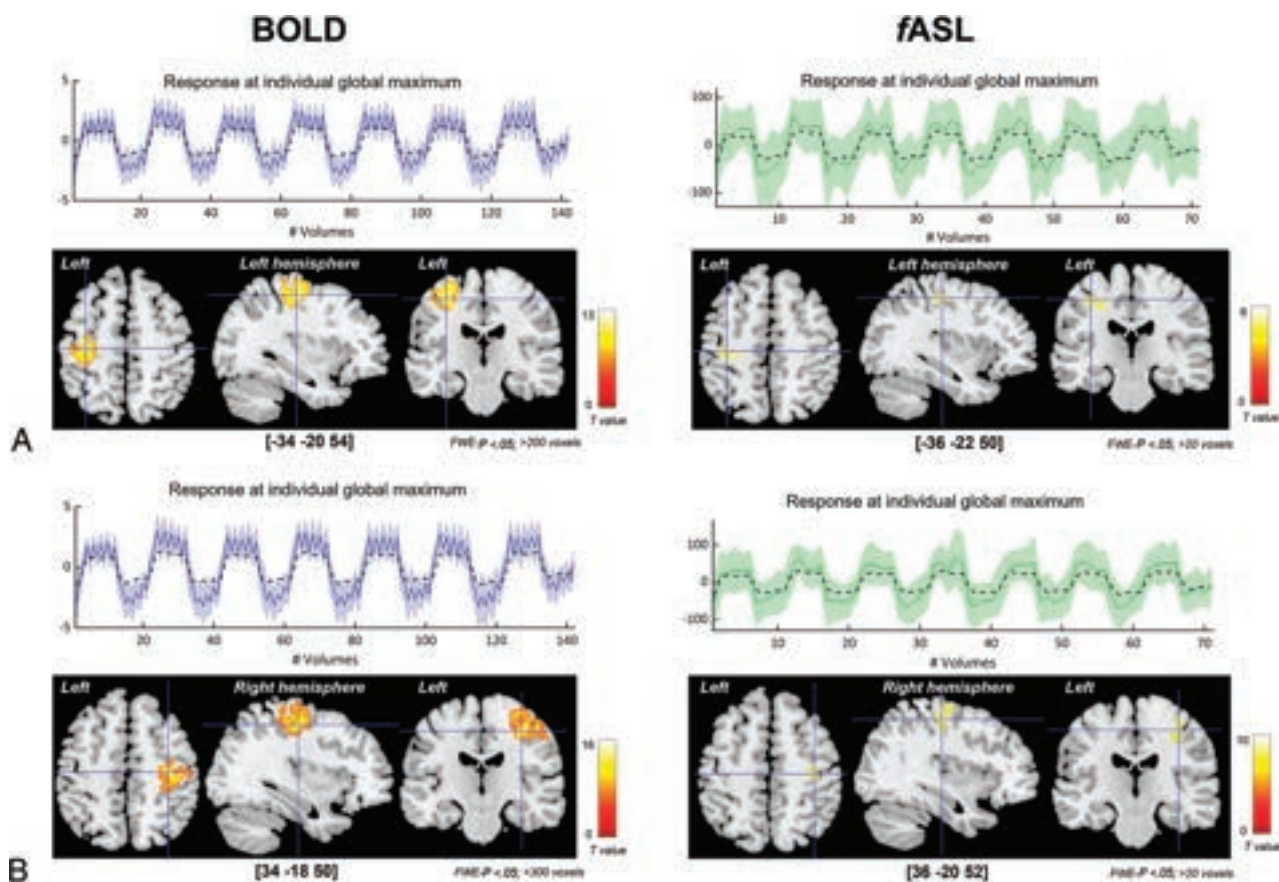


**FIG 1.** Group analysis of clenching hand task. Results of the clenching of the right (A) and left (B) hand across the subjects are shown for BOLD (left side) and fASL (right side). Blue crosslines point at the global maxima of the group-level activation. Coordinates are reported in squared parentheses. Plots on top of each brain-view represent the BOLD (in blue) and fASL (green) timeseries of the individual global maxima. Straight lines and shaded areas indicate the means and the standard deviations evaluated at each timepoint across the subjects. The dashed black line represents the experimental design.

a threshold of  $P < .01$  was used, this choice was even more difficult. To avoid localization bias by visual inspection, we excluded the possibility of relying on a statistical comparison at the level of coordinates of activation at the individual level. However, at the group level, the comparison between MAX showed that fASL localized more medially, anteriorly, and deeper than BOLD imaging (Online Supplemental Data).

## DISCUSSION

This work assessed the role of fASL as a complementary or alternative solution to BOLD imaging for mapping the eloquent cortex. We selected motor and somatosensory tasks and reviewed the shift between fASL and BOLD imaging in a cohort of healthy participants. Instead of deriving the BOLD signal from ASL or considering a separate BOLD session,<sup>26,30,31</sup> we used a simultaneous BOLD-fASL acquisition.<sup>27-29,32,33</sup> Additionally, we addressed the localization specificity between the 2 MR imaging modalities, while comparing motor task results with the hand somatotopy depicted by TMS (ie, TMS assumed as ground truth).

TMS is known to noninvasively identify the  $\omega$ -shaped hand knob with millimeter resolution,<sup>42</sup> demonstrating high spatial concordance with intraoperative and direct cortical stimulation.<sup>43</sup>

## Selection of Experimental Paradigms

Given the extent of hand representation in the human brain,<sup>44</sup> known from 1937,<sup>45</sup> we used well-established hand sensorimotor stimulations to activate the primary motor (M1) and sensory (S1) cortices. In fMRI studies, hand-clenching is used for mapping M1, specifically the Rolandic region.<sup>46</sup> Similarly, cutaneous low-threshold vibration on the fingertips reproduces the functional organization of S1.<sup>10,47</sup> Brain activated regions have been compared across different imaging techniques. In the hand motor task, fMRI showed a more posterior and lateral localization with respect to electrical source imaging.<sup>48</sup> The posterior shift has been confirmed between fMRI and motor TMS.<sup>9</sup> For pneumatic stimulation, fMRI activated the central gyrus more laterally (8–20 mm) with respect to electromagnetic techniques.<sup>10,48,49</sup>

In our cohort, we confirmed that during hand-clenching, BOLD imaging localized more posteriorly and laterally than fASL for both hands (Table 1 and the Online Supplemental Data). For somatosensory stimulation, we found fASL more anterior than BOLD imaging for both thumbs and fASL more medial than BOLD imaging only for the left thumb. Most interesting, the Montreal Neurological Institute coordinates of the MAX were comparable with the results obtained in a previous work (Online Supplemental Data and Lascano et al<sup>10</sup>). Although derived from a

**Table 2: Results of the distances to TMS of fASL and BOLD**

		X: Left →Right (mean)	Y: Anterior→Posterior (mean)	Z: Inferior→Superior (mean)	Euclidean Distance (mean)
MAX					
Right Hand	TMS-fASL	3.51 (SD, 7.03)	3.45 (SD, 4.71)	4.85 (SD, 8.02) <sup>b</sup>	11.31 (SD, 4.89)
	TMS-BOLD	1.02 (SD, 5.79)	2.19 (SD, 5.73)	−10.90 (SD, 5.3) <sup>b</sup>	14.52 (SD, 4.23)
Left hand	TMS-fASL	0.38 (SD, 4.35)	5.21 (SD, 4.10)	5.82 (SD, 7.53) <sup>b</sup>	11.33 (SD, 4.87) <sup>a</sup>
	TMS-BOLD	0.83 (SD, 5.57)	4.28 (SD, 6.87)	−10.08 (SD, 5.62) <sup>b</sup>	14.51 (SD, 4.23) <sup>a</sup>
CoG					
Right hand	TMS-fASL	3.32 (SD, 5.85) <sup>a</sup>	4.32 (SD, 4.87)	4.41 (SD, 6.42) <sup>b</sup>	9.03 (SD, 4.04)
	TMS-BOLD	1.30 (SD, 3.39) <sup>a</sup>	3.58 (SD, 4.21)	−3.45 (SD, 7.51) <sup>b</sup>	9.15 (SD, 4.56)
Left hand	TMS-fASL	−0.61 (SD, 3.29) <sup>a</sup>	4.59 (SD, 3.53)	5.78 (SD, 4.35) <sup>b</sup>	9.03 (SD, 4.05)
	TMS-BOLD	2.51 (SD, 6.78) <sup>a</sup>	3.57 (SD, 3.42)	−2.31 (SD, 5.04) <sup>b</sup>	9.12 (SD, 4.57)

<sup>a</sup>  $P < .05$ .

<sup>b</sup>  $P < .001$ .

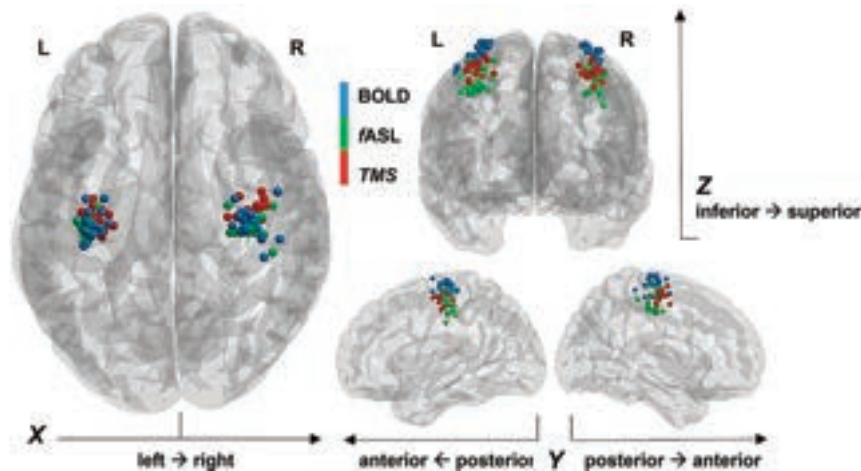


**FIG 2.** Representation of CoG on MNI template. For each healthy participant, blue and green spheres are positioned on the MNI coordinates of the CoG for BOLD and fASL activations during the clenching motor task for each hand. The red spheres correspond to the MNI coordinates of the points with the highest motor evoked potential during TMS for each hand.

group-level analysis, compared with BOLD imaging, fASL in the somatosensory task seems to share characteristics with electrical source imaging, leading to the hypothesis that fASL could be a more direct measure of spiking neurons. An fASL shift toward the midline with respect to BOLD imaging could be ascribed to the digit-specific somatotopy, which attributes a more medial location to the thumb, which, in our case, received the stimulation.<sup>42</sup>

**Influence of Cerebral Vasculature**

Across studies, the localization distance between BOLD-fMRI and other modalities during motor and somatosensory tasks is variable (10–30 mm).<sup>10,49</sup>

In patients with brain tumors, though there is a good concordance between preoperative BOLD-fMRI with intra- or extraoperative electrocortical stimulation, some localization discrepancies have been observed.<sup>50,51</sup> The different origins of electrocortical and hemodynamic signals may affect the localization as well as cerebrovascular characteristics. Quantitative assessment of cerebral perfusion with ASL allowed overcoming the influence of the venous blood of BOLD imaging.

In our cohort, activations in somatosensory tasks showed a systematic anterior shift of fASL compared with BOLD for both

hands. This finding could highlight the specificity of fASL in localizing arterial blood changes and the limitation of BOLD imaging affected by draining veins. Notably, the somatosensory area possesses a rich venous system, including the middle part of the anastomotic vein of Trolard, which runs into the postcentral sulcus, draining the adjacent cortex and the Rolandic vein, anterior to the vein of Trolard, which irrigates the pre- and postcentral sulci.<sup>52</sup>

**The Choice of the Threshold**

In fMRI localization, the spatial extent of the results depends on the thresholding procedure (ie,  $P$  value and minimum cluster size). For hand-clenching, we opted for a conservative threshold and reproduced and confirmed the findings of similar work.<sup>31</sup> Somatosensory stimulation required a more flexible approach.

In addition, the choice of the “most representative” activation point is debatable.<sup>39,53</sup> While the MAX seems less representative than the center of the mass and the CoG, it is less affected by thresholding. We analyzed our data both in terms of MAX and CoG, providing concordant intermodality results on both the strength and the distribution of activations. Notably, CoG was calculated for the first activation cluster (ie, containing the



MAX). Thus, we restricted the analysis to the area around the central sulcus by avoiding central and contralateral coactivated regions, observed in some subjects.

### TMS as Ground Truth

TMS was used to compare *f*ASL and BOLD localizations of the hand motor task. As opposed to previous studies using the maximal fMRI activation as a reference point for TMS stimulation,<sup>31</sup> in our study, the TMS operator was blinded to fMRI results and mapped the motor region using a structural MR imaging–navigated approach.

In line with previous studies, we reproduced the shift between *f*ASL and BOLD imaging,<sup>26,31,54</sup> along the inferior-to-superior and posterior-to-anterior axes. Moreover, we found that *f*ASL was more proximal to TMS than BOLD imaging along the inferior-superior and mediolateral axes.

### Limitations and Perspectives

The accuracy of our results should be interpreted in light of the intrinsic limitations of ASL, characterized by low spatial and temporal resolution. This limitation can be explained by the low SNR of the perfusion signal, which depends on the scarce tissular microvasculature in the voxel volume and the decay of the relaxation time during postlabeling delay.<sup>55</sup>

The spatial accuracy of *f*ASL demonstrated in this work would be beneficial in patients with a potential modification of the neurovascular coupling. This is the case in patients with brain tumors, cerebral arteriovenous malformations, epileptic lesions, or stroke. In such instances, the alteration of the cerebral vascularity can, indeed, induce false-negative BOLD activations on the definition of functional areas.

### CONCLUSIONS

In the current study, we investigated the spatial accuracy of *f*ASL in delineating functional brain regions. In a cohort of 26 healthy subjects, using hand sensorimotor tasks, we found significant shifts between *f*ASL and the standard BOLD imaging along all brain directions, and we observed that *f*ASL targeted the sulci anatomy better than BOLD imaging. Moreover, the comparison with TMS showed that *f*ASL is more proximal than BOLD imaging to the areas excited by stimulation and can, therefore, be a more direct representation of neuronal spiking. These findings make *f*ASL a valid alternative or complement to the standard functional imaging, particularly in patients with potentially altered neurovascular coupling, which could bias localization of the eloquent cortex.

### ACKNOWLEDGMENTS

This work was performed using the imaging platform at the Brain Behaviour Laboratory (BBL), University of Geneva, which received the financial support of Swiss National Science Foundation (R'Equip grant, 326030\_205728). The authors thank the technical staff of the BBL and of the CIBM Center for Biomedical Imaging for their support. We acknowledge the receipt of the dual-echo pseudocontinuous arterial spin-labeling sequence from the University of Southern California's Stevens Neuroimaging and Informatics Institute. We also acknowledge

The Regents of the University of California, on behalf of its Los Angeles campus, as the source of portions of the licensed technology. We acknowledge the Clinical Research Center, University Hospitals and Faculty of Medicine in Geneva.

Disclosure forms provided by the authors are available with the full text and PDF of this article at [www.ajnr.org](http://www.ajnr.org).

### REFERENCES

1. Glover GH. Overview of functional magnetic resonance imaging. *Neurosurg Clin N Am* 2011;22:133–39, vii CrossRef Medline
2. Boubela RN, Kalcher K, Huf W, et al. fMRI measurements of amygdala activation are confounded by stimulus correlated signal fluctuation in nearby veins draining distant brain regions. *Sci Rep* 2015;5:10499 CrossRef Medline
3. Fujiwara N, Sakatani K, Katayama Y, et al. Evoked-cerebral blood oxygenation changes in false-negative activations in BOLD contrast functional MRI of patients with brain tumors. *Neuroimage* 2004;21:1464–71 CrossRef Medline
4. Giussani C, Roux FE, Ojemann J, et al. Is preoperative functional magnetic resonance imaging reliable for language areas mapping in brain tumor surgery? Review of language functional magnetic resonance imaging and direct cortical stimulation correlation studies. *Neurosurgery* 2010;66:113–20 CrossRef Medline
5. Pittau F, Fahoum F, Zelman R, et al. Negative BOLD response to interictal epileptic discharges in focal epilepsy. *Brain Topogr* 2013;26:627–40 CrossRef Medline
6. Rathakrishnan R, Moeller F, Levan P, et al. BOLD signal changes preceding negative responses in EEG-fMRI in patients with focal epilepsy. *Epilepsia* 2010;51:1837–45 CrossRef Medline
7. Carusone LM, Srinivasan J, Gitelman DR, et al. Hemodynamic response changes in cerebrovascular disease: implications for functional MR imaging. *AJNR Am J Neuroradiol* 2002;23:1222–28 Medline
8. Gerloff C, Grodd W, Altenmüller E, et al. Coregistration of EEG and fMRI in a simple motor task. *Hum Brain Mapp* 1996;4:199–209 CrossRef Medline
9. Inuggi A, Filippi M, Chieffo R, et al. Motor area localization using fMRI-constrained cortical current density reconstruction of movement-related cortical potentials, a comparison with fMRI and TMS mapping. *Brain Res* 2010;1308:68–78 CrossRef Medline
10. Lascano AM, Grouiller F, Genetti M, et al. Surgically relevant localization of the central sulcus with high-density somatosensory-evoked potentials compared with functional magnetic resonance imaging. *Neurosurgery* 2014;74:517–26 CrossRef Medline
11. Pike GB. Quantitative functional MRI: concepts, issues and future challenges. *Neuroimage* 2012;62:1234–40 CrossRef Medline
12. Hyder F, Sanganahalli BG, Herman P, et al. Neurovascular and neuro-metabolic couplings in dynamic calibrated fMRI: transient oxidative neuroenergetics for block-design and event-related paradigms. *Front Neuroenergetics* 2010;2:18 CrossRef Medline
13. Detre JA, Rao H, Wang DJ, et al. Applications of arterial spin labeled MRI in the brain. *J Magn Reson Imaging* 2012;35:1026–37 CrossRef Medline
14. Krainik A, Villien M, Tropres I, et al. Functional imaging of cerebral perfusion. *Diagn Interv Imaging* 2013;94:1259–78 CrossRef Medline
15. Liu TT, Wong EC. A signal processing model for arterial spin labeling functional MRI. *Neuroimage* 2005;24:207–15 CrossRef Medline
16. Hernandez-Garcia L, Aramendia-Vidaurreta V, Bolar DS, et al. Recent technical developments in ASL: a review of the state of the art. *Magn Reson Med* 2022;88:2021–42 CrossRef Medline
17. Pinto J, Chappell MA, Okell TW, et al. Calibration of arterial spin labeling data-potential pitfalls in post-processing. *Magn Reson Med* 2020;83:1222–34 CrossRef Medline
18. Wang Z. Improving cerebral blood flow quantification for arterial spin labeled perfusion MRI by removing residual motion artifacts



- and global signal fluctuations. *Magn Reson Imaging* 2012;30:1409–15 CrossRef Medline
19. Borogovac A, Habeck C, Small SA, et al. Mapping brain function using a 30-day interval between baseline and activation: a novel arterial spin labeling fMRI approach. *J Cereb Blood Flow Metab* 2010;30:1721–33 CrossRef Medline
  20. Stewart SB, Koller JM, Campbell MC, et al. Arterial spin labeling versus BOLD in direct challenge and drug-task interaction pharmacological fMRI. *PeerJ* 2014;2:e687 CrossRef Medline
  21. Hoogenraad FG, Pouwels PJ, Hofman MB, et al. Quantitative differentiation between BOLD models in fMRI. *Magn Reson Med* 2001;45:233–46 CrossRef Medline
  22. Hassanpour MS, Yan L, Wang DJ, et al. How the heart speaks to the brain: neural activity during cardiorespiratory interoceptive stimulation. *Philos Trans R Soc Lond B Biol Sci* 2016;371:20160017 CrossRef Medline
  23. Tancredi FB, Lajoie I, Hoge RD. Test-retest reliability of cerebral blood flow and blood oxygenation level-dependent responses to hypercapnia and hyperoxia using dual-echo pseudo-continuous arterial spin labeling and step changes in the fractional composition of inspired gases. *J Magn Reson Imaging* 2015;42:1144–57 CrossRef Medline
  24. Hodkinson DJ, Krause K, Khawaja N, et al. Quantifying the test-retest reliability of cerebral blood flow measurements in a clinical model of on-going post-surgical pain: a study using pseudo-continuous arterial spin labelling. *Neuroimage Clin* 2013;3:301–10 CrossRef Medline
  25. Gardumi A, Ivanov D, Havlicek M, et al. Tonotopic maps in human auditory cortex using arterial spin labeling. *Hum Brain Mapp* 2017;38:1140–54 CrossRef Medline
  26. Pimentel MA, Vilela P, Sousa I, et al. Localization of the hand motor area by arterial spin labeling and blood oxygen level-dependent functional magnetic resonance imaging. *Hum Brain Mapp* 2013;34:96–108 CrossRef Medline
  27. Storti SF, Galazzo IB, Pizzini FB, et al. Dual-echo ASL based assessment of motor networks: a feasibility study. *J Neural Eng* 2018;15:026018 CrossRef Medline
  28. Jann K, Orosz A, Dierks T, et al. Quantification of network perfusion in ASL cerebral blood flow data with seed based and ICA approaches. *Brain Topogr* 2013;26:569–80 CrossRef Medline
  29. Storti SF, Boscolo Galazzo I, Montemezzi S, et al. Dual-echo ASL contributes to decrypting the link between functional connectivity and cerebral blood flow. *Hum Brain Mapp* 2017;38:5831–44 CrossRef Medline
  30. Raoult H, Petr J, Bannier E, et al. Arterial spin labeling for motor activation mapping at 3T with a 32-channel coil: reproducibility and spatial accuracy in comparison with BOLD fMRI. *Neuroimage* 2011;58:157–67 CrossRef Medline
  31. Diekhoff S, Uludağ K, Sparing R, et al. Functional localization in the human brain: gradient-echo, spin-echo, and arterial spin-labeling fMRI compared with neuronavigated TMS. *Hum Brain Mapp* 2011;32:341–57 CrossRef Medline
  32. Faraco CC, Strother MK, Dethrage LM, et al. Dual echo vessel-encoded ASL for simultaneous BOLD and CBF reactivity assessment in patients with ischemic cerebrovascular disease. *Magn Reson Med* 2015;73:1579–92 CrossRef Medline
  33. Tak S, Wang DJ, Polimeni JR, et al. Dynamic and static contributions of the cerebrovasculature to the resting-state BOLD signal. *Neuroimage* 2014;84:672–80 CrossRef Medline
  34. McGonigle DJ, Howseman AM, Athwal BS, et al. Variability in fMRI: an examination of intersession differences. *Neuroimage* 2000;11:708–34 CrossRef Medline
  35. Rossi S, Antal A, Bestmann S, et al; basis of this article began with a Consensus Statement from the IFCN Workshop on Present, Future of TMS: Safety, Ethical Guidelines, Siena, October 17–20, 2018, updating through April 2020. Safety and recommendations for TMS use in healthy subjects and patient populations, with updates on training, ethical and regulatory issues: Expert Guidelines. *Clin Neurophysiol* 2021;132:269–306 CrossRef Medline
  36. Rossini PM, Barker AT, Berardelli A, et al. Non-invasive electrical and magnetic stimulation of the brain, spinal cord and roots: basic principles and procedures for routine clinical application. Report of an IFCN committee. *Electroencephalogr Clin Neurophysiol* 1994;91:79–92 CrossRef Medline
  37. Wang Z, Aguirre GK, Rao H, et al. Empirical optimization of ASL data analysis using an ASL data processing toolbox: ASLtbx. *Magn Reson Imaging* 2008;26:261–69 CrossRef Medline
  38. Aguirre GK, Detre JA, Zarahn E, et al. Experimental design and the relative sensitivity of BOLD and perfusion fMRI. *Neuroimage* 2002;15:488–500 CrossRef Medline
  39. Vidyasagar R, Parkes LM. Reproducibility of functional MRI localization within the human somatosensory cortex. *J Magn Reson Imaging* 2011;34:1439–44 CrossRef Medline
  40. Sondergaard RE, Martino D, Kiss ZHT, et al. TMS motor mapping methodology and reliability: a structured review. *Front Neurosci* 2021;15:709368 CrossRef Medline
  41. Lotze M, Kaethner RJ, Erb M, et al. Comparison of representational maps using functional magnetic resonance imaging and transcranial magnetic stimulation. *Clin Neurophysiol* 2003;114:306–12 CrossRef Medline
  42. Numssen O, Zier AL, Thielscher A, et al. Efficient high-resolution TMS mapping of the human motor cortex by nonlinear regression. *Neuroimage* 2021;245:118654 CrossRef Medline
  43. Takahashi S, Vajkoczy P, Picht T. Navigated transcranial magnetic stimulation for mapping the motor cortex in patients with Rolandic brain tumors. *Neurosurg Focus* 2013;34:E3 CrossRef Medline
  44. Wilson M, Dadachanji H, Greenwell D. The motor homunculus: linking the past with the present. *J Physiol* 2021;599:1731–32 CrossRef Medline
  45. Penfield W, Boldrey E. Somatic motor and sensory representation in the cerebral cortex of man as studied by electrical stimulation. *Brain* 1937;60:389–443 CrossRef
  46. Tieleman A, Deblaere K, Van Roost D, et al. Preoperative fMRI in tumour surgery. *Eur Radiol* 2009;19:2523–34 CrossRef Medline
  47. Schweisfurth MA, Frahm J, Schweizer R. Individual fMRI maps of all phalanges and digit bases of all fingers in human primary somatosensory cortex. *Front Hum Neurosci* 2014;8:658 CrossRef Medline
  48. Kober H, Nimsky C, Moller M, et al. Correlation of sensorimotor activation with functional magnetic resonance imaging and magnetoencephalography in presurgical functional imaging: a spatial analysis. *Neuroimage* 2001;14:1214–28 CrossRef Medline
  49. Christmann C, Ruf M, Braus DF, et al. Simultaneous electroencephalography and functional magnetic resonance imaging of primary and secondary somatosensory cortex in humans after electrical stimulation. *Neurosci Lett* 2002;333:69–73 CrossRef Medline
  50. Korvenoja A, Kirveskari E, Aronen HJ, et al. Sensorimotor cortex localization: comparison of magnetoencephalography, functional MR imaging, and intraoperative cortical mapping. *Radiology* 2006;241:213–22 CrossRef Medline
  51. Ulmer JL, Hacein-Bey L, Mathews VP, et al. Lesion-induced pseudo-dominance at functional magnetic resonance imaging: implications for preoperative assessments. *Neurosurgery* 2004;55:569–79; discussion 580–61 CrossRef Medline
  52. Tomasi SO, Umana GE, Scalia G, et al. The superficial anastomosing veins of the human brain cortex: a microneurosurgical anatomical study. *Front Surg* 2021;8:817002 CrossRef Medline
  53. Fesl G, Braun B, Rau S, et al. Is the center of mass (COM) a reliable parameter for the localization of brain function in fMRI? *Eur Radiol* 2008;18:1031–37 CrossRef Medline
  54. Kallioniemi E, Pitkanen M, Kononen M, et al. Localization of cortical primary motor area of the hand using navigated transcranial magnetic stimulation, BOLD and arterial spin labeling fMRI. *J Neurosci Methods* 2016;273:138–48 CrossRef Medline
  55. Alsop DC, Detre JA, Golay X, et al. Recommended implementation of arterial spin-labeled perfusion MRI for clinical applications: a consensus of the ISMRM perfusion study group and the European consortium for ASL in dementia. *Magn Reson Med* 2015;73:102–16 CrossRef Medline

# Prevalence of Cochlear-Facial and Other Non-Superior Semicircular Canal Third Window Dehiscence on High-Resolution Temporal Bone CT

Vladislav Razskazovskiy, Andrew A. McCall, and Barton F. Branstetter



## ABSTRACT

**BACKGROUND AND PURPOSE:** The radiologic prevalence of superior semicircular canal dehiscence in the asymptomatic population has been widely studied, but less is known about the rates of other forms of third window dehiscence. Per the existing literature, the radiologic prevalence of cochlear-facial nerve dehiscence, for example, exceeds that seen in histologic studies, suggesting that conventional CT is unreliable for cochlear-facial dehiscence. These studies relied on nonisometric CT acquisitions, however, and underused multiplanar reformatting techniques, leading to false-positive findings. Our purpose was to determine the rate of cochlear-facial dehiscence and other non-superior semicircular canal third window dehiscences on optimized CT in asymptomatic patients.

**MATERIALS AND METHODS:** Sixty-four-channel temporal bone CT scans from 602 patients in emergency departments were assessed for cochlear-facial and other non-superior semicircular canal third window dehiscences by using high-resolution, multiplanar oblique reformats. Confidence intervals for dehiscence prevalence were calculated using the Newcombe 95% interval confidence method.

**RESULTS:** Of 602 patients, 500 were asymptomatic, while 102 had an imaging indication consistent with possible third window syndrome (symptomatic). Eight asymptomatic patients (1.6%) had cochlear-facial dehiscence, while 43 (8.4%) had jugular bulb-vestibular aqueduct dehiscence. There was no statistically significant difference between the prevalence of cochlear-facial dehiscence or jugular bulb-vestibular aqueduct dehiscence in asymptomatic patients compared with symptomatic patients. Cochlear-carotid canal, cochlear-internal auditory canal, and cochlear-petrosal sinus dehiscences were not observed.

**CONCLUSIONS:** Sixty-four-channel CT with multioblique reformatting is sensitive and specific for identifying cochlear-facial dehiscence, with rates similar to those in postmortem series. Jugular bulb-vestibular aqueduct dehiscence is a common incidental finding and is unlikely to produce third window physiology. Other non-superior semicircular canal third window dehiscences are rare in asymptomatic patients.

**ABBREVIATIONS:** CFD = cochlear-facial nerve dehiscence; JVD = jugular bulb-vestibular aqueduct dehiscence; OCD = otic capsule dehiscence; SSCD = superior semicircular canal dehiscence

There are 2 anatomic locations where pressure is normally transmitted between the middle and inner ear, the oval and round windows. Third window syndromes occur when an additional communication forms between the inner ear and surrounding spaces, resulting in altered perilymph hydrodynamics and symptoms including hearing loss, tinnitus, autophony, and sound- or pressure-induced vertigo.<sup>1-3</sup> These most frequently

occur as a result of bony otic capsule dehiscence (OCD) as is seen with superior semicircular canal dehiscence (SSCD). Since the discovery of CT-positive SSCD in humans, other sites of OCD have been identified, including cochlear-facial nerve canal dehiscence (CFD), cochlear-carotid canal dehiscence, cochlear-internal auditory canal dehiscence, superior semicircular canal-superior petrosal sinus dehiscence, posterior semicircular canal dehiscence, lateral semicircular canal dehiscence, and vestibular dehiscence.<sup>1,4,5</sup> Although not an OCD, jugular bulb-vestibular aqueduct dehiscence (JVD) has also been reported to occasionally produce third window symptoms.<sup>6</sup> Additional examples of anatomic variants that can result in third window syndromes include an enlarged vestibular aqueduct, an X-linked stapes gusher, and bone dyscrasias.<sup>5</sup> While much research has been

Received July 16, 2023; accepted after revision September 14.

From the University of Pittsburgh School of Medicine (V.R., B.F.B.), Pittsburgh, Pennsylvania; and Departments of Radiology (A.A.M., B.F.B.), and Otolaryngology (A.A.M., B.F.B.), University of Pittsburgh Medical Center, Pittsburgh, Pennsylvania.

Please address correspondence to Barton Branstetter, MD, University of Pittsburgh Medical Center, Department of Radiology, 200 Lothrop St, PUH Room D132, Pittsburgh, PA, 15213; e-mail: BFB1@pitt.edu; @CharBranstetter

<http://dx.doi.org/10.3174/ajnr.A8032>

devoted to SSCD, the other forms of OCD have received relatively little attention. Importantly, diagnosis of OCD in patients experiencing auditory/vestibular symptoms allows surgical intervention, which has been shown to reduce often debilitating third window symptoms and improve quality of life.<sup>7,8</sup>

In the original literature on the CT diagnosis of OCD, CT was performed on scanners without the capability of submillimeter section thickness, resulting in increased rates of false-positive findings.<sup>9</sup> Modern 64-channel helical scanners are much more specific in detecting SSCD so that the rate of CT findings of SSCD in asymptomatic patients now approaches the rate of histologic findings in cadavers, and otolaryngology evaluation can be recommended when SSCD is incidentally discovered on CT.<sup>10</sup> It remains unclear whether this rate is true for CFD (and other non-SCC forms of OTC), however, because there is currently a discrepancy between the published prevalence of radiologic CFD (6.3%–9.2%) and the prevalence of histologic CFD seen on temporal bone analysis (0.59%–1.6%).<sup>11–14</sup>

The purpose of this study was to measure the rate of non-SSCD on high-resolution CT in asymptomatic individuals and compare that with the rate in patients with audiological or vestibular symptoms.

## MATERIALS AND METHODS

This study was approved by University of Pittsburgh Medical Center institutional review board as an exempt study of existing data.

### Patients

Pre-hoc power analysis indicated that for a 95% CI spanning 4% and a finding with an underlying rate of 5%, 500 patients would be required. Adult patients who had undergone high-resolution temporal bone CT in the emergency department of a large tertiary care academic medical center between February 2012 and December 2022 were retrospectively identified. Only patients scanned on a 64-channel CT scanner were eligible. Although we enrolled patients presenting to the emergency department at an adult hospital, we included the small number of adolescent patients (14–17 years of age) who met inclusion because existing evidence suggests that otic capsule development is generally complete by adolescence.<sup>15</sup> Patients with pathology within the otic capsule or fractures that prevented otic capsule evaluation were not included. Patients were divided into 2 groups based on the indication for imaging: patients with audiological or vestibular symptoms that might be consistent with a third window syndrome (symptomatic patients) and those with all other imaging indications (asymptomatic patients). For this study, symptoms consistent with third window syndrome were vertigo, hearing loss, dizziness, and tinnitus. Symptoms were based on review of systems obtained in the emergency department; for those with hearing loss, audiometric data were not available to differentiate between conductive and sensorineural hearing loss. Patients with auditory or vestibular symptoms were excluded from the asymptomatic patient group. We concluded enrollment when we had accumulated 500 asymptomatic patients, in keeping with our power analysis.

### Imaging Protocol and Techniques

CT was acquired using LightSpeed 64-channel CT scanners (GE Healthcare) with a section thickness of 0.63 mm, spacing of

0.375 mm, 120 kV(peak), 195 mA, pitch of 0.53°, a bone kernel, and a matrix of 512 × 512. Reformatted images in sagittal and coronal planes at 1-mm section thickness and 1-mm interslice spacing were routinely obtained on the CT scanners.

### Image Interpretation

The patient's indication for imaging, date of birth, date of imaging, and sex were recorded. Patient CT scans were reviewed by a Certificate of Added Qualification–certified neuroradiologist with fellowship training in head and neck radiology and 20 years of experience who was blinded to the indication for the examination. The presence of OCD was recorded and categorized as CFD, JVD, cochlear–internal auditory canal, cochlear–carotid canal, or other dehiscence (eg, posterior semicircular canal dehiscence, lateral semicircular canal dehiscence, and vestibular aqueduct dehiscence). Screening for dehiscence was in the axial plane, with 1-mm sagittal reformatted images serving to corroborate findings in the axial plane. In patients who demonstrated dehiscence on both axial and sagittal images, final confirmation of CFD was assessed using postprocessing software (Vitrea; Cannon Medical Systems) to produce high-definition multiplanar oblique reformats. These additional images were 0.625-mm thick with interslice spacing of 0.625 mm. The plane of reformat was a modified plane of Stenvers, along the basal turn of the cochlea and orthogonal to the labyrinthine portion of the facial nerve. The reformats were angled in both the coronal and sagittal plane to ensure that the entire basal turn of the cochlea was included in a single image. Interpretation was performed with a high threshold for positivity (ie, a barely perceptible bony covering was still considered intact) to avoid false-positive results.<sup>16</sup>

### Data Analysis

The prevalence of CFD and JVD was calculated, and 95% CIs were generated using the Newcombe method for binomial proportions.<sup>17</sup> If no events were recorded, 95% CIs were calculated using exact techniques. All statistical calculations were performed using SPSS software, Version 28 (IBM).

## RESULTS

Six hundred two patients were included in the study. For every patient, images from both temporal bones were interpreted, for a total of 1204 temporal bones. On the basis of their clinical indication for temporal bone imaging, 500 patients were asymptomatic and 102 were symptomatic. The median age at imaging for asymptomatic patients was 47 years with an age range of 15–93 years. The median age at imaging for symptomatic patients was 50.5 years with a range of 21–87 years. Reasons for examinations in asymptomatic and symptomatic patients are summarized in Tables 1 and 2.

In asymptomatic patients, 100 of 1000 temporal bones (10%) exhibited sufficient evidence of CFD on axial imaging to prompt evaluation in sagittal reformatted images (Fig 1). Of these 100 temporal bones, 14 (1.4% of the asymptomatic population) demonstrated apparent CFD dehiscence on the automated 1-mm-thick sagittal reformatted images. Following evaluation of these 14 temporal bones in high-definition multioblique reformatted images, only 8 temporal bones (0.8%) demonstrated CFD (Fig 2).

**Table 1: Asymptomatic patient characteristics and indications for temporal bone CT imaging**

Asymptomatic Patients	
Median age (range) (yr)	47 (15–93)
No. Male (%)	325 (65.0%)
Imaging indication	
Trauma	368 (73.6%)
Mass	45 (9.0%)
Infection	37 (7.4%)
Pain	20 (4.0%)
CSF leak/cephalocele	15 (3.0%)
Cranial nerve palsy	5 (1.0%)
Otosclerosis	4 (0.8%)
Surgical planning	2 (0.4%)
Other	4 (0.8%)

**Table 2: Symptomatic patient characteristics and indications for temporal bone CT imaging<sup>a</sup>**

Symptomatic Patients	
Median age (range) (yr)	50 (14–87)
No. of males (%)	43 (42.2%)
Imaging indication	
Dizziness	52 (51.0%)
Hearing loss	16 (15.7%)
Suspected SSCD	14 (13.7%)
Tinnitus	7 (6.9%)
Vertigo	6 (5.9%)
Otosclerosis	3 (2.9%)
Multiple auditory/vestibular symptoms	3 (2.9%)
Mass involving otic capsule	1 (1.0%)

<sup>a</sup>Symptomatic patients with multiple symptoms were classified on the basis of their primary symptom, so that there is no overlap between imaging indications.

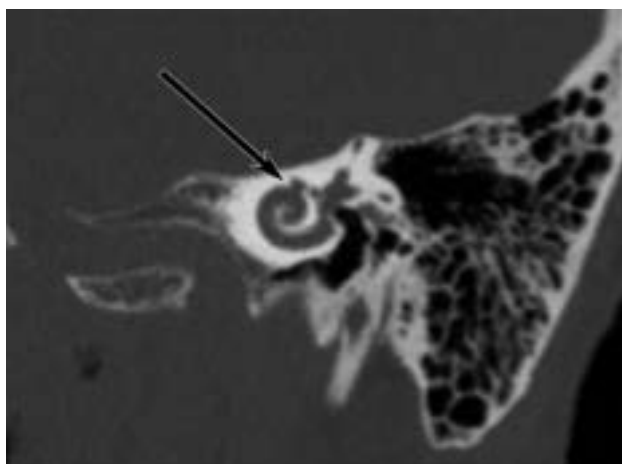


**FIG 1.** Cochlear-facial dehiscence. Oblique reformatted CT scan along the basal turn of the cochlea (modified Stenvers reformat) shows a dehiscence (arrow) between the middle turn of the cochlea and the labyrinthine segment of the facial nerve canal.

On a patient-level analysis, these represented 1.6% of the asymptomatic patient population (95% CI, 0.8%–3.1%). There were no cases of bilateral CFD.

In asymptomatic patients, 41 of the 1000 temporal bones had JVD (Fig 3), with 1 patient exhibiting bilateral JVD, yielding a dehiscence prevalence of 4.1% per ear and a patient-level prevalence of 8.0% (95% CI, 5.9%–10.7%).

Of the 102 symptomatic patients, 3 demonstrated CFD and 8 demonstrated JVD, resulting in a CFD and JVD patient prevalence of 2.9% (95% CI, 1.0%–8.3%) and 7.8% (95% CI, 4.0%–14.7%), respectively. One symptomatic patient presenting with hearing loss exhibited left-sided CFD with concomitant, contralateral JVD.

No statistically significant difference existed between the rates of CFD and JVD in symptomatic-versus-asymptomatic patients. No instances of cochlea-carotid, cochlea-internal auditory canal, or other sites of dehiscence were identified in the 1204 temporal bones studied (95% CI, 0.0%–0.2%; Fig 4).

## DISCUSSION

In the current study of 500 patients without third window symptoms and 102 patients with possible third window symptoms, 1.6% of asymptomatic patients exhibited CFD and 8.0% exhibited JVD. The values in patients with symptoms that might be attributable to third window dehiscence are similar (2.9% CFD and 7.8% JVD). This finding contrasts with the those in SSCD, in which symptomatic patients have a substantially higher rate of dehiscence.<sup>10</sup> This presumably reflects the rarity of symptomatic CFD and JVD, making it harder to discern any differences, even with a relatively large patient population.

Two previous radiologic studies using temporal bone CTs have reported a CFD prevalence ranging from 6.3% to 9.2%.<sup>11,12</sup> Both of these studies have limitations that likely contributed to the discrepancy between radiologic and histologic CFD prevalence, however. The first study examined only patients presenting to highly specialized, academic neurotology clinics with auditory and/or vestibular symptoms, making it difficult to extrapolate their findings to the general population. Additionally, this study included both conventional temporal bone CTs with section thickness up to 1 mm as well as images produced by conebeam CT, making it difficult to draw conclusions on the specificity of conventional, thin-section temporal bone CT in diagnosing CFD. The second study used a 16-section CT scanner for image acquisition and exclusively relied on image interpretation in conventional CT planes without using optimized oblique plane reformats to evaluate the labyrinthine section of the facial nerve in an orthogonal plane. Despite these design and technological limitations, authors in both studies concluded that CT overcalled CFD and that limitations in CT section thickness and volume-averaging protocol effects obfuscated specific radiologic detection of CFD. Our results contradict the assertion that modern CT scan techniques inherently overcall CFD.

The low prevalence rates of CFD that we identified were highly dependent on our use of multioblique images along the basal turn of the cochlea. When only axial slices were analyzed, the apparent prevalence was 12 times higher than the true prevalence. The use of routine sagittal reformats improved the false-positive rate, but it was still twice the true value. Thus, we recommend that high-resolution multiplanar oblique reformats be used before making a diagnosis of CFD on CT. This method contrasts with radiologic SSCD detection, in which conventional coronal reformatted images are sufficient for diagnosis.<sup>16</sup>

The radiologic CFD prevalence in the current study (0.9% of all temporal bones) is congruent with the rate in 2 prior histologic studies that reported rates of temporal bone dehiscence instead of



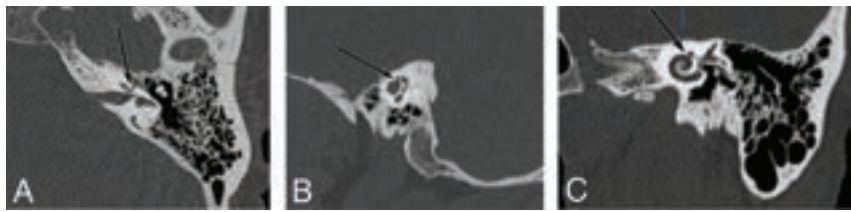


**FIG 2.** The importance of multiplanar oblique reformats for the diagnosis of cochlear-facial dehiscence. Axial CT image (A) shows an apparent dehiscence (arrow) between the middle turn of the cochlea and the labyrinthine segment of the facial nerve. Sagittal reformatted image (B) appears to confirm the dehiscence (arrow). However, multiple oblique reformats along the basal turn of the cochlea (C) reveal that the bone between the cochlea and the facial canal (arrow) is thin but intact.

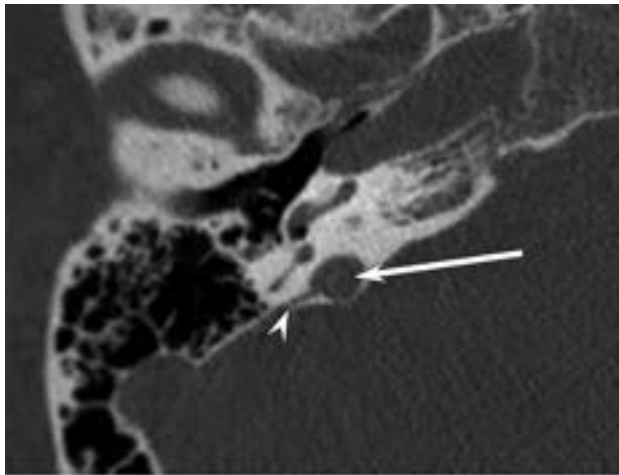


**FIG 3.** JVD. Axial CT image shows dehiscence between a diverticulum of the jugular bulb (arrow) and the vestibular aqueduct (arrowhead).

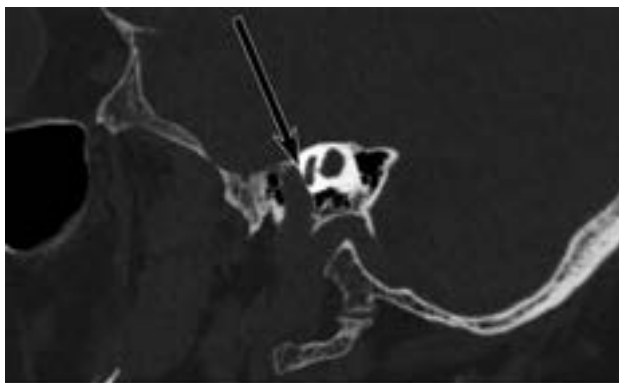


**FIG 4.** Cochlear-carotid plate. Sagittal reformatted CT image shows thin-but-intact bone (arrow) between the petrous segment of the ICA and the basal turn of the cochlea. None of the 1204 temporal bones in this study demonstrated a true dehiscence at this location.

patient-level prevalence. Fang et al<sup>13</sup> reported a CFD prevalence of 0.59% in a histologic survey of 1020 temporal bones at Johns Hopkins, while Schart-Morén et al<sup>14</sup> reported a slightly higher CFD prevalence of 1.6% in molds from 282 temporal bones at Uppsala University in Sweden. Differences between these 2 studies can be explained by small differences in CFD prevalence

rates among different ethnic groups as well as incomplete coverage of the otic capsule during the molding process used in the latter study. Unfortunately, neither of the histologic studies reported patients' clinical characteristics, so it is unknown whether patients that exhibited confirmed CFD dehiscence demonstrated third window symptoms, and conclusions cannot be drawn on the prevalence of histologic dehiscence in asymptomatic-versus-symptomatic patients.

Our observations on JVD, cochlear-carotid dehiscence, and cochlear-internal auditory canal dehiscence prevalence are consistent with those in prior studies.<sup>6,11,18,19</sup> While JVD was the most frequently observed OCD here, the lack of a difference in prevalence between symptomatic and asymptomatic patients suggests that it represents a benign anatomic variant in most individuals and is an infrequent cause of third window symptoms. This suggestion supports the conclusions of a prior study examining the association between JVD and auditory/vestibular symptoms in a cohort of 8325 patients undergoing temporal bone CT imaging for all causes.<sup>20</sup> The lack of observed cochlear-carotid, and cochlear-internal auditory canal dehiscences in this study suggests that very few individuals in the general population have these anatomic variants.

In patients with incidentally discovered SSCD, the rate of sub-clinical hearing and vestibular abnormalities is sufficiently high to recommend clinical evaluation, even in the absence of patient-reported symptoms.<sup>10</sup> In JVD and CFD, this relationship is less clear. Our study found no statistically significant difference in the rates of radiologic findings between patients with reported symptoms suggestive of a possible third window syndrome and those without auditory or vestibular symptoms; a prior report on JVD had similar findings as did a report of CFD in which only 1 patient had hearing loss unattributable to any other cause.<sup>12,18</sup> Surgical intervention has been proposed as an option for patients with symptomatic CFD, as has endovascular intervention for JVD.<sup>7,21</sup> We, thus, advise caution before ascribing symptomatology to these radiographic findings. In particular, our data show that JVD is a very common incidental finding among asymptomatic patients. Also, our data show that CFD is likely to be over-called, even with modern, multidetector CT scanners, unless particular attention is given to reconstructing in multiple planes, most notably the modified Stenvers plane along the basal turn of the cochlea orthogonal to the labyrinthine facial nerve.

Our study has several limitations. We included patients from a single institution, and interpretations were performed by a single radiologist. There was no attempt to assess intra- or inter-reader variability. Our asymptomatic patient population had a male predominance, likely due to the high proportion of trauma cases in the emergency department. Because our results are dependent on image generation using 64-section CT scanners with a section thickness of 0.63 mm and overlap of 0.375 mm, our results may not be generalizable to imaging protocols using different specifications.

## CONCLUSIONS

Modern 64-channel CT scanning techniques can demonstrate third window dehiscence such as CFD with rates similar to those in postmortem series. In asymptomatic patients, the radiologic prevalences of CFD and JVD are 1.6% and 8.0%, respectively. Excluding SSCD, no other third window dehiscences were observed in our study population. Diagnosis of non-SSCD requires that images be obtained with submillimeter section thickness and overlap, that images be reformatted in multiplanar oblique planes, and that images be interpreted with a high degree of specificity. JVD is a common incidental radiologic finding and is not necessarily indicative of third window pathophysiology, and neither CFD nor JVD, when seen incidentally in asymptomatic individuals, requires further testing. Cochlear-carotid and cochlear-internal auditory canal dehiscences are extremely rare in the asymptomatic population and were not observed in our study.

Disclosure forms provided by the authors are available with the full text and PDF of this article at [www.ajnr.org](http://www.ajnr.org).

## REFERENCES

1. Minor LB, Solomon D, Zinreich JS, et al. **Sound- and/or pressure-induced vertigo due to bone dehiscence of the superior semicircular canal.** *Arch Otolaryngol Head Neck Surg* 1998;124:249–58 CrossRef Medline
2. Iversen MM, Rabbitt RD. **Biomechanics of third window syndrome.** *Front Neurol* 2020;11:891 CrossRef Medline
3. Naert L, Ocak I, Griet M, et al. **Prospective analysis of an evidence-based symptom set in superior canal dehiscence syndrome.** *Otol Neurotol* 2021;42:186–92 CrossRef Medline
4. Shoman NM, Samy RN, Pensak ML. **Contemporary neuroradiographic assessment of the cochleo-carotid partition.** *ORL J Otorhinolaryngol Relat Spec* 2016;78:193–98 CrossRef Medline
5. Ho ML, Moonis G, Halpin CF, et al. **Spectrum of third window abnormalities: semicircular canal dehiscence and beyond.** *AJNR Am J Neuroradiol* 2017;38:2–9 CrossRef Medline
6. Tanrivermis Sayit A, Elmali M, Kemal O, et al. **Radiological, clinical and audiological evaluation of jugular bulb-vestibular aqueduct dehiscence.** *Acta Otolaryngol* 2017;137:1221–25 CrossRef Medline
7. Bi WL, Brewster R, Poe D, et al. **Superior semicircular canal dehiscence syndrome.** *J Neurosurg* 2017;127:1268–76 CrossRef Medline
8. Allsopp T, Kim AH, Robbins AM, et al. **Quality of life outcomes after transmastoid plugging of superior semicircular canal dehiscence.** *Am J Otolaryngol* 2020;41:102287 CrossRef Medline
9. Belden CJ, Weg N, Minor LB, et al. **CT evaluation of bone dehiscence of the superior semicircular canal as a cause of sound- and/or pressure-induced vertigo.** *Radiology* 2003;226:337–43 CrossRef Medline
10. Berning AW, Arani K, Branstetter BF. **Prevalence of superior semicircular canal dehiscence on high-resolution CT imaging in patients without vestibular or auditory abnormalities.** *AJNR Am J Neuroradiol* 2019;40:709–12 CrossRef Medline
11. Motasaddi Zarandy M, Kouhi A, Emami H, et al. **Prevalence of otic capsule dehiscence in temporal bone computed tomography scan.** *Eur Arch Otorhinolaryngol* 2023;280:125–30 CrossRef Medline
12. Song Y, Alyono JC, Bartholomew RA, et al. **Prevalence of radiographic cochlear-facial nerve dehiscence.** *Otol Neurotol* 2018;39:1319–25 CrossRef Medline
13. Fang CH, Chung SY, Blake DM, et al. **Prevalence of cochlear-facial dehiscence in a study of 1,020 temporal bone specimens.** *Otol Neurotol* 2016;37:967–72 CrossRef Medline
14. Schart-Morén N, Larsson S, Rask-Andersen H, et al. **Anatomical characteristics of facial nerve and cochlea interaction.** *Audiol Neurotol* 2017;22:41–49 CrossRef Medline
15. Sanverdi SE, Ozgen B, Dolgun A, et al. **Incomplete endochondral ossification of the otic capsule, a variation in children: evaluation of its prevalence and extent in children with and without sensorineural hearing loss.** *AJNR Am J Neuroradiol* 2015;36:171–75 CrossRef Medline
16. Branstetter BF, Harrigal C, Escott EJ, et al. **Superior semicircular canal dehiscence: oblique reformatted CT images for diagnosis.** *Radiology* 2006;238:938–42 CrossRef Medline
17. Newcombe RG. **Improved confidence intervals for the difference between binomial proportions based on paired data.** *Statist Med* 1998;17:2635–50 Medline
18. Hourani R, Carey J, Yousem DM. **Dehiscence of the jugular bulb and vestibular aqueduct: findings on 200 consecutive temporal bone computed tomography scans.** *J Comput Assist Tomogr* 2005;29:657–62 CrossRef Medline
19. Liu Z, Bi W, Li J, et al. **Superior semicircular canal dehiscence in relation to the superior petrosal sinus: a potential cause of pulsatile tinnitus.** *Clin Radiol* 2015;70:943–47 CrossRef Medline
20. Li S, Shen N, Cheng Y, et al. **The effect of jugular bulb-vestibular aqueduct dehiscence on hearing and balance.** *Acta Otolaryngol* 2015;135:1103–07 CrossRef Medline
21. Thénint MA, Barbier C, Hitier M, et al. **Endovascular treatment of symptomatic vestibular aqueduct dehiscence as a result of jugular bulb abnormalities.** *J Vasc Interv Radiol* 2014;25:1816–20 CrossRef Medline

# MR Imaging Appearance of Ruptured Rathke Cleft Cyst and Associated Bone Marrow Enhancement

Ian T. Mark and Christine M. Glastonbury



## ABSTRACT

**SUMMARY:** Rathke cleft cysts are common cystic pituitary lesions seen on MR imaging. A subset of Rathke cleft cysts can rupture within the sella and are uncommon. The imaging appearance of a ruptured Rathke cleft cyst has been previously described with nonspecific imaging findings. We present 7 cases of ruptured Rathke cleft cysts and basisphenoid bone marrow enhancement below the sella that could be used to potentially distinguish a ruptured Rathke cleft cyst from other cystic lesions.

**ABBREVIATIONS:** RCC = Rathke cleft cyst; rRCC = ruptured Rathke cleft cyst

Rathke cleft cysts (RCC) are benign epithelium-lined remnants originating from the craniopharyngeal duct between the anterior and posterior pituitary lobes.<sup>1</sup> RCCs are common, having been found in 11.3% of patients in a large cadaveric study<sup>2</sup> and are often asymptomatic. When symptomatic, RCCs manifest most frequently with headaches, visual deficits, or hormonal abnormalities,<sup>1</sup> often leading to a contrast-enhanced brain MR imaging. A subset of RCCs can rupture within the sella, and several prior case reports described nonspecific findings on MR imaging in this setting.<sup>3–8</sup> We present 7 cases of pathology-proved ruptured RCC (rRCC), each of which had basisphenoid bone marrow enhancement.

## MATERIALS AND METHODS

An internal database was reviewed from 2016 to 2022 for pathology-proved rRCC. Inclusion criteria were adults (18 years of age or older) with preoperative MR imaging that included fat-saturated postcontrast T1-weighted imaging. Pertinent patient history was reviewed, which included the following: sex, age, presenting symptoms, serum prolactin levels, presumed preoperative diagnosis, surgical approach, and postoperative follow-up.

Preoperative MR imaging was evaluated for lesion size and enhancement of the basisphenoid bone marrow directly below the sella. Additionally, the images were evaluated for lesion location (midline versus off-midline), T2 signal, T1 signal, and the

presence of a T2 dark nodule. The images were reviewed by a neuroradiology instructor (I.T.M.) and a neuroradiologist with 20 years of experience (C.M.G.). Sphenoid sinus pneumatization patterns were evaluated and graded as the following: type 1 conchal, type 2 presellar, type 3 sellar, and type 4 postsellar.<sup>9</sup>

Post hoc analysis was conducted of 7 consecutive patients (2019–2022) with pathology-proved cystic adenoma for enhancing basisphenoid bone marrow. Inclusion criteria matched those of the patients with rRCC; adults (18 years of age or older) with preoperative MRI, including fat-saturated postcontrast T1-weighted MR imaging.

## RESULTS

### Patients with rRCC

Seven patients with pathology-proved rRCC were included. Patient-specific demographics are listed in Table 1. All 7 patients were women and had an average age of 44.3 years (range, 30–72 years). The median serum prolactin level was 34.9  $\mu\text{g/L}$  (range, 2.7–113.2  $\mu\text{g/L}$ ). Pituitary adenoma was the presumed preoperative diagnosis in 5 (71.4%) cases. The average maximum lesion diameter was 11.2 mm (range, 8.2–14.0 mm). Three patients had type 2 (presellar) pneumatization of the sphenoid sinus, and 4 patients had type 3 (sellar) pneumatization.<sup>9</sup> Three patients had focal basisphenoid bone enhancement below the sella (Fig 1), while 4 patients had enhancement that extended diffusely in the axial plane (Figs 2 and 3). Patient-specific imaging findings are listed in Table 2.

### Patients with Cystic Pituitary Adenoma

The average age of our patients was 40.9 years (range, 28–62 years). The average maximum adenoma diameter was 20.1 mm (range, 9–44 mm). The median serum prolactin level was

Received February 3, 2023; accepted after revision August 30.

From the Department of Radiology (I.T.M.), Mayo Clinic, Rochester, Minnesota; and Department of Radiology and Biomedical Imaging (I.T.M., C.M.G.), University of California San Francisco, San Francisco, California.

Please address correspondence to Ian Mark, MD, 200 1st St SW, Rochester, MN 55905; e-mail: Mark.ian@mayo.edu; @iantmark

Indicates open access to non-subscribers at www.ajnr.org

<http://dx.doi.org/10.3174/ajnr.A8009>

**Table 1: Demographic information of the patients with rRCC proved at surgical resection**

Patient	Age (yr)	Sex	Prolactin ( $\mu\text{g/L}$ )	Presenting Symptom	Preop Diagnosis	Follow-Up
1	51	Female	33.2	HA	Adenoma	No recurrence at 6 mo
2	47	Female	n/a	HA, panhypopituitary	RCC	Recurrence at 3 yr
3	38	Female	2.7	HA	Adenoma	No recurrence at 4 yr
4	39	Female	22.4	Enlarging lesion	RCC	No recurrence at 1 mo
5	30	Female	36.5	Diabetes insipidus, vision changes	Adenoma	No recurrence at 2 mo
6	72	Female	42.4	Fatigue	Adenoma	No recurrence at 2 mo
7	33	Female	113.2	Hyperprolactinemia	Adenoma	No recurrence at 2 mo

**Note:**—HA indicates headache; Preop, preoperative; n/a, not available.

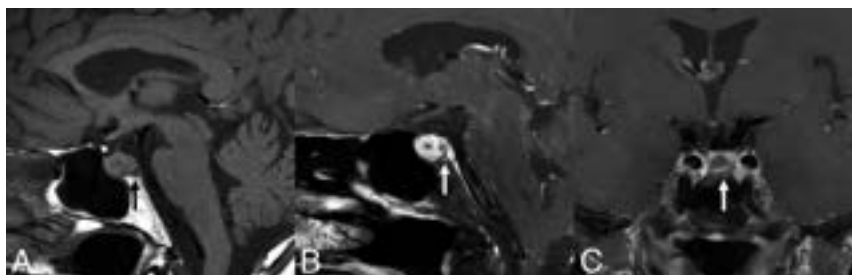


**FIG 1.** A 72-year-old woman who presented with fatigue and was found to have a bilobed pituitary lesion, preoperatively favored to be a pituitary adenoma. A, Precontrast T1-weighted imaging shows focal hypointense signal in the posterior basisphenoid bone marrow (arrows). Postcontrast imaging shows corresponding enhancement (B and C). Pathology confirmed an rRCC.

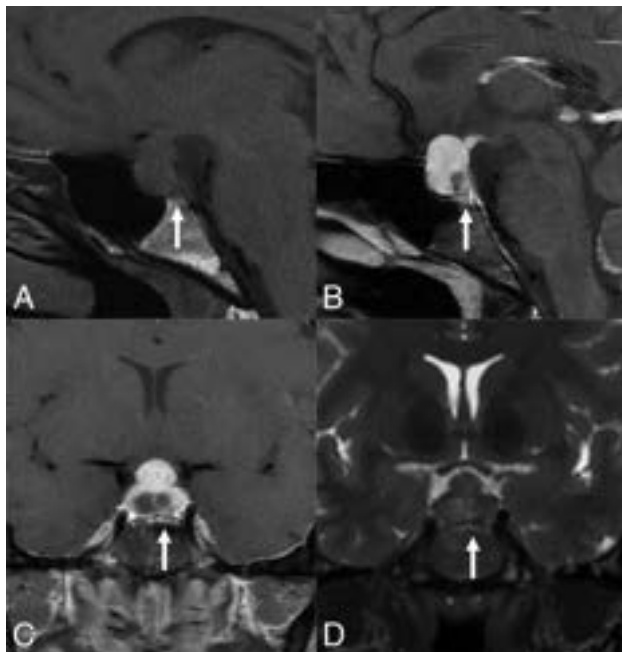


**FIG 2.** A 38-year-old woman presented with headaches for 6 months. MR imaging shows a sellar/suprasellar mass with a septated cystic lesion in the posterior aspect of the sella, preoperatively favored to represent a pituitary adenoma. Postcontrast MR imaging shows basisphenoid bone marrow (arrows) enhancement (B and C) with corresponding edema (D). There was no intrinsic basisphenoid T1-hyperintense signal on the precontrast imaging (A). Pathology confirmed the cystic lesion to be an rRCC. The enlarged suprasellar lesion was biopsied and found to be mixed inflammatory infiltrate and fibrosis, thought to represent inflammatory hypophysitis secondary to the rRCC.

30.8  $\mu\text{g/L}$  (range, 12.6–167.1  $\mu\text{g/L}$ ). Six patients had type 3 (sellar) pneumatization of the sphenoid sinus, and 1 patient had type 2 (presellar) pneumatization. None of the 7 patients had enhancing basisphenoid bone marrow below the sella.

## DISCUSSION

Our study is the first to describe enhancing basisphenoid bone marrow below the sella as an imaging finding of rRCC. We present 7 cases of rRCC, all of which showed bone marrow enhancement. This finding is potentially important because the leading differential for

an rRCC is cystic pituitary adenoma, which, in our limited experience reported here, does not have basisphenoid bone marrow enhancement.

RCCs arising from failed regression of the cleft between the adeno- and neurohypophysis are frequently incidental and asymptomatic findings.<sup>10</sup> RCCs can become symptomatic and present with headaches, visual deficits, or hormonal abnormalities and have an overlapping imaging appearance with cystic adenoma.<sup>11</sup> Park et al<sup>12</sup> created a diagnostic model using MR imaging to differentiate cystic pituitary adenoma and RCC, but the model does not specifically assess rRCC. Prior case reports of rRCCs have not described specific findings to differentiate them from a cystic adenoma.

Intrasellar rupture of an RCC was described in 1988,<sup>10</sup> with associated marked inflammation of the pituitary gland thought to be secondary to the spillage of RCC contents. Numerous additional case reports have since been presented in the literature of symptomatic patients with xanthogranulomatous changes of the pituitary gland.<sup>3–8,13</sup> It is thought that mucin leaking out of the rRCC can trigger a cascade of surrounding inflammation.<sup>14</sup> The abnormal bone marrow enhancement in our cases, therefore, likely represents an imaging manifestation of the adjacent inflammatory changes. This is most evident in the patient presented in Fig 2, in which the native pituitary was markedly enlarged with suprasellar extension, preoperatively thought to be an adenoma. In this case, the RCC was found to be ruptured, and the pituitary biopsy findings were thought to represent reactive hypophysitis. Further testing was not compatible with lymphocytic hypophysitis or immunoglobulin G4-related disease. Given that the bone marrow enhancement is likely secondary to the inflammatory cascade set





**FIG 3.** A 39-year-old woman with a history of gamma knife therapy to the sella for an undiagnosed lesion at another institution presented with an enlarging cystic pituitary lesion. T2-weighted imaging (A) shows a hypointense nodule and edema of the basisphenoid bone marrow (arrows). This area has corresponding T1-hypointense signal on precontrast imaging (B) and enhancement (C). Pathology confirmed an rRCC.

**Table 2. MR imaging characteristics of patients with pathologic rRCCs**

Patient	Max Dimension (mm)	Bone Marrow Enhancement	T2 Signal	T2 Dark Nodule	T1 Hyperintense Signal	Location
1	11.5	Focal	Hyperintense	No	No	Midline
2	14.0	Focal	Hypointense	No	Yes	Midline
3	10.8	Diffuse	Heterogeneous	No	No	Midline
4	10.8	Diffuse	Hyperintense	Yes	Yes	Off-midline
5	11.1	Diffuse	Hyperintense	Yes	No	Midline
6	8.2	Focal	Heterogeneous	No	No	Replaces entire pituitary
7	12.2	Diffuse	Hyperintense	Yes	No	Replaces entire pituitary

**Note:**—Max indicates maximum.

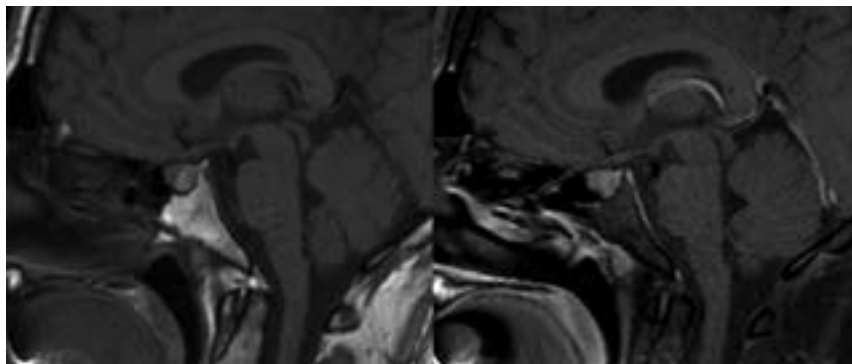


**FIG 4.** Example of a pathology-proved nonruptured RCC. The precontrast T1-weighted (left) images show normal signal of the basisphenoid bone marrow edema below the T1-hyperintense RCC. The fat-saturated postcontrast image (right) shows normal basisphenoid bone marrow without abnormal enhancement.

off by the RCC rupture, we would not expect to see abnormal enhancement with nonruptured RCCs (Fig 4).

Similar bone marrow imaging findings have been recently described with granulomatous hypophysitis,<sup>15</sup> which is a noncystic inflammatory process of the pituitary gland. In that article, 100 pituitary adenomas were evaluated, none of which had basisphenoid bone marrow enhancement. Therefore, bone marrow enhancement is reflective of an inflammatory process, regardless of the cystic or

solid nature of the sellar process. The current study is the first to describe bone marrow enhancement associated with an rRCC.

Differentiating between a RCC and a cystic pituitary adenoma can be challenging because they often have an overlapping imaging appearance. Pituitary adenomas have been described as off-midline in position and as having fluid levels, a hypointense T2 rim, and septations,<sup>12</sup> while RCCs are associated with T2-hypointense nodules and are typically midline in position.<sup>11</sup> Our study is limited by the small number of patients; however, none of our cystic adenomas had basisphenoid bone marrow enhancement, nor has this previously been described in the literature. The differential for cystic lesions of the pituitary gland extends beyond RCC and cystic adenoma, but such lesions are expected to demonstrate different imaging findings and clinical presentations. Adamantinomatous craniopharyngiomas occur more frequently in children and are typically suprasellar and calcified.<sup>16</sup> Pituitary abscess could also appear as a cystic lesion and, due to marked surrounding inflammatory changes, could also have bone marrow signal changes; however, an abscess should also present with restricted diffusion,<sup>17</sup> whereas an RCC would not.<sup>18</sup> Our patients did not have DWI for us to analyze. The broad category of hypophysitis has many primary and secondary causes, ranging from immunoglobulin G4-related disease to infectious causes such as tuberculosis.<sup>19</sup> While these entities, outside of granulomatous hypophysitis,<sup>15</sup> have not been previously described as having bone marrow enhancement, it is certainly possible, given the associated inflammation. These should present as solidly enhancing enlargement of the pituitary gland, however, rather than the cystic appearance expected for an RCC.

Diagnosing basisphenoid bone marrow inflammatory changes on MR imaging is predicated on having bone marrow below the sella (non-type 4 sphenoid pneumatization) and the correct MR imaging protocol, and this requirement limits generalization of this finding to all pituitary cases. The findings are most easily seen when the T2-weighted and postcontrast T1-weighted images are fat-saturated. Even in the absence of fat saturation, however, precontrast T1-weighted images can show dark bone marrow

signal (Fig 3). We believe that the presence of MR signal abnormalities consistent with basisphenoid inflammation is an important finding that can potentially help to identify an rRCC in the appropriate clinical setting. Although the small number of patients included in this report limits its generalizability, it can serve as a starting point for future studies that include more patients.

## CONCLUSIONS

RCCs are commonly seen on MR imaging as cystic pituitary lesions. Intracellular rupture of an RCC is uncommon and without previously described imaging findings to differentiate it from other pathologies. We present 7 cases of basisphenoid bone marrow enhancement below the sella that could be used to potentially identify an rRCC before surgical exploration.

Disclosure forms provided by the authors are available with the full text and PDF of this article at [www.ajnr.org](http://www.ajnr.org).

## REFERENCES

1. Elarjani T, Alhuthayl MR, Dababo M, et al. **Rathke cleft cyst apoplexy: hormonal and clinical presentation.** *Surg Neurol Int* 2021;12:504 CrossRef
2. Teramoto A, Hirakawa K, Sanno N, et al. **Incidental pituitary lesions in 1,000 unselected autopsy specimens.** *Radiology* 1994;193:161–64 CrossRef Medline
3. Duan K, Asa SL, Winer D, et al. **Xanthomatous hypophysitis is associated with ruptured Rathke's cleft cyst.** *Endocr Pathol* 2017;28:83–90 CrossRef Medline
4. Gezer E, Çabuk B, Bayrak BY, et al. **Xanthomatous hypophysitis secondary to a ruptured Rathke's cleft cyst: a case report.** *Brain Tumor Res Treat* 2022;10:48–54 CrossRef Medline
5. Neidert MC, Woernle CM, Leske H, et al. **Ruptured Rathke cleft cyst mimicking pituitary apoplexy.** *J Neurol Surg A Cent Eur Neurosurg* 2013;74(Suppl 1):e229–32 CrossRef Medline
6. Schittenhelm J, Beschoner R, Psaras T, et al. **Rathke's cleft cyst rupture as potential initial event of a secondary perifocal lymphocytic hypophysitis: proposal of an unusual pathogenetic event and review of the literature.** *Neurosurg Rev* 2008;31:157–63 CrossRef Medline
7. Sonnet E, Roudaut N, Mériot P, et al. **Hypophysitis associated with a ruptured Rathke's cleft cyst in a woman, during pregnancy.** *J Endocrinol Invest* 2006;29:353–57 CrossRef Medline
8. Yang C, Wu H, Bao X, et al. **Lymphocytic hypophysitis secondary to ruptured Rathke cleft cyst: case report and literature review.** *World Neurosurg* 2018;114:172–77 CrossRef Medline
9. Pirinc B, Fazliogullari Z, Guler I, et al. **Classification and volumetric study of the sphenoid sinus on MDCT images.** *Eur Arch Otorhinolaryngol* 2019;276:2887–94 CrossRef Medline
10. Albini CH, MacGillivray MH, Fisher JE, et al. **Triad of hypopituitarism, granulomatous hypophysitis, and ruptured Rathke's cleft cyst.** *Neurosurgery* 1988;22:133–36 CrossRef Medline
11. Byun WM, Kim OL, Kim D. **MR imaging findings of Rathke's cleft cysts: significance of intracystic nodules.** *AJNR Am J Neuroradiol* 2000;21:485–88 Medline
12. Park M, Lee SK, Choi J, et al. **Differentiation between cystic pituitary adenomas and Rathke cleft cysts: a diagnostic model using MRI.** *AJNR Am J Neuroradiol* 2015;36:1866–73 CrossRef Medline
13. Sprau A, Mahavadi A, Zhang M, et al. **Rathke's cleft cyst with xanthogranulomatous change: a case report and review of the literature.** *Surg Neurol Int* 2020;11:246 CrossRef Medline
14. Oka H, Kawano N, Suwa T, et al. **Radiological study of symptomatic Rathke's cleft cysts.** *Neurosurgery* 1994;35:632; discussion 636–37 CrossRef Medline
15. Mark IT, Glastonbury CM. **Diffuse basisphenoid enhancement: possible differentiating feature for granulomatous hypophysitis.** *AJNR Am J Neuroradiol* 2022;43:1341–45 CrossRef Medline
16. Sartoretti-Schefer S, Wichmann W, Aguzzi A, et al. **MR differentiation of adamantinous and squamous-papillary craniopharyngiomas.** *AJNR Am J Neuroradiol* 1997;18:77–87 Medline
17. Takayasu T, Yamasaki F, Tominaga A, et al. **A pituitary abscess showing high signal intensity on diffusion-weighted imaging.** *Neurosurg Rev* 2006;29:246–48 CrossRef Medline
18. Kunii N, Abe T, Kawano M, et al. **Rathke's cleft cysts: differentiation from other cystic lesions in the pituitary fossa by use of single-shot fast spin-echo diffusion-weighted MR imaging.** *Acta Neurochir (Wien)* 2007;149:759–69; discussion 769 CrossRef Medline
19. Langlois F, Varlamov EV, Flešeriu M. **Hypophysitis, the growing spectrum of a rare pituitary disease.** *J Clin Endocrinol Metab* 2022;107:10–28 CrossRef Medline

# The Influence of Nonaerated Paranasal Sinuses on DTI Parameters of the Brain in 6- to 9-Year-Old Children

Marjolein H.G. Dremmen, Dorottya Papp, Juan A. Hernandez-Tamames, Meike W. Vernooij, and Tonya White



## ABSTRACT

**BACKGROUND AND PURPOSE:** DTI is prone to susceptibility artifacts. Air in the paranasal sinuses can cause field inhomogeneity, thus affecting measurements. Children often have mucus in their sinuses or no pneumatization of them. This study investigated the influence of lack of air in the paranasal sinuses on measurements of WM diffusion characteristics.

**MATERIALS AND METHODS:** The study was embedded in the Generation R Study, a prospective population-based birth cohort in Rotterdam (the Netherlands). Brain MR imaging studies (1070 children, 6–9 years of age) were evaluated for mucosal thickening of the paranasal sinuses. Nonaeration of the paranasal sinuses (modified Lund-Mackay score) was compared with that in a randomly selected control group. The relationship between nonaerated paranasal sinuses and fractional anisotropy and mean diffusivity in the DTI fiber tracts was evaluated using ANCOVA and independent *t* tests.

**RESULTS:** The prevalence of mucosal thickening was 10.2% (109/1070). The mean modified Lund-Mackay score was 6.87 (SD, 3.76). In 52.3% (57/109),  $\geq 1$  paranasal sinus was not pneumatized. The results are reported in effect sizes (Cohen's *d*). Lower mean fractional anisotropy values were found in the uncinate fasciculus (right uncinate fasciculus/right frontal sinus,  $d = -0.60$ ), superior longitudinal fasciculus (right superior longitudinal fasciculus/right ethmoid sinus,  $d = -0.56$ ; right superior longitudinal fasciculus/right sphenoid sinus,  $d = -2.09$ ), and cingulate bundle (right cingulum bundle/right sphenoid sinus,  $d = -1.28$ ; left cingulum bundle/left sphenoid sinus,  $d = -1.49$ ). Higher mean diffusivity values were found in the forceps major/right and left sphenoid sinuses,  $d = 0.78$ .

**CONCLUSIONS:** Nonaeration of the paranasal sinuses is a common incidental finding on pediatric MR imaging brain scans. The amount of air in the paranasal sinuses can influence fractional anisotropy and, to a lesser degree, mean diffusivity values of WM tracts and should be considered in DTI studies in pediatric populations.

**ABBREVIATIONS:** CGB = cingulum bundle; FA = fractional anisotropy; FDR = false discovery rate; FMa = forceps major; ILF = inferior longitudinal fasciculus; IQ = intelligence quotient; MD = mean diffusivity; SLF = superior longitudinal fasciculus; UF = uncinate fasciculus; VBA = voxel-based analysis

The use of DTI to study WM microstructural development and degeneration has shown an exponential increase during the past decade. In pediatric research, DTI serves as a promising

tool for monitoring brain maturation and development from fetal life onward, and multiple studies have demonstrated age-related differences or changes in WM microstructure.<sup>1–4</sup> A disadvantage of echo-planar DTI sequences, however, is susceptibility artifacts resulting from field inhomogeneities of the static magnetic field, for example, at air/tissue or air/bone interfaces.<sup>5</sup> These inhomogeneities result in geometric distortion and signal loss, which can distort DTI measurements in the vicinity of these areas. To a certain degree, field map imaging can compensate for these artifacts, however; but it cannot completely remove the geometric distortion, and areas of complete signal loss cannot be restored.<sup>6</sup>

Received June 9, 2023; accepted after revision September 20.

From the Departments of Radiology and Nuclear Medicine (M.H.G.D., D.P., J.A.H.-T., M.W.V., T.W.) and Epidemiology (M.W.V.), Erasmus University Medical Center, Rotterdam, the Netherlands; The Generation R Study Group (M.H.G.D.), and Department of Child and Adolescent Psychiatry (T.W.), Erasmus Medical Center Sophia, Rotterdam, the Netherlands; and Section on Social and Cognitive Developmental Neuroscience (T.W.), National Institute of Mental Health, Bethesda, Maryland.

This study is financially supported through Netherlands Organization for Health Research and Development TOP project number 91211021. The general design of Generation R Study is made possible by financial support from the Erasmus Medical Center, Rotterdam; the Erasmus University Rotterdam; the Netherlands Organization for Health Research and Development; the Netherlands Organization for Scientific Research; and the Ministry of Health, Welfare and Sport. Furthermore, this study is part of the BRAIN development, Imaging trajectories and Deviations in brain morphology in the pEdiatric population (BRIDGE), BRIDGing the gap study. The BRIDGE gap study is made possible through financial support of an internal Erasmus Medical Center grant and of the Department of Radiology and Nuclear Medicine, Erasmus University Medical Center, Rotterdam, the Netherlands.

Please address correspondence to Marjolein Dremmen, MD, Erasmus MC Sophia, Department of Radiology and Nuclear Medicine, Room Sb-1654, PO Box 2060, 3000 CB Rotterdam, the Netherlands; e-mail: m.dremmen@erasmusmc.nl

Indicates open access to non-subscribers at www.ajnr.org

Indicates article with online supplemental data.

<http://dx.doi.org/10.3174/ajnr.A8033>

## Demographic characteristics of the sample

	Total Group ( <i>n</i> = 208) (100%)	Controls ( <i>n</i> = 105) (50.5%)	Nonaerated Sinuses ( <i>n</i> = 103) (49.5%)	<i>P</i> Value
Age (mean) (SD) (yr)	8.00 (1.00)	8.17 (1.01)	7.83 (0.97)	.02
Sex (%)				.78
Male	51.9	50.5	53.4	
Female	48.1	49.5	46.6	
Ethnicity (%) <sup>a</sup>				.37
Dutch	65.9	65.7	66.0	
Other Western	8.2	9.5	6.8	
Non-Western	22.1	19.0	25.2	
Nonverbal IQ (mean) (SD) <sup>b</sup>	102.81 (14.42)	103.87 (15.72)	101.78 (13.04)	.33
Maternal education (%) <sup>c</sup>				.19
Low	4.8	1.9	7.8	
Medium	36.1	34.3	37.9	
High	46.2	50.4	41.7	
Handedness (%) <sup>d</sup>				.45
Right	87.5	89.5	85.4	
Left	9.6	7.6	11.7	

<sup>a</sup>Missing data on ethnicity (3.8%).

<sup>b</sup>Missing data on nonverbal IQ (13.0%).

<sup>c</sup>Low indicates primary school/lower vocational education; Medium, intermediate vocational education; High, higher vocational education/university. Missing data on maternal education (11.5%).

<sup>d</sup>Missing data on handedness (2.9%).

The paranasal sinuses are in close approximation to anterior-inferior brain areas, and their air content may thus influence diffusion measurements in these areas. The presence of mucus or mucosal thickening is relatively high in children compared with the adult population, peaking between 3 and 8 years of age,<sup>7,8</sup> and it is a common incidental finding on MR imaging in pediatric populations.<sup>9</sup> Reported frequencies vary due to differences in the study design and the mean age of the populations studied and range from 12% to 48%.<sup>7,10,11</sup> Furthermore, the paranasal sinuses are still developing in children, resulting in different degrees of pneumatization of the paranasal sinuses during the first 2 decades of life.<sup>12,13</sup>

WM microstructure continues to change with time in typically developing children and adolescents, with greater change in the frontal regions for all DTI parameters.<sup>14,15</sup> In addition, nonlinear trajectories have been reported with a deceleration of age-related changes in specific WM tracts in children between 4 and 11 years of age.<sup>14</sup> Thus, there is a need to evaluate the possible effect of the degree of aeration of the paranasal sinuses on DTI parameters.

In this study, we used data from a large population-based study of child development to study the influence of the degree of aeration of the paranasal sinuses on DTI parameters in the pediatric brain.

## MATERIALS AND METHODS

### Participants

The current study was embedded in the longitudinal population-based Generation R Study. An overview of the Generation R Study design is published elsewhere.<sup>16,17</sup> Briefly, the Generation R Study is a prospective birth cohort study initiated in Rotterdam between 2002 and 2006. After we obtained informed consent, a total of 9778 pregnant women or women who had recently delivered were included in the study. Demographic characteristics included age, sex, ethnicity, and educational level of the mother (Table).<sup>17</sup> In addition, the intelligence quotient (IQ) of the child was measured using the Snijders-Oomen Nonverbal Intelligence

Test 2.5–7-Revised;<sup>18</sup> and handedness, using the Edinburgh Handedness Inventory.<sup>19</sup> A neuroimaging substudy of 6- to 9-year-old children was initiated in 2009 and involved a total of 1070 children.<sup>20</sup> Exclusion criteria were general contraindications for MR imaging examination (ie, pacemaker), neurologic disorders, and claustrophobia. Informed consent was obtained from the parents before participation, and the study was approved by the Medical Ethics Committee at the Erasmus Medical Center.<sup>20</sup>

### MR Imaging Acquisition

Children were familiarized with the MR imaging scanners using a mock scanning procedure.<sup>20</sup> MR images were acquired on a 3T scanner (Discovery MR750; GE Healthcare) using an 8-channel head coil. DTI data were

obtained with 3 *b*=0 volumes and 35 diffusion directions using an EPI sequence (TR = 11s, TE = 84 ms, section thickness = 2 mm, FOV = 256 × 256 mm, *b*=1000s/mm<sup>2</sup>). The EPI phase-encoding direction was anterior-posterior. No EPI with reversed phase-encoding directions or gradient-echo field maps was acquired. In addition, an axial proton density sequence (TR = 13,500 ms, TE = 6.7 ms, section thickness = 1.0 mm, FOV = 256 × 256 mm) and a high-resolution 3D T1-weighted inversion recovery fast-spoiled gradient recalled sequence (TR = 10.3 ms, TE = 4.2 ms, section thickness = 0.9 mm, FOV = 512 × 512 mm) were obtained.

### Paranasal Sinus Assessment

The paranasal sinuses were assessed in a standardized approach by a neuroradiologist blinded to subject information. The rater evaluated whether the neuroimaging scans (*n* = 1070) showed evidence of mucosal thickening in any sinus. Subsequently, the degree of mucosal thickening of the paranasal sinuses (*n* = 109) was scored by an experienced pediatric neuroradiologist according to a modified Lund-Mackay score (Online Supplemental Data). The Lund-Mackay score is used for radiologic staging of rhinosinusitis.<sup>21–23</sup> Each sinus was assigned a score of 0 (normal aeration), 1 (partial nonaeration), or 2 (complete nonaeration). The modification of the score consisted of not assessing the maxillary sinus (due to its distance from the anterior-inferior brain regions and no expectation of it causing relevant susceptibility artifacts) and not assessing the ostiomeatal complex (which is not relevant to our study). A nonpneumatized paranasal sinus received a separate score of 3 in the modified Lund-Mackay score. The Lund-Mackay score was originally designed for CT staging, but previous studies have shown that Lund-Mackay staging of sinus disease by MR imaging is closely correlated to corresponding staging based on CT.<sup>22,23</sup>

A control group (*n* = 110) without any signs of mucosal thickening of the paranasal sinuses and with pneumatization of all sinuses (modified Lund-Mackay score of 0) was randomly



selected from an age-matched group of 6- to 9-year-old children from the same source population. After excluding DTI scans of insufficient quality for image analysis, the subset of children with nonaeration of  $\geq 1$  paranasal sinus consisted of 89 children, and the control group was 85 children. To assure an adequate sample size and because the maximum effect of nonaerated sinuses on DTI measures of the adjacent brain was hypothesized to occur in sinuses without any amount of air (so without susceptibility artifacts), we clustered the 4 groups into 2 contrasting groups: a nonaerated group with complete filling by mucosal thickening and/or no pneumatization of paranasal sinuses (score 2/3) and a control group consisting of children with normal aeration and/or partial filling by mucosal thickening (score 0/1) of the paranasal sinuses. For more detail see the flow chart in the Online Supplemental Data.

### DTI Analysis

Images were preprocessed the FMRIB Software Library, Version 6.0.2 (FSL; <http://www.fmrib.ox.ac.uk/fsl>).<sup>24</sup> Nonbrain tissue was removed, and correction for eddy current-induced artifacts and volume realignment was applied.<sup>25</sup> A weighted least-squares method was used to fit the diffusion tensor at each voxel. Probabilistic fiber tractography was run by leveraging the FSL plugin AutoPtx (<https://fsl.fmrib.ox.ac.uk/fsl/fslwiki/AutoPtx>), including the uncinate fasciculus (UF), superior and inferior longitudinal fasciculus (SLF/ILF), forceps major (FMA) and minor, cingulum bundle (CGB), and the corticospinal tract.<sup>26,27</sup> Target and exclusion masks were defined by using atlases and transferred to subject native space using nonlinear registrations obtained with FNIRT (<https://fsl.fmrib.ox.ac.uk/fsl/fslwiki/FNIRT>).<sup>28</sup> Normalization of connectivity distributions was based on successful seed-to-target attempts. Voxels unlikely to be part of the true distribution were removed by thresholding.<sup>28</sup> Average values for fractional anisotropy (FA) and mean diffusivity (MD) of each WM tract were obtained after weighting voxels on the basis of connectivity distributions. For bilateral tracts, left and right hemisphere values were averaged. To obtain global connectivity measures, we averaged all FA or MD values across the commonly used tracts and weighted this average on the basis of the volume of each tract.<sup>29</sup>

For the analysis, we focused primarily on mean FA and MD values of the WM tracts, because FA and MD values are the most widely used DTI parameters in pediatric brain imaging studies.<sup>1,4,30</sup> In addition, we developed and applied a voxel-based analysis (VBA) to study the effect of paranasal sinus content on DTI parameters in greater detail. The VBA was performed following nonlinear registration of FA maps to a study-specific EPI template in standard space.<sup>31</sup> Subsequently, an FA mask was created in standard space defined by  $FA > 0.1$  of the mean FA image. A voxelwise linear regression was performed in Python, Version 3.8.2, for each voxel within the FA mask to visualize the global effect of paranasal sinus content on FA values of adjacent WM tracts. To correct for multiple testing, we applied the Benjamini-Hochberg false discovery rate (FDR) correction, using all individual voxels within the FA mask.<sup>32</sup>

The image quality of the DTI data set was assessed using both manual and automated approaches. The manual approach included visual inspection to assess the presence of major artifacts and to assess the sum-of-squares error of tensor calculation and tract reconstructions. We also applied automatic quality control to

assess the number of slices and volumes with signal drop-out, and we excluded data with excessive motion based on translation and rotation motion parameters.<sup>29</sup> These procedures resulted in 5.0% ( $n = 11$ ) of the scans being rated as of insufficient quality, and those scans were excluded from analysis (Online Supplemental Data).<sup>27</sup>

### Statistical Analyses

Demographic differences between the nonaerated and control groups were analyzed using a  $\chi^2$  test for categorical variables (sex, ethnicity, maternal education level, handedness); and independent  $t$  tests, for continuous variables (age, nonverbal IQ). Differences in DTI parameters between the nonaerated and control groups were tested using ANCOVA. Covariates were added to the ANCOVA models if they resulted in a  $> 5\%$  change in the effect estimate. Covariates included the child's age at scanning and sex. Results were reported in effect sizes (Cohen's  $d$ ) with  $P$  values. The threshold for significance was set at  $P < .05$ .

Because the control group does include children with minor degrees of mucosal thickening of their sinuses (score 1) and the significance of this minor degree of mucosal thickening is not clear, 2 additional sensitivity analyses were performed assessing different WM tracts: an analysis comparing the 2 extreme categories (score 0 versus 2/3) and an analysis using a classification into 3 groups (score 0 versus 1 versus 2/3).

To account for possible age differences between the nonaerated and control groups seen in our total study population, we performed a subsequent subanalysis in children with nonaerated paranasal sinuses showing a significant effect on mean FA values of specific WM tracts in the ANCOVA. To perform this subanalysis, for each subgroup of nonaerated paranasal sinuses (Online Supplemental Data), we individually matched cases and controls so that the paired age difference was less than 6 months. The number of age-matched controls in each subgroup was identical to the number of children in the accompanying nonaerated group, ie, 54 and 46 controls in, respectively, the right and left nonaerated frontal sinus groups; 16 and 16 controls in, respectively, the right and left nonaerated ethmoid sinus groups; and 13 and 17 controls in, respectively, the right and left nonaerated sphenoid sinus groups (Online Supplemental Data). Because of the small number of cases in the subgroups of the nonaerated group, results were reported in effect sizes (Cohen's  $d$ ) with 95% CIs instead of  $P$  values. Only effect sizes found to exceed the Cohen's convention (1988) for a medium, large, or very large effect are given.<sup>33</sup>

A VBA of FA and MD values of WM microstructure was performed to provide greater spatial detail of the effect of nonaerated-versus-aerated paranasal sinuses. Because in this VBA a large number of voxels were compared simultaneously, the Benjamini-Hochberg FDR correction was applied to all voxels within the FA and MD masks to correct for multiple testing.<sup>32</sup>

All analyses were performed using R statistical and computing software, Version 4.0.1 (<http://www.r-project.org/>) or the scikit-learn module (<https://scikit-learn.org/stable/>) in Python, Version 3.8.2.

## RESULTS

### Sample Characteristics

Sample characteristics are presented in the Table. A total of 109 children were included in the group with nonaeration of  $\geq 1$

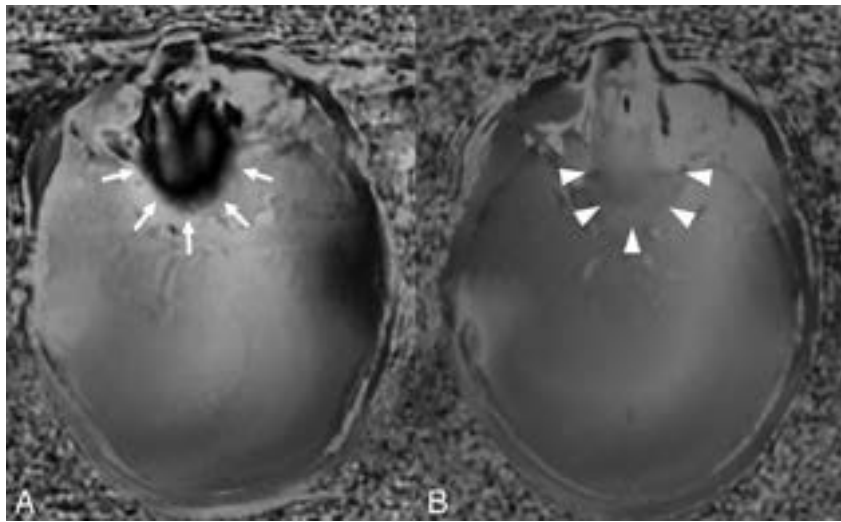


**FIGURE.** DTI phase maps of the brain at the level of ethmoid and sphenoid sinuses. Prominent susceptibility artifacts (arrows) are seen in a participant with well-aerated paranasal sinuses (A). In a participant with nonaerated ethmoid and sphenoid sinuses (B), much fewer susceptibility artifacts are seen (arrowheads).

paranasal sinus, and 110 children were included in the control group. DTI data of 6 and 5 children, respectively, were of insufficient quality and were, therefore, excluded from analysis. Children in the nonaerated sinus and control groups significantly differed in age at the time of scanning ( $t(206) = 2.45, P = .02$ ). There was no difference in sex ( $P = .78$ ), ethnicity ( $P = .37$ ), non-verbal IQ ( $t(171) = 0.97, P = .33$ ), maternal education ( $P = .19$ ), and handedness ( $P = .45$ ) between groups.

### Paranasal Sinuses

The prevalence of neuroimaging signs of mucosal thickening in our cohort was 10.2% (109/1070). The mean modified Lund-Mackay score was 6.56 (SD, 3.60). The Online Supplemental Data show, in more detail, the distribution and degree of nonaerated paranasal sinuses.

DTI phase maps are shown to visualize the distortion (Figure), to demonstrate the effect on magnetic susceptibility caused by well-aerated paranasal sinuses versus nonaerated paranasal sinuses.

### FA and MD Values of Major WM Tracts

The Online Supplemental Data show the differences in mean FA values of major WM tracts between the nonaerated and control groups. Children with nonaerated ethmoid sinuses demonstrated lower mean FA values of the ipsilateral UF (right ethmoid sinus:  $d = -0.03, P = .02$  and left ethmoid sinus:  $d = -0.03, P = .02$ ). Lower mean FA values of the ipsilateral UF were shown in children with nonaerated left sphenoid sinuses ( $d = -0.02, P = .04$ ) and right frontal sinuses ( $d = -0.02, P = .03$ ). The mean FA value of the ipsilateral SLF was lower in children with nonaerated right ethmoid sinuses ( $d = -0.03, P \leq .005$ ), right frontal sinuses ( $d = -0.06, P \leq .005$ ), and right sphenoid sinuses ( $d = -0.04, P \leq .005$ ); there was significant influence of FA values of the ILF in children with nonaerated left frontal sinuses ( $d = -0.02, P = .02$ ). The ipsilateral CGB mean FA value was negatively influenced by the nonaerated left frontal sinus ( $d = -0.02, P = .03$ )

and the right and left sphenoid sinuses (respectively,  $d = -0.04, P \leq .005$ , and  $d = -0.02, P = .04$ ). A lower mean FA value was found in the FMa in children with nonaerated right and left frontal sinuses (respectively,  $d = -0.04, P = .005$ , and  $d = -0.02, P = .03$ ) and the right sphenoid sinuses ( $d = -0.02, P = .04$ ).

The sensitivity analysis of FA values of the major WM tracts in the 3 groups (score 0 versus 1 versus 2/3), and the 2 extreme groups (score 0 versus 2/3) had predominantly similar results. Comparing the 2 extreme groups did show additional lower FA values of the ipsilateral CGB in children with nonaerated right and left ethmoid sinuses as well (respectively,  $d = -0.02, P = .04$ , and  $d = -0.02, P = .03$ ).

In addition, the Online Supplemental Data show the differences in the mean MD values of major WM tracts between the nonaerated and control groups with

the mean MD values of certain major WM tracts demonstrating significant influence caused by nonaerated paranasal sinuses. The mean MD values changed in the opposite direction compared with FA values. Higher mean MD values of the ipsilateral UF were shown in children with nonaerated right and left sphenoid sinuses (respectively,  $d = 0.03, P = .007$ , and  $d = 0.02, P = .04$ ) and nonaerated right frontal sinuses ( $d = 0.02, P = .02$ ). The mean MD value of the ipsilateral SLF was higher in children with nonaerated right frontal sinuses ( $d = 0.02, P = .02$ ), whereas there was no significant influence of MD values of the ILF. A higher mean MD value was found in the FMa in children with nonaerated right and left frontal sinuses (respectively,  $d = 0.05, P \leq .005$ , and  $d = 0.07, P \leq .005$ ) and right and left sphenoid sinuses (respectively,  $d = 0.04, P \leq .005$ , and  $d = 0.02, P = .02$ ).

The subanalysis of the nonaerated paranasal sinuses in which the ANCOVA demonstrated significantly lower mean FA and/or higher mean MD values, using age-matched controls, showed a persistent negative effect on the mean FA values of the UF, SLF, and CGB. The mean FA value of the ipsilateral UF remained lower in children with nonaerated right frontal sinuses ( $n = 24, d = -0.60$ ; 95% CI,  $-0.31$  to  $-1.52$ ). In the ipsilateral SLF, the mean FA value remained lower in children with nonaerated right ethmoid sinuses ( $n = 14, d = -0.56$ ; 95% CI,  $-0.63$  to  $-1.75$ ) and right sphenoid sinuses ( $n = 12, d = -2.09$ ; 95% CI,  $-0.24$  to  $-3.64$ ). The negative effect of nonaerated right sphenoid sinuses ( $n = 12, d = -1.28$ ; 95% CI,  $-0.32$  to  $-2.75$ ) and the left sphenoid sinuses ( $n = 12, d = -1.49$ ; 95% CI,  $-0.19$  to  $-2.94$ ) persisted in the ipsilateral CGB. The results of this subanalysis are shown in the Online Supplemental Data. The mean MD values remained higher only in the FMa in children with nonaerated right and left sphenoid sinuses (respectively,  $n = 12, d = 0.78$ ; 95% CI,  $0.69$ – $.24$ , and  $n = 12, d = 0.78$ ; 95% CI,  $0.69$ – $2.24$ ).

The proximity of some of the above-mentioned WM tracts to the specific paranasal sinuses is shown in the Online Supplemental data.

## Voxel-Based Analyses

To provide greater spatial detail, we analyzed the effect of nonaerated ethmoid, frontal, and sphenoid sinuses on the FA and MD values of the WM microstructure of the adjacent brain regions using VBA. Overall, the VBA showed focal changes in mean FA and MD values in the WM tracts, consistent with our tract-based approach. The lower FA was localized very focally in the regions of the UF, SLF, and CGB, near the region of the paranasal sinuses. After we performed the FDR correction on all voxels within the FA and MD masks, the VBA showed similar results.

## DISCUSSION

The potential impact of paranasal sinus aeration status and mucosal disease on neuroimaging sequences susceptible to magnetic field inhomogeneity has not been previously reported. DTI is known to be vulnerable to susceptibility artifacts.<sup>5</sup> Most important, analyses of DTI parameters are used increasingly in research projects evaluating typical and atypical brain development in children and adolescents. Our study results show that the amount of air in the paranasal sinuses in close proximity to brain tissue influences the measurements of diffusion characteristics of adjacent WM. The highly regional effect of this impact is further supported by the results of the VBA. This outcome is likely caused by changes in susceptibility directly resulting from different amounts of air that are near the WM tracts of interest.

Previous studies have demonstrated that susceptibility effects can lead to misinterpretation of DTI parameters of the involved brain tissue.<sup>34-36</sup> At tissue-air interface, susceptibility values demonstrate more variation, leading to diminished quality of the local magnetic field and creating field inhomogeneities. The frequency shift in *k*-space results in a spatial shift of voxel intensity and thus images deviating from true brain anatomy.<sup>37-39</sup> If the shifted voxel is still within the volume of the calculated WM tract, there will be less effect on the mean FA value. We focused on major WM tracts, and some of the susceptibility effects from the DTI acquisition seen on the voxel level may have had less influence on the level of a WM tract. Tract-based DTI analyses are the workhorse in the current published studies investigating the microstructure of the pediatric brain.<sup>1-4</sup> We think that only focusing on voxel-based FA and MD would ignore the common practice in this research field. This study shows that the amount of air in the paranasal sinuses affects FA and MD values of the WM in close proximity to those sinuses and also translates into the effects on mean FA and MD values of some of the major WM tracts. Susceptibility distortions can potentially be diminished using geometric corrections of the structural image, estimate maps of  $B_0$  inhomogeneities acquired using gradient-echo scans, and estimates of the underlying distortions derived from additional data acquired using reversed phase-encoding.

Typically, FA and MD change in opposite directions; however, susceptibility effects can change them in a similar manner.<sup>40,41</sup> Because FA reflects directionality in diffusion, there is a more direct relation to WM microarchitecture, in contrast to MD.<sup>42,43</sup> Our results illustrate less influence of aerated-versus-nonaerated paranasal sinuses on mean MD values of major WM tracts than on FA values. MD values by themselves are nonspecific, however, and should be used in conjunction with other diffusion

tensor parameters.<sup>44</sup> The lower FA values in the nonaerated group likely better reflect the true underlying values because nonaerated sinuses lead to fewer susceptibility-related distortions. This reasoning is in line with previous studies showing that susceptibility distortion-correction methods cause reductions in whole-brain WM FA values and corresponding higher MD values.<sup>37,45</sup>

This study demonstrates the relevance of considering the extent of mucosal thickening or the degree of pneumatization of the paranasal sinuses in the region of the skull base (ie, as a covariate or using it in sensitivity analyses) before interpreting DTI parameters of the brain, especially in pediatric populations. In studies focusing on typical development of the pediatric brain, changes in DTI parameters of specific WM tracts, such as the ILF, UF, and CGB, are described.<sup>14</sup> Knowledge of potential factors that can modify the signal, such as nonaerated paranasal sinuses, is especially relevant when the study population includes a relative large sample of children between 3 and 8 years of age (peak age of inflammatory paranasal sinus disease<sup>7,8</sup>). In addition, because some neurodevelopmental disorders may increase the risk of sinusitis (eg, craniofacial syndromes, neuromuscular disorders),<sup>46,47</sup> it is important to incorporate knowledge of the potential effect of the degree of aeration of paranasal sinuses on DTI parameters in these study designs. Because we excluded the maxillary sinus from our analyses (due to the relatively large separation between the maxillary sinus and the anterior-inferior brain regions), we did not assess the potential effects of nonaerated maxillary sinuses on measurements of WM diffusion characteristics. This assessment could be an interesting focus for future research.

There are a number of strengths of the population-based study, including standardized DTI measurements obtained in a large sample derived from the general pediatric population. However, there are also limitations. We were unable to determine a distortion-correction factor due to the small number of children with completely nonaerated paranasal sinuses. In addition, the younger children did show more mucosal thickening and less pneumatization of the paranasal sinuses. Although we tried to take age differences into account, we cannot completely exclude residual confounding. Additionally, DTI phase maps (instead of field maps) were acquired in the study protocol. The lack of acquired field maps is a limitation of the study because we were able to create distortion maps to further illustrate the effect of air/nonaeration. To minimize the effect of geometric distortion, we applied a nonlinear registration of the FA maps to a study-specific EPI template in standard space, a method favoring other distortion-correction methods as shown in the literature.<sup>31</sup>

## CONCLUSIONS

Nonaeration of the paranasal sinuses is a common incidental finding on MR imaging of the pediatric brain. We demonstrate that the amount of mucosal thickening or the degree of pneumatization of the paranasal sinuses influences FA and, to a lesser degree, MD values of major WM tracts close to the skull base region in 6- to 9-year-old children.

**Disclosure forms** provided by the authors are available with the full text and PDF of this article at [www.ajnr.org](http://www.ajnr.org).

## REFERENCES

- López-Vicente M, Lamballais S, Louwen S, et al. **White matter microstructure correlates of age, sex, handedness and motor ability in a population-based sample of 3031 school-age children.** *Neuroimage* 2021;227:117643 CrossRef Medline
- Lebel C, Walker L, Leemans A, et al. **Microstructural maturation of the human brain from childhood to adulthood.** *Neuroimage* 2008;40:1044–55 CrossRef Medline
- Schmithorst VJ, Yuan W. **White matter development during adolescence as shown by diffusion MRI.** *Brain Cogn* 2010;72:16–25 CrossRef Medline
- Giorgio A, Watkins KE, Chadwick M, et al. **Longitudinal changes in grey and white matter during adolescence.** *Neuroimage* 2010;49:94–103 CrossRef Medline
- Atlas SW, ed. **Magnetic resonance imaging of the brain and spine.** Vol. 1. Lippincott Williams & Wilkins; 2009
- Tax CM, Vos SB, Leemans A. **Checking and Correcting DTI Data.** In: Van Hecke W, Emsel L, Sunaert S, eds. *Diffusion Tensor Imaging.* Springer-Verlag; 2016:127–50
- von Kalle T, Fabig-Moritz C, Heumann H, et al. **Incidental findings in paranasal sinuses and mastoid cells: a cross-sectional magnetic resonance imaging (MRI) study in a pediatric radiology department.** *Rofo* 2012;184:629–34 CrossRef Medline
- Gordts F, Clement PA, Destryker A. **Prevalence of sinusitis signs on MRI in a non-ENT pediatric population.** *Rhinology* 1997;35:154–57 Medline
- Jansen PR, Dremmen M, van den Berg A, et al. **Incidental findings on brain imaging in the general pediatric population.** *N Engl J Med* 2017;377:1593–95 CrossRef Medline
- Kim BS, Illes J, Kaplan RT. **Incidental findings on pediatric MR images of the brain.** *AJNR Am J Neuroradiol* 2002;23:1674–77 Medline
- Lim WK, Ram B, Fasulakis S, et al. **Incidental magnetic resonance image sinus abnormalities in asymptomatic Australian children.** *J Laryngol Otol* 2003;117:969–72 CrossRef Medline
- Scuderi AJ, Harnsberger HR, Boyer RS. **Pneumatization of the paranasal sinuses: normal features of importance to the accurate interpretation of CT scans and MR images.** *AJR Am J Roentgenol* 1993;160:1101–04 CrossRef Medline
- Adibelli ZH, Songu M, Adibelli H. **Paranasal sinus development in children: a magnetic resonance imaging analysis.** *Am J Rhinol Allergy* 2011;25:30–35 CrossRef Medline
- Krogsrud SK, Fjell AM, Tamnes CK, et al. **Changes in white matter microstructure in the developing brain: a longitudinal diffusion tensor imaging study of children from 4 to 11 years of age.** *Neuroimage* 2016;124:473–86 CrossRef Medline
- Mukherjee P, Miller JH, Shimony JS, et al. **Normal brain maturation during childhood: developmental trends characterized with diffusion-tensor MR imaging.** *Radiology* 2001;221:349–58 CrossRef Medline
- Jaddoe VW, Mackenbach JP, Moll HA, et al. **The Generation R Study: design and cohort profile.** *Eur J Epidemiol* 2006;21:475–84 CrossRef Medline
- White T, Muetzel RL, El Marroun H, et al. **Paediatric population neuroimaging and the Generation R Study: the second wave.** *Eur J Epidemiol* 2018;33:99–125 CrossRef Medline
- Basten M, van der Ende J, Tiemeier H, et al. **Nonverbal intelligence in young children with dysregulation: the Generation R Study.** *Eur Child Adolesc Psychiatry* 2014;23:1061–70 CrossRef Medline
- Oldfield RC. **The assessment and analysis of handedness: the Edinburgh inventory.** *Neuropsychologia* 1971;9:97–113 CrossRef Medline
- White T, El Marroun H, Nijs I, et al. **Pediatric population-based neuroimaging and the Generation R Study: the intersection of developmental neuroscience and epidemiology.** *Eur J Epidemiol* 2013;28:99–111 CrossRef Medline
- Lund VJ, Kennedy DW. **Staging for rhinosinusitis.** *Otolaryngol Head Neck Surg* 1997;117:S35–40 CrossRef
- Lin HW, Bhattacharyya N. **Diagnostic and staging accuracy of magnetic resonance imaging for the assessment of sinonasal disease.** *Am J Rhinol Allergy* 2009;23:36–39 CrossRef Medline
- Yousefi F, Mollabashi M, Shokri A, et al. **Magnetic resonance imaging study of incidental findings in the paranasal sinuses and ostiomeatal complex.** *Imaging Sci Dent* 2022;52:11–18 CrossRef Medline
- Smith SM, Jenkinson M, Woolrich MW, et al. **Advances in functional and structural MR image analysis and implementation as FSL.** *Neuroimage* 2004;23(Suppl 1):S208–19 CrossRef Medline
- Andersson JL, Sotiropoulos SN. **An integrated approach to correction for off-resonance effects and subject movement in diffusion MR imaging.** *Neuroimage* 2016;125:1063–78 CrossRef Medline
- Mulder TA, Kocavska D, Muetzel RL, et al. **Childhood sleep disturbances and white matter microstructure in preadolescence.** *J Child Psychol Psychiatry* 2019;60:1242–50 CrossRef Medline
- Muetzel RL, Mous SE, van der Ende J, et al. **White matter integrity and cognitive performance in school-age children: a population-based neuroimaging study.** *Neuroimage* 2015;119:119–28 CrossRef Medline
- de Groot M, Vernooij MW, Klein S, et al. **Improving alignment in tract-based spatial statistics: evaluation and optimization of image registration.** *Neuroimage* 2013;76:400–11 CrossRef Medline
- Dall'Aglia L, Xu B, Tiemeier H, et al. **Longitudinal associations between white matter microstructure and psychiatric symptoms in adolescence.** *medRxiv* 22279298;2022. <https://www.medrxiv.org/content/10.1101/2022.08.27.22279298v1>. Accessed September 30, 2022
- Luque Laguna PA, Combes AJE, Streffer J, et al. **Reproducibility, reliability and variability of FA and MD in the older healthy population: a test-retest multiparametric analysis.** *Neuroimage Clin* 2020;26:102168 CrossRef Medline
- Calhoun VD, Wager TD, Krishnan A, et al. **The impact of T1 versus EPI spatial normalization templates for fMRI data analyses.** *Hum Brain Mapp* 2017;38:5331–42 CrossRef Medline
- Benjamini Y, Hochberg Y. **Controlling the false discovery rate: a practical and powerful approach to multiple testing.** *J R Stat Soc* 1995;57:289–300 CrossRef
- Cohen J. *Statistical Power Analysis for the Behavioral Sciences.* Academic press, 2013
- Hiwatashi A, Kinoshita T, Moritani T, et al. **Hypointensity on diffusion-weighted MRI of the brain related to T2 shortening and susceptibility effects.** *AJR Am J Roentgenol* 2003;181:1705–09 CrossRef Medline
- Haris M, Gupta RK, Husain N, et al. **Measurement of DTI metrics in hemorrhagic brain lesions: possible implication in MRI interpretation.** *J Magn Reson Imaging* 2006;24:1259–68 CrossRef Medline
- Pfefferbaum A, Adalsteinsson E, Rohlfing T, et al. **Diffusion tensor imaging of deep gray matter brain structures: effects of age and iron concentration.** *Neurobiol Aging* 2010;31:482–93 CrossRef Medline
- Lahti K, Parkkola R, Jääsaari P, et al; PIPARI Study Group. **The impact of susceptibility correction on diffusion metrics in adolescents.** *Pediatr Radiol* 2021;51:1471–80 CrossRef Medline
- Huang H, Ceritoglu C, Li X, et al. **Correction of B0 susceptibility induced distortion in diffusion-weighted images using large-deformation diffeomorphic metric mapping.** *Magn Reson Imaging* 2008;26:1294–302 CrossRef Medline
- Embleton KV, Haroon HA, Morris DM, et al. **Distortion correction for diffusion-weighted MRI tractography and fMRI in the temporal lobes.** *Hum Brain Mapp* 2010;31:1570–87 CrossRef Medline
- Lebel C, Gee M, Camicioli R, et al. **Diffusion tensor imaging of white matter tract evolution over the lifespan.** *Neuroimage* 2012;60:340–52 CrossRef Medline
- Schmithorst VJ, Wilke M, Dardzinski BJ, et al. **Correlation of white matter diffusivity and anisotropy with age during childhood and adolescence: a cross-sectional diffusion-tensor MR imaging study.** *Radiology* 2002;222:212–18 CrossRef Medline



42. Mukherjee P, Berman JI, Chung SW, et al. **Diffusion tensor MR imaging and fiber tractography: theoretic underpinnings.** *AJNR Am J Neuroradiol* 2008;29:632–41 CrossRef Medline
43. Mukherjee P, Chung SW, Berman JI, et al. **Diffusion tensor MR imaging and fiber tractography: technical considerations.** *AJNR Am J Neuroradiol* 2008;29:843–52 CrossRef Medline
44. Sijens PE, Irwan R, Potze JH, et al. **Relationships between brain water content and diffusion tensor imaging parameters (apparent diffusion coefficient and fractional anisotropy) in multiple sclerosis.** *Eur Radiol* 2006;16:898–904 CrossRef Medline
45. Irfanoglu MO, Sarlls J, Nayak A, et al. **Evaluating corrections for eddy-currents and other EPI distortions in diffusion MRI: methodology and a dataset for benchmarking.** *Magn Reson Med* 2019;81:2774–87 CrossRef Medline
46. Leo G, Triulzi F, Incorvaia C. **Diagnosis of chronic rhinosinusitis.** *Pediatr Allergy Immunol* 2012;23(Suppl 22):20–26 CrossRef Medline
47. Heath J, Hartzell L, Putt C, et al. **Chronic rhinosinusitis in children: pathophysiology, evaluation, and medical management.** *Curr Allergy Asthma Rep* 2018;18:37 CrossRef Medline

# Fetal MR Imaging Anatomy of the Transverse Temporal Gyrus (Heschl Gyrus)

Eleonora Piccirilli, Chiara Marchetti, Valentina Panara, Claudio Celentano, Francesco D'Antonio, Stefano Sensi, Andrea Righini, and Massimo Caulo

## ABSTRACT

**BACKGROUND AND PURPOSE:** The human auditory system develops early in fetal life. This retrospective MR imaging study describes the in vivo prenatal anatomic development of the transverse temporal gyrus (Heschl gyrus) site of the primary auditory cortex.

**MATERIALS AND METHODS:** Two hundred seventy-two MR imaging studies of the fetal brain (19–39 weeks' gestational age) acquired from a single institution's 1.5T scanner were retrospectively examined by 2 neuroradiologists. MR imaging with pathologic findings and extreme motion artifacts was excluded. Postnatal Heschl gyrus landmarks were used as a reference on T2-weighted ssFSE sequences in the 3 orthogonal planes. The frequency of the Heschl gyrus was reported for gestational age, hemisphere, and planes. Descriptive statistics and a McNemar test were performed.

**RESULTS:** Two hundred thirty MR imaging studies were finally included. Fetal brains were divided by gestational age (in weeks) into 8 groups (parentheses indicate the number of observations): 19–21 (29), 22–23 (32), 24–25 (21), 26–27 (18), 28–29 (35), 30–31 (30), 32–33 (33) and >34 (32). The Heschl gyrus appeared on MR imaging between 24 and 25 weeks' gestational age (14/21 fetuses, 67%) and was visible in all fetuses after the 28th week of gestation. By its appearance (24–28 weeks' gestational age), the sagittal plane was the most sensitive in its detectability. After 28–29 weeks' gestational age, the Heschl gyrus was evident in all acquisition planes and fetuses. Results did not differ between hemispheres.

**CONCLUSIONS:** The Heschl gyrus appears on MR imaging at 24–25 weeks' gestational age, paralleling the functional activation of the auditory system. We propose the Heschl gyrus as an early additional MR imaging marker of fetal brain development.

**ABBREVIATIONS:** GA = gestational age; HG = Heschl gyrus; SI = sulcus intermedius; ssFSE = single-shot fast spin-echo

The human auditory system is a unimodal sensory system developed to receive, interpret, and respond to complex language and plays a major role in musical skills.<sup>1</sup> As the acoustic waves reach the auditory receptor cells in the organ of Corti,

sound vibrations are transformed into electric signals. Then, the acoustic nerve transmits the auditory stimuli to the cochlear nuclei in the brainstem, and signals ascend through the auditory pathway to the auditory cortex.

The primary auditory cortex is located in the transverse temporal gyrus and was first described in 1878 by Heschl on post-mortem specimens, and since then, it has been identified as the Heschl gyrus (HG).<sup>2–4</sup> From an evolutionary perspective, the HG is relatively new because it can be found only in a subset of chimpanzee brains, while it is not present in the macaque monkey.<sup>5,6</sup>

The HG runs diagonally across the superior temporal plane, hidden in the depth of the Sylvian fissure.<sup>4</sup> Its characteristic shape and location can be readily identified on MR images using specific landmarks.<sup>4</sup> Axial images passing through the interthalamic adhesion identify the HG as a thin gyrus running anterior-laterally from the posterior aspect of the insula to the lateral convexity. Coronal and sagittal images passing through the planum temporale identify the HG as having a mushroom- or omega-like shape, respectively.<sup>7</sup> In adults, the inconstant presence of the sulcus

Received June 11, 2023; accepted after revision August 30.

From the Department of Neuroscience (E.P., S.S., M.C.), Imaging and Clinical Sciences, and Center for Fetal Care and High-Risk Pregnancy (F.D.), Department of Obstetrics and Gynecology, University of Chieti, Chieti, Italy; Neuro-Oncology Unit (E.P.), Department of Imaging, Bambino Gesù Children's Hospital, Istituto di Ricovero e Cura a Carattere Scientifico, Rome, Italy; Radiology Unit (C.M.), San Pio Da Pietrelcina Hospital, Vasto, Chieti, Italy; Department of Radiology (V.P., M.C.), Santissima Annunziata Hospital, Chieti, Italy; Obstetrics and Gynaecology Unit (C.C.), Santo Spirito Hospital, Pescara, Italy; and Neuroradiology Unit (A.R.), Pediatric Radiology Department, Vittore Buzzi Children's Hospital, Milan, Italy; ITAB-Institute of Advanced Biomedical Technologies, Department of Neuroscience, Imaging and Clinical Sciences (E.P., C.M., V.P., S.S., M.C.), University G. d'Annunzio of Chieti-Pescara, Chieti, Italy.

Eleonora Piccirilli and Chiara Marchetti share first authorship.

Please address correspondence to Massimo Caulo, MD, PhD, Department of Neuroscience, Imaging and Clinical Sciences, Institute for Advanced Biomedical Technologies, University G. d'Annunzio of Chieti-Pescara, Via Luigi Polacchi 11, 66100 Chieti, Italy; e-mail: massimo.caulo@unich.it

<http://dx.doi.org/10.3174/ajnr.A8026>

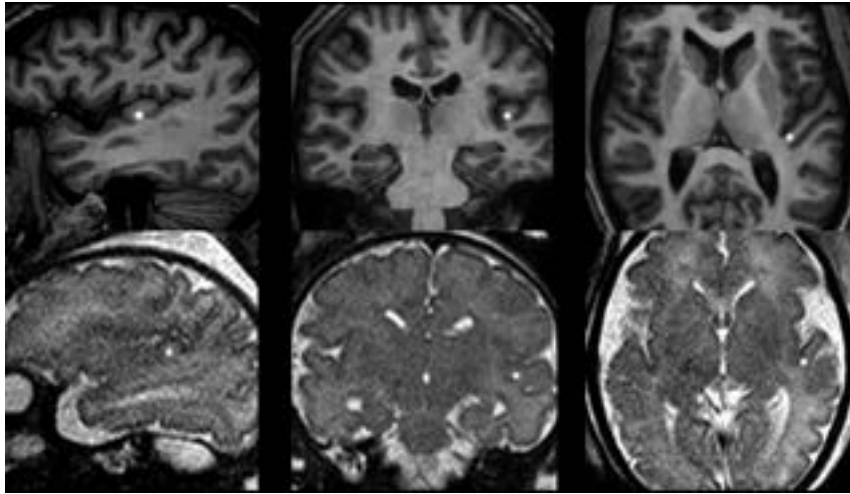


**FIG 1.** Representative images of adult (*upper row*) and fetal (*lower row*, 28 weeks' GA) HGs on the 3 orthogonal planes. Adult landmarks were used to correctly identify the HG on the fetal brains (*asterisk*).

intermedius (SI) may split the HG, leading to different inter- or intraindividual configurations.<sup>6</sup> Morphologic variability has been described more often in the right than in the left hemisphere.<sup>8</sup>

Unlike vision, in which the visual experience begins after birth, the auditory system develops in utero and fully functions at birth. Its functional development begins around 25–29 weeks' gestation when the ganglion cells of the spiral nucleus in the cochlea connect the inner cells to the brainstem and the temporal lobe.<sup>1</sup> By 32 weeks' gestational age (GA), fetuses can discriminate tones, mothers' voices, and simple music.<sup>9</sup> Bilateral activation of the HG by maternal internal acoustic stimulus was demonstrated using blood oxygen level–dependent fMRI between 33 and 38 weeks' GA.<sup>9</sup> Furthermore, fetuses at 28–32 weeks' GA show a heart rate increase to music stimulation, indicating in utero functioning.<sup>10</sup>

Such extensive functional characterization of the auditory cortex in fetuses contrasts with the limited knowledge of its prenatal anatomic development. To date, relatively few studies have concentrated on the prenatal anatomic development of the HG. By sectioning 207 fetal brains in the 3 orthogonal planes, Chi et al<sup>11</sup> could recognize the HG from 31 weeks' gestation.

More recently, López Ramón Y Cajal<sup>12</sup> used 3D ultrasound to characterize the in vivo development of the HG in a cohort of 224 human fetuses between 18 and 41 weeks' gestation.

Remarkably, the anatomic development of the HG has never been investigated using prenatal MR imaging, and currently, it is not included among potential markers of normal brain development in clinical fetal MR imaging. Thus, the purpose of the present study was to describe the anatomic development of the transverse temporal gyrus assessed on fetal brain MR imaging.

## MATERIALS AND MATERIALS

### Study Population

Due to the retrospective nature of the study, the need for ethics committee approval was waived by our institutional review board.

A total of 272 fetal MR images were obtained between June 2019 and August 2022 at the Institute for Advanced Biomedical Technologies of the G. D'Annunzio Chieti-Pescara University. Scans were then retrospectively evaluated.

Fetuses underwent MR imaging for the following indications:

- Suspicion of abnormal CNS and non-CNS features (ventricular dilation, anomalies of cortical development, posterior fossa abnormalities, abnormal fetal brain biometry, extracerebral malformations) as indicated by fetal ultrasound
- Pregnancy at risk: toxoplasmosis, rubella, cytomegalovirus, herpes simplex, and HIV (TORCH) maternal seroconversion, intrauterine growth restriction, twin-to-twin transfusion syndrome
- Family history of genetic disorders.

Scans of fetal brains with physiologic gyration and biometric parameters at MR imaging (according to Parazzini et al<sup>13</sup> [younger than 24 weeks' GA] and to Garel et al<sup>14</sup> [older than 24 weeks' GA]) were included in the study.<sup>15</sup> Fetal brains with pathologic findings on MR imaging (ie, ventriculomegaly, agenesis of the corpus callosum, posterior fossa malformations, intracerebral hemorrhage, stroke, and malformations of cortical development) were excluded and underwent postnatal MR imaging.

### Fetal MR Imaging

Images were acquired on a 1.5T scanner (Achieva; Philips Healthcare) using a 16-channel SENSE XL Torso Coil (Philips Healthcare). Patients were scanned supine. When feasible, the mother was fasting for at least 4 hours to limit fetal motion artifacts.

The standardized fetal brain MR imaging protocol included single-shot fast spin-echo T2-weighted sequences (ssFSE-T2-weighted TSE) in the 3 orthogonal planes (section thickness = 3 mm, in-plane resolution = 1.0–1.2 mm<sup>2</sup>), axial T1-weighted TSE sequences, and DWI (*b* factors: *b*=0, *b*=500, and *b*=700).

The size of the fetal head determined the FOV.

### MR Imaging Analysis

All MR images were analyzed in consensus by 2 neuroradiologists with >5 years' experience in prenatal neuroradiology. Postnatal HG landmarks were used as a reference on T2WI (Fig 1). On axial sections, the HG was visualized on the slice passing through the interthalamic adhesion as an oblique structure of the planum temporale with a posterior-anterior and medial-lateral dislocation.<sup>7,16</sup> On sagittal and coronal sections, the HG appears as a protrusion above the posterior part of the superior temporal gyrus (Fig 1).<sup>4–6</sup>

MR images were analyzed in descending order of GA to increase HG detection in earlier stages of fetal life.

On each plane, the HG was classified as “visible” when identified in at least 1 scan plane and “not visible” when uncertain or not identified.

We also tried to evaluate SI detectability. Because the SI splits the HG, leading to a heart-shaped configuration in the sagittal plane, this characteristic feature was used for identification (Fig 2).

### Statistical Analysis

HG frequencies were reported for GAs and hemispheres. A McNemar test was performed to compare HG detection between hemispheres using SPSS Statistics for Mac, Version 25.0 (IBM) ( $P < .05$ ).

## RESULTS

### Fetal Demographics

Of the initial 272 fetal MR images, 230 were eventually included. Seventeen examinations were excluded due to pathologic findings (ventriculomegaly, callosal agenesis, posterior fossa malformations, cerebral hemorrhages, and abnormalities of cortical development), and 25, due to motion artifacts (Fig 3).

The GA ranged from 19 to 39 weeks (mean, 28 weeks; median, 29 weeks).

The cases were subdivided into eight 2-week GA groups: 19–21 GA (29 fetuses), 22–23 GA (32 fetuses), 24–25 GA (21 fetuses),

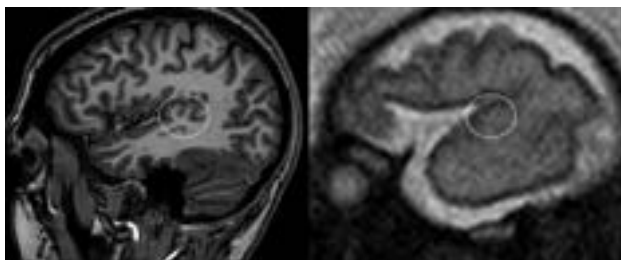


**FIG 2.** The SI of the HG in representative adult (*left*) and fetal (*right*, 28 weeks' GA) brains. The characteristic adult heart-shaped configuration in the sagittal plane was used for SI identification on fetal scans.

26–27 GA (18 fetuses), 28–29 GA (35 fetuses), 30–31 GA (30 fetuses), 32–33 GA (33 fetuses), and >34 GA (32 fetuses). The distribution of fetuses according to GA is given in Figs 3 and 4.

The 2-week GA range was chosen because no substantial changes in gyrational patterns are observed in this timeframe.<sup>15</sup> Fetuses between 34 and 39 weeks' GA were grouped because by the 34th week of GA, all the primary sulci are already present on MR imaging.<sup>15</sup>

### HG Fetal Development

The HG became visible between 24 and 25 weeks' GA and was detectable in 14/21 fetuses (67% of cases); between 26 and 27 weeks' GA, the HG was detectable in 17/18 fetuses (94% of cases); and by the 28th week of GA onward, the HG was always detectable (Table).

The chart in Figs 4 and 5 summarizes the time of HG appearance in each plane. Figure 6 shows HG changes with GA as assessed on 3 orthogonal planes.

The HG becomes detectable in the earliest gestational weeks of the sagittal plane (24–25 weeks). The structure emerges as a little hump on the posterior part of the superior temporal gyrus. It then reaches a mushroom-like shape abutting the Sylvian fissure from 28 to 29 weeks' GA and further beyond.

On the coronal sections, the HG begins to be visible from 26 to 27 weeks' GA in the upper and most medial part of the superior temporal gyrus. In these earliest stages, the HG emerges as a little point. With GA progression, the HG becomes an evident protrusion, and from the 34 weeks' GA onward, it appears as a hill-shaped structure.

On axial sections, the HG begins to be visible around 26 weeks' GA, when it emerges as a blurred oblique gyrus with a posterior-anterior and medial-lateral course, deep in the lateral fissure. The HG becomes more defined in the intermediate stages of gestation (28–29 and 30–31 weeks) and reaches a thin,

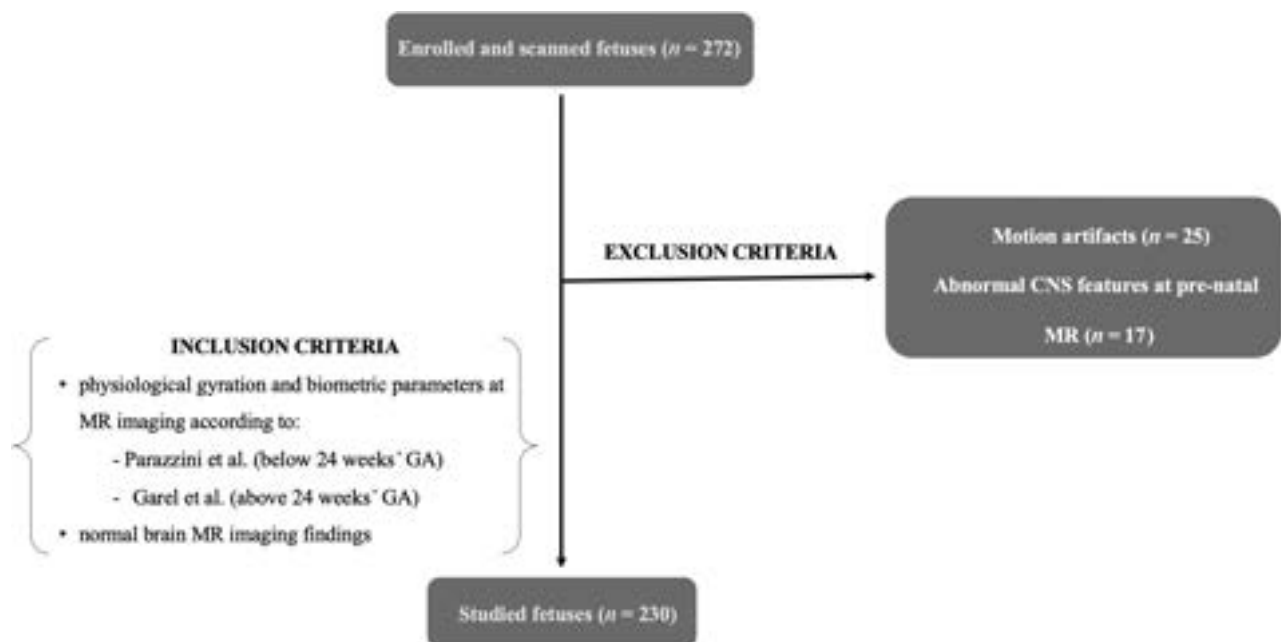


**FIG 3.** Flow chart detailing inclusion and exclusion criteria.



undulated gyral morphology at the edges of the Sylvian fissure in more advanced GA stages (>32 weeks).

By 28–29 weeks' GA, the HG becomes visible in all fetuses and planes (Table and Figs 5 and 6).

**HG and SI**

The SI becomes detectable from the 28th to 29th week onward. Of the 103 fetal brains with a GA of >28–29 weeks, the SI was detectable in 30 fetuses (29%).

**HG and Hemispheric Differences**

No statistically significant differences existed between right and left HG detection ( $P = .38$ ).

**DISCUSSION**

MR imaging has been used to describe the normal anatomy of the HG in adults and its abnormal development.<sup>2,8,17</sup> Fetal maturational changes of the HG have been studied using only ultrasound or in ex vivo specimens.<sup>12,18</sup> Our study focused on the description of HG development as assessed by fetal MR imaging.

We demonstrated that the HG becomes detectable during the second trimester of gestation, specifically between the 24th and 25th week, and that it is visible on MR images in all fetuses from 28 weeks.

Similar to other in vivo sulcations detected by Garel et al,<sup>14</sup> there was a 2-week mean lag time between the first HG detection and its presence in >75% of the cases.

We hypothesized that the early identification of the HG is driven by auditory development during intrauterine life. During

embryogenesis, sulci and gyri develop with a predefined and predictable sequence that reflects their phylogeny and hierarchy so that gyri containing eloquent areas are the first to appear.<sup>19,20</sup>

Such anatomic development likely underlies a progressive functional maturation. The auditory activity has been demonstrated to begin in utero, because the processing of acoustic stimuli is part of the fetal experience.<sup>1,21</sup> Graven and Browne<sup>1</sup> found that the human auditory system becomes functional at around 25 weeks' GA, thereby overlapping with the time in which the HG becomes macroscopically detectable. Later, as early as 27 gestational weeks when the HG becomes more defined, MEG studies demonstrated that fetuses can perceive sounds and discriminate them.<sup>22,23</sup>

At the initial time of its appearance (24–25 weeks' GA), the HG was best demonstrated on the sagittal plane, followed by the coronal plane.

As the HG gets thicker and bulges toward the Sylvian fissure, morphing to its final, adultlike shape, it becomes visible on the axial plane, approximately 4 weeks after its initial detection on the sagittal plane.

The HG tends to develop in an anterior-posterior and oblique and upward fashion, thus explaining the greater sensitivity of the sagittal and coronal planes in its recognition during the earliest stages of gestation.

Likewise, the minimal width of the HG before 28 weeks' GA may account for its limited detectability in the axial plane. It is known that the prenatal recognizability of gyri on imaging usually lags behind their histologic appearance. Our results raise an apparent contradiction between histopathologic and MR imaging data, because the original observations of Chi et al<sup>18</sup> date the appearance of the HG at 31 weeks' GA as assessed on postmortem fetal brain specimens. However, this discrepancy may stem from methodologic issues. In that study,<sup>18</sup> only 20% of the fetal brains were sectioned in the sagittal plane, which we found to be the most sensitive in the earliest phases of HG appearance, possibly owing to its pattern of growth and orientation. Therefore, their relatively late finding<sup>18</sup> likely reflects an underestimation of the actual timing of the appearance of HG. Moreover, brain fixation and consequent tissue shrinking may have impaired the detection of smaller structures, including the HG, in younger fetuses.

Some comments are also required on the study of López Ramón Y Cajal,<sup>12</sup> which, with intrauterine ultrasound, detected the HG well before 24 weeks' gestation. Intrinsic technical differences between ultrasound and prenatal MR imaging, particularly the lower spatial resolution of the latter, should be considered. Therefore, ultrasound data cannot be used as a reference in prenatal MR imaging practice. Both normative data, ours and y Cajal's, need to be confirmed by further studies.

Due to the left hemispheric dominance for language, interhemispheric morphologic differences of the HG have been postnatally investigated in

**Frequencies of HG appearance in the three orthogonal planes according to GA groups**

GA (week)	Sagittal Plane (%)	Coronal Plane (%)	Axial Plane (%)
19–21	0	0	0
22–23	0	0	0
24–25	67	9.5	0
26–27	94	88.8	67
28–29	100	100	100
30–31	100	100	100
32–33	100	100	100
34–39	100	100	100

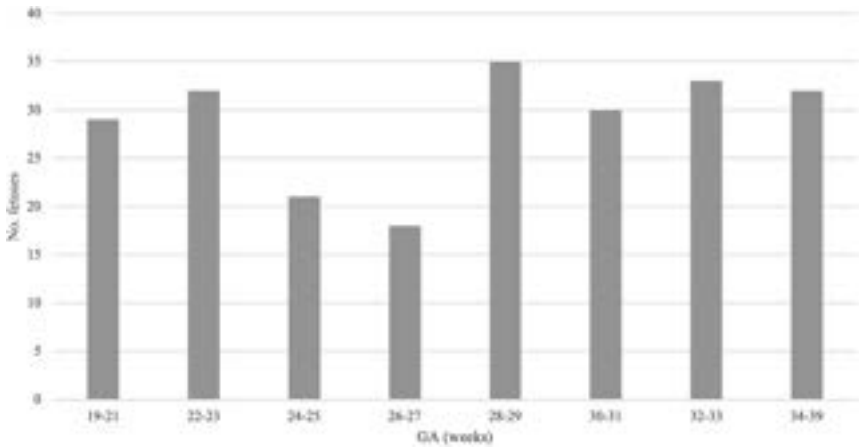


**FIG 4.** Distribution of the number of fetuses as a function of GA.

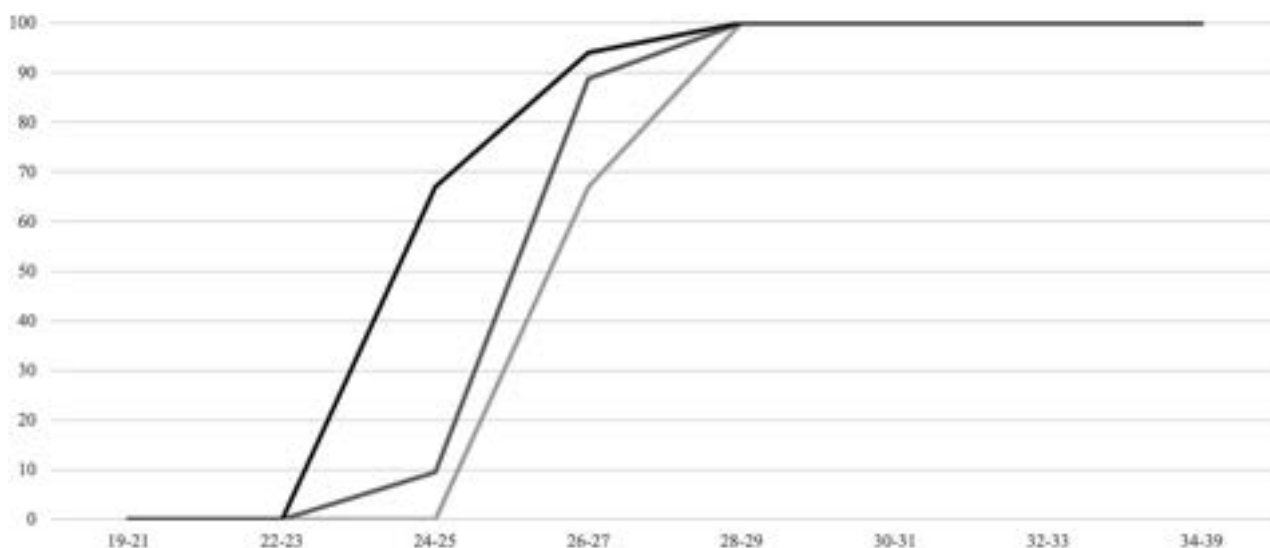


**FIG 5.** Detection of the HG on sagittal (black line), coronal (gray line), and axial (light gray line) T2-weighted SSf MR images with increasing GA (in weeks).

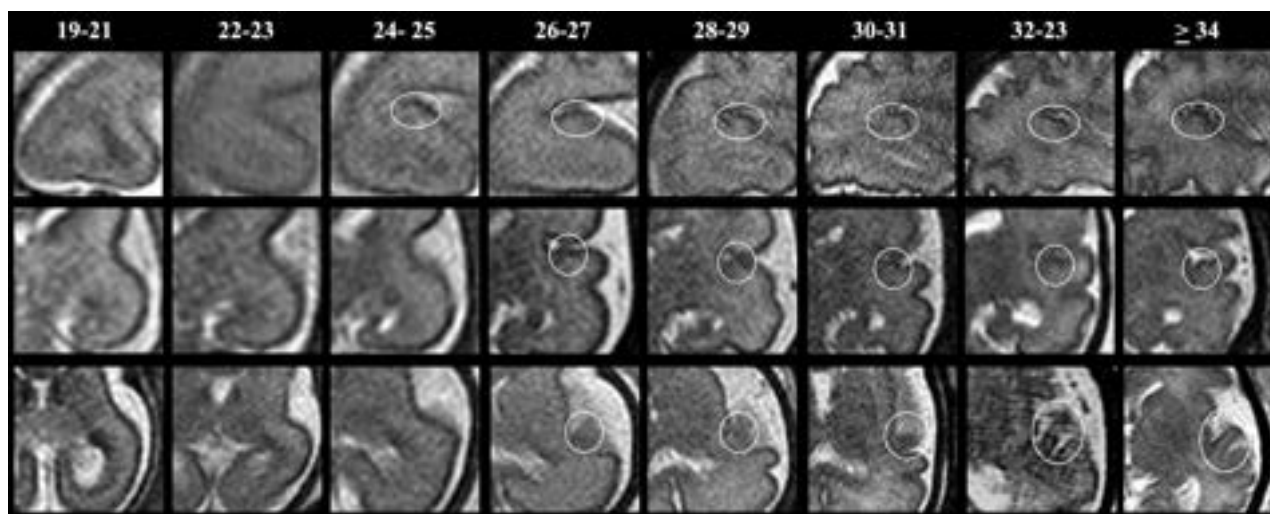


**FIG 6.** SSf T2WI sagittal (upper row), coronal (middle row), and axial (lower row) MR images illustrating changes in HG morphology with increasing GA.

relation to auditory processing. Furthermore, HG high morphologic variability across individuals and brain hemispheres has been used as a surrogate for functional lateralization.<sup>24</sup> Thus, the HG might appear in one hemisphere before the other, though the link between interhemispheric anatomic variability and function remains elusive because the results are inconsistent among studies. Indeed, a rightward asymmetry, a leftward asymmetry, and no asymmetry have all been reported.<sup>25-27</sup> Such inconsistencies may be biased by the studied features (gyrification versus morphometry/volumetry), handedness, and age, but also by the different examination methods and the complexity of the HG and its sulcal landmarks.<sup>4,8</sup>

Anatomic investigations of fetuses have revealed that the right HG appears 1-2 weeks earlier than the left and is a more frequent side of duplication.<sup>11</sup> On the contrary, although the left HG seemed to slightly anticipate the right in our cohort, we found no significant differences in HG appearance between the 2

hemispheres. Similarly, López Ramón Y Cajal<sup>12</sup> did not observe between-hemisphere differences. Our findings do not necessarily contradict those in previous studies. In that respect, although Chi et al<sup>11</sup> reported slight anticipation of the right HG development, statistical significance was not sought. Moreover, the most frequent finding in both MR imaging and postmortem studies is a symmetric single HG in adults,<sup>2,4,8</sup> thus questioning whether interhemispheric anatomic differences can be considered a reliable marker of functional lateralization.

To add to the complexity of the matter, our findings seem to question whether fetuses exhibit anatomic asymmetry in this area. This feature could emerge later in life as an advantage in sound processing or due to multiple influences. Of note, given the resolution constraints of the sequences used, we did not search for the possibility of hemispheric differences in size and morphology of the HG. In this regard, high-resolution volumetric sequences, such as a 3D-T2 sampling perfection with application-

optimized contrasts by using different flip angle evolution (SPACE sequence; Siemens) or volume isotropic turbo spin-echo acquisition (VISTA), together with the use of stronger magnetic fields allowing higher image quality, would help.

In adults, the HG is variably divided by the presence and the depth of the SI into 4 anatomic variants, single HG, common stem duplication, complete posterior duplication, and multiple duplications that protrude over the posterior part of the superior temporal gyrus in the coronal and sagittal slices as a single omega, a mushroom, a heart, a bow tie, or 2 separate S.<sup>4</sup> Due to the higher consistency, we used this peculiar heart-shaped configuration of the HG in the sagittal plane as a marker of its presence.

We found that the SI can be detected from 28 to 29 weeks' GA, with a prevalence of 29%. Our results are similar to the reported frequency, ranging between 24% and 33%, in prenatal and postnatal subjects.<sup>4,12</sup>

However, the SI is a very thin structure. Thus, the resolution threshold of our sequences combined with motion artifacts may have contributed to underestimating its prevalence. The section-thickness constraints have also prevented us from reaching greater anatomic detail.

HG duplication is considered a physiologic, anatomic variant, usually associated with phonologic and musical expertise.<sup>28</sup> Nonetheless, HG duplication has been proved to be an important clinical finding. Its increased presence has been reported in patients with learning disabilities, autism, and neuropsychiatric disorders.<sup>29–31</sup> The link between the presence of SI in fetal brains and its clinical and functional significance warrants further investigation.

The study has limitations, including its retrospective design. Also, another difficulty we encountered was the limited spatial resolution of 2D sequences since high-resolution 3D T2 images became part of our routine protocol from January 2023. High-resolution 3D-T2 sequences are of great value in fetal brain biometry to obtain proper orthogonal planes. We also recognize that smaller anatomic structures such as the SI might have been underestimated. However, previous studies on fetal gyration mainly relied on 2D images, which represent the current spatial resolution of prenatal MR imaging to assess primary and secondary sulcation processes. Finally, while beyond the scope of our article, a certain limitation of this study is that clinical correlations between the appearance timeline of the HG and disorders were not explored.

## CONCLUSIONS

The HG can be detected on fetal brain MR imaging from 24 to 25 weeks' GA onward, conceivably around the time the auditory system becomes functional. Our normative data about the timing of HG detection could represent an additional marker to be applied to clinical fetal MR imaging.

**Disclosure forms** provided by the authors are available with the full text and PDF of this article at [www.ajnr.org](http://www.ajnr.org).

## REFERENCES

- Graven SN, Browne JV. **Auditory development in the fetus and infant.** *Newborn Infant Nurs Rev* 2008;8:187–93 CrossRef
- Penhune V, Zatorre R, MacDonald J, et al. **Interhemispheric anatomical differences in human primary auditory cortex: probabilistic mapping and volume measurement from magnetic resonance scans.** *Cereb Cortex* 1996;6:661–72 CrossRef Medline
- Khalighinejad B, Patel P, Herrero JL, et al. **Functional characterization of human Heschl's gyrus in response to natural speech.** *Neuroimage* 2021;235:118003 CrossRef Medline
- Abdul-Kareem IA, Sluming V. **Heschl gyrus and its included primary auditory cortex: structural MRI studies in healthy and diseased subjects.** *J Magn Reson Imaging* 2008;28:287–99 CrossRef Medline
- Moerel M, De Martino F, Formisano E. **An anatomical and functional topography of human auditory cortical areas.** *Front Neurosci* 2014;8:225 CrossRef Medline
- Benner J, Wengenroth M, Reinhardt J, et al. **Prevalence and function of Heschl's gyrus morphotypes in musicians.** *Brain Struct Funct* 2017;222:3587–603 CrossRef Medline
- Yousry TA, Fesl G, Büttner A, et al. **Heschl's gyrus: anatomic description and methods of identification in MRI.** *Int J Neuroradiol* 1997;3:2–12
- Marie D, Jobard G, Crivello F, et al. **Descriptive anatomy of Heschl's gyri in 430 healthy volunteers, including 198 left-handers.** *Brain Struct Funct* 2015;220:729–43 CrossRef Medline
- Goldberg E, McKenzie CA, de Vrijer B, et al. **Fetal response to a maternal internal auditory stimulus.** *J Magn Reson Imaging* 2020;52:139–45 CrossRef Medline
- Kisilevsky BS, Hains S, Jacquet AY, et al. **Maturation of fetal responses to music.** *Dev Sci* 2004;7:550–59 CrossRef Medline
- Chi JG, Dooling EC, Gilles FH. **Left-right asymmetries of the temporal speech areas of the human fetus.** *Arch Neurol* 1977;34:346–48 CrossRef Medline
- López Ramón Y Cajal C. **Antenatal study of the Heschl's gyrus: the first step to understanding learning.** *Med Hypotheses* 2019;130:109290 CrossRef Medline
- Parazzini C, Righini A, Rustico M, et al. **Magnetic resonance imaging: brain normal linear biometric values below 24 gestational weeks.** *Neuroradiology* 2008;50:877–83 CrossRef Medline
- Garel C, Chantrel E, Elmaleh M, et al. **Fetal MRI: normal gestational landmarks for cerebral biometry, gyration and myelination.** *Childs Nerv Syst* 2003;19:422–25 CrossRef Medline
- Garel C, Chantrel E, Brisse H, et al. **Fetal cerebral cortex: normal gestational landmarks identified using MR imaging.** *AJNR Am J Neuroradiol* 2001;22:184–89 Medline
- Simon E, Perrot X, Linne M, et al. **Morphometry and localization of the temporal transverse Heschl's gyrus in magnetic resonance imaging: a guide for cortical stimulation of chronic tinnitus.** *Surg Radiol Anat* 2013;35:115–24 CrossRef Medline
- Leonard CM, Puranik C, Kuldau JM, et al. **Normal variation in the frequency and location of human auditory cortex landmarks. Heschl's gyrus: where is it?** *Cereb Cortex* 1998;8:397–406 CrossRef Medline
- Chi JG, Dooling EC, Gilles FH. **Gyral development of the human brain.** *Ann Neurol* 1977;1:86–93 CrossRef Medline
- Das S, Bal K, Bhattacharjee S. **Morphological development of sulci in fetal brain: an anatomical study.** *Asian J Med Sci* 2022;13:45–50 CrossRef
- Nishikuni K, Ribas GC. **Study of fetal and postnatal morphological development of the brain sulci.** *J Neurosurg Pediatr* 2013;11:1–11 CrossRef Medline
- Ghio M, Cara C, Tettamanti M. **The brain readiness for speech processing: a review on foetal development of auditory and primordial language networks.** *Neurosci Biobehav Rev* 2021;128:709–19 CrossRef Medline
- Schleussner E, Schneider U. **Developmental changes of auditory-evoked fields in fetuses.** *Exp Neurol* 2004;190(Suppl 1):S59–64 CrossRef Medline
- Draganova R, Eswaran H, Murphy P, et al. **Serial magnetoencephalographic study of fetal and newborn auditory discriminative evoked responses.** *Early Hum Dev* 2007;83:199–207 CrossRef Medline

24. Dorsaint-Pierre R, Penhune VB, Watkins KE, et al. **Asymmetries of the planum temporale and Heschl's gyrus: relationship to language lateralization.** *Brain* 2006;129:1164–76 CrossRef Medline
25. Galaburda A, Sanides F. **Cytoarchitectonic organization of the human auditory cortex.** *J Comp Neurol* 1980;190:597–610 CrossRef Medline
26. Economo C, Horn L. **Gyral relief, size, and cortical architectonics of the supratemporal surface: their individual and lateral differences.** *Z Ges Neurol Psychiatr* 1930;130:678–757
27. Campain R, Minckler J. **A note on the gross configurations of the human auditory cortex.** *Brain Lang* 1976;3:318–23 CrossRef Medline
28. Turker S, Reiterer SM, Seither-Preisler A, et al. **“When music speaks”: auditory cortex morphology as a neuroanatomical marker of language aptitude and musicality.** *Front Psychol* 2017;8:2096 CrossRef Medline
29. Leonard CM, Eckert MA, Lombardino LJ, et al. **Anatomical risk factors for phonological dyslexia.** *Cereb Cortex* 2001;11:148–57 CrossRef Medline
30. Prigge MD, Bigler ED, Fletcher PT, et al. **Longitudinal Heschl's gyrus growth during childhood and adolescence in typical development and autism.** *Autism Res* 2013;6:78–90 CrossRef Medline
31. Takahashi T, Sasabayashi D, Takayanagi Y, et al. **Heschl's gyrus duplication pattern in individuals at risk of developing psychosis and patients with schizophrenia.** *Front Behav Neurosci* 2021;15:647069 CrossRef Medline



# Factors Predictive of Treatment Success in CT-Guided Fibrin Occlusion of CSF-Venous Fistulas: A Multicenter Retrospective Cross-Sectional Study

Andrew L. Callen, Lalani Carlton Jones, Vincent M. Timpone, Jack Pattee, Daniel J. Scoffings, David Butteriss, Thien Huynh, Peter Y. Shen, and Mark D. Mamlouk



## ABSTRACT

**BACKGROUND AND PURPOSE:** CSF-to-venous fistulas contribute to spontaneous intracranial hypotension. CT-guided fibrin occlusion has been described as a minimally invasive treatment strategy; however, its reproducibility across different institutions remains unclear. This multi-institution study evaluated the clinical and radiologic outcomes of CT-guided fibrin occlusion, hypothesizing a correlation among cure rates, fibrin injectate spread, and drainage patterns.

**MATERIALS AND METHODS:** A retrospective evaluation was conducted on CT-guided fibrin glue treatment in patients with CSF-to-venous fistulas from 6 US and UK institutions from 2020 to 2023. Patient information, procedural characteristics, and injectate spread and drainage patterns were examined. Clinical improvement assessed through medical records served as the primary outcome.

**RESULTS:** Of 119 patients at a mean follow-up of 5.0 months, fibrin occlusion resulted in complete clinical improvement in 59.7%, partial improvement in 34.5%, and no improvement in 5.9% of patients. Complications were reported in 4% of cases. Significant associations were observed between clinical improvement and concordant injectate spread with the fistula drainage pattern ( $P = .0089$ ) and pretreatment symptom duration ( $P < .001$ ). No associations were found between clinical improvement and cyst puncture, intravascular extension, rebound headache, body mass index, age, or number of treatment attempts.

**CONCLUSIONS:** Fibrin occlusion performed across various institutions shows cure when associated with injectate spread matching the CVF drainage pattern and shorter pretreatment symptom duration, emphasizing the importance of accurate injectate placement and early intervention.

**ABBREVIATIONS:** BMI = body mass index; CTM = CT myelography; CVF = CSF-to-venous fistula; SIH = spontaneous intracranial hypotension

CSF-to-venous fistulas (CVFs) have been increasingly recognized as a cause of spontaneous intracranial hypotension (SIH) since their first description in 2014.<sup>1</sup> Initially, surgical ligation of the associated nerve root or adjacent draining veins was

the primary treatment strategy for CVF.<sup>2</sup> More recently, less invasive treatment strategies have been described with high degrees of efficacy, including fibrin occlusion and transvenous embolization.<sup>3,4</sup> Fibrin occlusion is performed percutaneously using either fluoroscopic or CT guidance, whereas transvenous embolization is performed via an endovascular approach using a liquid embolic agent under live fluoroscopy. Both procedures have been described by a few quaternary SIH referral centers as safe, having low adverse effect profiles and relatively high rates of radiologic and clinical improvement.<sup>5,6</sup> However, the replicability of these techniques and outcomes across other institutions and patient populations is unknown.

The use of fibrin sealant as a neurosurgical adjunct for postoperative CSF leaks is well-known, and its use under image guidance for treatment of SIH has been documented since at least 2004.<sup>7</sup> The relatively high cure rates described in the 2021 reports of CVF fibrin occlusion were somewhat surprising, given that prior reports stated minimal response to epidural patching.<sup>3,8</sup> However, unlike traditional epidural patching, the fibrin occlusion technique described needle positioning at the junction of the meningeal diverticulum and/or downstream draining vein, sometimes

Received July 21, 2023; accepted after revision August 27.

From the Department of Radiology (A.L.C., V.M.T.), Neuroradiology Section, University of Colorado Anschutz Medical Campus, Aurora, Colorado; Imaging Department (L.C.J.), Guys and St Thomas's and Kings College Hospital Foundation Trusts, London, UK; Department of Biostatistics and Informatics (J.P.), Colorado School of Public Health, University of Colorado-Denver Anschutz Medical Campus, Aurora, Colorado; Department of Radiology (D.J.S.), Cambridge University Hospitals National Health Service Foundation Trust, Cambridge, UK; Department of Neuroradiology (D.B.), Newcastle upon Tyne Hospitals National Health Service Foundation Trust, Newcastle upon Tyne, UK; Department of Radiology (T.H.), Division of Neuroradiology, Mayo Clinic, Jacksonville, Florida; Department of Radiology (P.Y.S., M.D.M.), The Permanente Medical Group, Kaiser Permanente Medical Center, Santa Clara, Santa Clara, California; and Department of Radiology and Biomedical Imaging (M.D.M.), University of California, San Francisco, San Francisco, California.

Please address correspondence to Andrew L. Callen, MD, University of Colorado Anschutz Medical Campus, 12401 E 17th Ave, Aurora, CO 80045; e-mail: andrew.callen@cuanschutz.edu; @AndrewCallenMD

Indicates open access to non-subscribers at [www.ajnr.org](http://www.ajnr.org)

<http://dx.doi.org/10.3174/ajnr.A8005>

with >1 needle (Fig 1). The resultant spread of fibrin injectate was often predominantly foraminal, paraspinal, and sometimes even within a meningeal diverticulum and/or intravascular, rather

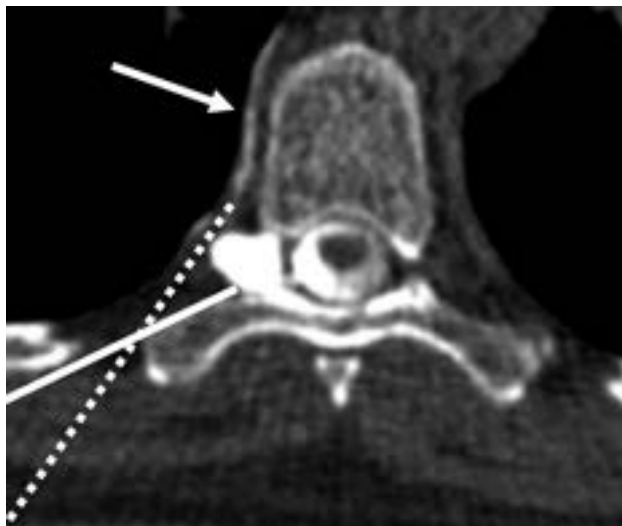


**FIG 1.** Expected needle trajectories for a typical transforaminal epidural steroid injection (solid line) compared with that for a fibrin CVF occlusion (dotted line), targeting a CVF with paraspinal drainage (arrow).

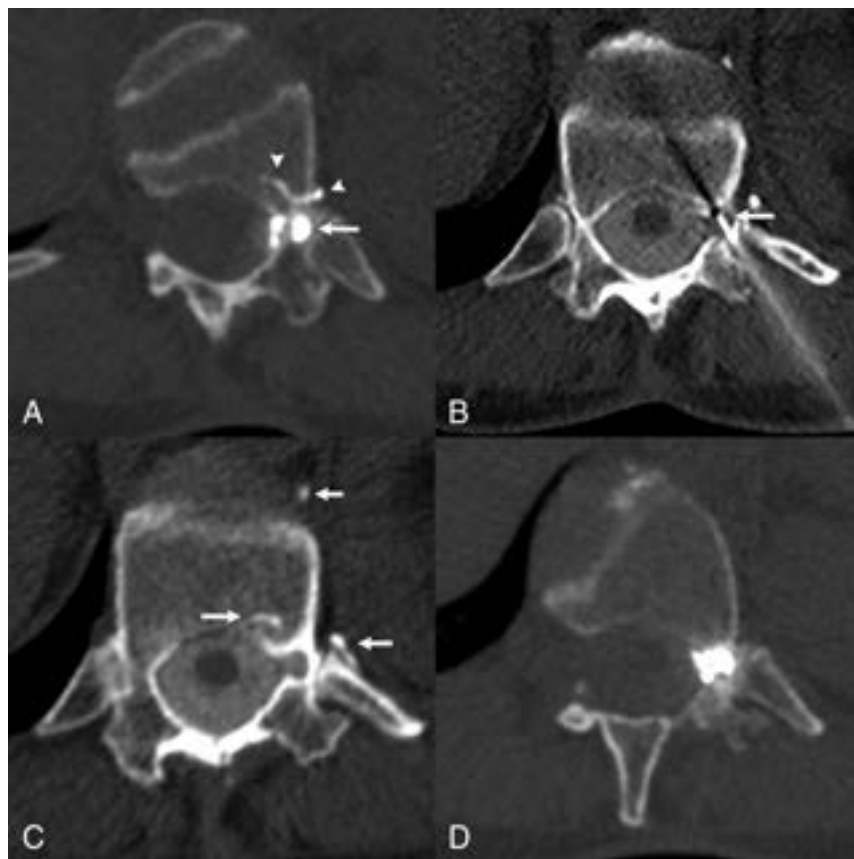


**FIG 2.** Direct cyst puncture of a CVF in a 64-year-old woman. A, Axial left decubitus CTM shows an intraosseous left T12 CVF embedded within the pedicle (arrow) with intraosseous and segmental venous drainage (arrowheads). B, Axial prone CT shows a needle intentionally directly puncturing the intraosseous meningeal diverticulum (arrow). C, Axial image slightly cranial to B shows contrast-enhanced glue within the osseous and paraspinal veins (arrows). D, Posttreatment left decubitus CTM 1 month later shows resolution of the CVF.

than within the dorsal or ventral spinal epidural space as would be achieved in a traditional dorsal interlaminar or transforaminal epidural injection (Fig 2).

The aim of this study was to characterize clinical and radiologic treatment outcomes of CT-guided fibrin occlusion across multiple institutions, hypothesizing that fibrin injectate spread patterns that more closely approximated the drainage pattern of the targeted CVF would be associated with a relatively higher cure rate and that injectate spread patterns that did not match the CVF drainage pattern would be associated with treatment failure. A secondary aim of this study was to characterize the safety profile and success rate of fibrin occlusion when performed by various proceduralists across multiple institutions.

## MATERIALS AND METHODS

### Patients

This was a retrospective cross-sectional cohort study involving 6 institutions across the United States and the United Kingdom from March 1, 2020, through March 31, 2023. Approval from each respective institution's ethics board was obtained or considered exempt as appropriate, and written informed consent was waived. Inclusion criteria included the following: 1) SIH diagnosis according to the "International Classification of Headache Disorders, 3rd ed"; 2) a CVF diagnosed by decubitus CT myelography (CTM); 3) CT-guided fibrin occlusion as a first-line therapy; and 4) a documented clinical response in the patient's electronic medical record.<sup>9</sup> Patient information including age, sex, body mass index (BMI), CVF level and side, pretreatment brain MR imaging, Bern score, and duration of symptoms was recorded.<sup>10</sup>

### CT-Guided Fibrin Glue Technique

The fibrin glue technique for CVF has been described previously, but briefly, the patient is positioned prone on the CT table and scanning is performed at the CVF level.<sup>3,6</sup> Spinal needles are placed along the CVF course using anatomic landmarks. A test dose of 0.2–0.5 mL of air and/or iodinated contrast is injected, depending on the preference of the proceduralist to outline the eventual glue location, and the needle position is modified if needed. Occasionally, if 2 needles were not placed initially, an additional needle may be placed after a test injection to optimize injectate spread. After adding 0.2 mL of preservative-free contrast into both hubs of the fibrin glue syringe (Tisseel or Artiss fibrin sealant, 4 mL; Baxter), the contrast-enhanced fibrin glue is injected into the spinal needle along the CVF course.

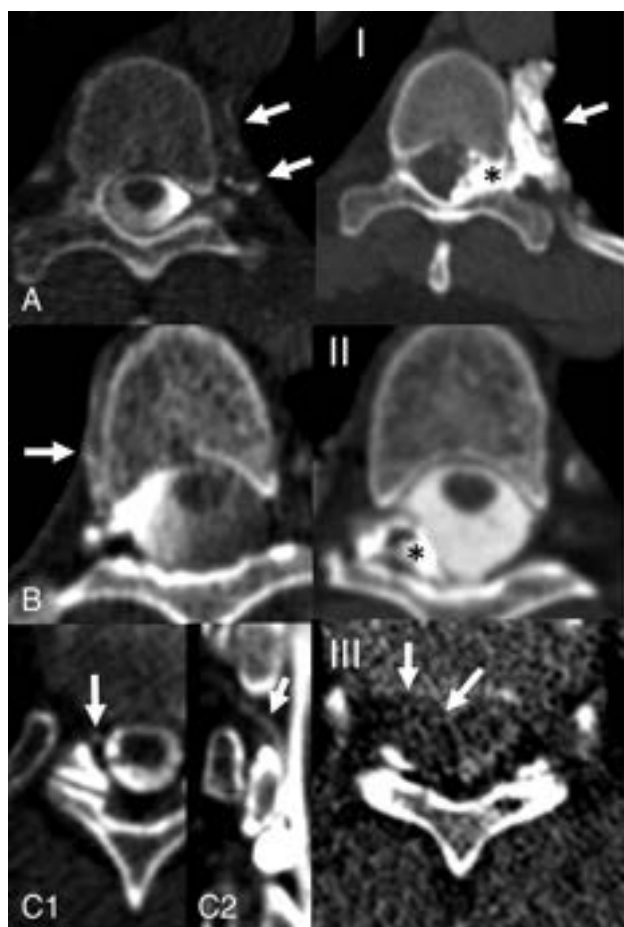


**FIG 3.** Examples of fibrin spread in 3 patients with a CVF. *A*, Left decubitus dynamic CTM demonstrates a CVF with paraspinal drainage (*A*, arrows), which was adequately covered by fibrin injectate in the paraspinal space (*I*, arrow), with additional extension into the lateral epidural space (*I*, asterisk). This injectate coverage was considered concordant with the CVF drainage. *B*, Right decubitus dynamic CTM demonstrating a CVF with paraspinal drainage (*B*, arrow), with fibrin injectate confined only to the dorsolateral epidural space (*II*, asterisk). This injectate coverage was considered discordant from the CVF drainage. *C*, Axial (*C1*) and coronal (*C2*) images from a right decubitus dynamic CTM demonstrating a CVF draining into the right epidural venous plexus (arrows), and axial (*III*) post injection image demonstrating fibrin injectate spreading along the right epidural space (arrows). This injectate coverage was considered concordant with the CVF drainage.

### CVF Characteristics

Each initial dynamic myelogram of a CVF was assessed for the primary venous drainage pattern and classified by the proceduralist as either paraspinal, internal epidural, or both. Postpatch images were then assessed, and the distribution of fibrin injectate was classified as either paraspinal, epidural, or both. Fibrin glue injection spread patterns were then compared with CVF drainage patterns and assessed for concordance of the injectate spread and CVF drainage. For example, a CVF that had paraspinal drainage but epidural injectate spread would be considered discordant, whereas a CVF that had paraspinal drainage and paraspinal injectate spread would be considered concordant (Fig 3).

### Procedural Characteristics

Additional treatment characteristics were recorded, including needle gauge and number of needles within a single procedure, as well as the type and volume of fibrin sealant used. The total number of fibrin occlusion attempts was also recorded, and if >1 procedure was performed, variables from the final procedure were used. Whether any postprocedural adverse event occurred was recorded.

### Clinical and Radiologic Evaluation

The primary outcome was the patient's clinical response, which was assessed by retrospective review of the patient's medical record by the proceduralist team for written documentation of either complete, partial, or no clinical improvement, along with the clinical follow-up time. This documentation consisted of either clinic or telephone encounter notes written by either the patient's primary care physician, referring neurologist, a radiology nurse/nurse practitioner, or the proceduralist. Whether there was a documented clinical record, either in the immediate postprocedural period or in the days to weeks following the procedure, of a patient developing symptoms suspicious for rebound intracranial hypertension was recorded. If the patient underwent postprocedural MR imaging of the brain, the posttreatment Bern score and brain MR imaging follow-up time were also recorded. Procedural covariates such as the number of total attempts, needles, needle gauge, and whether there was intravascular extension of fibrin or a direct cyst puncture were recorded.

### Statistical Analysis

The primary outcome of the study was clinical improvement, which was treated as a 3-category variable (no improvement, partial improvement, complete improvement). All exposures were tested univariately for association with clinical improvement. Dichotomous exposures (concordant spread, cyst puncture, intravascular extension, rebound headache) were tested via logistic regression, with the exposure as the outcome and clinical improvement as a covariate. BMI, age, and the number of attempts were tested via linear regression with the exposure as the outcome. Symptom duration was tested via robust linear regression with Huber weights; robust regression was used to ensure valid inference in the presence of outliers. For logistic regression models, association of categorical clinical improvement with the exposure was tested via a likelihood ratio test. For linear regression models, an *F*-test was used, and for robust linear models, a robust *F*-test was used. In the case of a significant association for the 3-category outcome, pair-wise comparisons were tested using the Tukey post hoc correction. A 6-fold Bonferroni multiple testing correction was applied to secondary exposures. All data analyses were performed using R statistical and computing software, Version 4.1.2 (<http://www.r-project.org/>).

## RESULTS

### Patients

Patients' descriptive statistics are summarized in Tables 1 and 2. One hundred nineteen total patients with 120 total CVFs were included in the analysis. Three patients did not have documentation of their clinical response in the medical record and thus were not

**Table 1: Descriptive statistics of patients**

Overall (n = 119)	
Age	
Mean (SD)	59.3 (11.7)
Median (Q1, Q3)	61.0 (53.0–66.0)
BMI	
Mean (SD)	27.1 (5.22)
Median (Q1, Q3)	26.6 (23.6–29.3)
Sex	
Female	63 (52.9%)
Male	56 (47.1%)
Symptom duration (yr)	
Mean (SD)	2.9 (6.1)
Median (Q1, Q3)	0.58 (0.25–3.0)
MR imaging follow-up (mo)	
Mean (SD)	3.5 (5.9)
Median (Q1, Q3)	2.0 (1.0–3.0)
Missing	27 (22.7%)
Clinical follow-up (mo)	
Mean (SD)	5.0 (5.8)
Median (Q1, Q3)	2.5 (1.0–6.0)

**Table 2: Descriptive statistics of fistulas**

Overall (n = 120)	
Fistula side	
Left	44 (36.7%)
Right	76 (63.3%)
Lumbar	
No	117 (97.5%)
Yes	3 (2.5%)
Thoracic	
No	6 (5.0%)
Yes	114 (95.0%)
Cervical	
No	117 (97.5%)
Yes	3 (2.5%)
Paraspinal drainage only	
No	33 (27.5%)
Yes	87 (72.5%)
Epidural drainage only	
No	109 (90.8%)
Yes	11 (9.2%)
Paraspinal and epidural drainage	
No	98 (81.7%)
Yes	22 (18.3%)
Bern score pretreatment	
Mean (SD)	6.4 (2.3)
Median (Q1, Q3)	7.0 (5.0, 8.0)
Missing	1 (0.8%)

included in the analysis. One hundred eighteen patients had 1 CVF, and 1 patient had 2 CVFs. The 2 CVFs in the single patient were on opposite sides but at adjacent levels at T7 and T8. The mean patient age was 59.3 (SD, 11.7) years. The mean patient BMI was 27.1 (SD, 5.2). Sixty-three of 119 (52.9%) patients were women, and 56/119 (47.1%) patients were men. Mean patient symptom duration was 34.6 (SD, 73.4) months. One hundred eighteen of 119 (99.2%) patients had a pretreatment MR imaging, and the mean pretreatment Bern score was 6.4 (SD, 2.3).

### CVF Characteristics

Seventy-six of 120 (63.3%) fistulas were on the right. One hundred fourteen of 120 (95.0%) originated in the thoracic spine, 3/120

**Table 3: Descriptive statistics of procedures (subject level)**

Overall (n = 119)	
Complications	
No	114/119 (96%)
Yes	5/119 (4%)
Rebound headache	
No	86 (72.3%)
Yes	33 (27.7%)
Clinical improvement	
Complete	71 (59.7%)
None	7 (5.9%)
Partial	41 (34.5%)

**Table 4: Descriptive statistics of procedures (fistula level)**

Overall (n = 120)	
Needle gauge	
18	1 (0.8%)
20	75 (62.5%)
22	44 (36.7%)
No. of needles	
1	88 (73.3%)
2	28 (23.3%)
3	4 (3.3%)
Fibrin type	
Artiss	1 (0.8%)
Tisseel	119 (99.2%)
Fibrin volume (mL)	
Mean (SD)	4.2 (1.6)
Median (Q1, Q3)	4.0 (3.5–4.0)
Intravascular fibrin extension	
No	83 (69.2%)
Yes	37 (30.8%)
Cyst puncture	
No	100 (83.3%)
Yes	20 (16.7%)
No. of fibrin attempts	
Mean (SD)	1.5 (0.90)
Median (Q1, Q3)	1.0 (1.0–2.0)

(2.5%) originated in the lumbar spine, and 3/120 (2.5%) originated in the cervical spine. Eighty-seven of 120 (72.5%) CVFs had only paraspinal drainage, 11/120 (9.2%) CVFs had only epidural drainage, and 22/120 (18.3%) had paraspinal and epidural drainage.

### Procedural Characteristics

Tables 3 and 4 summarize the procedural characteristics. Seventy-five of 120 (62.5%) CVFs were treated with 20-ga needles, 44/120 (36.7%) were treated with 22-ga needles, and 1/120 (0.8%) was treated with an 18-ga needle. One needle was used in 88/120 (73.3%) cases, 2 needles were used in 28/120 (23.3%) cases, and 3 needles were used in 4/120 (3.3%) cases. Tisseel fibrin sealant was used in all except 1 case, in which Artiss fibrin sealant was used. In 9 cases, 2–9 mL of autologous blood was injected with fibrin, and in the remaining cases, fibrin sealant was injected in isolation. The mean and median (Q1, Q3) of fibrin sealant used were 4.15 (SD, 1.63) mL, and 4.00 (3.5–4.00) mL, respectively. Intravascular extension of fibrin was noted in 37/120 (30.8%) cases. A direct cyst puncture was performed in 20/120 (16.7%) cases. The mean number of procedural attempts per patient was 1.5 (SD, 0.9).



### Clinical Outcome

One hundred nineteen patients all had documentation of the degree of clinical improvement or lack thereof following the procedure in their electronic medical record. The mean clinical follow-up time was 5.0 (SD, 5.8) months (range, 0.25–20 months). Complete clinical improvement was documented in 71/119 (59.7%) patients, partial clinical improvement was documented in 41/119 (34.5%) patients, and no clinical improvement was documented in 7/119 (5.9%) patients. Mean injectate volume stratified by clinical improvement was 4.0 (SD, 1.5) mL in complete, 4.4 (SD, 2.0) mL in partial, and 3.7 (SD, 0.5) mL in no improvement. More than 1 needle was used in 18/71 (25.3%) patients with complete improvement, 12/41 (29.2%) patients with partial improvement, and 2/7 (28.6%) patients with no improvement. Postprocedural complications occurred in 5/119 (4%) cases. These included asymptomatic pulmonary embolism in 2 patients (noted on routine postprocedural imaging performed to assess injectate spread, not prompted by any change in clinical status) and self-limiting radicular pain in 3 patients. Thirty-three of 119 (27.7%) patients experienced a new nonorthostatic headache postprocedure, which was clinically suspected to reflect rebound intracranial hypertension.

Within the complete response group, injectate spread was concordant with the fistula drainage pattern in 60/72 (83.3%) fistulas, compared with 30/41 (73.1%) in the partial response group and 2/7 (28.6%) in the no response group. There was a statistically significant association between concordant spread and clinical improvement ( $P = .0089$ ). Pair-wise group tests further revealed that subjects with complete clinical improvement had significantly higher odds of concordant spread compared with those with no clinical improvement (OR = 12.5; 95% CI, 1.53–101.7;  $P = .013$ ).

The mean pretreatment symptom duration was 1.3 years in the complete response group, 4.7 years in the partial response group, and 8.2 years in the no response group. There was a highly significant association between pretreatment symptom duration and clinical improvement ( $P < .001$ ). Pair-wise group tests indicated that subjects with no clinical improvement had significantly longer symptom duration compared with those with complete clinical improvement (estimate = 3.0; 95% CI, 1.5–4.4;  $P < .001$ ). Likewise, subjects with partial clinical improvement had significantly longer symptom duration compared with those with complete improvement (estimate = 1.1; 95% CI, 0.4–1.9;  $P < .001$ ), whereas subjects with partial improvement had significantly shorter symptom duration than those with no improvement (estimate = 1.8; 95% CI, 0.3–3.3;  $P = .01$ ).

After Bonferroni correction for multiple comparisons, no statistically significant associations were found between clinical improvement and cyst puncture ( $P = .22$ ), intravascular extension ( $P = .85$ ), rebound headache ( $P = .42$ ), BMI ( $P = .95$ ), age ( $P = .06$ ), or the number of attempts ( $P = .31$ ).

### Radiologic Outcome

Of the 119 subjects, 92 underwent follow-up MR imaging, while 27 had not at the time of data analysis. Postprocedural MR imaging was performed at a mean duration of 3.5 months. Logistic regression analysis indicated no significant association between

missing follow-up MR imaging and clinical improvement. The mean change in the Bern score (calculated as posttreatment Bern score minus pretreatment Bern score) in those with a complete response was  $-5.4$ , compared with  $-2.9$  in the partial response group and  $0.6$  in the no response group. Figure 3 shows pre- and posttreatment Bern scores stratified by clinical improvement. No inferential analysis was performed due to the incomplete data.

### DISCUSSION

This study aimed to assess the clinical and radiologic treatment outcomes achieved through CT-guided fibrin occlusion of CVFs across multiple institutions. Our results suggest that treatment success may be in part driven by whether the spread of fibrin injectate matches the target drainage pathway of the CVF and thus provides a potential explanation to account for the failure of a fibrin patch to treat a CVF. Specifically, when a technique mirroring a traditional transforaminal epidural steroid injection is used, achieving a robust epidural spread of injectate is often desirable. However, these data suggest that such a spread pattern is only desirable if there is concurrent drainage of the CVF into the internal epidural venous plexus; otherwise, the needle tip should be positioned more laterally, anterior or posterior to the foramen to target the CVF anatomy (Fig 1). Therefore, rather than using a standard transforaminal technique for all CVFs, we suggest mapping each CVF drainage pattern preprocedurally to plan needle positions accordingly. Before the termination of a procedure, postinjection imaging should be performed and studied for such adequate coverage, and if it is not achieved, additional injections should be considered. Historically, reports of patching for CVF described minimal treatment success; however, exact details such as the image-guidance technique and injectate location and amount were not reported.<sup>8,11</sup> Our experience suggests that CT-guided fibrin glue injections that cover the CVF drainage are one of the main keys to successful treatment.

We found that this procedure demonstrates a favorable safety profile while achieving a relatively high clinical and radiologic cure rate. At a mean follow-up of 5.0 months, 59.7% of patients reported complete symptom improvement. This rate is lower than that of the initial reports describing fibrin occlusion, which may more closely approximate the effectiveness of this procedure in the hands of multiple proceduralists across various institutions.<sup>3,6</sup> As centers build continued experience with this procedure, particularly with the unique needle placement required for successful fibrin occlusion, we speculate that there will be a step-wise improvement in clinical outcomes. Further research should continue to evaluate the success rate of this procedure as techniques are refined and more experience is gained.

Secondary analysis did not suggest that direct cyst puncture, intravascular spread of injectate, or the development of rebound intracranial hypertension independently predicted treatment success. There were no cases of confirmed or suspected arachnoiditis in our cohort despite a direct cyst puncture performed in 20 cases, and despite 37 cases of intravascular fibrin extension, there were only 2 instances of an incidentally imaged pulmonary embolism, neither of which were symptomatic. Despite the lack of clinically meaningful thromboembolic complications related to the procedure in our cohort, fibrin sealant does carry a black box

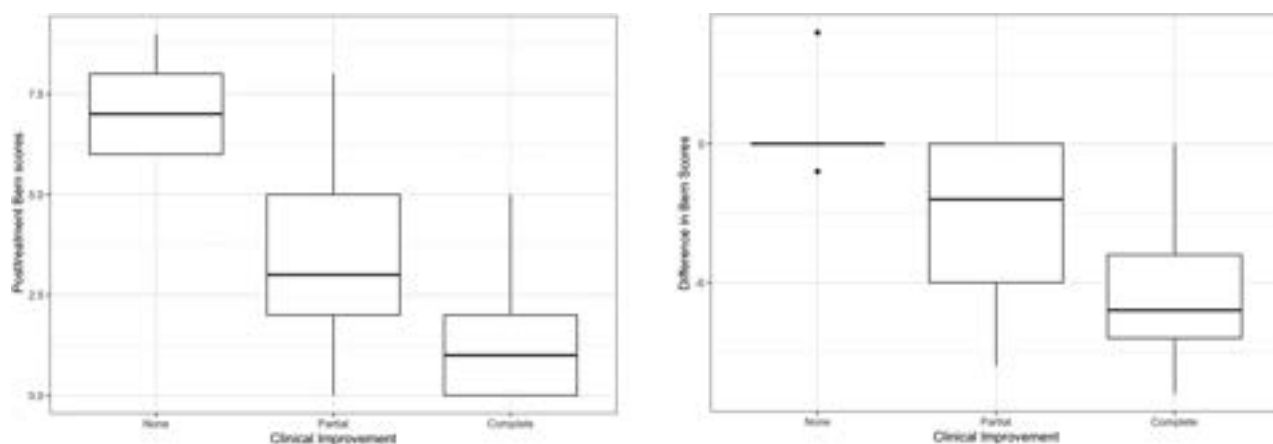


**FIG 4.** Posttreatment Bern score (*left*) and change in Bern scores (*right*) stratified by clinical improvement.

warning in the United States advising against intravascular injection.

In our cohort, most (63.3%) CVFs were found on the right side, which is in keeping with several prior reports of CVF stratified by laterality.<sup>12–14</sup> Given this repeat evidence suggesting a right-sided predilection for CVF, we suggest starting digital subtraction myelography or decubitus CT myelography with the patient in the right decubitus position in the absence of other guiding factors. Also, in keeping with prior literature, most patients in our cohort were overweight, with a mean BMI of 27.1.<sup>12,15</sup> Others have postulated that CSF hypertension secondary to obesity could lead to damage to spinal arachnoid granulations in the de novo or postsurgical setting.<sup>8,16</sup> Further research should continue to investigate the associations between these factors and CVF pathophysiology.

Longer clinical duration of symptoms preceding treatment was inversely related to treatment success. This finding is in keeping with a recent report by Häni et al,<sup>17</sup> which concluded that a shorter duration of preoperative symptoms was the strongest predictor of favorable response to the surgical treatment of type 1 and 2 CSF leaks. The enduring significance of this discovery in an alternative type of leak and treatment approach reinforces the understanding that SIH is intricately influenced by symptom duration in not only its clinical and imaging manifestations but also its susceptibility to treatment.<sup>18–21</sup> While we believe that there is likely some pathophysiologic underpinning to this phenomenon, this relationship may also in part reflect regression to the mean independent of treatment as a result of selection bias in patients with longer symptoms. Nonetheless, we believe that prompt and decisive treatment strategies should be used for patients with spinal CSF leaks or CVF, without any unnecessary delays.

This study has important limitations, including its modest sample size (particularly in the no clinical response group) and retrospective nature. Specifically, due to the lack of universal prospective implementation of standardized or validated clinical response scoring criteria at the participating institutions, assessment of clinical response was obtained through a retrospective review and secondary classification of notes in each patient's medical record. This approach is potentially prone to interpretation

bias, which may limit the generalizability of these findings. While the post hoc use of such measurement tools (such as the Headache Impact Test [HIT-6] headache questionnaire) could have been retrospectively administered to patients, this would have also introduced bias and therefore was not pursued. Institutions providing care for patients with SIH should consider routine, prospective, pre- and postprocedural use of such tools. Despite this potential limitation, we noted a concurrent stepwise improvement in the imaging response paralleling that in the patients with no, partial, or complete clinical improvement (Fig 4), which strengthens the overall validity of this classification schema and supports the potential reliability of the findings of this study. Additional limitations include the potential for missing cases of rebound intracranial hypertension because, in general, these symptoms are subjective and their documentation was subject to self-reporting by the patient.

## CONCLUSIONS

CT-guided fibrin occlusion is a safe and effective treatment for CVF, achieving a relatively high clinical and radiologic cure rate with a small adverse effect profile across multiple institutions. The alignment between the spread pattern of fibrin injectate and the drainage pathway of CVFs appears to play a significant role in treatment success, emphasizing the importance of preprocedural mapping and tailored needle positions. Additionally, the shorter duration of symptoms preceding treatment was associated with a higher likelihood of treatment success, highlighting the significance of prompt intervention in patients with SIH.

Disclosure forms provided by the authors are available with the full text and PDF of this article at [www.ajnr.org](http://www.ajnr.org).

## REFERENCES

- Schievink WI, Moser FG, Maya MM. CSF-venous fistula in spontaneous intracranial hypotension. *Neurology* 2014;83:472–73 CrossRef Medline
- Wang TY, Karikari IO, Amrhein TJ, et al. Clinical outcomes following surgical ligation of cerebrospinal fluid-venous fistula in patients with spontaneous intracranial hypotension: a prospective case series. *Oper Neurosurg (Hagerstown)* 2020;18:239–45 CrossRef Medline

3. Mamlouk MD, Shen PY, Sedrak MF, et al. **CT-guided fibrin glue occlusion of cerebrospinal fluid-venous fistulas.** *Radiology* 2021;299:409–18 CrossRef Medline
4. Borg N, Oushy S, Savastano L, et al. **Transvenous embolization of a cerebrospinal fluid-venous fistula for the treatment of spontaneous intracranial hypotension.** *J Neurointerv Surg* 2022;14:948 CrossRef Medline
5. Brinjikji W, Garza I, Whealy M, et al. **Clinical and imaging outcomes of cerebrospinal fluid-venous fistula embolization.** *J Neurointerv Surg* 2022;14:953–56 CrossRef Medline
6. Mamlouk MD, Shen PY, Dahlin BC. **Headache response after CT-guided fibrin glue occlusion of CSF-venous fistulas.** *Headache* 2022;62:1007–18 CrossRef Medline
7. Schievink WI, Marcel Maya M, Moser FM. **Treatment of spontaneous intracranial hypotension with percutaneous placement of a fibrin sealant: report of four cases.** *J Neurosurg* 2004;100:1098–100 CrossRef Medline
8. Kranz PG, Amrhein TJ, Gray L. **CSF venous fistulas in spontaneous intracranial hypotension: imaging characteristics on dynamic and CT myelography.** *AJR Am J Roentgenol* 2017;209:1360–66 CrossRef Medline
9. **Headache classification committee of the International Headache Society (IHS) the International Classification of Headache Disorders, 3rd edition.** *Cephalalgia* 2018 38:1–211 CrossRef Medline
10. Dobrocky T, Grunder L, Breiding PS, et al. **Assessing spinal cerebrospinal fluid leaks in spontaneous intracranial hypotension with a scoring system based on brain magnetic resonance imaging findings.** *JAMA Neurol* 2019;76:580–87 CrossRef Medline
11. Schievink WI, Maya MM, Moser FG, et al. **Lateral decubitus digital subtraction myelography to identify spinal CSF-venous fistulas in spontaneous intracranial hypotension.** *J Neurosurg Spine* 2019 Sep 13. [Epub ahead of print] CrossRef Medline
12. Mamlouk MD, Shen PY, Jun P, et al. **Spontaneous spinal CSF leaks stratified by age, body mass index, and spinal level.** *AJNR Am J Neuroradiol* 2022;43:1068–72 CrossRef Medline
13. Kim DK, Carr CM, Benson JC, et al. **Diagnostic yield of lateral decubitus digital subtraction myelogram stratified by brain MRI findings.** *Neurology* 2021;96:e1312–18 CrossRef Medline
14. Mark I, Madhavan A, Oien M, et al. **Temporal characteristics of CSF-venous fistulas on digital subtraction myelography.** *AJNR Am J Neuroradiol* 2023;44:492–95 CrossRef Medline
15. Schievink WI, Maya M, Prasad RS, et al. **Spinal CSF-venous fistulas in morbidly and super obese patients with spontaneous intracranial hypotension.** *AJNR Am J Neuroradiol* 2021;42:397–401 CrossRef Medline
16. Malinzak MD, Kranz PG, Gray L, et al. **Postsurgical recurrence of CSF-venous fistulas in spontaneous intracranial hypotension.** *Neurol Clin Pract* 2021;11:e356–58 CrossRef Medline
17. Häni L, Fung C, Jesse CM, et al. **Outcome after surgical treatment of cerebrospinal fluid leaks in spontaneous intracranial hypotension—a matter of time.** *J Neurol* 2022;269:1439–46 CrossRef Medline
18. Häni L, Fung C, Jesse CM, et al. **Insights into the natural history of spontaneous intracranial hypotension from infusion testing.** *Neurology* 2020;95:e247–55 CrossRef Medline
19. Callen A, Pattee J, Thaker AA, et al. **Relationship of Bern score, spinal elastance, and opening pressure in patients with spontaneous intracranial hypotension.** *Neurology* 2023;100:e2237–46 CrossRef Medline
20. Kranz PG, Amrhein TJ, Choudhury KR, et al. **Time-dependent changes in dural enhancement associated with spontaneous intracranial hypotension.** *AJR Am J Roentgenol* 2016;207:1283–87 CrossRef Medline
21. Chen ST, Wu JW, Wang YF, et al. **The time sequence of brain MRI findings in spontaneous intracranial hypotension.** *Cephalalgia* 2022;42:12–19 CrossRef Medline

# Likelihood of Discovering a CSF Leak Based on Intracranial MRI Findings in Patients without a Spinal Longitudinal Extradural Collection: A New Probabilistic Scoring System

John C. Benson, Ajay A. Madhavan, Ian T. Mark, Jeremy K. Cutsforth-Gregory, Waleed Brinjikji, and Jared T. Verdoorn

## ABSTRACT

**BACKGROUND AND PURPOSE:** The likelihood of discovering a CSF leak can be determined by assessing intracranial abnormalities. However, the Dobrocky scoring system, which is used to determine this likelihood, did not incorporate patients with CSF-venous fistulas. This study sought to create a new probabilistic scoring system applicable to patients without a spinal longitudinal extradural collection.

**MATERIALS AND METHODS:** A retrospective review was completed of patients with suspected spontaneous intracranial hypotension who underwent brain MR imaging followed by digital subtraction myelography with same-day CT myelography. Patients with and without leaks found on digital subtraction myelography were included. MRIs were assessed for numerous reported stigmata of spontaneous intracranial hypotension and were compared between cohorts.

**RESULTS:** One hundred seventy-four patients were included; 113 (64.9%) were women (average age, 52.0 [SD, 14.3] years). A CSF leak was found in 98 (56.3%) patients, nearly all of which (93.9%) were CSF-venous fistulas. Diffuse dural enhancement, internal auditory canals dural enhancement, non-Chiari cerebellar descent, pituitary engorgement, brain sag, dural venous sinus engorgement, and decreased suprasellar cistern size were associated with a CSF leak. A probabilistic scoring system was made in which a single point value was assigned to each of those findings: 0–2 considered low probability and  $\geq 3$  considered intermediate-to-high probability of a CSF leak.

**CONCLUSIONS:** This study offers a new probabilistic scoring system for evaluating the likelihood of discovering a CSF leak on the basis of intracranial MR imaging findings, though the new system is not superior to that of the Dobrocky method for predicting the presence of CSF leaks.

**ABBREVIATIONS:** AUC = area under the curve; CTM = CT myelography; DSM = digital subtraction myelography; IAC = internal auditory canal; SIH = spontaneous intracranial hypotension; SLEC = spinal longitudinal extradural fluid collection

Spontaneous intracranial hypotension (SIH) is a condition caused by spinal CSF leaks.<sup>1,2</sup> The condition can be extremely debilitating. SIH is classically characterized by orthostatic headaches but can also lead to long-term disability, decreased consciousness, and even coma.<sup>3,4</sup> In recent years, much has been learned about the characteristics and frequency of various types of spinal CSF leaks, particularly with the rise of digital subtraction myelography (DSM) and dynamic CT myelography (CTM).<sup>5,6</sup> Nevertheless, accurately diagnosing patients with SIH is difficult, and clinicians often rely on radiologic findings.<sup>3</sup> Specifically,

patients with SIH typically have some combination of intracranial abnormalities best seen on brain MR imaging: dural thickening and enhancement, brain sag, and engorgement of the pituitary and/or dural venous sinuses,<sup>7</sup> a set of findings that is explained by physiologic responses to loss of CSF volume according to the Monroe-Kellie doctrine.<sup>8</sup>

Many of the aforementioned imaging findings can mimic those of other pathologies.<sup>9</sup> In 2019, Dobrocky et al<sup>10</sup> developed a method to determine the likelihood of discovering a spinal CSF leak based on intracranial findings. This probability score, commonly called the “Bern score,” uses 6 imaging findings: pachymeningeal enhancement, venous sinus engorgement, effacement of the suprasellar cistern, the presence of subdural fluid collections, effacement of the prepontine cistern, and decreased mamillo-pontine distance. By assigning point values to these findings, the authors created a scoring system to categorize someone as having a high, intermediate, or low probability of a spinal CSF leak.

Received June 20, 2023; accepted after revision September 14.

From the Departments of Radiology (J.C.B., A.A.M., I.T.M., W.B., J.T.V.), and Neurology (J.K.C.-G.), Mayo Clinic, Rochester, Minnesota.

Please address correspondence to John C. Benson, MD, Department of Radiology, Mayo Clinic, 723 6th St SW, Rochester, MN 55902; e-mail: benson.john3@mayo.edu

<http://dx.doi.org/10.3174/ajnr.A8030>



Undoubtedly, the widely adopted probabilistic scoring method developed by Dobrocky et al<sup>10</sup> has had a positive impact on the field of SIH. It created a simplified approach to diagnosing an often underrecognized condition. However, the cohort used for analysis in the study was based on patients with so-called “fast” CSF leaks, which are typically caused by ventral or posterolateral dural tears and associated with spinal longitudinal extradural fluid collections (SLECs). Thus, the study did not include patients for whom a probabilistic scoring system would be most useful, namely patients without a SLEC in whom CSF-venous fistulas are the most common leak type,<sup>11</sup> and in rarer cases patients with distal nerve root sleeve tears. Although the scoring system was later demonstrated to stratify the probability of finding a leak on lateral decubitus DSM in a predominantly “slow” leak cohort,<sup>11</sup> the original scoring system development did not include any patients with fistulas.

The current study set out to create a new probabilistic scoring system of intracranial findings that can determine whether a patient suspected of having SIH but having no SLEC on spine MR imaging will ultimately have a spinal CSF leak identified. Thus, we assessed brain MR images in patients with clinically suspected SIH and compared findings between patients with and without a spinal CSF leak.

## MATERIALS AND METHODS

### Patient Cohort

This study was performed following exemption by the local institutional review board. A retrospective review was completed of consecutive patients with suspected SIH who underwent DSM between December 30, 2021, and November 30, 2022. All included patients underwent lateral decubitus DSM. Patients were excluded if they did not have a pre-DSM brain MR imaging or if images were of poor quality or substantially degraded by artifacts. Patients were also excluded if an SLEC was observed on pre-DSM spinal MR imaging (per our institution’s diagnostic algorithm, no patients with an SLEC underwent DSM imaging). For any patients who had undergone a previous DSM (ie, before the study inclusion date), either the first DSM performed that identified a CSF leak or the first DSM performed at our institution (in patients in whom a CSF leak was not identified) and the most recent brain MR imaging preceding the DSM were used for analysis. The number of days between the pre-DSM brain MR imaging and the analyzed DSM was recorded. When we used these criteria, dates for all reviewed DSM examinations ranged from December 21, 2018, to November 15, 2022.

### DSM Technique

All DSMs were performed during 2 days, the first with the patient in the right lateral decubitus position and the second with the patient in the left lateral decubitus position.<sup>6</sup> Imaging was completed with the patient placed on a wedge-shaped cushion on a tiltable table to position the patient’s hips superior to his or her shoulders. After placement of a 20-ga spinal needle into the thecal sac (typically at L2–3 or L3–4), 2 separate DSM acquisitions were performed per side: the first with the flat panel detector focused over the upper spine and the second focused over the lower spine. A total of 11 mL of intrathecal Omnipaque 300 (GE Healthcare)

was administered for both runs. Following completion of DSM imaging, the patient was kept in lateral decubitus positioning and transferred to CT for a subsequent entire spine CTM. DSM and CTM images were interpreted as part of a single examination.

### Brain MR Imaging Protocol

MR imaging was performed on either a 1.5T or 3T scanner. Nearly all imaging analyses were based on fat-saturated post-contrast 3D T1 sampling perfection with application-optimized contrasts by using different flip angle evolutions (SPACE; Siemens) sequences (TR = 600 ms, TE = 7.2 ms, flip angle = 120°, section thickness = 1 mm, FOV = 250 × 250 mm<sup>2</sup>). Evaluation of superficial siderosis was based on SWI sequences (TR = 49 ms, TE = 40 ms, flip angle = 15°, section thickness = 3 mm, FOV = 201 × 240 mm<sup>2</sup>). Assessment of subdural fluid collections was performed by comparing axial postcontrast T1 SPACE sequences with axial T2 FLAIR images (TR = 9000 ms, TE = 149 ms, flip angle = 180°, section thickness = 4 mm, FOV = 220 × 220 mm<sup>2</sup>).

### Image Analysis

Four neuroradiologists reviewed the DSM and pre-DSM brain MR images, with the entire cohort split evenly among the reviewers. Thus, each patient in the cohort was reviewed by only a single radiologist, who reviewed the MRIs, DSMs, and CTMs. The reviewers were blinded to clinical information but not blinded to the official reports or annotations in the PACS system.

Each reviewer individually evaluated all DSMs for the presence or absence of an identified CSF leak (specified as positive, negative, or indeterminate), laterality of the leak, and location of the leak (ie, spinal segment). Leaks were further stratified by subtype, according to a previously validated categorization: type 1 (ventral dural tear with an SLEC), type 2 (posterolateral dural tear/nerve root sleeve tear with an SLEC), type 3 (CSF-venous fistula), type 4 (distal nerve root sleeve tear), and type 5 (other).<sup>12</sup>

MR imaging brain scans were assessed for multiple potential stigmata of SIH: smooth dural enhancement, smooth dural enhancement specifically involving the internal auditory canals (IACs), subdural fluid collections, superficial siderosis, pituitary engorgement, non-Chiari cerebellar tonsillar descent of >5 mm (meaning tonsillar descent without pointed or “peglike” morphology of the tonsils), dural venous sinus engorgement, “layered” hyperostosis of the calvaria, or descent of the cerebral aqueduct iter below the incisural line.

The definition of layered hyperostosis was based on prior studies in which a secondary layer of bone was seen subjacent to the primary calvarial structure.<sup>13,14</sup> Pituitary engorgement was considered positive if the superior margin of the gland was convex on sagittal images. The presence or absence of dural venous sinus engorgement was based on assessment of the midportion of the dominant transverse sinus on sagittal images for convexity of the inferior border of the sinus wall.<sup>15</sup> Given the ambiguity of this finding, results were categorized as positive, negative, or indeterminate. Multiple measurements were made on fat-saturated post-contrast sagittal images (or the available T1-weighted image if contrast was not used for the examination, typically sagittal

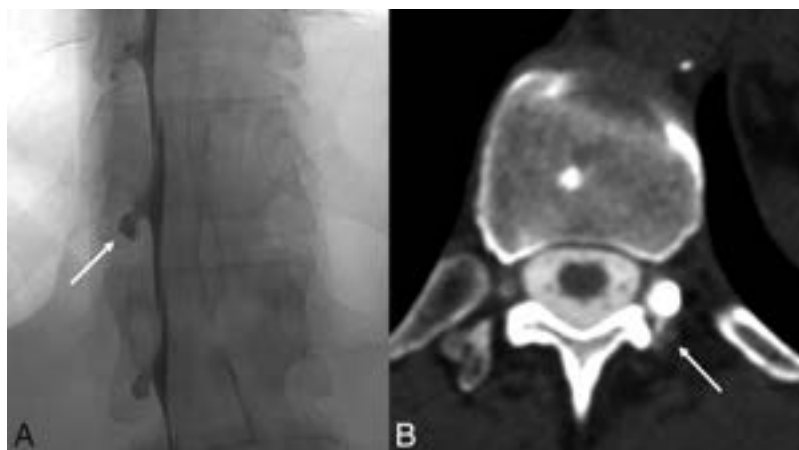


**FIG 1.** An example of a distal nerve root sleeve tear (type 4 leak) diagnosed using a combination of DSM and delayed CTM findings. Left lateral decubitus unsubtracted image from a DSM (A) demonstrates contained contrast within a left T12 meningeal diverticulum (A, arrow). On a 30-minute delayed left decubitus CTM (B), there is a subtle contrast leak posterior to the diverticulum (B, arrow). The combined findings from a DSM and delayed CTM are often necessary to confidently diagnose type 4 leaks.

MPRAGE) of the following: mamillopontine distance, suprasellar cistern height (measured between the inferior aspect of the optic chiasm and the superior border of the pituitary), and prepontine cistern width.

### Statistical Analysis

All statistical calculations were performed using BlueSky Statistics software (BlueSky Statistics). Means and SDs were calculated for all continuous variables. A  $\chi^2$  test was used to assess statistically significant differences among categorical variables, and the Student *t* test was used for differences among continuous variables. To obtain a cutoff for any continuous variables that were significantly associated with CSF leaks (in this case, only the suprasellar cistern measurement), we created a receiver operating characteristic curve using a logistic regression model to select the optimal cutoff. These continuous variables were then converted to binary variables on the basis of their relationship to the cutoff point. For all calculations, the threshold for statistical significance was set to  $P = .05$ .

To create a scoring system, we put any variables that were found to be significantly associated with the presence of a CSF leak into a multivariable analysis with a logistic regression. Following the methodology of the prior study,<sup>10</sup> any variable that could not be assessed (in this case, dural enhancement in 8 patients who did not undergo contrast-enhanced MR imaging) was counted as negative. Any variables that had a coefficient of  $>2$  were planned to be given a score of 2 for the final system (though none were noted in our analysis); all others were given a score of 1. The scores of all patients were then calculated, and a final logistic regression with the Youden index was performed to assess the optimal cut-point for a scoring system.

Logistic regression analyses were used to assess correlations between a CSF leak and both the scoring system developed in the current study and that of Dobrocky et al.<sup>10</sup> Areas under curve (AUCs) were compared between both scoring systems.

## RESULTS

### Patient Cohort and CSF Leaks

Of 175 patients, one was excluded due to an inability to undergo brain MR imaging due to a neurostimulator in place. None were excluded for poor brain MR image quality. Thus, the final cohort was composed of 174 patients. One hundred thirteen (64.9%) were women, with average age 52.0 (SD, 14.3) years. At least 1 CSF leak was found on DSM in 76 (43.7%) patients, while indeterminate findings were noted in 22 (12.6%). Because indeterminate findings were considered suspicious and treated in all except 1 patient (21/22; 95.5%), such cases were considered positive. Thus, at least 1 CSF leak was discovered in 98 (56.3%) patients. There was no significant difference in sex makeup between patients without and with CSF leaks ( $P = .91$ ).

For the entire cohort, the mean Dobrocky et al.<sup>10</sup> score was 4.0 (SD, 2.7). The average Dobrocky et al score among patients with a CSF leak (5.0) was significantly higher than in those without a CSF leak (2.6) ( $P < .001$ ).

Regarding leak sites, 61/98 (62.2%) were on the right side, 29 (29.6%) were on the left side, 6 (6.1%) were bilateral, 1 (1.0%) was ventral, and 1 (1.0%) was into the internal epidural venous plexus. Ninety-three (94.9%) were classified as type 3 leaks (CSF-venous fistulas), 1 (2.0%) was type 1 (ventral dural leak), and 4 (4.1%) were type 4 (distal nerve root sleeve tears) (Fig 1).

### Brain Imaging

The average time between pre-DSM MR imaging and DSM was 91.0 (SD, 163.1) days. Eight patients did not have postcontrast imaging available for review.

Among the entire cohort, smooth dural enhancement was present in 63/166 patients (38.0%) and dural enhancement in the IACs was present in 38/166 (23.0%) (Fig 1). Unilateral or bilateral subdural fluid collections were observed in 13 (7.5%) patients. Superficial siderosis was present in 4 (2.3%) patients, though 1 of the 4 with superficial siderosis had a known history of prior head and spine trauma. Pituitary engorgement was observed in 73 (42.0%); non-Chiari cerebellar tonsillar descent, in 30 (17.2%); descent of the cerebral aqueduct iter below the incisural line, in 48 (27.6%); and layered hyperostosis, in 11 (6.3%). Venous sinus engorgement was clearly present in 30 (17.2%) patients and was indeterminate in 31 (17.8%). The average mamillopontine distance was 5.6 (SD, 1.9) mm, the average prepontine cistern width was 4.1 (SD, 1.5) mm, and the average suprasellar cistern height was 3.9 (SD, 2.5) mm.

### Comparisons between Cohorts

Comparisons of brain MR imaging findings in patients with and without a CSF leak identified on DSM are detailed in Table 1. Abnormalities significantly more common in patients with a CSF leak were smooth dural enhancement, dural enhancement

**Table 1: Frequency and measurements of intracranial findings<sup>a</sup>**

	CSF Leak (n = 76)	No CSF Leak (n = 98)	P Value
Smooth dural enhancement	54 (57.4%)	9 (12.5%)	$P < .001^b$
Dural enhancement in IACs	34 (36.2%)	4 (5.6%)	$P < .001^b$
Subdural fluid collections	9 (9.2%)	4 (5.3%)	$P = .32$
Superficial siderosis	3 (3.1%)	1 (1.3%)	$P = .44$
Pituitary engorgement	56 (57.1%)	17 (22.4%)	$P < .001^b$
Non-Chiari cerebellar tonsillar descent of >5 mm	22 (22.4%)	8 (10.5%)	$P = .04^b$
Dural venous sinus engorgement	Yes = 25 (25.8%) Indeterminate = 27 (27.8%)	Yes = 5 (6.6%) Indeterminate = 4 (5.3%)	$P < .001^b$
Layered hyperostosis	8 (8.2%)	3 (3.9%)	$P = .25$
Cerebral aqueduct iter below incisural line	33 (33.7%)	15 (19.7%)	$P = .04^b$
Average mamillopontine distance (mm)	5.5 (SD, 2.1) mm	5.9 (SD, 1.7) mm	$P = .13$
Average prepontine cistern size (mm)	4 (SD, 1.5) mm	4.2 (SD, 1.6) mm	$P = .35$
Average suprasellar cistern size (mm)	3.2 (SD, 2.1) mm	4.8 (SD, 2.7) mm	$P < .001^b$

<sup>a</sup> Indeterminate dural sinus engorgement is counted as positive in this analysis.

<sup>b</sup> Statistically significant  $P$  values.

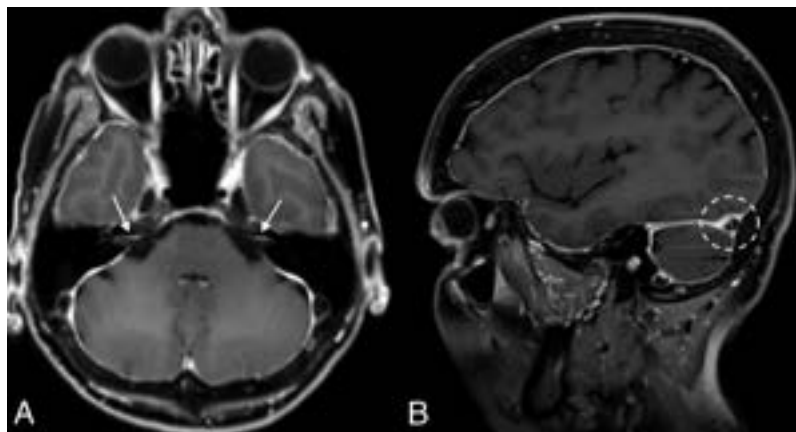


**FIG 2.** An example of multiple intracranial sequelae of SIH in a 69-year-old woman. Axial (A) and sagittal (B) postcontrast images demonstrate diffuse smooth dural enhancement, with involvement of the IACs (arrows, A). The right transverse sinus is engorged (dashed circle, B).

**Table 2: Scoring system based on 7 intracranial imaging findings**

Finding	Points
Smooth dural enhancement	1
Dural enhancement in the IACs	1
Pituitary engorgement	1
Non-Chiari cerebellar descent of >5 mm	1
Dural venous sinus engorgement	1
Cerebral aqueduct iter below incisural line	1
Suprasellar cistern $\leq 2.5$ mm	1

**Table 3: Proposed probabilistic scoring system for determining whether a spinal CSF leak is present**

Score	Probability of CSF Leak
0–2	Low
$\geq 3$	Intermediate to high

involving the IACs, non-Chiari cerebellar descent of >5 mm below the foramen magnum, pituitary engorgement, dural venous sinus engorgement, descent of the cerebral aqueduct iter below the incisural line, and decreased suprasellar cistern height (Fig 2). Although subdural fluid collections, layered hyperostosis, and superficial siderosis were more common among patients with a CSF leak, the differences did not reach statistical significance.

Similarly, the average mamillopontine distance and prepontine cistern width were smaller in patients with a CSF leak, though these differences did not reach statistical significance.

Dural venous sinus engorgement was associated with a CSF leak when allowing for categorization into 1) present, 2) absent, or 3) indeterminate classifications ( $P < .001$ ). To incorporate this finding into the statistical analysis for the scoring system, we combined present and indeterminate into 1 category. By means of this method, the presence of definite or indeterminate dural venous sinus engorgement was still significantly associated with a CSF leak ( $P < .001$ ).

By means of receiver operating characteristic analysis, the cutoff for the suprasellar cistern was 2.5 mm. A follow-up  $\chi^2$  analysis assessing a suprasellar cistern size of  $\leq 2.5$  mm found that this size was significantly associated with the presence of a CSF leak (OR = 3.2; 95% CI, 1.6–6.3;  $P = .0008$ ).

### Development of Scoring System

All statistically significant variables were given 1 point for the scoring system (Tables 2 and 3 and Fig 3). The average score for all patients was 2.1 (SD, 0.2) (range, 0–7). Higher scores were significantly associated with a CSF leak (OR = 1.7; 95% CI, 1.4–2.2;  $P < .001$ ).

Statistical analysis demonstrated the optimal cut-point for a probabilistic scoring system to be 3. No other cut-points were identified. Thus, our scoring system dichotomized the outcomes into “low” and “intermediate-to-high” probabilities of a CSF leak, divided into scores of 0–2 and  $\geq 3$ , respectively. By means of this system, 65 patients were considered to have an intermediate-to-high probability of a CSF leak. Forty-three of 109 (39.4%) patients with a low-probability had a leak, while 55/65 (84.6%) patients with intermediate-to-high probability of a leak were found to have a leak.

The scoring system was significantly associated with finding a leak (OR = 8.4; 95% CI, 3.9–18.3;  $P < .001$ ). By means of the



**FIG 3.** Schematics of intracranial findings used for the probabilistic scoring system developed in this study. Pertinent findings included diffuse dural enhancement and dural enhancement involving the walls of the IACs (pink lines, A), engorgement of the transverse sinus and non-Chiari cerebellar descent (B), and pituitary engorgement, effacement of the suprasellar cistern, and descent of the aqueduct of Sylvius below the incisural line (dotted line, C). Used with permission of Mayo Foundation for Medical Education and Research, all rights reserved.

scoring system of Dobrocky et al,<sup>10</sup> both intermediate (OR = 1.4; 95% CI, 0.6–3.3) and high (OR = 8.3; 95% CI, 3.8–19.1) scores were associated with leaks ( $P < .001$ ). There was no significant difference in the AUC for the scoring system of Dobrocky et al (AUC = 0.72) and the one developed for the current study (AUC = 0.70;  $P = .51$ ).

## DISCUSSION

We set out to create a new probabilistic scoring method for determining the likelihood of finding a spinal CSF leak in a patient with clinically suspected SIH. The results found that none of the “minor” criteria of the Dobrocky et al<sup>10</sup> score were associated with a leak, while 7 of the studied intracranial findings were associated with a leak. From these, we developed a scoring system that dichotomized patients as having a low or intermediate-to-high probability of a CSF leak.

However, there was no significant difference between the 2 scoring systems in their ability to predict the presence or absence of a CSF leak, likely, due to a few major reasons. First, many of the same imaging findings are used by both systems. For example, our system uses the descent of the aqueduct below the incisural line as a stand-in for subjective brain sag used previously. Next, many of the imaging findings coexist in patients with CSF leaks. Finally, the original study by Dobrocky et al<sup>10</sup> had many strengths, including the use of statistical rigor and incorporation of a validation cohort to confirm its findings.

What then should be done with the 2 scoring systems: the one developed by Dobrocky et al<sup>10</sup> and the scoring system developed in the current study? Ultimately, we believe that the scoring system developed in this study has some benefits over the prior system: It has less dependence on the measurement of minute structures and does not include the 3 minor findings that were not found to be associated with leaks. Nevertheless, the imperfections of both scoring systems highlight the concept that CSF leaks cannot be ruled in or out on the basis of imaging alone.

Next, the results of this study ultimately do serve as further validation of the Dobrocky et al<sup>10</sup> system. Already, the Dobrocky system has been validated using both DSMs and dynamic CTMs.<sup>16,17</sup> Therefore, the results of the current study, though

they seek to reshape our assessment of intracranial findings in patients with suspected SIH, should also be thought to highlight the strengths of the Dobrocky et al scoring system.

The results of the current study should be interpreted in the context of its methodology. For example, superficial siderosis is commonly associated with fast CSF leaks, thought to be related to slow oozing of blood at the site of the dural defect.<sup>18</sup> This superficial siderosis tends to be infratentorial and can regress after repair of the CSF leak.<sup>19</sup> Prior reports have suggested that infratentorial siderosis is present in up to 20% of patients with a ventral spinal CSF leak.<sup>18</sup> Because the current study excluded patients with an SLEC (and therefore a fast CSF leak), superficial siderosis was infrequently observed. The results of the current study should not be incorrectly interpreted to suggest that siderosis is not associated with spinal CSF leaks in general. Similarly, although subdural fluid collections did not reach the statistical threshold of being associated with a CSF leak in this study, these findings should not be misinterpreted to suggest that subdural collections are unrelated to SIH.

Finally, although nearly 40% of patients with a low probability of a score were found to have a leak, there is a substantial selection bias in the patients included in this cohort, all of whom had clinically suspected SIH. Nevertheless, given this large incidence of patients with relatively normal intracranial findings, the results of this study might suggest that DSMs may be warranted for patients with a high clinical suspicion of SIH.

This study has several limitations. First, the conclusions are based on a retrospective review. Prospective studies are needed to validate our results. In addition, because each patient was only reviewed by a single neuroradiologist, this study was not able to provide interobserver agreement analyses. Next, 2 findings were allowed to be given an “indeterminate” score during the initial assessment: whether a leak was visualized on DSM and/or the subsequent CT, and the presence or absence of dural venous sinus engorgement. In both cases, we lumped indeterminate findings into “positive” categories to best match the clinical realities. Also, there was some selection bias intrinsic to the methodology of this study, given that only patients without an SLEC were included. In addition, the reviewers were not blinded to the official reports or annotations in the PACS system. Finally, the



statistical analysis of our data allowed the development of only a dichotomized scoring system, rather than the prior 3-tiered (low, indeterminate, high) system. For the clinician, however, this may actually simplify the decision to proceed or not to myelography.

## CONCLUSIONS

This study set out to determine the likelihood of having a CSF leak based on intracranial MR imaging findings in patients without an SLEC. A new scoring system was developed on the basis of 7 intracranial findings associated with a leak. Some of the criteria used by the established scoring system did not meet the statistical threshold to include them in this new scoring system. Although this system was not significantly more accurate at predicting leaks than the Dobrocky method, it has potential benefits that could make it worthy of future studies.

Disclosure forms provided by the authors are available with the full text and PDF of this article at [www.ajnr.org](http://www.ajnr.org).

## REFERENCES

1. Callen AL, Timpone VM, Schwertner A, et al. **Algorithmic multimodality approach to diagnosis and treatment of spinal CSF leak and venous fistula in patients with spontaneous intracranial hypotension.** *AJR Am J Roentgenol* 2022;219:292–301 CrossRef Medline
2. Madhavan AA, Benson JC, Cutsforth-Gregory JK, et al. **Co-existing fast CSF leaks and CSF-venous fistulas on dynamic CT myelography.** *Radiol Case Rep* 2022;17:2968–71 CrossRef Medline
3. Dobrocky T, Nicholson P, Häni L, et al. **Spontaneous intracranial hypotension: searching for the CSF leak.** *Lancet Neurol* 2022;21:369–80 CrossRef Medline
4. Mark I, Madhavan A, Oien M, et al. **Temporal characteristics of CSF-venous fistulas on digital subtraction myelography.** *AJNR Am J Neuroradiol* 2023;44:492–95 CrossRef Medline
5. Madhavan AA, Verdoorn JT, Shlapak DP, et al. **Lateral decubitus dynamic CT myelography for fast cerebrospinal fluid leak localization.** *Neuroradiology* 2022;64:1897–903 CrossRef Medline
6. Kim DK, Brinjikji W, Morris PP, et al. **Lateral decubitus digital subtraction myelography: tips, tricks, and pitfalls.** *AJNR Am J Neuroradiol* 2020;41:21–28 CrossRef Medline
7. Schievink WI. **Spontaneous spinal cerebrospinal fluid leaks and intracranial hypotension.** *JAMA* 2006;295:2286–96 CrossRef Medline
8. Benson JC, Madhavan AA, Cutsforth-Gregory JK, et al. **The Monroe-Kellie doctrine: a review and call for revision.** *AJNR Am J Neuroradiol* 2023;44:2–6 CrossRef Medline
9. Bond KM, Benson JC, Cutsforth-Gregory JK, et al. **Spontaneous intracranial hypotension: atypical radiologic appearances, imaging mimickers, and clinical look-alikes.** *AJNR Am J Neuroradiol* 2020;41:1339–47 CrossRef Medline
10. Dobrocky T, Grunder L, Breiding PS, et al. **Assessing spinal cerebrospinal fluid leaks in spontaneous intracranial hypotension with a scoring system based on brain magnetic resonance imaging findings.** *JAMA Neurol* 2019;76:580–87 CrossRef Medline
11. Pradeep A, Madhavan AA, Brinjikji W, et al. **Incidence of spontaneous intracranial hypotension in Olmsted County, Minnesota: 2019–2021.** *Interv Neuroradiol J* 2023 March 22. [Epub ahead of print] CrossRef Medline
12. Farb RI, Nicholson PJ, Peng PW, et al. **Spontaneous intracranial hypotension: a systematic imaging approach for CSF leak localization and management based on MRI and digital subtraction myelography.** *AJNR Am J Neuroradiol* 2019;40:745–53 CrossRef Medline
13. Babcock JC, Johnson DR, Benson JC, et al. **Diffuse calvarial hyperostosis and spontaneous intracranial hypotension: a case-control study.** *AJNR Am J Neuroradiol* 2022;43:978–83 CrossRef Medline
14. Johnson DR, Carr CM, Luetmer PH, et al. **Diffuse calvarial hyperostosis in patients with spontaneous intracranial hypotension.** *World Neurosurg* 2021;146:e848–53 CrossRef Medline
15. Farb RI, Forghani R, Lee SK, et al. **The venous distension sign: a diagnostic sign of intracranial hypotension at MR imaging of the brain.** *AJNR Am J Neuroradiol* 2007;28:1489–93 CrossRef Medline
16. Kim DK, Carr CM, Benson JC, et al. **Diagnostic yield of lateral decubitus digital subtraction myelogram stratified by brain MRI findings.** *Neurology* 2021;96:e1312–18 CrossRef Medline
17. Callen AL, Pattee J, Thaker AA, et al. **Relationship of Bern score, spinal elastance, and opening pressure in patients with spontaneous intracranial hypotension.** *Neurology* 2023;100:e2237–46 CrossRef Medline
18. Schievink WI, Maya MM, Nuño M. **Chronic cerebellar hemorrhage in spontaneous intracranial hypotension: association with ventral spinal cerebrospinal fluid leaks: clinical article.** *J Neurosurg Spine* 2011;15:433–40 CrossRef Medline
19. Schievink WI, Maya M. **Regression of infratentorial superficial siderosis following surgical repair of a spontaneous spinal CSF leak.** *Neurol Clin Pract* 2021;11:e359–60 CrossRef Medline

# Clinical Outcomes and Safety Comparison of Vertebroplasty, Balloon Kyphoplasty, and Vertebral Implant for Treatment of Vertebral Compression Fractures

✉ Taibo Li, Sharon Pang, ✉ Ryan England, Anna Gong, ✉ David Botros, Sasicha Manupipatpong, ✉ Ferdinand K. Hui, and ✉ Majid Khan



## ABSTRACT

**BACKGROUND AND PURPOSE:** Vertebral compression fracture represents a major health burden for the aging populations globally. However, limited studies exist on the relative efficacy and safety of surgical interventions for vertebral compression fracture. Here, we aim to compare clinical and patient-reported outcomes following vertebral augmentation using balloon kyphoplasty, vertebroplasty, and SpineJack vertebral implant.

**MATERIALS AND METHODS:** An institutional review board–approved, retrospective, multi-institutional review of patients undergoing vertebral augmentation with kyphoplasty, vertebroplasty, and/or a SpineJack vertebral implant was performed between 2018 and 2021. Primary outcomes included pre- and postprocedural pain ratings and vertebral body height restoration. The secondary outcome was a change in the local kyphotic angle. The Kruskal-Wallis test was used to compare outcomes across 3 treatment options. Complications were reviewed during and 30–90 days after the procedure.

**RESULTS:** Vertebral augmentation of 344 vertebral compression fracture levels was performed during the study period. Sixty-seven patients had 79 kyphoplasty procedures (55% women; mean age, 64.2 [SD, 12.3] years). Seventy-four patients underwent a mean of 84 vertebroplasty procedures (51% women; mean age, 63.5 [SD, 12.8] years), and 61 patients had a mean of 67 SpineJack vertebral implant procedures (57.4% women; mean age, 68.3 [SD, 10.6] years). Following kyphoplasty, vertebroplasty, and SpineJack vertebral implant, pain scores improved significantly ( $P < .001$ ). Resting pain improvement was similar across the 3 procedures, whereas improvement of “worst pain” was significantly better following a SpineJack vertebral implant compared with kyphoplasty and vertebroplasty ( $P < .001$ ). Patients with a SpineJack vertebral implant had greater improvement in vertebral body height restoration and local kyphotic angle compared with those undergoing kyphoplasty and vertebroplasty. Adjacent level fractures (6.7% incidence) occurred similarly in the 3 procedure types. There were no other peri- or postoperative complications.

**CONCLUSIONS:** The SpineJack vertebral implant showed equivalent pain improvement compared with vertebroplasty and kyphoplasty, but it had superior vertebral body height restoration and local kyphotic angle improvement. This study supports the SpineJack vertebral implant as a safe and effective alternative (adjunct) for vertebral augmentation, especially in patients with moderate-to-severe vertebral compression fractures for greater improvement in vertebral body height restoration.

**ABBREVIATIONS:** KP = balloon kyphoplasty; LKA = local kyphotic angle; PMMA = polymethylmethacrylate; SJ = SpineJack vertebral implant; VCF = vertebral compression fracture; VH = vertebral body height; VP = vertebroplasty

Vertebral compression fractures (VCFs) are common throughout the world, especially affecting older populations.<sup>1</sup> In the

United States alone, there have been up to 1.5 million VCFs annually.<sup>2,3</sup> VCFs are caused by trauma, infection, cancer, and, most commonly, osteoporosis—especially in postmenopausal women.<sup>3,4</sup> VCFs frequently cause severe pain and disability, limiting activities of daily living and resulting in decreased quality of life.<sup>5,6</sup> Limiting

Received March 18, 2023; accepted after revision September 14.

From the Department of Biomedical Engineering (T.L.), Johns Hopkins School of Medicine, Baltimore, Maryland; Department of Emergency Medicine (S.P.), Massachusetts General Hospital, Boston, Massachusetts; Russell H. Morgan Department of Radiology and Radiological Science (R.E., F.K.H.), The Johns Hopkins Hospital, Baltimore, Maryland; Johns Hopkins School of Medicine (A.G., D.B., S.M.), Baltimore, Maryland; Neurointerventional Surgery Division (F.K.H.), The Queen's Medical Center, Honolulu, Hawaii; Non-Vascular Interventional Neuroradiology (M.K.), Department of Radiology, Thomas Jefferson University Hospital, Philadelphia, Pennsylvania; and Division of Neuroradiology and Division of Interventional Radiology (M.K.), Russell H. Morgan Department of Radiology and Radiological Science, The Johns Hopkins Hospital, Baltimore, Maryland.

F.K. Hui and M. Khan are senior authors.

Please address correspondence to Taibo Li, MS, Medical Scientist Training Program, Department of Biomedical Engineering, Johns Hopkins School of Medicine, 1830 E Monument St, Suite 2-130 Baltimore, MD, 21205; e-mail: taiboli@jhu.edu; @taibo\_li

✉ Indicates open access to non-subscribers at [www.ajnr.org](http://www.ajnr.org)

☰ Indicates article with online supplemental data.

<http://dx.doi.org/10.3174/ajnr.A8031>

activities of daily living and concurrent medical conditions can complicate patients' health and nutrition and increase morbidity and mortality rates compared with the general population.<sup>3</sup> Most important, patients who have had a VCF are at higher risk for recurrent fracture, further limiting the quality of life of the patient and leading to repeat hospital visits and increased costs.

There are multiple nonsurgical and surgical treatment options for VCFs. Nonsurgical treatments include bed rest, analgesics, hyperextension braces (used for benign fractures), and radiation therapy for pathologic fractures (including stereotactic body radiation therapy and proton beam therapy for oligometastatic and diffuse pathologic osseous involvement). However, these treatments may not be effective and can result in multiple complications; for example, immobilization from bed rest can lead to weakness, pressure ulcers, and venous thromboembolism. Minimally invasive surgical treatments include balloon kyphoplasty (KP), percutaneous vertebroplasty (VP), internal bracing, and, more recently, vertebral implants such as the SpineJack vertebral implant (SJ) system (Stryker). Surgical options have become increasingly popular because their effects have been found to be rapid and sustained.<sup>7-11</sup> Vertebral augmentation strategies have been shown to greatly reduce stresses for various preaugmentation vertebral heights in 3D reconstruction models of compression fractures.<sup>10</sup> There have been controversial studies considering serious complications following surgical treatments, such as new vertebral fractures, but more recent meta-analyses did not replicate these conclusions.<sup>9,12</sup> Furthermore, patients with osteoporotic compression fractures were found to have decreased mortality following vertebral augmentation compared with nonsurgical treatment.<sup>8</sup> Nevertheless, older patients who present with VCF along with multiple comorbidities often face risks and contraindications to vertebral augmentation, leading to poorer outcomes, such as increased morbidity and mortality and postoperative complications.<sup>13-15</sup>

Vertebral implant procedures such as SJ introduce permanent titanium implants to help restore vertebral height, and received FDA approval in 2018.<sup>16</sup> While with VP, polymethylmethacrylate (PMMA) is directly injected into the VCF space and KP uses an inflated balloon to prepare a cavity before injection of PMMA, SJ uses a bilateral transpedicular approach with placement of implants within the vertebral body,<sup>9,17,18</sup> allowing progressive and well-controlled reduction of vertebral fractures.<sup>17</sup> The amount of PMMA injected is lower than in VP or KP, theoretically decreasing the risk of PMMA leakage and adjacent vertebral body fractures.<sup>17</sup> While the SJ has only been approved for osteoporotic and traumatic fractures, its efficacy in vertebral height restoration may aid in reducing other vertebral fractures, such as fractures secondary to tumors.<sup>17,19</sup>

In this study, we hypothesized that a vertebral implant is a safe and effective approach for patients with VCF under broad indications. Consequently, we aimed to evaluate patient outcomes of KP, VP, and SJ by comparing clinical outcomes (pre- and postprocedural pain scores), radiologic measurements (anterior and middle vertebral body height [VH] and local kyphotic angle [LKA]), and complications following vertebral augmentation among the 3 types of procedures.

## MATERIALS AND METHODS

This was an institutional review board–approved, retrospective, multi-institutional cohort study, located at 2 tertiary care hospital

centers (The Johns Hopkins Hospital and Thomas Jefferson University Hospital), of 202 patients who received vertebral augmentation for a total of 344 vertebral levels from November 1, 2018, to September 1, 2021. Medical records including demographics, pain scores, and imaging measurements were obtained and reviewed. Treatment efficacy was defined by primary and secondary objectives. Primary outcome variables included pre- and postprocedural pain ratings and VH restoration. The secondary outcome variable was a change in the LKA. Complications of the cohort during and after procedures (follow-up time varied) were reviewed to assess safety.

### Inclusion Criteria

We included patients experiencing intractable mechanical back pain from osteoporotic or pathologic vertebral fractures, which were augmented using KP, VP, and/or SJ during the study period. Pathologic compression fractures were included in this study on an off-label basis.

### Exclusion Criteria

We excluded patients who experienced primarily radicular back pain without a mechanical component and patients experiencing pathologic fractures with epidural tumor extension or spinal canal and/or cord compression.

### Clinical Assessment

Clinical outcomes collected included patient-reported pain scores (both “at rest” and “at worst”) before and after the vertebral augmentation procedure (KP, VP, and/or SJ) and complication rates. Preprocedural evaluation occurred generally 1 month before the procedure. Postprocedural clinic evaluations occurred 3 weeks to 3 months after the procedure. The pain scale used was a 10-point numeric scale, in which 0 indicates no pain and 10 indicates the “worst pain” ever experienced. Pain scores were assessed both in the presurgical assessment and during a follow-up clinic visit, in which patients were asked about their level of pain at baseline (at rest) and about their worst ever level of pain during the assessment periods regardless of triggering events (at worst).

### Radiographic Assessment

Technical outcomes involved radiographic assessments of LKA and VHs in the craniocaudal dimension at the mid and anterior vertebral body levels before and immediately after the procedure for all patients (Fig 1), which were reviewed by attending radiologists (F.K.H., M.K.). An increase in VH and a decrease in the LKA represented improvement in vertebral height restoration.

### Safety Assessment

Follow-up evaluations ranged from 30 to 90 days after the procedure. Procedural and clinic notes were reviewed to evaluate complications. Complications assessed included perisurgical technical complications, device removal, cement leakage, and postprocedural compression fractures. Follow-up imaging with radiographs or CT performed during follow-up clinic visits between 3 and 6 months was used to assess any evidence of adjacent level fractures or other adverse events.

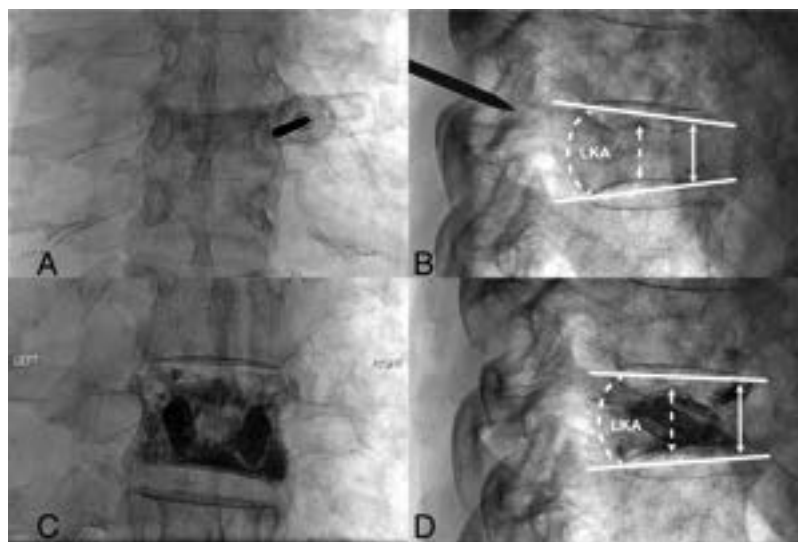


**FIG 1.** Sample radiographic measurements. A 72-year-old man with a history of osteoporosis presented with severe midthoracic back pain. Anterior-posterior (A) and lateral (B) projections of fluoroscopic images of the thoracic spine with the needle at the level of T8 demonstrate a preprocedural T8 vertebral compression fracture, as shown by an increased LKA formed by *solid white lines* along the superior and inferior endplates and decreased midvertebral (*dashed arrow*) and anterior-vertebral (*solid arrow*) body heights. Following vertebral augmentation with SJ, anterior-posterior (C) and lateral (D) projections show postprocedural changes with improvement in LKA and VH at T8.

**Table 1: Patient demographics**

	Kyphoplasty	Vertebroplasty	SJ
No. of patients	67	74	61
No. of total procedures	79	84	67
Age (mean) (yr)	64.2 (SD, 12.3)	63.5 (SD, 12.8)	68.3 (SD, 10.6)
No. of female (%)	37 (55.2)	38 (51.4)	35 (57.3)
No. of African American (%)	12 (17.9)	15 (20.3)	14 (22.9)
No. of European (%)	46 (68.6)	49 (66.2)	37 (60.7)
No. of other race (%)	9 (13.4)	10 (13.5)	10 (16.4)
BMI (mean)	28.2 (SD, 7.3)	26.8 (SD, 5.8)	28.7 (SD, 7.1)
No. of pathologic fractures <sup>a</sup>	46	59	19
No. of structural fractures <sup>a</sup>	19	15	42
No. of treatment sessions			
1 Procedure	58	64	57
2 Procedures	7	10	2
3 Procedures	1	0	2
4 Procedures	1	0	0
Median follow-up period (days)	39.5	70	94

<sup>a</sup> Not all patients had recorded fracture type.

### Statistical Analysis

Baseline characteristics of total procedures were summarized as count, mean (SD), and frequency. Some patients underwent multiple procedures on the same day (ie, KP at 1 vertebral level and SJ at another). In those cases, each type of procedure performed was counted in the total count of procedures. To account for patients who received >1 type of VCF treatment, we applied a bootstrapping algorithm to assess changes in pain scores and radiographic augmentation outcomes pre- and postsurgery, so that for each outcome variable, a total of 1000 subsamples were drawn from the patient cohort in which data from each patient appeared only once. A 2-sample *t* test was then conducted to assess statistical significance between bootstrapped sample means, and the

Kruskal-Wallis H test was used to compare among different procedures (KP, VP, and SJ). Pain score and adjacent level fracture outcomes were assessed during individual clinical visits and may occur in patients having undergone >1 type of procedure. In these cases, an additional subgroup analysis was performed using data from those patients with only 1 type of augmentation procedure. A mixed-effect linear logistic model was constructed to assess the influence of demographic (age, sex, race) and clinical (body mass index, total levels operated, type of procedure) variables on adjacent level fractures using patient as the random effect. Statistical significance was assessed at  $\alpha = .05$ . All statistical computation was performed using the R statistical and computing software (Version 3.4.0; <http://www.r-project.org/>).

## RESULTS

### Demographics and Case Characteristics

Sixty-seven patients underwent 79 KP procedures (55.2% women; mean age, 64.2 [SD, 12.3] years), 74 patients had 84 VP procedures (51.4% women; mean age, 63.5 [SD, 12.8] years), and 61 patients had 67 SJ procedures (57.4% women; mean age, 68.3 [SD, 10.6] years). Additional demographic data are reported in Table 1. Because the number of treatment sessions varied on the basis of the patient's clinical presentation and progression, total treatment sessions are also reported in Table 1. KP and VP were more often performed for pathologic fractures, whereas SJ was performed more for structural fractures (Table 1). SJ procedures had the longest median follow-

up of 94 days, followed by VP (70 days) and KP (40 days). There were no major complications immediately postprocedure in all cases. Of note, 1 augmentation procedure was aborted due to patient oxygen desaturations while supine, before starting the procedure.

### Patient-Reported Outcomes

In all 3 procedures, pain scores reported both at rest and at worst improved significantly after the procedure compared with prior to it (all,  $P < .001$ , Fig 2 and Table 2). Patients' worst pain scores improved following KP (8.3 to 4.1; 95% confidence interval of the change [95% CI  $\Delta$ ]: 3.4–5.1;  $P < .001$ ), VP (7.8 to 4.1; 95% CI  $\Delta$ : 2.9–4.4;  $P < .001$ ), and SJ (8.6 to 3.7; 95% CI  $\Delta$ : 4.3–5.5;  $P < .001$ ).



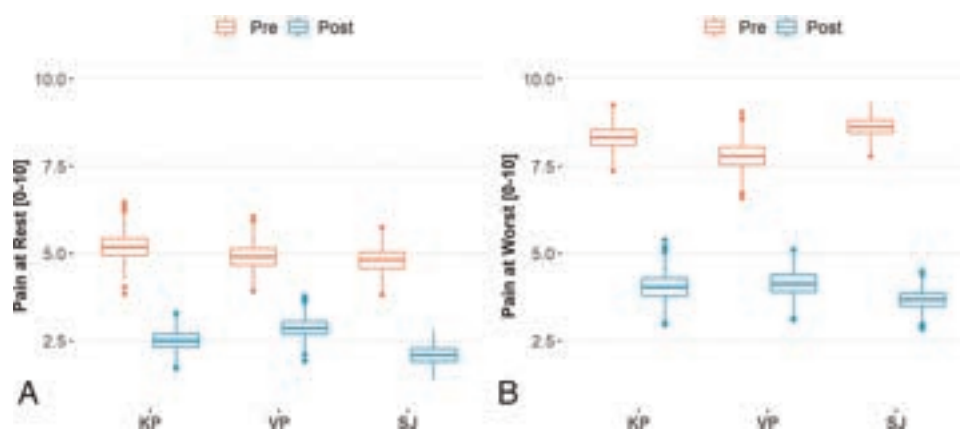


**FIG 2.** Pain score comparison. A, Distribution of patient-reported pain scores on a scale between 0 and 10 at rest for 3 procedure types pre- (red) and postprocedure (blue). B, The same pain score distribution reported at worst. Shown are median and interquartile ranges.

**Table 2: Patient-reported outcomes**

Pain Score at Rest (0–10)	KP	VP	SJ	P Value <sup>a</sup>
Pre (mean)	5.2	4.9	4.8	>.05
Post (mean)	2.5	2.9	2.1	
Δ 95% CI	(1.9–3.5)	(1.3–2.7)	(2.1–3.3)	
P value <sup>b</sup>	<.001	<.001	<.001	
Pain score at worst (0–10)				
Pre (mean)	8.3	7.8	8.6	<.001
Post (mean)	4.1	4.1	3.7	
Δ 95% CI	(3.4–5.1)	(2.9–4.4)	(4.3–5.5)	
P value <sup>b</sup>	<.001	<.001	<.001	

<sup>a</sup> The P value was calculated with Kruskal-Wallis  $\chi^2$  tests across procedures.

<sup>b</sup> The P value was calculated with bootstrapping.

Following SJ, patients reported a larger reduction in pain at worst compared with VP and KP, though improvement in pain scores at rest was comparable in all procedure types. Similar results were obtained if comparisons were restricted to patients who underwent only 1 type of procedure (44 patients with KP [8.2 to 3.8 at worst; 5.3 to 2.5 at rest], 45 patients with VP [6.9 to 3.6 at worst; 4.9 to 2.9 at rest], and 37 patients with SJ [8.8 to 3.4 at worst; 4.6 to 1.6 at rest]). Notably, in a subanalysis on the underlying pathology of these procedures, patients' pain scores improved more following SJ for pathologic fractures compared with structural fractures (Online Supplemental Data).

### Radiographic Outcomes

Anterior and middle vertebral body measurements from before and after vertebral augmentation procedures showed improved height restoration following KP, VP, and SJ (Table 2). Both absolute change in VH (craniocaudal length) and percentage change of VH were significantly increased in all procedure groups when comparing pre- with postprocedural measurements ( $P < .001$ , Fig 3, and Table 3). Most important, SJ had significantly greater VH restoration, both in the anterior and middle columns of the vertebral body, compared with both KP and VP (each,  $P < .001$ , Table 2). The kyphotic angle was also measured before and after procedures, which showed patients having undergone SJ with a significantly improved LKA compared with both KP and VP (each  $P < .001$ , Table 2).

### Complications

There were no perioperative adverse events, symptomatic cement leakage, or device-removal complication in any of the cases in this study. However, of the 344 VCF levels treated, there were 23 adjacent vertebral fractures, representing a 6.7% adjacent level fracture rate. Lumbar levels were over-represented in all procedures in which combination treatment was performed in multilevel fractures on the basis of vertebral height loss (Online Supplemental

Data). Overall, adjacent level fractures were rare among patients undergoing only 1 type of procedure (1/44 KP, 3/46 VP, and 1/37 SJ visits, Table 4). There were a total of 23 adjacent level fractures in 13 patients. The logistic regression model revealed that there was no difference in the fraction of these fractures across the 3 procedure types ( $P > .05$ ). Demographic variables such as sex, race, and body mass index were not significantly associated with the outcome of adjacent level fracture, while the total number of levels operated were, so that each increased level of augmentation resulted in a 2.4-fold increase in the odds of having an adjacent level fracture (95% CI, 1.8–3.2).

### DISCUSSION

Among the many distinct types of surgical interventions for VCFs, vertebral implant systems such as the SJ were the most recently approved by the FDA.<sup>16</sup> Therefore, limited data exist to benchmark clinical outcomes between vertebral implant and other vertebral augmentation procedures, representing a major gap in the current knowledge on treatment-planning for patients with VCF. In this multi-institutional retrospective study, patient-reported and radiographic outcomes were compared in patients receiving balloon KP, VP, and SJ vertebral implant for VCFs. We hypothesized that vertebral implant systems such as SJ will lead to comparable, if not better, clinical improvement for patients with increased vertebral height restoration, therefore justifying its application in a wide range of indications, including osteoporotic and pathologic fractures.

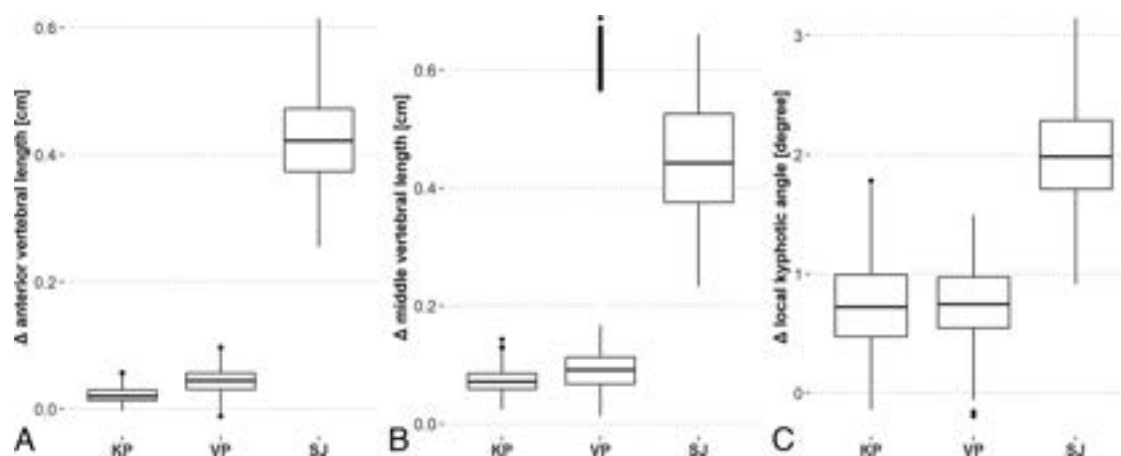


**FIG 3.** Vertebral augmentation radiologic changes. A, Distribution of changes in radiographic vertebral augmentation measurements for anterior vertebral length for the 3 procedures B, The same distribution of changes for middle vertebral length. C, The same distribution of changes for local kyphotic angle. Shown are median and interquartile ranges.

**Table 3: Augmentation measurement outcomes**

	KP	VP	SJ	P Value <sup>a</sup>
Anterior vertebral length (mm)				
Pre (mean)	18.4	20.6	13.0	<.001
Post (mean)	18.6	21.0	17.3	
Δ 95% CI	(0.03–0.4)	(0.09–0.79)	(3.1–5.6)	
% Increase (mean)	1.1	2.2	32.4	
% CI	(0.14–2.59)	(0.4–3.9)	(23.5–43.6)	
Middle vertebral length (mm)				
Pre (mean)	15.9	17.9	12.7	<.001
Post (mean)	16.6	19.5	17.2	
Δ 95% CI	(0.4–1.1)	(0.4–6.5)	(3.0–6.0)	
% Increase (mean)	4.5	5.0	35.6	
% CI	(2.3–7.1)	(2.1–36.8)	(24.0–46.4)	
LKA				
Pre (mean)	7.6°	6.8°	8.9°	<.001
Post (mean)	6.9°	6.1°	6.9°	
Δ Angle				
Δ 95% CI	(0.09°–1.38°)	(0.15°–1.33°)	(1.24°–2.80°)	

<sup>a</sup> The P value calculated with Kruskal-Wallis  $\chi^2$  tests across procedures.

In a pilot study with 30 patients with osteoporotic VCFs, patients having undergone SJ had better vertebral height and local kyphotic angle restoration compared with those undergoing KP.<sup>20</sup> In another early study following 77 patients who had undergone SJ for 5 years, patients experienced improvement in pain relief, self-sufficiency quality of life, and vertebral height.<sup>21</sup> While there has been promising data on the use of SJ for VCFs, existing studies remain limited in the scope of comparison and/or monocenter design because a comprehensive study involving VP, KP, and SJ is lacking. Our data show that pain score improvement for resting pain after SJ procedures was comparable with that after KP and VP. Moreover, patients having undergone SJ reported larger pain score improvement for pain at worst over the other 2 procedures. Vertebral height and kyphotic angle improvement were all significantly greater in patients having undergone SJ than in those having undergone KP and VP.

Our conclusions are similar to findings from previous studies which showed improved pain scores, VH, and LKA after vertebral implant compared to kyphoplasty,<sup>17,20,22–24</sup> although vertebroplasty was not included in those comparisons. Additionally,

most previous studies comparing vertebral augmentation outcomes have compared KP with VP. One meta-analysis showed that KP tended to have significantly better pain reduction than non-surgical management and better height restoration than VP, while VP had better pain reduction (though not statistically significant) than nonsurgical treatment.<sup>25</sup> This result was in contrast to no significant difference in pain and disability outcomes between KP and VP in a separate meta-analysis by Gu et al.<sup>26</sup> Another review study noted multiple randomized controlled trials,<sup>9</sup> including the Kyphoplasty And Vertebroplasty In the Augmentation and Restoration of Vertebral Body Compression Fractures (KAVIAR) trial,<sup>27</sup> showing longer proce-

dural times with KP, but no difference in clinical outcomes or rates of complication.<sup>9</sup> Furthermore, a retrospective study found that KP and VP were both safe and effective procedures for patients, but it noted complications of PMMA leakage and epidural hematomas.<sup>28</sup> Among the few studies on clinical outcomes and safety involving SJ, one small study compared KP with SJ and VP patient groups, which found improved kyphotic angle and middle VH restoration in the KP with the SJ group, and no difference in pain scores or complication rates.<sup>29</sup> Nevertheless, that study combined KP with SJ in the comparison. In the present study, we directly compared SJ outcomes with KP and VP outcomes, a comparison that is more clinically relevant because KP and VP are the currently accepted and popular procedures for VCFs, while SJ is only approved for osteoporotic and traumatic fractures and more recently approved for use in clinical practice in the United States.

Although SJ is a much newer vertebral augmentation method, as shown in our study and in a handful of others, it presents better improvement in terms of pain scores and shows significant improvement of VH and LKA compared with KP and VP.

**Table 4: Adjacent level fracture statistics**

	KP	VP	SJ
By visit <sup>a</sup>			
Total No. of procedures	44	46	37
No. of visits with adj. fracture	1	3	1
Total No. of individuals with adj. fracture	1	3	1
No. of levels with adj. fractures	6	8	9
By level <sup>b</sup>			
Total No. of levels	113	132	102
Total No. of individuals with adj. fracture	5	8	4

**Note:**—adj. indicates adjacent.

<sup>a</sup> Only visits with 1 type of procedure (KP, VP, or SJ) were included.

<sup>b</sup> All visits were considered.

Furthermore, because it is currently only FDA-approved to treat osteoporotic and traumatic VCFs, our direct outcome comparison including pathologic or secondary VCFs informs the interventional community of benefit in off-label use of SJ and may support future approval of use in other pathologies. We found that pain scores showed greater improvement for pathologic fractures following vertebral implants in our subanalysis. In practice, we performed microwave ablation on approximately 25% of pathologic fractures regardless of the choice of surgical procedures, which, in itself, could palliate the pain during coagulation necrosis of the tumor and destruction of the nerve ending. Future research is warranted to optimize the combination of ablation and surgical interventions for VCF management. Notably, our data suggest that major complications such as adjacent level fractures were not more common in vertebral implants compared with well-established procedures, advocating the use in a wider range of future clinical applications.

In our multi-institutional cohort, patients selected for SJ had less anterior and middle vertebral heights and larger local kyphotic angles than patients selected for KP and VP before each procedure. This outcome was because patients with moderate-to-severe height loss were preferentially selected to receive vertebral implants because of the suspected clinical advantage of height restoration in these patients. This secondary benefit of SJ was confirmed by this study, further supporting the potential utility of a vertebral implant as a safe and effective treatment for moderate-to-severe VCFs. However, the observed benefits of SJ in comparison with those from other procedures should be interpreted with caution, given the retrospective nature of this study.

Additional limitations of this study include retrospective review and a moderately sized patient population, particularly in the vertebral implant group. This limitation is partially due to the novelty of this procedure and the lack of FDA approval for cancer-related VCF indications. Although this may limit the generalizability of our results, we noted that our multi-institutional, multiprovider study design was aimed at minimizing confounding effects on clinical outcomes. Additionally, we found a potential trend toward improved reduction in worst pain with SJ in patients with VCF, but we may be limited in the power to detect benefits of one procedure type over another. Future larger randomized controlled trials would be needed to directly compare these procedures. Another limitation is that some patients received >1 type of vertebral augmentation, which may introduce correlations in our data set and violate the independence assumptions of statistical testing. We addressed this challenge by

designing a rigorous bootstrapping procedure to avoid inflation of type 1 errors. We further confirmed our findings by performing a separate analysis using data from visits with only 1 type of vertebral augmentation, which did not alter our findings.

Overall, we present the first systematic study analyzing patient-reported and radiographic outcomes following 3 types of VCF procedures, demonstrating vertebral implants as safe and effective alternatives to VP or KP in a wide variety of clinical scenarios. With vertebral implants becoming more common and consistent across the United States, this study may contribute to better understanding of their implications in patients in comparison with alternative therapies.

## CONCLUSIONS

Vertebral implant systems demonstrated similar pain improvement in patients with structural and pathologic VCFs compared with KP and VP, but they showed superior VH restoration and LKA improvement. Our findings support the vertebral implant as a safe and effective treatment option for vertebral augmentation. Future studies are warranted to establish comparative advantages of each procedure for optimal treatment-planning of specific groups of patients with VCFs.

**Disclosure forms** provided by the authors are available with the full text and PDF of this article at [www.ajnr.org](http://www.ajnr.org).

## REFERENCES

- Dewar C. **Diagnosis and treatment of vertebral compression fractures.** *Radiol Technol* 2015;86:301–20; quiz 321–23 Medline
- Wong CC, McGirt MJ. **Vertebral compression fractures: a review of current management and multimodal therapy.** *J Multidiscip Healthc* 2013;6:205–14 CrossRef Medline
- Alexandru D, So W. **Evaluation and management of vertebral compression fractures.** *Perm J* 2012;16:46–51 CrossRef Medline
- Tobert DG, Schwab JH. **Pathologic vertebral fractures: diagnosis, treatment, complications, and controversies through case-based learning.** *Instr Course Lect* 2019;68:585–91 Medline
- Jung HJ, Park YS, Seo HY, et al. **Quality of life in patients with osteoporotic vertebral compression fractures.** *J Bone Metab* 2017;24:187–96 CrossRef Medline
- Lips P, Cooper C, Agnusdei D, et al. **Quality of life in patients with vertebral fractures: validation of the Quality of Life Questionnaire of the European Foundation for Osteoporosis (QUALEFFO): Working Party for Quality of Life of the European Foundation for Osteoporosis.** *Osteoporos Int* 1999;10:150–60 CrossRef Medline
- Health Quality Ontario. **Vertebral augmentation involving vertebroplasty or kyphoplasty for cancer-related vertebral compression fractures: a systematic review.** *Ont Health Technol Assess Ser* 2016;16:1–202 Medline
- Hinde K, Maingard J, Hirsch JA, et al. **Mortality outcomes of vertebral augmentation (vertebroplasty and/or balloon kyphoplasty) for osteoporotic vertebral compression fractures: a systematic review and meta-analysis.** *Radiology* 2020;295:96–103 CrossRef Medline
- Chandra RV, Maingard J, Asadi H, et al. **Vertebroplasty and kyphoplasty for osteoporotic vertebral fractures: what are the latest data?** *AJNR Am J Neuroradiol* 2018;39:798–806 CrossRef Medline
- Zhao WT, Qin DP, Zhang XG, et al. **Biomechanical effects of different vertebral heights after augmentation of osteoporotic vertebral compression fracture: a three-dimensional finite element analysis.** *J Orthop Surg Res* 2018;13:32 CrossRef Medline
- Descamps J, Lamerain M, Chenguel Z, et al. **Vertebral compression fractures treated in acute by instrumented kyphoplasty: early and**

- mid-term clinical and radiological results. *Biomed Res Int* 2019;2019:1386510 CrossRef Medline
12. Zhang H, Xu C, Zhang T, et al. Does percutaneous vertebroplasty or balloon kyphoplasty for osteoporotic vertebral compression fractures increase the incidence of new vertebral fractures? A meta-analysis. *Pain Physician* 2017;20:E13–28 Medline
  13. Deiner S, Westlake B, Dutton RP. Patterns of surgical care and complications in elderly adults. *J Am Geriatr Soc* 2014;62:829–35 CrossRef Medline
  14. Turrentine FE, Wang H, Simpson VB, et al. Surgical risk factors, morbidity, and mortality in elderly patients. *J Am Coll Surg* 2006;203:865–77 CrossRef Medline
  15. Story DA. Postoperative complications in elderly patients and their significance for long-term prognosis. *Curr Opin Anaesthesiol* 2008;21:375–79 CrossRef Medline
  16. Melkerson M. K181262 Trade/Device Name: SpineJack® Expansion Kit: FDA U.S Food & Drug Administration. [https://www.accessdata.fda.gov/cdrh\\_docs/pdf18/K181262.pdf](https://www.accessdata.fda.gov/cdrh_docs/pdf18/K181262.pdf). Accessed March 16, 2023
  17. Vanni D, Galzio R, Kazakova A, et al. Third-generation percutaneous vertebral augmentation systems. *J Spine Surg* 2016;2:13–20 CrossRef Medline
  18. El-Fiki M. Vertebroplasty, kyphoplasty, lordoplasty, expandable devices, and current treatment of painful osteoporotic vertebral fractures. *World Neurosurg* 2016;91:628–32 CrossRef Medline
  19. England RW, Gong A, Li T, et al. Clinical outcomes and safety of the SpineJack vertebral augmentation system for the treatment of vertebral compression fractures in a United States patient population. *J Clin Neurosci* 2021;89:237–42 CrossRef Medline
  20. Noriega DC, Rodriguez-Monsalve F, Ramajo R, et al. Long-term safety and clinical performance of kyphoplasty and SpineJack® procedures in the treatment of osteoporotic vertebral compression fractures: a pilot, monocentric, investigator-initiated study. *Osteoporos Int* 2019;30:637–45 CrossRef Medline
  21. Renaud C. Treatment of vertebral compression fractures with the cranio-caudal expandable implant SpineJack®: technical note and outcomes in 77 consecutive patients. *Orthop Traumatol Surg Res* 2015;101:857–59 CrossRef Medline
  22. Rotter R, Schmitt L, Gierer P, et al. Minimum cement volume required in vertebral body augmentation: a biomechanical study comparing the permanent SpineJack device and balloon kyphoplasty in traumatic fracture. *Clin Biomech (Bristol, Avon)* 2015;30:720–25 CrossRef Medline
  23. Noriega D, Marcia S, Theumann N, et al. A prospective, international, randomized, noninferiority study comparing an implantable titanium vertebral augmentation device versus balloon kyphoplasty in the reduction of vertebral compression fractures (SAKOS study). *Spine J* 2019;19:1782–95 CrossRef Medline
  24. Premat K, Vande Perre S, Cormier É, et al. Vertebral augmentation with the SpineJack® in chronic vertebral compression fractures with major kyphosis. *Eur Radiol* 2018;28:4985–91 CrossRef Medline
  25. Beall D, Lorio MP, Yun BM, et al. Review of vertebral augmentation: an updated meta-analysis of the effectiveness. *Int J Spine Surg* 2018;12:295–321 CrossRef Medline
  26. Gu CN, Brinjikji W, Evans AJ, et al. Outcomes of vertebroplasty compared with kyphoplasty: a systematic review and meta-analysis. *J Neurointerv Surg* 2016;8:636–42 CrossRef Medline
  27. Dohm M, Black CM, Dacre A, et al; KAVIAR investigators. A randomized trial comparing balloon kyphoplasty and vertebroplasty for vertebral compression fractures due to osteoporosis. *AJNR Am J Neuroradiol* 2014;35:2227–36 CrossRef Medline
  28. Yaltirik K, Ashour AM, Reis CR, et al. Vertebral augmentation by kyphoplasty and vertebroplasty: 8 years experience outcomes and complications. *J Craniovertebr Junction Spine* 2016;7:153–60 CrossRef Medline
  29. Lin JH, Wang SH, Lin EY, et al. Better height restoration, greater kyphosis correction, and fewer refractures of cemented vertebrae by using an intravertebral reduction device: a 1-year follow-up study. *World Neurosurg* 2016;90:391–96 CrossRef Medline



# A Novel Patient-Positioning Device for Dynamic CT Myelography

Andrew L. Callen, Rich Wojcik, and Michael Bojanowski



## ABSTRACT

**SUMMARY:** We describe a novel patient-positioning device for dynamic CT myelography. Dynamic CT myelography requires angling the patient's spine to distribute dense contrast along the dependent thecal sac. The proposed device is constructed of a low-density reinforced polymer frame and can be raised or lowered to various heights with a hand-operated mechanism, allowing precise adjustment of the spinal angle and control of the contrast bolus, increasing the safety, reproducibility, and sensitivity of dynamic CT myelography.

**ABBREVIATION:** dCTM = dynamic CT myelography

Dynamic CT myelography (dCTM) is an effective technique for the localization of CSF leaks and the detection of CSF venous fistulas.<sup>1</sup> Unlike conventional CT myelography, in which the goal is the even diffusion of contrast material throughout the subarachnoid space, in dCTM, the goal is to distribute dense, unmixed contrast along the dependent thecal sac.<sup>2</sup> When one looks for a CSF venous fistula or a ruptured meningeal diverticulum, the patient is in a decubitus position so that dense contrast fills the nerve root sleeves and meningeal diverticula. When a ventral dural defect is suspected, the patient is positioned prone with the hips elevated to localize the site of subarachnoid contrast extravasation into the ventral epidural space.<sup>3</sup> Unlike digital subtraction myelography, which can use a tilt table to facilitate gravity-dependent egress of contrast from the lumbar puncture site toward the craniocervical junction, patient positioning in CT typically relies on the use of either a foam wedge or an inflatable mattress device positioned under the patient's hips to angle the spine.<sup>4</sup> A foam wedge can lead to a predictable, constant movement of contrast, but positioning a patient on top of the wedge from the beginning of the procedure precludes the accurate measurement of spinal opening pressure, and the prone position can

often require additional pillows or other material to elevate the hips sufficiently to overcome a patient's lumbar lordosis (Fig 1). Additionally, beginning the patient in the angled position can often result in decreased tension of the thecal sac, causing difficulty achieving a subarachnoid puncture. An inflatable mattress allows the patient to begin the examination in the horizontal position, followed by temporary inflation and deflation before scanning. However, the time required for inflation can be variable, and patient positioning can be unstable, often requiring assistants to secure the patient while the device is in the inflated position. In the case of type 1 or 2 CSF leaks, misjudging the timing of the contrast bolus or delays due to needing to reposition a patient after contrast injection can lead to poorer visualization of a dural defect and decreased diagnostic accuracy (Fig 2). To overcome the drawbacks of each commonly used technique, we designed a unique patient-positioning device to accurately and safely manipulate the spinal angle during dCTM, to increase the safety, reproducibility, and sensitivity of the examination.

## Device Description

The device consists of a reinforced polymer frame covered with heavy duty canvas fabric and supportive foam cushioning, secured to the CT table at the end distal to the gantry by straps and 3D-printed plastic inserts. The inserts are specific to the channel along the length of the patient's bed, which can vary among manufacturers. The device was initially designed for a Somatom Alpha CT table (Siemens). This CT table uses a channel size of 0.219 inches (5.6 mm) in diameter with a 0.129-inch (3.3-mm) slot opening. If the channel diameter and opening on the patient bed are within  $\pm 0.010$  inches ( $\pm 0.25$  mm) of the dimensions above, then the straps will be compatible with other CT tables. If the channel

Received August 2, 2023; accepted after revision September 3.

From the Department of Radiology (A.L.C.), Neuroradiology Section, University of Colorado Anschutz Medical Campus, Aurora, Colorado; and KIC Consulting LLC (R.W., M.B.), Denver, Colorado.

Grant support from the Considine Family Foundation was used for the development of this device.

Please address correspondence to Andrew L. Callen, MD, 12401 E 17th Ave, Aurora, CO 80045; e-mail: andrew.callen@cuanschutz.edu; @AndrewCallenMD

Indicates open access to non-subscribers at [www.ajnr.org](http://www.ajnr.org)

Indicates article with supplemental online video.

<http://dx.doi.org/10.3174/ajnr.A8023>

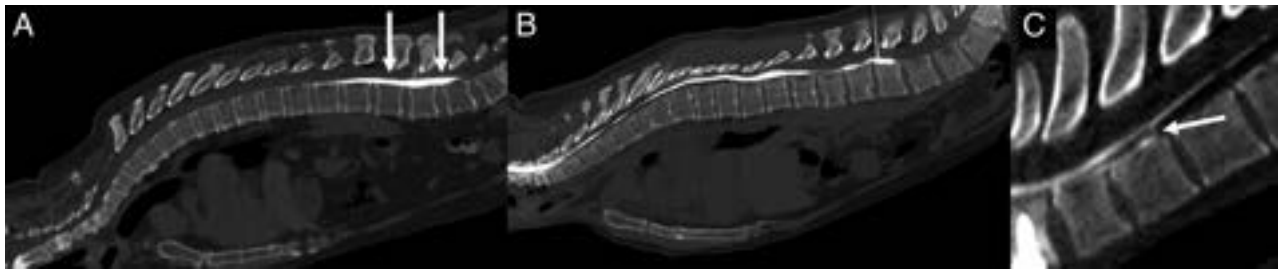


**FIG 1.** Spine angulation using a foam wedge versus using the elevation device in suspected ventral dural defects. *A*, A patient with a suspected ventral dural defect, positioned on top of a foam wedge for dCTM. CT image obtained after contrast injection shows pooling of contrast at the patient's lumbar lordosis (arrows) due to insufficient hip elevation. *B*, A separate patient with a suspected ventral dural defect on top of the novel positioning device. CT image obtained after contrast injection demonstrates egress of contrast from the puncture site to the craniocervical junction. *C*, Smaller FOV image demonstrates extravasation of contrast from the subarachnoid space into the ventral epidural space at C7–T1 (arrow), consistent with a ventral dural defect.

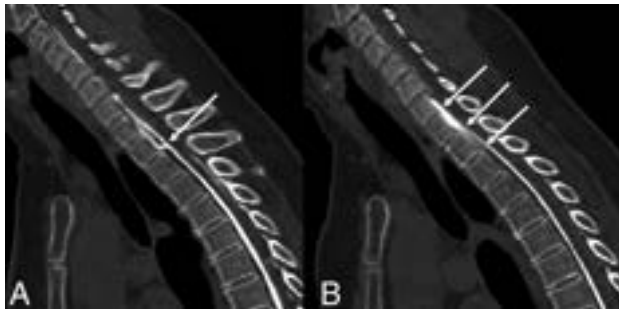


**FIG 2.** A ventral dural defect at T2–T3. *A*, Image obtained immediately after contrast injection demonstrates clear extravasation of contrast (arrow) from the subarachnoid space into the ventral epidural space, precisely localizing this patient's dural defect. *B*, A second image obtained 38 seconds after the first demonstrates rapid diffusion of contrast throughout the ventral epidural fluid collection (arrows), obscuring the precise site of the dural defect.

diameters vary more than these dimensions, new inserts may be 3D-printed at minimal cost. The device is bisected by a pivot point. At the fixed end, there is a hand-operated winch, which connects to the other end of the device by a polyester strap that runs beneath the frame (Fig 3). Underneath the mobile end proximal to the gantry, there are polyurethane wheels that allow translation along the Z-axis of the bore, depending on the length of the strap, which is controlled by the hand winch. The portion of the device that is included in the FOV is constructed of reinforced

polymer and engineered polymers to minimize streak artifacts and the patient dose (Fig 4). The only metallic components present are along the most distal and proximal ends of the device, which remain outside of the FOV.

The overall device measures 91 inches long  $\times$  21 inches wide  $\times$  9 inches tall (231  $\times$  54  $\times$  23 cm), with the bed portion measuring 77 inches long  $\times$  20 inches wide (196  $\times$  51 cm). It can support a patient weighing up to 300 pounds (136 kg) and up to 76 inches (193 cm) in height. Initially designed for the Somatom Alpha CT machine, the fixation straps can accommodate multiple CT machine types as long as the CT table uses a patient bed that is 17–19 inches wide with a minimum length of 91 inches and a curvature height of 2 inches from the edges to the bottom of the bed.

#### Device Use

The device can be unpacked and secured to the CT table in <5 minutes, best achieved with 2 operators. The patient can be positioned either decubitus or prone and is secured to the device with 2 fabric straps (Fig 5). At the mobile end proximal to the gantry, there are 2 fixed handles that can be held by the patient in the prone position. The patient can begin the examination in the horizontal or elevated position, depending on the preference of the operator. The height of the device can be adjusted depending on the size of the patient and is limited only by the width of his or her hips to allow the maximal elevation possible without obstructing movement into the gantry. Patient elevation takes

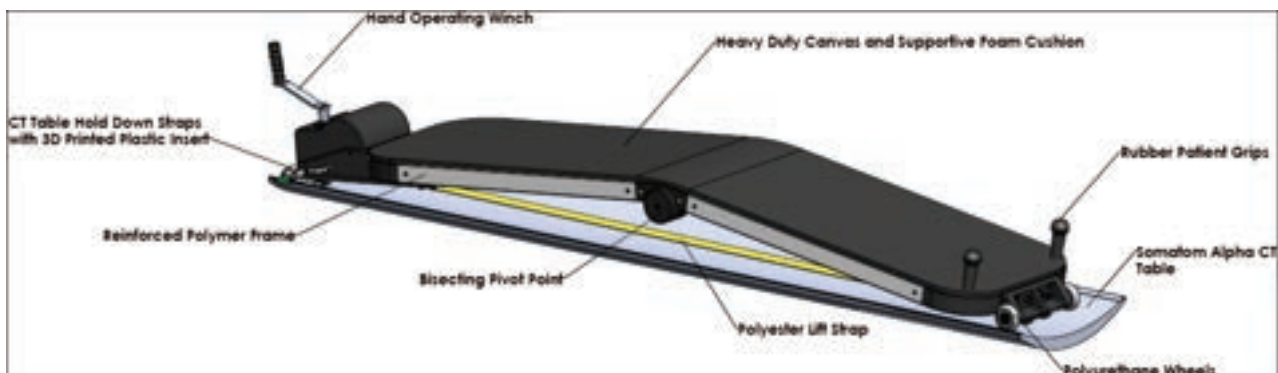


**FIG 3.** Device schematic.

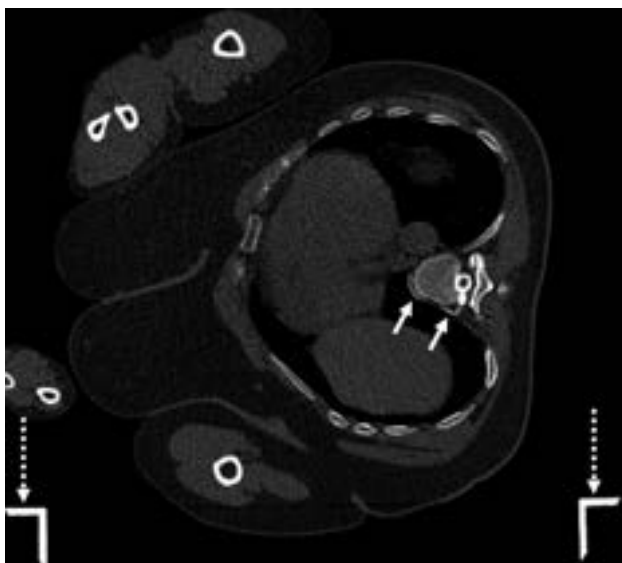


**FIG 4.** Localization of a CSF venous fistula using the positioning device. Axial CT image with a wide FOV demonstrates a patient in the right lateral decubitus position on top of the positioning device during dCTM with a CSF venous fistula (solid arrows) arising from a right T8–T9 meningeal diverticulum. The device frame (dashed arrows) generates no streak artifacts.

the patient, if desired, may allow needle trajectories that would otherwise require tilting of the CT gantry.

## CONCLUSIONS

We describe a dCTM patient-positioning device that offers several practical advantages over current commonly used methods for angling the spine on the CT table. By providing accurate and safe manipulation of the spinal angle, the device has the potential to increase diagnostic accuracy and procedural reproducibility and can accommodate patients of varying sizes. Patients can be positioned decubitus or prone and can start the examination in a horizontal or angled position. Because elevation is smooth and controlled, height can be adjusted while leaving the needle in place if needed. We believe that the incorporation of this device in clinical practice will improve patient outcomes and streamline the dCTM procedure for radiologists. Further studies are warranted to validate its effectiveness, assess patient and provider satisfaction as well as explore potential applications for manipulating the spinal angle in other CT-guided procedures. To date, we have performed 32 dCTM examinations using the device, all of which have been executed without compromised image quality. A patent is pending for the device, and it is our hope that it will be commercially available soon.

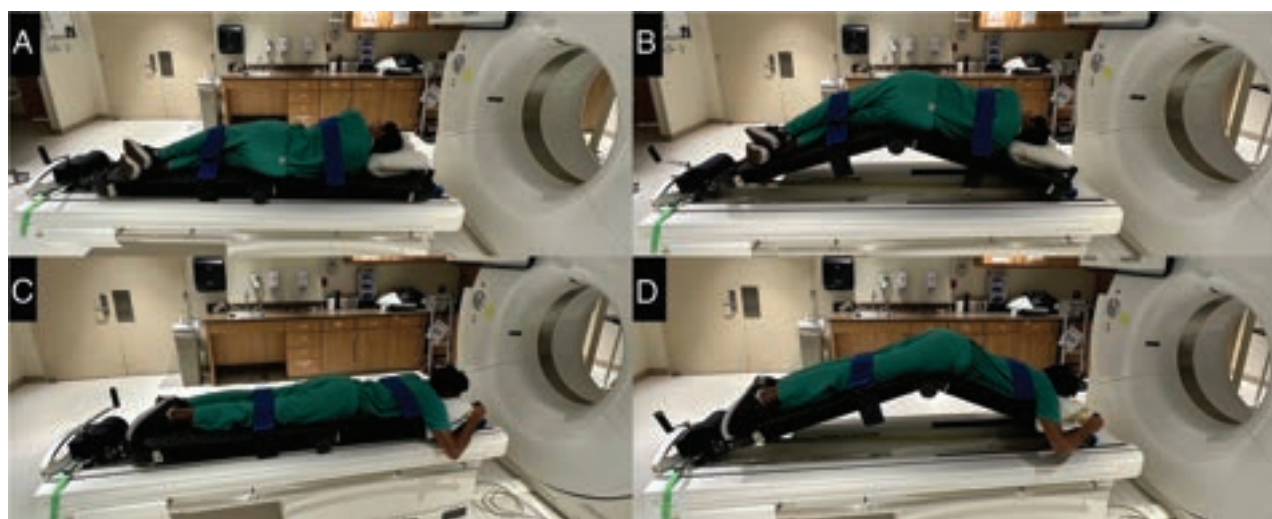


**FIG 5.** Example of the device in use in decubitus (A, Flat, B, Elevated) and prone (C, Flat, D, Elevated) patient positions.

approximately 8–12 seconds (Supplementary Online Video). Because the patient's elevation is controlled and predictable, the needle may be left in the patient during height adjustment to allow additional contrast administration during the examination if necessary. If the patient is too large to fit in the gantry in the elevated position, the device can be elevated and subsequently lowered with the patient outside the gantry before scanning. Because the device is secured to the CT table, the patient may rotate to the contralateral decubitus position while remaining on the device if desired. Additionally, the patient may remain on the device during patching or other CT-guided procedures. Angling

## ACKNOWLEDGMENTS

We acknowledge Ashesh A. Thaker, MD, Vincent M. Timpone, MD, and Josh Grip for input early in the design process.

Disclosure forms provided by the authors are available with the full text and PDF of this article at [www.ajnr.org](http://www.ajnr.org).

## REFERENCES

1. Kranz PG, Gray L, Amrhein TJ. Decubitus CT myelography for detecting subtle CSF leaks in spontaneous intracranial

- hypotension.** *AJNR Am J Neuroradiol* 2019;40:754–56 CrossRef Medline
2. Mamlouk MD, Ochi RP, Jun P, et al. **Decubitus CT myelography for CSF-venous fistulas: a procedural approach.** *AJNR Am J Neuroradiol* 2021;42:32–36 CrossRef Medline
3. Thielen KR, Sillery JC, Morris JM, et al. **Ultrafast dynamic computed tomography myelography for the precise identification of high-flow cerebrospinal fluid leaks caused by spiculated spinal osteophytes.** *J Neurosurg Spine* 2015;22:324–31 CrossRef Medline
4. Callen AL, Timpone VM, Schwertner A, et al. **Algorithmic multimodality approach to diagnosis and treatment of spinal CSF leak and venous fistula in patients with spontaneous intracranial hypotension.** *AJR Am J Roentgenol* 2022;219:292–301 CrossRef



## Professor Antonios (Anton) Valavanis, MD

This memorial aims to celebrate the life and the many clinical, educational, and scientific accomplishments of Professor Antonios Valavanis who recently passed away.<sup>1</sup> Antonios Valavanis has impacted and shaped the specialty of diagnostic and interventional neuroradiology like few have done before. He was born in Athens, Greece, graduated from medical school at the University of Zurich, completed his training in radiology and neuroradiology at the University Hospital of Zurich, received his *venia legendi* in neuroradiology at the University of Zurich, and founded and chaired the Clinic of Neuroradiology at the University Hospital Zurich until his retirement. Together with Professor Peter Huber from Bern, Switzerland, he is considered the father of neuroradiology in Switzerland. His relentless effort to develop neuroradiology as an integral diagnostic and interventional part of the clinical care of patients with neurologic, neurosurgical, or otorhinolaryngeal diseases is legendary.

Antonios Valavanis's curiosity and expertise were stimulated and shaped early in his career by 2 Zurich giants in medicine: Professor M. Gazi Yaşargil and Professor Ugo Fish, who, respectively, served as the Chair of the Department of Neurosurgery and Chair of the Department of Otorhinolaryngology at the University Hospital of Zurich (Fig 1). In the many years of his illustrious career, Antonios Valavanis became a professional and often also close personal friend of many more exceptional physicians around the globe, including companion colleagues like Pierre Lasjaunias (Fig 2), Luc Picard, Giovanni di Chiro, Guido Guglielmi, Marco Leonardi, Alex Berenstein (Fig 3), Scott Atlas, Timo Krings, Karel ter Brugge, and many more. Antonios Valavanis will be especially remembered as an extremely talented innovator, who, on the basis of a detailed knowledge and deep understanding of the functional neuroarchitecture, explored and developed revolutionary neurointerventional approaches to treat patients. He embraced new technologies with ease, always focused on offering the best care possible for patients. Next to his clinical and academic accomplishments, he was also a great representative of all aspects of neuroradiology in

Europe and the world. Furthermore, he was an exceptionally gifted teacher, who was able to dissect complex topics in an exemplary way, allowing both junior and senior colleagues to better understand diseases and how to best treat them. In addition, his intelligence, critical thinking, and knowledge of history, combined with a good sense of humor and charisma, made him very well-recognized and successful internationally.



**FIG 2.** Antonios Valavanis and Pierre Lasjaunias, First International Zurich Course on Interventional Neuroradiology, March 1992.



**FIG 1.** Ugo Fish, M. Gazi Yaşargil, and Antonios Valavanis (1991).



**FIG 3.** Alejandro (Alex) Berenstein and Antonios Valavanis, First International Zurich Course on Interventional Neuroradiology, March 1992.

His academic achievements are extensive, including numerous scientific articles, book chapters, books, invited lectures, visiting professorships, scientific awards, honorary memberships, gold medals, and much more. His legacy is, however, best celebrated by the way he is remembered by his colleagues.

### **M. Gazi Yaşargil**

Anton, an outstanding and talented neuroradiologist in endovascular surgery and neurodiagnostics, was a valuable colleague and a loyal friend for more than 40 years. Neuroradiologic diagnosis plays a major role in planning surgical strategy. In Zurich, Anton presided over our daily conference, and with respect, we followed his evaluation of MR and angiographic images and listened attentively to his precise and clear descriptions of the anatomy in relation to the location of the lesion. We miss his quiet presence at our congresses and his exceptional, well-organized lectures, distinguished by the systematic structure of the content.

For me personally, Anton was also a partner for discussion and conversations on a philosophical level. He demonstrated a profound knowledge of Greek philosophers and Greek mythology and a deep understanding of old and new Greek languages. His wisdom was exceptional and supplemented my own readings and great interest in these subjects.

I admired Anton for his placid frame of mind and his dignity and composure throughout a long and distressing illness. His defiance to withstand the frustrations of poor health and negative effects of treatment and to continue his research and publications was impressive.

We recognize his many achievements, and mourn our loss.

### **Alejandro (Alex) Berenstein**

Anton was my dear friend and a very special doctor, scientist, intellectual, colleague, friend, and unique human being.

I miss our interactions so much and his analytical mind, sensitivity, humor, and, most of all, his contagious laughing. The many hours of discussions and then rich consensus advanced our understanding of a topic such as interventional neuroradiology or any topic from science, politics, history (mostly Greek . . .) to human behavior. I will never forget our walk through Zurich's Zoo and how we saw anatomy and evolution as we observed the various animals and how similar and different they were and how they related to everything. We finished with unstoppable laughter as we enjoyed dinner. My beloved friend, what a loss you are to our field, to medicine, to your beautiful family, and personally to me. You will always be my most loved friend.

### **Scott W. Atlas**

My colleague and friend, Professor Anton Valavanis, passed away after a long battle, persevering for years like no one else could have, against all odds. I had the absolute honor of working with Anton beginning in 2013 as Visiting Professor in his world-renowned Neuroradiology Department and to serve as Co-Director of his celebrated course on Interventional Neuroradiology when he added a section on Imaging and Diagnostic Neuroradiology. Everyone who ever worked with him immediately recognized his intellect and unparalleled attention to detail, including his relentless drive to

truly understand neurologic diseases at their most basic level—far deeper than the level of knowledge that dominates the field.

Virtually at once, we became close friends and remained so. I also have the great pleasure of knowing his wonderful wife and daughters, in whom he had great pride. Initially, being an American from California, I was stunned at his intimidating and formal presence to his students, who jumped to stand at attention on his entrance. I quickly came to understand and enjoy his humor and warmth over our many memorable dinners and long discussions over fine wine in Zurich. Beyond sharing an intolerance for superficial thinking and appreciating the humor in recognizing the “Emperor's New Clothes” in our field and elsewhere, we shared many great times enjoying what can be best described as a quest for high quality.

Anton Valavanis led a truly remarkable life—a one-of-a-kind man who will never be replaced. I will miss him.

### **Timo Krings**

Having had the unique opportunity to teach with Professor Valavanis in the Zurich Course between 2009 and 2016 allowed me to get to know the many facets of a giant in our field, who truly excelled at whatever he did—whether it was in sports (he competed for the Greek national swimming team), philosophy (in particular his love for the cephalocentric view of Plato and his deepfelt antagonism of the Aristotelian cardiocentrism), neuroanatomy, or catheter handling.

Professor Valavanis was an amazing storyteller, who was able to hold his audience captive, whether he talked about the history of neurointervention, his theories on brain AVM development, or the art of medicine.

However, it was not only serious talking. He had an amazing sense of humor, and his stories about past encounters with luminaries in our fields could easily entertain the faculty of the Zurich Course for an entire evening.

As a neurointerventionalist, he was rooted deeply in neuroanatomy but still embraced new materials and techniques. However, he regarded those as mere tools and was skeptical about those innovations that were mainly driven by companies. His main focus was always the well-being of the patient, and he taught us that the neurointerventional procedure is but one part of the treatment journey of the patient.

He was always sharp, present in the moment, and remained inquisitive and open-minded. He will be missed by his family, his friends and pupils, and his patients.

### **Karel G. ter Brugge**

Anton Valavanis stood out for me not only for being an exceptional interventional neuroradiologist but also because of his outstanding knowledge of neuroanatomy. His ongoing search to understand the phylogenetic evolution of the human brain was unique and revealing. He demonstrated the relevance of such knowledge in the understanding of the neuroimaging characteristics of the various parts of the brain and their relevance for the location of certain pathologies. He taught us the importance of such knowledge because it allowed him to treat his patients safely using tools with which he was thoroughly familiar and rejecting the use of the latest devices with no proved records of superiority.

Anton Valavanis organized, for more than 2 decades, the Zurich Course on Diagnostic and Interventional Neuroradiology, a premier course in its field, attended each year by hundreds of neuroradiologists and neurosurgeons from all over the world. I was fortunate to be part of Zurich Course faculty for many years and witnessed Anton's unique program choices and teaching abilities. It was during the Zurich Course in 2008 that Pierre Lasjaunias, one of Anton's closest friends and a course faculty member since its inception, unexpectedly died. In consultation with Professor Yasargil, former head of neurosurgery at the Zurich University Hospital, Anton decided to continue the program and dedicate it to his friend Pierre Lasjaunias. This choice was made with the understanding that education must continue independent of any given teacher, no matter how outstanding his or her contributions were. The contributions of Anton Valavanis to our field will always be a guidance for future research, education, and patient care.

#### ***Finally, How Will I (Thierry Huisman) Remember Professor Antonios Valavanis?***

I started 1991 as a fellow in neuroradiology at the University Hospital of Zurich (Fig 4). Training under him was hard but fair. The days of work were long, very long; the evenings and nights as well as the weekends were there for reading and study. A detailed knowledge and understanding of functional neuroanatomy, including embryology, were (and of course still are) a *sine qua non*. Imaging should always be approached from a clinical perspective, the brain is unique and extremely fascinating, and neuroradiology is one of the best medical specialties there is. Most of all, I learned that critical thinking is very, very important. He advised me to read a text from Eugen Bleuler, Professor of Psychiatry at the University of Zurich in the early 1900s. This text was entitled "*Undisciplined Thinking in Medicine and How To Overcome It.*" I integrated this line into my doctorate thesis,



**FIG 4.** Thierry A. Huisman and Antonios Valavanis during the welcome reception of the XIX Annual Scientific Meeting of the European Society of Neuroradiology, September 8–12, 1993.

which I completed under his supervision/mentorship. This line is today as true as ever. I will always be grateful for all I learned from him. He is one of the true giants in neuroradiology, and because of him, I became a neuroradiologist. I miss him dearly.

#### **REFERENCE**

1. Wanke I, Lövblad KO, Remonda L. **Professor Antonios Valavanis.** *AJNR Am J Neuroradiol* 2023;44:E33–34 CrossRef Medline

**Thierry A.G.M. Huisman**  
**Scott W. Atlas**  
**Alejandro Berenstein**  
**Timo Krings**  
**Karel ter Brugge**  
**M. Gazi Yaşargil**

<http://dx.doi.org/10.3174/ajnr.A8010>

# Medicare Coverage of Amyloid PET: Implications for Clinical Practice

On July 17, 2023, the Centers for Medicare & Medicaid Services (CMS) issued a memo proposing to permit Medicare coverage determinations for beta amyloid ( $A\beta$ )-targeted PET to be made by Medicare Administrative Contractors. As neuroradiologists, neurologists, and nuclear medicine physicians, we highlight the relevance of this decision to our clinical practice.

Alzheimer disease (AD) is the leading cause of dementia, affecting more than 6 million patients in the United States, with health care costs expected to exceed \$1 trillion by 2050.<sup>1</sup>  $A\beta$  plaques are a widely accepted AD biomarker, as well as a promising therapeutic target, despite recent studies questioning the pathophysiologic significance of  $A\beta$  in AD.<sup>2</sup>

The Imaging Dementia: Evidence for Amyloid Scanning (IDEAS) study enrolled more than 18,000 Medicare beneficiaries 65 years of age or older, aiming to answer 2 central questions: “Does  $A\beta$ -targeted PET change management?” and “Does  $A\beta$ -targeted PET improve outcomes?”<sup>3</sup> While the first question was answered affirmatively, providing the strongest evidence supporting the clinical utility of  $A\beta$ -targeted PET to date,<sup>3</sup> and evaluation of the second question is ongoing because the IDEAS study had important limitations. Most notably, Black and Hispanic/Latino patients were markedly underrepresented, despite well-documented racial disparities in AD risk, diagnosis, and outcomes.<sup>1</sup> The ongoing New IDEAS study seeks to address these disparities by emphasizing an accrual of patients from underrepresented groups.

Recently,  $A\beta$ -targeted therapies have been approved by the FDA, including aducanumab and lecanemab. While there are important adverse events to consider, including amyloid-related imaging abnormalities,<sup>1</sup> this approval represents the most promising therapeutic option for AD to date, with understandably strong interest from both patients and referring neurologists. Eligibility for  $A\beta$ -targeted therapies requires a positive  $A\beta$ -targeted PET or CSF analysis. Any emerging and future AD therapies are likely to include  $A\beta$ -targeted PET as part of their inclusion criteria. Even as serologic and CSF assays of  $A\beta$  show the promise of approximating levels of overall brain  $A\beta$ , no other technology allows the assessment of its geographic distribution. Furthermore,  $A\beta$ -PET is much preferred to CSF testing from the patients’ and caregivers’ perspective, due to its noninvasive nature.

Clinicians and scientists at our major academic urban medical center are collaborating closely in studying  $A\beta$ -targeted PET in the clinical and research settings, participating in the IDEAS/New IDEAS studies, developing imaging-centered clinical trials evaluating different aspects of AD pathophysiology, and optimizing quan-

titative analysis methods of  $A\beta$ -targeted PET.<sup>4</sup> Access to  $A\beta$ -PET will improve clinical trial accrual and will increase our understanding of the geographic distribution of brain  $A\beta$  levels and how they are affected by emerging disease-modifying therapies. We therefore applaud this decision by CMS to commence reimbursement of  $A\beta$ -targeted PET studies in the clinical setting. We further encourage increased training opportunities for practicing radiologists and radiology residents and fellows in the interpretation of  $A\beta$ -targeted PET, along with educational opportunities for neurologists and other dementia specialists, and the incorporation of  $A\beta$ -targeted PET into national clinical guidelines for imaging of patients with cognitive impairment. It is important for our community to ensure the availability of  $A\beta$ -targeted PET, particularly in underserved populations.

Disclosure forms provided by the authors are available with the full text and PDF of this article at [www.ajnr.org](http://www.ajnr.org).

## REFERENCES

- 2023 Alzheimer’s disease facts and figures. *Alzheimers Dement* 2023;19:1598–695 CrossRef Medline
- Jack CR Jr, Bennett DA, Blennow K, et al. NIA-AA Research Framework: toward a biological definition of Alzheimer’s disease. *Alzheimers Dement* 2018;14:535–62 CrossRef Medline
- Rabinovici GD, Gatzonis C, Apgar C, et al. Association of amyloid positron emission tomography with subsequent change in clinical management among Medicare beneficiaries with mild cognitive impairment or dementia. *JAMA* 2019;321:1286–94 CrossRef Medline
- Smith NM, Ford JN, Haghdel A, et al. Statistical parametric mapping in amyloid positron emission tomography. *Front Aging Neurosci* 2022;14:849932 CrossRef Medline

● J. Ivanidze

Department of Radiology  
Weill Cornell Medicine  
New York, New York

● A.S. Nordvig

Department of Neurology  
Weill Cornell Medicine  
New York, New York

● A.R. Fajardo

A.J. Tsiouris

● G.C.-Y. Chiang

● J.R. Osborne

Department of Radiology  
Weill Cornell Medicine  
New York, New York